

Modified Dental Composites For Bone Repair

Thesis submitted by

Mayda Arshad

For the degree of

DOCTOR OF PHILOSOPHY

Eastman Dental Institute

Division of Biomaterials and Tissue Engineering

UNIVERSITY COLLEGE LONDON

- 2021 -

Dedicated to

My children

DECLARATION

I, **Mayda Arshad** confirm that the work presented in this thesis is my own. Where information has been derived from other sources, I confirm that this has been indicated in the thesis.

ACKNOWLEDGMENTS

First and foremost I would like to show my deepest gratitude to my supervisor Professor Anne Young for providing me with limitless guidance, support, advice and patience during my PhD. I would also like to sincerely thank my second supervisor Professor Patrizia Ferretti for her valuable input and direction.

I am grateful to the Institute of Biomedical Engineering, now known as the Institute of Healthcare Engineering for offering me this PhD. Extending my gratitude to the funding body, Research Councils UK for the studentship that allowed me to conduct my thesis.

I am thankful to Dr. Wendy Xia for always assisting me in labs. I am also extremely thankful to Dr George Georgiou, Dr Graham Palmer, Dr. Nicky Morden and Dr. Isabel Kingston for their continuous technical assistance throughout my PhD. Additionally I would like to show appreciation to Dr. Panpisut Piyaphong for training me on equipment during the initial stages of my PhD. Thank you to Dr. António HS Delgado for assisting me with the statistics using SPSS.

Grateful to the staff from the Royal Orthopaedic hospital and Institute of child health for the training and use of facilities to carry out the experiments in my project.

I truly appreciate all my friends and colleagues at the Eastman and within the Biomaterials and Tissue Engineering Department who have always found a way to help me. Especially Dr. Nazanin Owji, Alessandra Grillo, Taleen Shakouri and Zalike Keskin Erdogan.

Finally, I am exceptionally grateful to my family, my parents, siblings, husband and in-laws who have always encouraged and believed in me. My husband has stood by me through my academic journey, immensely supportive and loving, while my parents have been actively involved with taking care of my children.

Publications and Talks (2015-2021)

A) Publication

Panpisut P, Khan MA, Main K, **Arshad M**, Xia W, Petridis H, et al. (2019) Polymerization kinetics stability, volumetric changes, apatite precipitation, strontium release and fatigue of novel bone composites for vertebroplasty. PLoS ONE 14(3): e0207965. <https://doi.org/10.1371/journal.pone.0207965>

B) Talks

- | | |
|---|--------------|
| 1. 3 Minute Thesis Competition - Runner up | -2017 |
| 2. 5 minute Thesis Presentation Competition - First Prize | -2018 |
| 2. Gibco Cell Culture Cell for heroes Webinar talk Thermo fisher | -2020 |
| 3. World Biomaterials Congress * | -2020 |

***Cancelled due to COVID-19**

ABSTRACT

The aim of this project was to develop modified dental composites for bone repair with additional remineralising monocalcium phosphate monohydrate (MCPM) and antibacterial polylysine (PLS).

Bone composites were prepared with the powder to monomer weight ratio of 3:1. The monomer phase consisted of dimethacrylate monomers with chemical curing initiator and activator. Powder phase consisted of glass filler, PLS as antibacterial agent and MCPM as the mineralising agent. The level of remineralising agent and PLS were varied amongst formulations. Commercial polymethylmethacrylate (PMMA) (Simplex™ P) and bone composite (Cortoss®) were used for comparison. Degree of monomer conversion (DC) was assessed using fourier transform infrared spectroscopy (FTIR) (n=3). Biaxial flexural strength (BFS), tested by means of ball on ring technique, was used to compare the mechanical properties of each formulation (n=6). Surface apatite forming ability was carried out using scanning electron microscopy (SEM). Toxicity of monomers were assessed with sheep mesenchymal stem cells (MSCs) and MG63 cells using an Alamar Blue assay. Chick Embryo Chorioallantoic Membrane (CAM) assay was carried out to assess angiogenesis and development of a chick embryo upon contact with the experimental bone composite.

Optimised initiator (benzoyl peroxide (BP)) and activator (N-(2-hydroxy-3-((2-methyl-1-oxo-2-propenyl)oxy)propyl)-N-tolyl glycine (NTGGMA)) levels enabled working times comparable to commercial cement, and advantageously higher conversion and lower heat generation. Increasing PLS resulted in decreased strength and cell activity. Conversely higher MCPM had lesser detrimental effect

on these properties and increased surface mineral precipitation both in-vitro and in-ovo. CAM assay showed, the set discs were generally not toxic (particularly those with high MCPM). Over time the CAM also showed strong adherence for the experimental bone composite discs but not the commercial PMMA.

The experimental bone composites show promising potential, since it encouraged apatite precipitation, which is known to promote bone bonding and did not show toxicity to the developing chicks embryos.

IMPACT STATEMENT

There are 1 million osteoporotic vertebral fractures diagnosed annually in the USA and EU, a further 90% go undiagnosed (Borgström et al., 2020; Williams et al., 2020). Problems with the cements currently employed to stabilise the fractures include placement difficulty, leakage, toxicity, continuing disease / fractures and infection. Furthermore, cementation typically provides only short-term (<1 year) pain relief.

Vertebral fractures are the most common complication of osteoporosis, comprising approximately 1/5th of the 5 million osteoporotic fractures in the EU and the USA annually. Minimally invasive treatment via polymethyl methacrylate (PMMA) bone cement injection (vertebroplasty) is employed to help stabilise fractures, relieve pain and increase mobility. An issue with PMMA is cement leakage leading to poor fixation and complications in distant organs. New bone composites have partially addressed concerns over PMMA leakage, placement difficulties, toxicity and heat generation. Neither materials, however, match the mechanical properties of the vertebra nor do they bond well to the living bone. The materials also do not address the problem of continuing bone destruction and further fractures thus preventing long-term treatment benefit. Finally, these materials have limited or no antibacterial actions to prevent post-operative infection; a potentially life-threatening complication.

Unlike PMMA cements, supplied as a powder and liquid, the experimental bone composite will be supplied in double-barrelled syringes with automatic mixing

tips. This enables a controllable short delay period to allow injection before setting, decreasing the chance of composite leakage from the site of application. It also provides flexibility by facilitating easy application at multiple sites.

Through slight modifications in composite chemistry, biocompatibility, mechanical and initial bone adhering properties have all been substantially improved and heat generation reduced. Long-term bonding to the bone is further improved through the addition of reactive calcium phosphate which promotes localised bone mineralisation. Furthermore, release of PLS, a food preservative, addresses the problem of increasing antibiotic resistance.

The vertebroplasty procedure typically costs ~£1,000. For this, the cost of the PMMA cement would be ~£100. For the composite cement, cost triples due to a lack of competition and obvious advantages of easy application. Of the current 1 million EU and USA vertebral fractures only around 5% are presently treated by vertebroplasty. This is likely due to the short-term benefit. The market will rise because of the increasing average age of the population but could also be substantially increased with the development of a more effective material. Initial development of the material for tooth restoration will enable easier translation into the orthopaedic market. Coverage of the materials by patents will allow licensing of the technology. Once the new material has been accepted in the vertebroplasty market its use could be extended to a wide range of other applications, e.g. hip and knee replacements.

Table of Contents

Chapter 1 Literature Review -----	1
1.1 Human Bone -----	1
1.1.1 Vertebrae -----	1
1.1.2 Trabecular and cortical -----	2
1.1.3 Remineralisation in bone -----	6
1.2 Osteoporotic Fractures -----	6
1.2.1 Aetiology -----	7
1.2.2 Epidemiology-----	9
1.3 Current Treatment -----	11
1.3.1 Vertebroplasty and Kyphoplasty -----	12
1.4 Bone Cements -----	13
1.4.1 Different types of bone cements -----	14
1.4.1.2 Strontium-Substituted Calcium Phosphates-----	16
1.4.1.3 Magnesium Phosphate Cement (MPC) -----	16
1.4.1.4 Incorporation of Bioactive Additives and Cells-----	17
1.4.1.5 PMMA -----	17
1.4.1.6 Composite Cements -----	22
1.5 Complications and failure of bone composite due to limitations in PMMA and other commercial products -----	24
1.6 Components of experimental bone composites -----	26
1.6.1 Monocalcium Phosphate Monohydrate (MCPM) -----	26
1.6.2 Polylysine (PLS)-----	29
-----	30
1.6.3 Glass Fillers -----	31
1.6.4 Organic Polymer Matrix -----	32
1.6.5 Flexible Diluent Monomer -----	33
1.6.7 Initiator/Activator systems -----	35
1.7 Osteoconductive bone cement/composite -----	36
1.8 Regulatory Approval of Bone Composite -----	38
1.9 Statement of the Problem -----	39

Chapter 2 Materials and Methods	41
2.1 Materials	41
2.1.1 Commercial Materials	42
2.1.2 Monomers	43
2.1.3 Remineralisation agent and antibacterial agent	43
2.1.4 Fillers	44
2.1.5 Initiator, Activator	44
2.2 Methods	44
2.2.1 Commercial material samples preparation	44
2.2.1.1 Simplex™ P (PMMA)	44
2.2.1.2 Cortoss®	45
2.2.2 Experimental Composite Preparation	45
2.2.3 Filler (Powder) Phase	46
2.2.4 Paste Mixing and Syringe Filling	46
2.2.5 Fourier Transform Infrared Spectroscopy (FTIR)	47
2.2.5.1 FTIR Background	48
2.2.5.2 FTIR Instrumentation	48
2.2.5.3 Curing Profile and Degree of Conversion	50
2.2.5.4 Polymerisation Equations	52
2.2.6 Heat Rise	56
2.2.7 Composite Disc preparation	57
2.2.7.1 Sterilisation for in-vitro and in-ovo	57
2.2.8 Mechanical Testing	58
2.2.8.1 Biaxial Flexural Testing	58
2.2.8.2 Biaxial Flexural Testing background	58
2.2.8.3 Poisson's Ratio	60
2.2.8.4 Biaxial flexural strength test	61
2.2.8.5 Young's modulus (YM)	62
2.2.9 In-vitro Studies With Experimental Bone Composite Discs	62
2.2.9.1 Bone Marrow Derived Sheep MSCs	64
2.2.9.2 MG63 Cells	64
2.2.10 In-ovo Chick Embryo Chorioallantoic Membrane assay (CAM)	65
2.2.10.1 Preparation of CAM	65

2.2.11 Scanning Electron Microscope -----	67
2.2.11.1 In-vitro Sample Preparation for SEM -----	68
2.2.11.2 In-ovo Sample Preparation for SEM -----	68
2.2.12 Antibody Staining -----	68
2.2.12.1 In-vitro -----	68
2.2.12.2 In-Ovo -----	69
Chapter 3 Kinetics of Composite Formulation Settings -----	71
3.1 Abstract -----	71
3.2 Introduction -----	72
3.3 Aims -----	73
3.4 Objectives -----	74
3.5 Materials and Methods -----	75
3.6 Results -----	76
3.6.1 Monomer Conversion of Experimental Bone Composite -----	76
3.6.2 Inhibition Time and Half-life of Experimental Composites -----	80
3.6.3 Rate of Polymerisation -----	82
3.6.4 Monomer Conversion Comparison with Commercial Products -----	83
3.6.5 Inhibition Time and Half-life Comparison with Commercial Products	85
3.6.6 Rate of Polymerisation Comparison with Commercial Products -----	87
3.6.7 Temperature Rise Comparison of Preferred Formulation versus PMMA (Simplex™ P) -----	88
3.7 Discussion -----	89
3.7.1 Monomer Conversion of Experimental Bone Composite -----	89
3.7.2 Inhibition Time and Half-life of Experimental Composite -----	92
3.7.3 Rate of Polymerisation -----	93
3.7.4 Monomer Conversion Comparison with Commercial Products -----	94
3.7.5 Inhibition Time and Half-life Comparison with Commercial Products	96
3.7.6 Rate of Polymerisation Comparison with Commercial Products -----	98
3.7.7 Temperature Rise Comparison of Preferred Formulation versus PMMA (Simplex™ P) -----	99
3.8 Conclusions -----	101

Chapter 4 Mechanical and Dimensional Properties of Optimised Formulations -----	102
4.1 Abstract -----	102
4.2 Introduction -----	104
4.3 Aims -----	106
4.4 Objectives -----	106
4.5 Materials and Methods -----	107
4.5.1 Discs for Gravimetric and Volumetric and pH Analysis-----	107
4.5.2 Discs for Biaxial Flexural Strength Test and Youngs Modulus---	109
4.5.3 Discs for SEM-----	109
4.5.4 Statistical Analysis-----	109
4.6 Results -----	110
4.6.1 Mass and Volume change-----	110
4.6.2 Potential of hydrogen (pH) change-----	115
4.6.3 Biaxial Flexural Strength (BFS) -----	118
4.6.4 Youngs Modulus (YM)-----	121
4.6.5 Remineralisation on Disc Surface -----	124
4.7 Discussion -----	129
4.7.1 Mass and Volume Change -----	129
4.7.2 Potential of Hydrogen (pH) Change -----	131
4.7.3 Biaxial Flexural Strength (BFS) -----	133
4.7.4 Youngs Modulus (YM)-----	134
4.7.5 Remineralisation on Disc Surface -----	136
4.8 Conclusions -----	138
Chapter 5 Different Cell Viability In-vitro with Optimised Formulation Discs -----	139
5.1 Abstract -----	139
5.2 Introduction -----	140
5.3 Aims -----	142
5.4 Objectives -----	142
5.5 Materials and Methods -----	143
5.5.1 Experimental Bone Composite Discs-----	143

5.5.2 Bone Marrow Derived Sheep MSCs-----	143
5.5.2.1 Assessing PLS Concentration on Bone Marrow Derived Sheep MSCs -----	143
5.5.2.2 Cell Morphology Assessment -----	144
5.5.2.3 Influence of Disc Extract on Sheep Mesenchymal Stem Cell Activity-----	144
5.5.3 MG63 Cells-----	145
5.5.3.1 Assessing PLS and MCPM vs HCl Concentration on MG63 Cells -----	145
5.5.3.2 Disc extract toxicity on MG63 cells -----	146
5.5.4 Statistical Analysis-----	146
5.6 Results -----	147
5.6.1 Sheep Mesenchymal Stem Cell: Morphology on Disc Surfaces ----	147
5.6.2 Bone Marrow Derived Sheep MSCs: Effect of Disc Extract Solution -----	153
5.6.3 Bone Marrow Derived Sheep MSCs: Polylysine Toxicity -----	156
5.6.4 MG63 cells: Effect of Disc Extract Solution -----	159
5.6.5 MG63 cells: Polylysine, Monocalcium phosphate and Hydrochloric Acid Toxicity -----	163
5.7 Discussion-----	165
5.7.1 Sheep Mesenchymal Stem Cell: Morphology on Disc Surfaces ----	165
5.7.2 Bone Marrow Derived Sheep MSCs: Effect of Disc Extract Solution -----	168
5.7.3 Bone Marrow Derived Sheep MSCs: Polylysine Toxicity -----	170
5.7.4 MG63 cells: Effect of disc extract solution -----	173
5.7.5 MG63 Cells: Polylysine, Monocalcium phosphate and Hydrochloric Acid Toxicity -----	175
5.8 Conclusions-----	177
Chapter 6 CAM grafting In-ovo of Composite Discs -----	178
6.1 Abstract-----	178
6.2 Introduction -----	179
6.3 Aims-----	181
6.4 Objectives-----	182

6.5 Materials and Methods	183
6.5.1 MCPM and PLS Added Individually in Disc Implants	183
6.5.2 MCPM 8 wt% and PLS 5 wt% Added Individually in Disc Implants	183
6.5.3 Experimental Bone Composite Formulations Versus Commercial PMMA Bone Cement for Disc Implants	187
6.5.4 Vascular density, junctions and branches quantification	187
6.6 Results	188
6.6.1 MCPM and PLS Added Individually in Formulations for Disc Implants	188
6.6.2 MCPM 8 wt% and PLS 5 wt% Added Individually in Disc Implants	198
6.6.3 Experimental Bone Composite Formulations Versus Commercial PMMA Bone Cement for Disc Implants	204
6.7 Discussion	209
6.7.1 MCPM and PLS Added Individually in Disc Implants	209
6.7.2 MCPM 8 wt% and PLS 5 wt% Added Individually in Disc Implants	214
6.7.3 Experimental Bone Composite Formulations Versus Commercial PMMA Bone Cement for Disc Implants	215
6.8 Conclusion	219
Chapter 7 Conclusions and Further Work	220
7.1 Conclusions	220
7.2 Further work	221
Chapter 8 Appendix A	238
Chapter 9 Appendix B	251

List of Abbreviations

2D	2-Dimensional
3D	3-Dimensional
NaHCO₃	Sodium Bicarbonate
4-META	4-Methacryloxyethyl trimellitic anhydride
ACP	Amorphous calcium phosphate
BFS	Biaxial flexural strength
Bis-GMA	Bisphenol A Glycidyl Methacrylate
BP	Benzoyl peroxide
CAM	Chick Embryo Chorioallantoic Membrane assay
CE	Conformité Européenne
CO₂	Carbon dioxide
CQ	Camphorquinone
DC	Degree of conversion
DCPA	Dicalcium phosphate anhydrate
dH₂O	De-ionised water
DMEM	Dulbecco's Modified Eagle's Medium
DMPT	N, N-Dimethyl para-toluidine
ED	Embryonic Day
EDD	Embryo development day
EDAX	Energy Dispersive Spectroscopy
FBS	Foetal bovine serum
FDA	Food and Drug Administration
FTIR	Fourier Transform Infrared Spectroscopy
HA	Hydroxyapatite

HCl	Hydrochloric acid
HEMA	Hydroxyethylmethacrylate
HEPES	N-2-hydroxyethylpiperazine-N-ethanesulfonic acid
ISO	International Organization for Standardisation
MCPM	Monocalcium phosphate monohydrate
MG63	Human osteoblast-like cells
MMA	Methyl methacrylate
MPC	Magnesium phosphate cement
MSCs	Mesenchymal Stem cells
NDS	Normal donkey serum
NTGGMA	N-(2-hydroxy-3-((2-methyl-1-oxo-2-propenyl)oxy)propyl)-N-tolyl glycine
PBS	Phosphate Buffer Saline
PBST	Phosphate Buffer Saline + Tween
PFA	Paraformaldehyde
pH	Potential of hydrogen
PLS	Polylysine
PMMA	Poly(methyl methacrylate)
PPGDMA	Polypropylene-glycol-dimethacrylate
rpm	rotations per minute
SBF	Simulated body fluid
SEM	Scanning Electron Microscope
TEGDMA	Triethylene Glycol Dimethacrylate
TetCP	Tetra calcium phosphate

T_g	Glass transition temperature
THR	Total hip replacement
UDMA	Urethane Dimethacrylate
UV	Ultraviolet
WHO	World Health Organisation
YM	Young's modulus

List of Symbols

Greek letters

β	Beta
β_c	Centre of deflection
Δ	Change
σ	Biaxial flexural strength
σ_y	Yield strength
Σ	Sum
μ	Micro
ν	Poisson's ratio
ρ	Density

Units

%	Percentage
€	Euro
°C	Degrees Celsius
μl	Microlitre
μm	Micrometre
a.u.	Arbitrary unit
cm^{-1}	Centimetre inverse
cm^2	Square centimetre
cc	Cubic centrimetre
g/mol	Molecular weight
g	Grams

GPa	Giga Pascal
H⁺	Hydrogen ion
hr	hour/s
kV	Kilovoltage
J/g	Heat capacity
mA	milliamperes
mg/kg	Miligram per kilogram
mins	Minutes
mm	Millimetre
mM	Millimolar
MPa	Megapascal
s	Second/s
v/v	Volume per volume
wt%	Weight percentage concentration

English letters

R_i	Initiator rate
A	Activator concentration
C_f	Fraction of monomer
I	Initiator concentration
k_d	Initiation constant
k_p	Reaction rate of propagation

k_t	Reaction rate for termination
M_0	Mass at initial time
M_n^*	Total concentration of polymer + monomer radicals
M_t	Mass at time t
P_t	Density of disc at time t
P_w	Density of water
®	Registered trademark
R_p	Rate of propagation
R_t	Rate of termination
R_{t50}	Rate of reaction at half life
R_x	Rate of inhibition
$t_{0.5} / t_{50}$	Half-life
t_i	Inhibition time
™	Trademark
V	Volume
V_0	Volume at initial time
V_t	Volume at time t
X_0	Initial concentration of inhibitors
§	Initiator efficiency

List of Figures

- Figure 1.1 Image of vertebra with essential features of thoracic vertebrae. Reprinted from Surgery, volume 36, Mahadevan V. Anatomy of the vertebral column. Page 329, with permission from Elsevier.1
- Figure 1.2 The articulated vertebral column in an adult. Reprinted from Surgery, volume 36, Mahadevan V. Anatomy of the vertebral column. Page 328, with permission from Elsevier.2
- Figure 1.3 In bone, macroscale arrangements involve both compact/cortical bone at the surface and spongy/trabecular bone (foam-like material with $\sim 100\text{-}\mu\text{m}$ -thick struts) in the interior. Reprinted from nature materials, volume 14, Ulrike G.K. Wegst. Bioinspired structural materials. Page 27, with permission from nature materials3
- Figure 1.4 Typical thoracic vertebra. Reprinted from Surgery, volume 36, Mahadevan V. Anatomy of the vertebral column. Page 329, with permission from Elsevier.4
- Figure 1.5 The two basic tissue types of bones are trabecular and cortical. Trabecular (spongy) and cortical (compact) bone tissue differ in their microarchitecture porosity. Reprinted from An introduction to Nutrition, section 9.1. Bone Structure and Function. This book is licenced under a Creative Commons Attribution Non-commercial licence 3.0 licence.....5
- Figure 1.6 MRI showing L2 and L3 compression fracture with no epidural bleed. Reprinted from The Archives of Bone and Joint Surgery, volume 3, T.R Ravi Kumar. An unusual case of a large hematorrachis associated with multi-level Osteoporotic Vertebral Compression Fractures; a Case Report. Page 135. This article is licenced under a Creative Commons Attribution Non-commercial licence 3.0 licence.....9
- Figure 1.7 Chemical structure of MMA 18

- Figure 1.8 The initiation of the polymerisation of MMA: BP from the powder and DMPT from the liquid react to form radicals, starting the curing of bone cements. Adapted from ‘The Acrylic Bone Cement in Arthroplasty’(Hamid Reza Seyyed Hosseinzadeh, 2013)..... 19
- Figure 1.9 Cement leakage into the Batson’s paravertebral venous system. Reprinted from Case Reports in Surgery, volume 2013, Giorgio Lo Iacono,1 Chiara Lo Nigro,1 Fabio Cannizzaro,1 Massimo Cajozzo,1 and Giuseppe Modica1, Asymptomatic Bone Cement Pulmonary Embolism after Vertebroplasty: Case Report ad Literature Review. Page 2. This article is licenced under a Creative Commons Attribution Non-commercial licence 3.0 licence25
- Figure 1.10 SEM images of MCPM particles. Retrieved from Kangwankai et al. (2017), licensed under CC BY 4.027
- Figure 1.11 SEM images of PLS particles. Retrieved from Kangwankai et al. (2017), licensed under CC BY 4.030
- Figure 1.12 SEM images of glass filler particles, 7µm and 0.7µm. Retrieved from Kangwankai et al. (2017), licensed under CC BY 4.031
- Figure 1.13 Chemical structure of Bis-MA.....32
- Figure 1.14 Chemical structure of TEGDMA32
- Figure 1.15 Chemical structure of UDMA.....32
- Figure 1.16 Chemical structure of PPGDMA.....33
- Figure 1.17 Chemical structure of 4-META34
- Figure 1.18 Chemical structure of HEMA34
- Figure 1.19 Chemical structure of BP.....35
- Figure 1.20 Chemical structure of NTG-GMA35
- Figure 2.1 Illustrating the incorporation of monomers (liquid) within fillers (powder).46
- Figure 2.2 Preparation of experimental bone composite A=The monomer phase with magnetic mixer, B= Double barrel syringe with activator and initiator, C=Double barrel syringe dispensing gun, D= 10mm mould with experimental bone composite disc.47

- Figure 2.3 Schematic of Michelson Interferometer, representing the light source splitting between the moving and fixed mirror, reaching the detector with a different path depending on the position of the moving mirror.....50
- Figure 2.4 FTIR spectra of a curing experimental bone composite consisting of 3.5 % BP and 2.1 % NTGGMA (Levels of initiator and activator after mixing in monomer phase) at 20 °C. Inset shows change in absorbance used to determine cure profile. The 1320 cm⁻¹ peak is used to measure peak height corresponding to C-O bond in the polymerising methacrylate group. Peaks corresponding to methacrylate groups are changing-implying one reaction (polymerisation) is occurring.52
- Figure 2.5 Time line presentation of CAM model66
- Figure 3.1 Monomer conversion (%) versus time (seconds) over 1 hour from mixing with increasing levels of BP (indicated on graph) in the initiator paste. Activator NTGGMA levels are 3/5 of BP wt%.....76
- Figure 3.2 Monomer conversion (%) versus time (seconds) over 10 minutes with increasing levels of BP (indicated on graph). Activator NTGGMA levels are 3/5 of BP wt%.....77
- Figure 3.3 Final Monomer conversion values at 1 hour compared with final conversion values determined by extrapolation to infinite time. (Error bars = 95 % CI, n=3).78
- Figure 3.4 Final Monomer conversion values at 10 minutes compared with final values determined by extrapolation to infinite time. (Error bars = 95 % CI, n=3).79
- Figure 3.5 Linear regression analysis of half-life and inhibition time versus inverse concentration of BP and NTGGMA of the two batches. Data fits for high concentration, however there is significant curvature if there is low concentration.....81
- Figure 3.6 Rate of reaction (s⁻¹) of varying BP levels before mixing in composite paste from 1.5 to 3.5 wt %. BP. NTGGMA was kept at a consistent ratio of 5:3.82

- Figure 3.7 Monomer conversion of composite formulations with 2.5 % BP and 1.5 % NTGGMA compared with the commercial bone composite Simplex™ P (PMMA) and Cortoss® . PMMA data was collected by Dr. Piyapong Panpisut.83
- Figure 3.8 Percentage of monomer reacted vs inverse time (s^{-1}), for the formulation with 2.5 BP and 1.5 NTGGMA in initiator and activator paste respectively (%), Cortoss® and Simplex™ P (PMMA).84
- Figure 3.9 Inhibition time for 2.5 % BP and 1.5 % NTGGMA formulation, Cortoss® and Simplex™ P (PMMA) (Error bars = 95 % CI, n=3).86
- Figure 3.10 Rate of reaction (s^{-1}) of 2.5 % BP and 1.5 % NTGGMA formulation, Cortoss® and PMMA (n=3)87
- Figure 3.11 Heat rise of experimental composite (volume of composite ~44.7 cc. (2.5 % BP and 1.5 % NTGGMA) and Simplex™ P (PMMA) (volume of PMMA ~45.3 cc). Arrows indicate the time point at which the experimental composite and PMMA were added to the DSC chamber..88
- Figure 4.1 Mass change plotted against the square root of time. Samples have varying levels of MCPM and PLS and were kept in distilled water. (Error bars = 95 % CI n=3). Significant differences found, 8% MCPM 2 % PLS vs 4 % MCPM 4 % PLS (Games-Howell, $p=0.006$)111
- Figure 4.2 Volume change (%) of discs with varying levels of MCPM and PLS in distilled water plotted against square root of time (hrs). (Error bars = 95 % CI n=3). There was no significant differences found between the different formulations ($p>0.05$).112
- Figure 4.3 Factorial analysis of (A) Mass change and (B) Volume change of formulation discs after submersion in distilled water at 37 °C after 1 month with increasing levels of MCPM and PLS. (Error bars = 95 % CI n=6).....114

- Figure 4.4 pH of deionised water in which discs with varying levels of MCPM and PLS were placed for a period of 12 weeks. (Error bars = 95 % CI n=6). Significant differences found: 8%MCPM 5%PLS vs. 4% MCPM 5%PLS (Games-Howell, $p=0.001$), 8% MCPM 5% PLS vs. 4% MCPM 2% PLS (Games-Howell, $p=0.001$), 8% MCPM 2 %PLS vs. 4% MCPM 5% PLS (Games-Howell, $p=0.022$), 8% MCPM 2% PLS vs. 4% MCPM 2% PLS (Games-Howell, $p=0.013$). 115
- Figure 4.5 Factorial analysis for pH of deionised water in which discs were submerged in after 12 weeks. (Error bars = 95 % CI n=6). 116
- Figure 4.6 Hydrogen ion concentration of deionised water in which discs with varying levels of MCPM and PLS were placed in for 12 weeks versus square root of time (hrs). (Error bars = 95 % CI n=6). 117
- Figure 4.7 BFS of composite formulation with varying levels of MCPM wt % and PLS wt % at different time points; 24 hours to 3 months. (Error bars = 95 % CI n=6). At 0 hours, the significant differences found were: 8% MCPM 5% PLS vs. 4% MCPM 2% PLS ($p=0.022$), 8% MCPM 5% PLS vs. 8% MCPM 2% PLS ($p=0.001$), 8% MCPM 2% PLS vs. 4% MCPM 5% PLS ($p=0.041$). At 24 hours, the significant differences found were: 8% MCPM 5% PLS vs. 4% MCPM 5% PLS ($p=0.025$), 8% MCPM 5% PLS vs. 4% MCPM 2% PLS ($p=0.006$). At 7 days the significant differences found were: 8% MCPM 5% PLS vs. 4% MCPM 2% PLS ($p=0.001$), 4% MCPM 5% PLS vs. 4% MCPM 2% PLS ($p=0.011$), 8% MCPM 2% PLS vs. 4% MCPM 2% PLS ($p=0.014$). At 1 month, the significant differences found were: 8% MCPM 5% PLS vs. 4% MCPM 5% PLS ($p=0.037$), 8% MCPM 5% PLS vs. 8% MCPM 2% PLS ($p=0.006$), 8% MCPM 5% PLS vs 4% MCPM 2% PLS ($p<0.001$). At 3 months, the significant differences found were: 8% MCPM 5% PLS vs 4% MCPM 5% PLS ($p=0.05$), 8% MCPM 2% PLS vs. 4% MCPM 5% PLS ($p=0.05$), 8% MCPM 5% PLS vs. 8% MCPM 2% PLS ($p<0.001$), 8% MCPM 5% PLS vs. 4% MCPM 2% PLS ($p<0.014$). 119

- Figure 4.8 Factorial analysis for ultimate strength of discs (MPa) with varying levels of MCPM and PLS for each time point (Error bars = 95 % CI n=6) 120
- Figure 4.9 Youngs Modulus of composite formulations with varying levels of MCPM wt. % and PLS wt. % at different time points; 24 hours to 3 months. (Error bars = 95 % CI n=6). At 24 hours, the significant differences were found: 8% MCPM 5% PLS vs. 4% MCPM 5% PLS (p=0.009), 8% MCPM 5% PLS vs. 4% MCPM 2% PLS (p=0.005), 8% MCPM 5% PLS vs. 8% MCPM 2% PLS (p=0.010). At 7 days, the significant differences found were: 8% MCPM 5% PLS vs. 4% MCPM 2% PLS (p=0.001), 8% MCPM 2% PLS vs. 4% MCPM 2% PLS (p=0.020). At 1 month, the significant differences found were: 4% MCPM 5% PLS vs. 4% MCPM 2% PLS (p=0.018), 8% MCPM 2% PLS vs. 4% MCPM 2% PLS (p=0.027), 8% MCPM 5% PLS vs. 4% MCPM 2% PLS (p<0.001). At 3 months, the significant differences found were: 8% MCPM 5% PLS vs. 4% MCPM 5% PLS (p=0.030), 8% MCPM 5% PLS vs. 4% MCPM 2% PLS (p=0.020), 8% MCPM 5% PLS vs. 8% MCPM 2% PLS (p=0.011). 122
- Figure 4.10 Factorial analysis of mean Youngs Modulus (GPa) with varying levels of MCPM and PLS for each time point. (Error bars = 95 % CI n=6). 123
- Figure 4.11 Representation of surface discs at low magnification at time 0, prior to immersing discs in SBF..... 124
- Figure 4.12 High magnification SEM images of specimen's surfaces of each formulation after 24 hours of incubation in SBF at magnification (A) 4 % MCPM 2 % PLS, (B) 4 % MCPM 5 % PLS, (C) 8 % MCPM 2 % PLS and (D)8 % MCPM 5 % PLS. 125
- Figure 4.13 Low magnification SEM images of specimen's surfaces of each formulation after 7 days of incubation in SBF (A)4 % MCPM 2 % PLS, (B) 4 % MCPM 5 % PLS, (C) 8 % MCPM 2 % PLS and (D)8 % MCPM 5 % PLS. 126

- Figure 4.14 High magnification SEM images of specimen's surfaces of each formulation after 7 days of incubation in SBF at magnification (A)4% MCPM 2% PLS, (B) 4 % MCPM 5 % PLS, (C)8 % MCPM2 % PLS and (D) 8% MCPM 5% PLS. 127
- Figure 4.15 High magnification SEM images of specimen's surfaces of each formulation after 1 month of incubation in SBF (A)4% MCPM 2 % PLS, (B) 4 % MCPM 5 % PLS, (C) 8% MCPM 2 % PLS and (D)8 % MCPM 5 % PLS. 128
- Figure 5.1 SEM images of disc surface of formulation disc with MCPM and PLS (A) 8% MCPM 5% PLS, edge of disc. (B) 8% MCPM 2 % PLS and (C) 4% MCPM 5% PLS. random location near centre of discs. (D) PMMA after 24 hours of seeding bone marrow derived sheep MSCs.. 148
- Figure 5.2 SEM images of cells on disc surfaces, formulation 8% MCPM and 2 % PLS; increasing magnification from low to high (A-C) after 24 hours of seeding bone marrow derived sheep MSCs..... 149
- Figure 5.3 SEM images of cell surfaces on disc surfaces, formulation 4% MCPM and 5% PLS; increasing magnification from low to high (A-C) after 24 hours of seeding bone marrow derived sheep MSCs..... 150
- Figure 5.4 SEM images of disc surfaces after 3 days of seeding bone marrow derived sheep MSCs experimental composite (A) 4% MCPM 2% PLS and commercial (B) PMMA..... 151
- Figure 5.5 Confocal microscopy images of experimental bone composite with 4% MCPM and 5% PLS. Blue is the Hoechst staining (cell nucleus) and green staining is phalloidin (cell's actin). (A) Edge of disc, (B-C) Areas near the centre of disc (D) Near centre of PMMA disc after 24 hours of seeding bone marrow derived sheep MSCs..... 152
- Figure 5.6 Metabolic activity of bone marrow derived sheep MSCs assessed via Alamar blue. Fluorescence following exposure to disc extracts from formulations and a commercial cement after 24 hours and 7 days (including the first 24 hours). (Error bars = 95 % CI n=6). Bonferroni, (P<0.05)..... 154

- Figure 5.7 Factorial analysis for metabolic activity of bone marrow derived sheep MSCs exposed to disc extract of varying levels of MCPM and PLS after 24 hours and 7 day incubation. (Error bars = 95 % CI n=6).
..... 155
- Figure 5.8 Disc extract solutions after 24 hours sample storage at 37 °C.
..... 155
- Figure 5.9 Fluorescence intensity versus bone marrow derived sheep MSCs exposure to increasing concentration of PLS (3200 mM to 0.32 mM) after 24 hours. Metabolic activity was assessed used Alamar blue. Control was cells exposed to cell culture media. (Error bars = 95 % CI n=3). Brackets indicate significant differences among groups, Bonferroni, (P<0.05). 157
- Figure 5.10 Visual indication of DMEM colour change due to the different amounts of PLS concentration in a 96 well plate in replicates of 3. PLS concentrations decreasing from wells 1 to 7. 158
- Figure 5.11 Metabolic activity of MG63 cells assessed after 24 hour exposure to disc extracts of experimental bone composite with varying levels of MCPM and PLS (Error bars = 95 % CI n=9). Bonferroni (P<0.05). 159
- Figure 5.12 Factorial analysis of MG63 cells exposed to disc extract of varying MCPM and PLS formulation after 24 hour (Error bars = 95 % CI n=3)..... 160
- Figure 5.13 Metabolic activity of MG63 cells after 24 hour incubation with disc extracts of varying formulations for 24 hours and 7 days. Metabolic activity was assessed using Alamar blue and absorbance was measured. (Error bars = 95 % CI n=9). 161
- Figure 5.14 Factorial analysis of MG63 cells exposed to disc extract of varying MCPM and PLS formulation after 24 hour incubation and) after 7 days incubation. (Error bars = 95 % CI n=3). 162

- Figure 5.15 Metabolic activity of MG63 cells against decreasing concentrations of HCl, PLS and MCPM after 24 hour incubation. Metabolic activity was assessed using Alamar blue. Fluorescence was measured (a.u.) (Error bars = 95 % CI n=3). Kruskal-Wallis $P < 0.05$, Bonferroni ($P < 0.05$)..... 164
- Figure 6.1 (A) Low speed hand piece used to cut the discs in quarters. (B) Discs before and after cutting..... 184
- Figure 6.2 Whole disc of the experimental bone composite(0 wt % MCPM and 0 wt% PLS) photographed in ovo 7 days after CAM-grafting 185
- Figure 6.3 Discs cut in quarters of experimental bone composite (0 wt% MCPM and 0 wt% PLS) photographed in-ovo at ED 7 after CAM-grafting. 186
- Figure 6.4 Macroscopic timeline from day 7 to 14 days of in-ovo features with disc implants (diameter 8mm) of the experimental bone composite with different formulations; 2 % PLS, 10 % PLS, 4 % MCPM and 16 % MCPM. (n=5)..... 188
- Figure 6.5 Disc implants of the experimental bone composite at ED 11 on the CAM. 189
- Figure 6.6 Disc implants (diameter 8mm) of the experimental bone composite with different formulations harvested 7 days after CAM-grafting; 0% PLS and MCPM, 2 % PLS, 10 % PLS, 4 % MCPM and 16 % MCPM. (A) Side placed on the CAM, (B) Upper side. (n=5) 190
- Figure 6.7 Microscope and binary images for disc implants (diameter 8mm) of the experimental bone composite with different formulations harvested 7 days after CAM-grafting; 0% PLS and MCPM, 2 % PLS, 10 % PLS, 4 % MCPM and 16 % MCPM. (n=3). See appendix for all images per group. 191

- Figure 6.8 Vascular density (%) of disc implants of the experimental bone composite with different formulations harvested 7 days after CAM-grafting; 0% PLS and MCPM, 2 % PLS, 10 % PLS, 4 % MCPM and 16 % MCPM. Formatted to binary using image J. (n=3). No differences were found, ANOVA to test differences in Vascular Density means, p=0.194. 192
- Figure 6.9 Junction points and branching vessel count on disc implants of the experimental bone composite with different formulations harvested 7 days after CAM-grafting; 0% PLS and MCPM, 2 % PLS, 10 % PLS, 4 % MCPM and 16 % MCPM.. (n=3). No differences were found, ANOVA to test differences in Branching means, p=0.639. ANOVA to test differences in Junction mean, p=0.754..... 192
- Figure 6.10 Graph representing the chick embryo's that survived out of 25 chicks at day 14 in different groups exposed to disc implants of experimental bone composite with different amounts of MCPM and PLS (wt. %). (n=5)..... 193
- Figure 6.11 SEM images of tissue on adhering to the experimental bone composite surface on the CAM sides 7 days after CAM grafting.(A) Disc surface with 0 % MCPM and PLS. Arrows pointing at tight junctions and red blood cells. (B) Disc surface with 2 % PLS. Arrows pointing at particles are the cell layer. (C) Disc surface with 10 % PLS. Arrows pointing at red blood cells and flat unidentified cells. (D) Disc surface with 4 % MCPM *Suspected macrophage. (D) Disc surface with 16 % MCPM. (n=5)..... 195
- Figure 6.12 High magnification SEM image of precipitate on fixed tissue in contact with experimental bone composite disc with 16 % MCPM. ... 196
- Figure 6.13 Antibody staining for epithelial cells (green), fibroblasts (red) and cell nucleus (blue) on experimental bone composite disc (0 wt% MCPM and PLS) in contact with the CAM (N=3)..... 197
- Figure 6.14 Images of disc implants (diameter 8mm) of the experimental bone composite with 5 % PLS and 8 % MCPM at day 9 and after harvest (n=5)..... 198

- Figure 6.15 Microscope and binary images of disc implants (diameter 8mm) of the experimental bone composite with different formulations harvested 7 days after CAM-grafting; 5 % PLS, 8 % MCPM and 0% PLS and MCPM. (n=3). See appendix for all images per group. 199
- Figure 6.16 Vascular density (%) of disc implants of the experimental bone composite with different formulations harvested 7 days after CAM-grafting; 5 % PLS, 8 % MCPM and 0% PLS and MCPM. Formatted to binary using image J. (n=3). ANOVA to test differences in Vascular Density, $p=0.715$ 199
- Figure 6.17 Junction points and branching vessel count on disc implants of the experimental bone composite with different formulations harvested 7 days after CAM-grafting; 5 % PLS, 8 % MCPM and 0% PLS and MCPM. Formatted to binary using image J. (n=3). ANOVA to test differences in Branching mean, $p=0.763$. ANOVA to test differences in Junction means, $p=0.938$ 200
- Figure 6.18 Graph representing the chick embryo's that survived out of 15 chicks at embryo day 14 in different groups exposed to disc implants of experimental bone composite with different amounts of MCPM and PLS (wt. %). (n=5)..... 201
- Figure 6.19 Images of disc implants (diameter 8mm) cut in quarters with 5 % PLS and 8 % MCPM at day 9 and after harvest (n=5). 202
- Figure 6.20 Graph representing the chick embryo's that survived out of 15 chicks at embryo day 14 in different groups exposed to disc implants in quarters of experimental bone composite with different amounts of MCPM and PLS (wt. %). (n=5). 203
- Figure 6.21 Disc mplants (diameter 8mm) with varying levels of PLS and MCPM (wt %) and PMMA at embryo day 9 and embryo day 14. 204
- Figure 6.22 Microscope and binary images of disc implants (diameter 8mm) of the experimental bone composite with different formulations harvested 7 days after CAM-grafting with varying levels of PLS and MCPM (wt %) and PMMA. (n=3). See appendix for all images per group. 205

- Figure 6.23 Vascular density (%) of disc implants of the experimental bone composite with different formulations harvested 7 days after CAM-grafting varying levels of PLS and MCPM (wt %) and PMMA. Formatted to binary using image J. (n=3). Add in caption nothing as observed for PMMA. (ANOVA p=0.201)206
- Figure 6.24 Junction points and branching vessel count on disc implants of the experimental bone composite with different formulations harvested 7 days after CAM-grafting varying levels of PLS and MCPM (wt %) and PMMA. Formatted to binary using image J. (n=3). Significant difference between 8% MCPM 5% PLS and PMMA (Branching ANOVA p=0.059), (Junction Tukey’s post-hoc p=0.049)207
- Figure 6.25 Graph representing the number of chick embryo’s that survived out of 25 chicks at embryo day 14 in different groups exposed to disc implants of PMMA and experimental bone composite with different amounts of MCPM and PLS (wt. %). (n=5).208
- Figure 8.1 Image of disc implants with 0 % PLS and MCPM of the experimental bone composite harvested 7 days, grey scaled and in binary format via image J (n=3).....238
- Figure 8.2 Image of disc implants with 2% PLS of the experimental bone composite harvested 7 days, grey scaled and in binary format via image J (n=3).....239
- Figure 8.3 Image of disc implants with 10% PLS of the experimental bone composite harvested 7 days, grey scaled and in binary format via image J (n=3).....240
- Figure 8.4 Image of disc implants with 4% MCPM of the experimental bone composite harvested 7 days, grey scaled and in binary format via image J (n=3).....241
- Figure 8.5 Image of disc implants with 16% MCPM of the experimental bone composite harvested 7 days, grey scaled and in binary format via image J (n=3).....242
- Figure 8.6 Image of disc implants with 5% PLS of the experimental bone composite harvested 7 days, grey scaled and in binary format via image J (n=3).....243

- Figure 8.7 Image of disc implants with 8% MCPM of the experimental bone composite harvested 7 days, grey scaled and in binary format via image J (n=3).....244
- Figure 8.8 Image of disc implants with 0 % PLS of the experimental bone composite harvested 7 days, grey scaled and in binary format via image J (n=3).....245
- Figure 8.9 Image of disc implants with 4 % MCPM and 2 % PLS of the experimental bone composite harvested 7 days, grey scaled and in binary format via image J (n=3).....246
- Figure 8.10 Image of disc implants with 4 % MCPM and 5 % PLS of the experimental bone composite harvested 7 days, grey scaled and in binary format via image J (n=3).....247
- Figure 8.11 Image of disc implants with 8% MCPM and 2 % PLS of the experimental bone composite harvested 7 days, grey scaled and in binary format via image J (n=3).....248
- Figure 8.12 Image of disc implants with 8% MCPM and 5 % PLS of the experimental bone composite harvested 7 days, grey scaled and in binary format via image J (n=3).....249
- Figure 8.13 Image of disc implants of PMMA harvested 7 days, grey scaled and in binary format via image J (n=3).....250
-

- **List of Tables**
- Table 1.1 Components of Simplex™ P PMMA; adaptation from Journal of Clinical Orthopaedics and Trauma, volume 4, Abishek et al. Bone cement. 18
- Table 2.1: Description of commercial materials used for this project with component information from manufacturer.....42
- Table 2.2: Monomer details including molecular weight and manufacturer information43
- Table 2.3 Remineralising agent and antibacterial agent with manufacture details.....43
- Table 2.4 Details of two glass fillers used in this project as fillers and information of manufacturer.44
- Table 2.5 Details of initiator, activator used in this project and details from manufacturer.....44
- Table 3.1 : Levels of BP and NTGGMA before mixing in composite monomer phase. Pastes were prepared using: UDMA (7.5 g), PPGDMA (2 g), HEMA (0.25 g). 4-META (0.3 g) was added in the initiator phase only.....75
- Table 3.2 Levels of BP and NTGGMA before mixing in composite monomer phase. Pastes were prepared using: UDMA (7.5 g), PPGDMA (2 g), HEMA (0.25 g). 4-META (0.3 g) was added in the initiator phase only.....75
- Table 3.3 Inhibition time (t_i) and half-life ($t_{0.5}$) of experimental formulation with varying levels of initiator (BP) and activator (NTGGMA). BP and NTGGMA ratio was kept consistent at 5:3. FTIR analysis as performed at room temperature of 24 °C. Formulation contains fixed levels of monomers 70 %, UDMA 20 % PPGDMA. Monomer content was fixed at 25 % (PLR 3:1) (Error bars = 95 % CI, n=3).....80

- Table 3.4 Inhibition time (t_i) and half-life(t_{50}) of experimental formulations with varying levels of initiator (BP) and activator (NTGGMA) further refined. BP and NTGGMA ratio was kept consistent at 5:3. FTIR analysis as performed at room temperature of 24 °C. Formulation contains fixed levels of monomers 70 %, UDMA 20 % PPGDMA. Monomer content was fixed at 25 % (PLR 3:1) (Error bars = 95 % CI, n=3).80
- Table 3.5 Gradients of the half-life time and inhibition time versus inverse BP and NTGGMA wt % with lower concentrations (BP concentrations from 2.5 to 0.5) (Error bars = 95%, CI, n=3).....81
- Table 3.6 Gradients of the half-life time and inhibition time versus inverse BP and NTGGMA wt % (BP concentrations from 3.5 to 1.5) (Error bars = 95%, CI, n=3).81
- Table 3.7 Percentage final conversion for 2.5 % BP and 1.5 % NTGGMA formulation, Cortoss® and PMMA. (Data range employed, shown in Figure 3.8).....84
- Table 3.8 Inhibition time (t_i) and half-life (t_{50}) of 2.5 % BP and 1.5 % NTGGMA formulation, Cortoss and PMMA (Simplex™ P) (n=3)85
- Table 3.9 Comparison of enthalpy between commercial PMMA and Composite88
- Table 4.1 MCPM and PLS percentages added to initiator and activator paste fillers in formulations 1-4. (Monomer phase: UDMA (7.5 g), PPGDMA (2 g), HEMA (0.25 g). 4-META (0.3 g) was added in the initiator phase only. 2.5 % BP and 1.5 % NTGGMA. Glass filler: 7 μ m and 0.7 μ m ratio 4:5. PLR 3:1) 107
- Table 4.2 Gradient and R^2 for hydrogen ion concentration ($H^+ = 10^{-pH}$) versus Sqrt time (hrs)..... 118
- Table 5.1 MCPM and PLS percentages added to initiator and activator paste fillers in formulations 1-4 (Monomer phase: UDMA (7.5 g), PPGDMA (2 g), HEMA (0.25 g). 4-META (0.3 g) was added in the initiator phase only. 2.5 % BP and 1.5 % NTGGMA. Glass filler: 7 μ m and 0.7 μ m ratio 4:5. PLR 3:1). 143

- Table 6.1 MCPM and PLS percentages added to initiator versus activator paste fillers in 5 formulations (Monomer phase: UDMA (7.5 g), PPGDMA (2 g), HEMA (0.25 g). 4-META (0.3 g) was added in the initiator phase only. 2.5 % BP and 1.5 % NTGGMA. Glass filler: 7 μ m and 0.7 μ m ratio 4:5.. PLR 3:1)..... 183
- Table 6.2 Intermediate levels of MCPM and PLS percentages added to initiator versus activator paste fillers in 5 formulations (Monomer phase: UDMA (7.5 g), PPGDMA (2 g), HEMA (0.25 g). 4-META (0.3 g) was added in the initiator phase only. 2.5 % BP and 1.5 % NTGGMA. Glass filler: 7 μ m and 0.7 μ m ratio 4:5.. PLR 3:1)..... 184
- Table 6.3 Combined levels of MCPM and PLS percentages added to initiator versus activator paste fillers in 5 formulations (Monomer phase: UDMA (7.5 g), PPGDMA (2 g), HEMA (0.25 g). 4-META (0.3 g) was added in the initiator phase only. 2.5 % BP and 1.5 % NTGGMA. Glass filler: 7 μ m and 0.7 μ m ratio 4:5.. PLR 3:1)..... 187

List of Equations

$M_c = 100(h_o - h_t)h_o$	Equation 2.1	51
$R_p = dDc/dt$	Equation 2.2	51
$R_i = 2\delta k_d [I][A]$	Equation 2.3	52
$R_p = k_p [M][M_n^*]$	Equation 2.4	53
$R_x = k_x [X][M_n^*]$	Equation 2.5	53
$R_t = 2k_t [M_n^*]^2$	Equation 2.6	53
$-d[M_n^*]/dt = -R_i + R_t + R_x = 0$	Equation 2.7	53
$-d[M_n^*]/dt = -R_i + 2k_t[M_n^*]^2 + k_x X[M_n^*] = 0$	Equation 2.8	54
$-d[X]/dt = k_x X[M_n^*]$	Equation 2.9	54
$-d[X]/dt = k_x X R_i / k_x [X]$	Equation 2.10	54
$[X] = [X_0] - R_i t$	Equation 2.11	54
$t_i = [X_0] R_i = [X_0] 2\delta k_d [I][A]$	Equation 2.12	54
$2\delta k_d [I][A] = 2k_t [M_n^*]$	Equation 2.13	55
$[M_n^*] = \delta k_d [I][A] / k_t$	Equation 2.14	55
$R_p = k_p [M][M_n^*] = k_m [M] \delta k_d [I][A] / k_t$	Equation 2.15	55
$R_{t50} = d[M]/dt = d\xi C_f / dt = 0.5 C_f t_{50} - t_i$	Equation 2.16	55
$t_{50} = 0.5 C_f R_p + t_i = 0.5 C_f 2k_t k_p [M] \delta k_d [I][A] + [X_0] 2\delta k_d [I][A]$	Equation 2.17	55
$\sigma_{max} = P t_{21} + v 0.4851 n a t + 0.52 + 0.48$	Equation 2.18	61
$E = \Delta P \Delta W c x (\beta c a 2 t^3)$	Equation 2.19	62
$\beta c = -0.642 - 0.19 m - 3 + 0.5687 + 3.254 m - 3 x 1 - v^2 + [-0.3973 + 11.0513 m - 3 + 0.5223 - 7.8535 m - 3 1 - v^2] t^3$	Equation 2.20	62
$M = 100(M_t - M_0) M_0$	Equation 4.1	108
$V = 100(V_t - V_0) V_0$	Equation 4.2	108
$p_t = M_t M_t - M_w \times p_w$	Equation 4.3	108
$pH = -\log_{10} [H^+]$	Equation 4.4	108
$H^+ = 10^{-pH} \text{ mol/l}$	Equation 4.5	108
$[H^+]_{\text{release}} = \Sigma([H^+]_s - [H^+]_{dw})$	Equation 4.6	108

Literature Review

1.1 Human Bone

1.1.1 Vertebrae

Bone in the human body can be classified into four general categories. The four general categories of bones are long bones, short bones, flat bones, and irregular bones. The vertebrae are classified as irregular bones (Clarke, 2008). All vertebrae have a common structure, consisting of an anterior vertebral body (the weight-bearing component), and a posterior vertebral arch. The vertebral body is made up of trabecular bone and red bone marrow covered with a thin layer of cortical bone (Whitney & Alastra, 2020) (Figure 1.1). Vertebrae in the lower portion of the column have larger bodies than those in the upper portion (to better support the increased weight) (Figure 1.2).

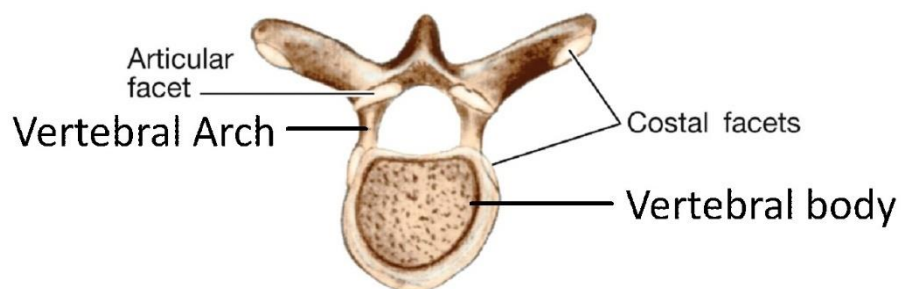


Figure 1.1 Image of vertebra with essential features of thoracic vertebrae. Reprinted from Surgery, volume 36, Mahadevan V. Anatomy of the vertebral column. Page 329, with permission from Elsevier.

Hyaline cartilage lines the superior and inferior aspects of the vertebral body. Each vertebral body is separated by a fibrocartilaginous intervertebral disc (Figure 1.2).

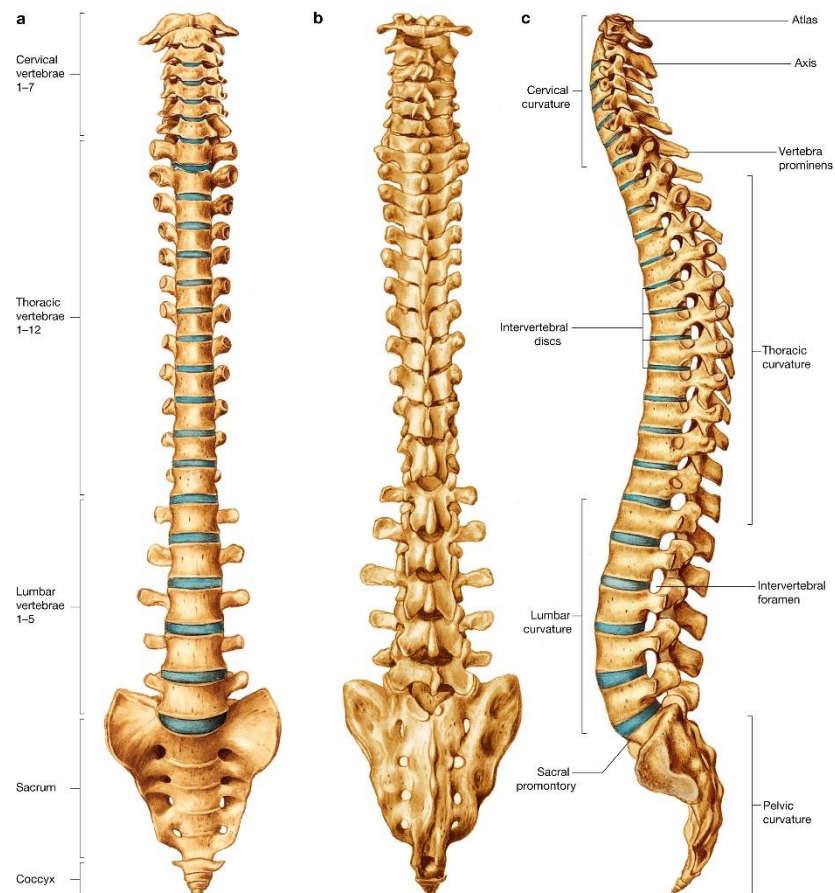


Figure 1.2 The articulated vertebral column in an adult. Reprinted from *Surgery, volume 36, Mahadevan V. Anatomy of the vertebral column. Page 328, with permission from Elsevier.*

1.1.2 Trabecular and cortical

Human bone consists of the trabecular bone and cortical bone. Trabecular bone is spongy while cortical bone is much more dense (Osterhoff et al., 2016). Cortical bone is the solid outer part of the bone with a higher modulus, surrounding the trabecular bone. The bone is an organised hierarchical structure (Figure 1.3), made up of the macrostructure trabecular and cortical bone; (1) the microstructure (from 10 to 500 μm): Haversian systems, osteons, single

trabeculae; (2) the sub-microstructure (1–10 μm): lamellae; (3) the nanostructure (from a few hundred nanometres to 1 μm): fibrillar collagen and embedded mineral; and (4) the sub-nanostructure (below a few hundred nanometres): molecular structure of constituent elements, such as mineral, collagen, and non-collagenous organic proteins (Reznikov, Shahar, & Weiner, 2014). The hard tissue of bone consists of oriented crystals of hydroxyapatite (HA) embedded within the type I collagen fibrils. (Yao et al., 2019).

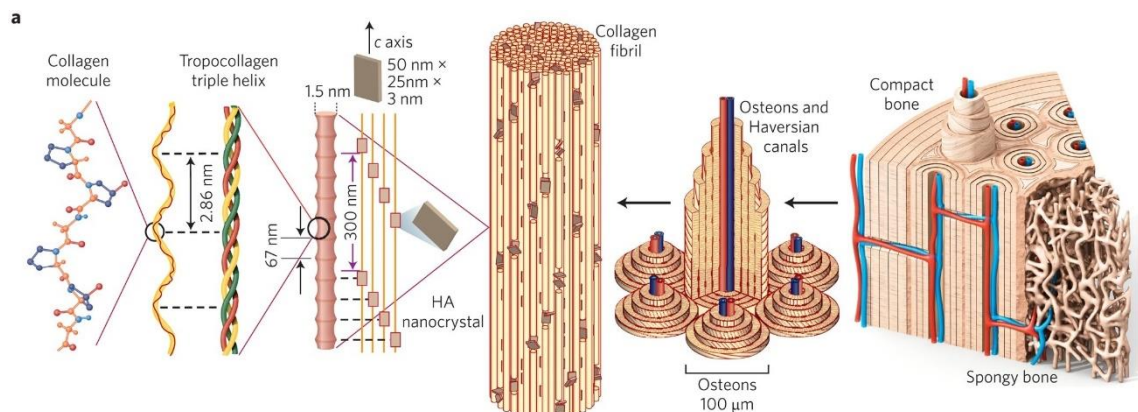


Figure 1.3 In bone, macroscale arrangements involve both compact/cortical bone at the surface and spongy/trabecular bone (foam-like material with $\sim 100\text{-}\mu\text{m}$ -thick struts) in the interior. Reprinted from nature materials, volume 14, Ulrike G.K. Wegst. Bioinspired structural materials. Page 27, with permission from nature materials

The characteristic microstructure and composition of bone is based on the location in the body. The vertebral bodies resist high and repetitive axial compression loads but experience little shear and tension loads (Osterhoff et al., 2016). A mature human skeleton is comprised of 80% cortical bone and 20% trabecular bone. Different bones and skeletal sites consist of different ratios of cortical to trabecular bone. Analysing the specific case of vertebrae, they are composed of cortical to trabecular bone in a ratio of 25:75 (Choksi, Jepsen, & Clines, 2018).

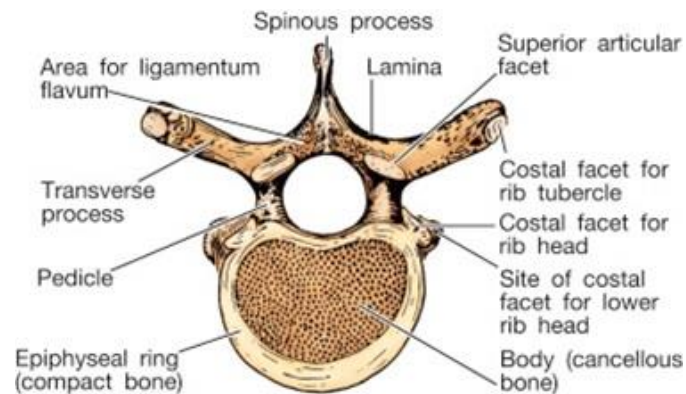


Figure 1.4 Typical thoracic vertebra. Reprinted from Surgery, volume 36, Mahadevan V. Anatomy of the vertebral column. Page 329, with permission from Elsevier.

Cortical bone is dense and solid surrounding the marrow space, whereas trabecular bone is composed of a honeycomb-like network of trabecular plates and rods interspersed in the bone marrow compartment. Since the axial compression load is applied across the centre of the spine, the spongy trabecular bone's alignment allows it to bear most of the load. Both cortical and trabecular bone are composed of osteons (Choksi et al., 2018). In compact bone osteons are tightly packed and they are also known as haversian systems (Härle & Boudrieau, 2012). They provide strength to the bone while also facilitating the transport of blood (Maggiano et al., 2016).

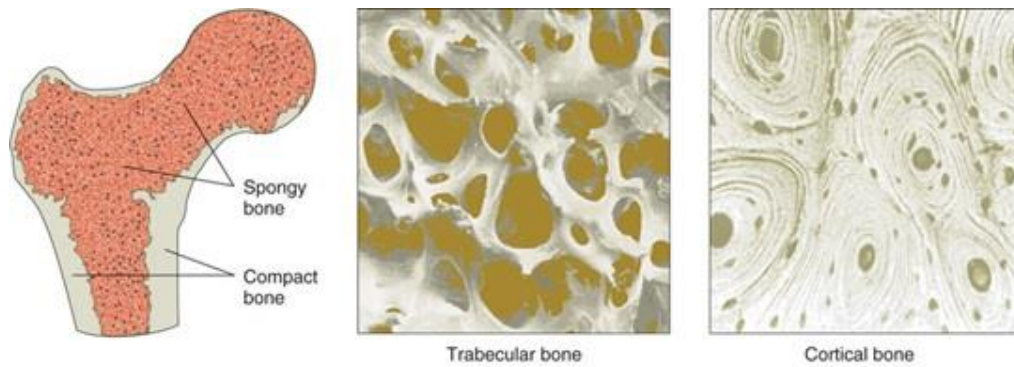


Figure 1.5 The two basic tissue types of bones are trabecular and cortical. Trabecular (spongy) and cortical (compact) bone tissue differ in their microarchitecture porosity. Reprinted from An introduction to Nutrition, section 9.1. Bone Structure and Function. This book is licenced under a Creative Commons Attribution Non-commercial licence 3.0 licence.

Bone maintains its strength and mineral homeostasis via bone remodelling. In response to mechanical forces, bone density may change due to removal or addition of bone by osteoblasts and osteoclasts, via resorption of old bone and formation of new bone (X. Feng & McDonald, 2011). This process, known as remodelling consists of constant removal of old bone with newly synthesised matrix and mineralisation of the matrix to establish new bone. During bone remodelling, mineralised bone is removed via osteoclasts, a process referred to as resorption. Next stage is known as reversal where mononuclear cells (blood cells) appear at the bone surface, followed by osteoblasts that form new bone matrix which later mineralises (Gutiérrez-Prieto, Perdomo-Lara, Diaz-Peraza, & Sequeda-Castañeda, 2019). Bone remodelling allows the bone to repair microdamage and to maintain skeletal integrity. Bone re-modelling decelerates with age, particularly in postmenopausal women and is thought to increase mildly in aging men (Clarke, 2008). As a result bone density decreases and the skeletal system is susceptible to fractures (Tu et al., 2018).

1.1.3 Mineralisation in bone

Mineralisation of bone involves the deposition of hydroxyapatite (HA) between collagen fibres within the bone. The long cylindrical structures within the compact bone (osteons) contribute to the mineralisation density via the bloody supply (Härle & Boudrieau, 2012). Blood supply to the bone contains minerals including calcium, phosphorous and water which forms calcium hydroxide and phosphoric acid. Both these components react and form hydroxyapatite. Slight increases in mineralisation results in large increase in strength of bone, however levels more than 60% have been shown to reduce bone strength (Wegst, Bai, Saiz, Tomsia, & Ritchie, 2015).

During the mineralisation of the bone matrix, osteoblasts deposit unmineralised organic tissue known as osteoids which later calcify. Osteoids are the unmineralised, organic portion of the bone matrix which forms before bone tissue matures. Type I collagen is the main component of the extracellular matrix of bone where HA is deposited. Crystals are formed between the type I collagen fibrils and have also been found to exist both within the external fibrils. The collagen matrix directs the interfibrillar mineralisation of collagen, resulting in nanostructured architecture with HA aligned parallel to the collagen fibril axis (Abou Neel et al., 2016).

1.2 Osteoporotic Fractures

5 million osteoporotic fractures occur approximately in the EU and USA every year (Hernlund et al., 2013). Fractures are prone due to osteoporosis, a condition in which bone mineral density is much lower in comparison to normal bone,

causing the bone to become more fragile. This results in higher risk of osteoporotic fractures (Tu et al., 2018).

1.2.1 Aetiology

The most common osteoporotic fractures are vertebral fractures, which may occur due to a minor accident or due to bending, lifting or turning (Pawel Szulc, 2011).

The prevalence of vertebral fractures rises drastically with age (Warriner et al., 2011), 10, 20, 40 and 66 % of 60, 70, 80 and 90 year old women respectively have osteoporosis with an increased risk of fragility fractures (Borgström et al., 2020). Regarding clinical symptoms of vertebral fractures, these can be back pain, loss of height and disability and limitation of spine mobility (C. C. Wong & McGirt, 2013). As a result, patients may experience difficulty in bending, rising, dressing, climbing stairs, as well as reduced pace of walking. Deterioration of quality of life is more pronounced in patients with several vertebral fractures (Yoon et al., 2014). Patients with fractures in lower thoracic and lumbar spine suffer from back pain, disability as well as struggling in performing daily activities. Figure 1.6 is an example of a vertebral fracture. Fractures in the mid-thoracic spine can result in mild reduction of pulmonary function (Baroud, Vant, & Wilcox, 2006). Clinical symptoms of vertebral fractures are often confused with osteoarthritis and other causes of back pain.

Radiological modalities are used to confirm the location of an osteoporotic fracture, how many vertebrae are damaged, vertebral height and if there is presence of concurrent spinal deformity. In addition, they allow evaluation of the area around the fracture. Often osteoporotic fractures are characterised by the semi-quantitative grading method of Genant (Genant et al., 1996). Severity is based on the extent of deformity (mild, moderate or severe) (Prost, Pesenti, Fuentes, Tropiano, & Blondel, 2020). Deterioration of quality of life is more pronounced in patients with several vertebral fractures (Yoon et al., 2014). Patients with fractures in lower thoracic and lumbar spine suffer from back pain, disability as well as struggling in performing daily activities. Figure 1.6 is an example of a vertebral fracture. Fractures in the mid-thoracic spine can result in mild reduction of pulmonary function (Baroud, Vant, & Wilcox, 2006). Clinical symptoms of vertebral fractures are often confused with osteoarthritis and other causes of back pain. Radiological modalities are used to confirm the location of an osteoporotic fracture, how many vertebrae are damaged, vertebral height and if there is presence of concurrent spinal deformity. In addition, they allow evaluation of the area around the fracture. Often osteoporotic fractures are characterised by the semi-quantitative grading method of Genant (Genant et al., 1996). Severity is based on the extent of deformity (mild, moderate or severe) (Prost, Pesenti, Fuentes, Tropiano, & Blondel, 2020).



Figure 1.6 MRI showing L2 and L3 compression fracture with no epidural bleed. Reprinted from The Archives of Bone and Joint Surgery, volume 3, T.R Ravi Kumar. An unusual case of a large hematorrachis associated with multi-level Osteoporotic Vertebral Compression Fractures; a Case Report. Page 135. This article is licenced under a Creative Commons Attribution Non-commercial licence 3.0 licence.

1.2.2 Epidemiology

Age-adjusted mortality rate increases with the number of vertebral fractures (Pawel Szulc, 2011). Fractures which are most likely because of osteoporosis have been found to be the femoral neck, pathologic fractures of the vertebrae, and lumbar and thoracic vertebral fractures (Warriner et al., 2011). Compression fractures of the vertebrae are difficult to diagnose because they are often asymptomatic (Rosen, 2000). Osteoporosis is less common in men than women due to hormonal differences. Unlike men, women experience a sudden drop in oestrogen during menopause and this can be accompanied by rapid bone loss (Ji & Yu, 2015).

However, in the past few years, the problem of osteoporosis in men has been recognised as an important public health issue. According to the US National Osteoporosis Foundation “men older than 70 will double by 2050” (Iqbal, 2000). Consequently, societal burden of osteoporosis in older men continues to rise, increasing the risk of osteoporotic fractures (Pawel Szulc, 2011).

The cost of osteoporotic fractures is increasing rapidly. Every year in the USA, 3.5 million hospital bed days are attributed to osteoporotic fractures and trends are similar in Europe, where the estimated cost of osteoporotic fractures was 36 billion euro in 2000. This is expected to double to 77 billion euro by 2050 (Borgström et al., 2020; Johnell & Kanis, 2005; Kanis et al., 2004).

Osteoporosis has become a serious public health concern due to an increase in aging population (InstituteOfBoneHealth, 2015). Often it is undertreated and diagnosed only after weakened bones have led to a fracture. Awareness of the disease has led to improved early diagnosis, although osteoporosis is still often detected after a fracture.

Osteoporotic fractures causes increased morbidity, mortality and costs thus it is a major health problem worldwide. Financially the condition is becoming a burden due to direct costs (hospital acute care, in-hospital rehabilitation, outpatient services, long term nursing care) and indirect costs (morbidity, loss of working days) (Pawel Szulc, 2011).

1.3 Current Treatment

Depending on the type of fracture and the patient's symptoms, history and expectations, the treatment is decided. Often conservative treatment involves bed rest with a back brace (3 months), patient-specific analgesia and medication to treat osteoporosis (Prost et al., 2020). Minimal; invasive surgical treatment involves pedicle cannulation with cement in the vertebral body. Pedicle cannulation involves, site of treatment to be anaesthetised then a small screw is inserted to support and aid in fixing the fracture site. The analgesic effect is quick, the vertebral body is stabilised once the cement is polymerised, resulting in immediate mobilisation without the support of a back brace (Prost et al., 2020). Traditional surgery is occasionally considered in managing osteoporotic fractures,

particularly in situations of neurological deficits where nerve decompression is needed (Santolini, Kanakaris, & Giannoudis, 2020).

1.3.1 Vertebroplasty and Kyphoplasty

Vertebroplasty refers to injection of bone cement into the fractured vertebral body. Vertebroplasty can be performed without the use of general anaesthetics in most patients (Cagli, Isik, & Zileli, 2010). For this reason, vertebroplasty is particularly useful in patients with risk factors for general anaesthesia. General anaesthesia is required only in patients unable to co-operate due to pain.

When the vertebral body is collapsed, either kyphoplasty or vertebroplasty is considered as one of the initial interventions (Denaro, Longo, Maffulli, & Denaro, 2009). Both vertebroplasty and kyphoplasty have been shown to prevent prolonged immobilisation, reduce pain within hours after the procedure, as well as improving physical mobility and quality of life (Pawel Szulc, 2011). Patients treated with either procedure have a high incidence of a succeeding vertebral fracture (Tseng, Yang, Tu, Lo, & Yang, 2009). Subsequent fractures occurring 30 to 60 days after treatment in the vertebrae adjacent to the initial fracture are of particular concern (Fribourg, Tang, Sra, Delamarter, & Bae, 2004).

In kyphoplasty, a void is created in the vertebral body by inflating a balloon, which is followed by the injection of cement. Kyphoplasty is a technique that is pursued on a patient under general anaesthetics. An X-ray method (fluoroscopy) is used

to enable the surgeon to see what is happening during the procedure (Boszczyk et al., 2006). Complications reported with kyphoplasty include cement extravasation as well as rib fractures, which in one study occurred in 2 of 30 patients (Denaro et al., 2009). Vertebroplasty and kyphoplasty in most patients improve quality of life because of pain relief, marked reduction of the amount of analgesics needed for pain control, and improvement in physical mobility (Denaro et al., 2009).

However based on clinical tests, due to the numerous risks current bone cements still pose, there is a need for superior bone composites.

1.4 Bone Cements

Bone cements are biomaterials designed to mimic and replace fractured areas as filling material, playing a vital part in the success of a vertebral or kyphoplasty procedure. The most common form of bone cement, known as PMMA comes in two phases composed of a liquid and solid powder phase. They chemically cure upon mixing and result in setting in to a solid phase eventually. Setting times vary between different bone cements, depending on different formulations. Injectable bone cements are administered at the fracture site in a paste form. It is essential the filling material have significant mechanical strength and are sustainable long term.

Bone cements are commonly categorised as acrylic bone cements, composites or calcium phosphate bone cements. Other combinations of bone composite cements have also been developed.

Poly(methyl methacrylate) (PMMA) is the most commonly used cement. Whilst originally developed for dental treatment. It is now used mostly for orthopaedic applications.

A composite is generally defined as a material that has physically distinct phases that differ in either material or form like concrete or carbon fibre composites. Bone cements can either remain within the body for many years (non-degradable) or be broken down by biological processes and replaced by new bone growth (degradable) (Kirsty Alexandra Iskrzycka Main, 2013).

Osseointegration is one of the desired outcomes after the bone cement is administered to the fractured site. This is where a direct interface between the bone cement and bone will form. An inert biomaterial that is not chemically or biologically bound at the interface can result in development of a non-adherent fibrous capsule between the tissue and the biomaterial (Chu et al., 2020). Thus different types of bone cements have been developed to encourage healing at the fractured site.

1.4.1 Different types of injectable bone cements

1.4.1.2 Calcium Phosphate Cements

Calcium phosphate cements consist of calcium and phosphate ions, making their composition similar to natural bone (Yousefi, 2019).

Types of calcium phosphates that are used in calcium phosphate cements include: Calcium phosphates phosphate compounds include; Monocalcium

phosphate (MCPM), monocalcium phosphate anhydrous (MCPA), Dicalcium phosphate anhydrate (DCPD), Dicalcium phosphate anhydrous (DCPA), Octacalcium phosphate (OCP), α -Tricalcium phosphate (α -TCP), β -Tricalcium phosphate (β -TCP), Hydroxyapatite (OHAP or simply HAP), Fluorapatite (FAP), Carbonated hydroxyapatite (dahllite), Tetracalcium phosphate (TTCP) (Wagh, 2016).

Many formulation combinations for calcium phosphate cements have been developed. Their end product is either HA or brushite (dicalcium phosphate dihydrate, DCPD) depending on the pH of the cement's environment. HA is the desired end product for injectable bone cements since it is also a naturally occurring mineral within bone (Anil, Venkatesan, Shim, Chalisserry, & Kim, 2017).

Calcium phosphate cements can be further categorised by the components in the solid-phase, their type of setting reaction (hydrolysis or acid-base reaction), their setting mechanisms and the type of end product. In comparison to acrylic bone cements that are used for high and medium load bearing applications, calcium phosphate cements are used for medium and low load-bearing applications (Yousefi, 2019). Calcium phosphate cements are an attractive alternative to acrylic bone cements due to their bioactivity, and ease in injecting during minimally invasive surgeries like percutaneous vertebroplasty and kyphoplasty (Şahin, 2018).

Calcium phosphates have been developed with other combined elements such as strontium and magnesium to enhance their biocompatible properties. These type of cements are also often referred to as hybrid cements (Wu et al., 2021).

1.4.1.3 Strontium-Substituted Calcium Phosphates

The intention of incorporating strontium in calcium phosphate cements, is to prevent bone loss and promote bone regeneration (Querido et al., 2014). The release of strontium ions stimulates bone formation as well as osseointegration.

Strontium (Sr) is believed to play a major role in the treatment of osteoporosis and enhancement of bone remineralisation as it is associated with a reduction of bone resorption *in-vivo*. Thus, several strontium containing materials have been extensively used as bone fillers (Luo et al., 2015). A study carried out in rats with a critical-size defect in the femur of rats with strontium calcium phosphates showed a significant increase in bone formation in comparison to rats who received just calcium phosphate cement (Thormann et al., 2013).

1.4.1.4 Magnesium Phosphate Cement (MPC)

Magnesium phosphate cements are biodegradable bone cements. The release of magnesium ions can encourage osteoblast activity thus functioning as a bioactive bone cement. However the setting time is very short (3 minutes) limiting their use (He et al., 2015).

1.4.1.5 Incorporation of Bioactive Additives and Cells

Incorporation of bioactive, osteogenic additives and cells increases the osteoconductivity of bone cements. Osteoconductive material enables new bone growth around the material encouraging integration with existing bone (H. H. K. Xu et al., 2017). Calcium phosphates cements are ideal carrier systems for growth factors due to their porosity and large surface area. To improve osteogenic and angiogenic ability of the calcium phosphate cements, growth factors such as bone morphogenetic proteins, basic fibroblasts growth factor and vascular endothelial growth factor have been added (He et al., 2015).

1.4.1.6 PMMA

PMMA was introduced in the use of a total hip replacement (THR) by Charnley in 1970, who used it to secure fixation of the acetabular and femoral components and to transfer loads to bone (Vaishya, Chauhan, & Vaish, 2013; Webb & Spencer, 2007). Simplex™ P is the commercial name for PMMA produced by Stryker® (2013 - 2021 Stryker Australia Pty Ltd).

PMMA is now widely used for implant fixation in various orthopaedic and trauma surgery and used to stabilise osteoporotic vertebral fractures.

PMMA is an acrylic polymer that is formed by mixing (Table 1.1); a liquid methyl methacrylate (MMA) (Figure 1.7) monomer and a powdered MMA-styrene copolymer. Upon mixing, the liquid monomer polymerises around the pre polymerised powder particles to form hardened PMMA. In the process, heat is generated, due to an exothermic reaction (Vaishya et al., 2013).

Table 1.1 Components of Simplex™ P PMMA; adaptation from *Journal of Clinical Orthopaedics and Trauma*, volume 4, Abishek et al. Bone cement.

Powder		Liquid	
Polymer	Polymethyl methacrylate/copolymer (PMMA)	Monomer	Methyl methacrylate (MMA)
Initiator	Benzoyl peroxide (BP)	Accelerator	N, N-Dimethyl para-toluidine (DMPT)
Radio-pacifer	Barium sulphate (BaSO ₄)/Zirconia (ZrO ₂)	Stabilizer	Hydroquinone
Antibiotics	e.g. Gentamycin	-	-

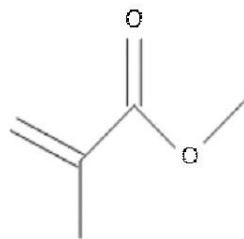


Figure 1.7 Chemical structure of MMA

The polymer PMMA is produced as a result of MMA polymerising. N, N-dimethyl-para-toluidine (DMPT) speeds up the polymerisation by acting as an accelerator to assist in setting the cement. MMA can spontaneously polymerise during storage, so small amounts of hydroquinone are added, preventing premature

polymerisation of monomers. MMA polymerizes by the mechanism of free radical polymerization, which consists of three steps: initiation, propagation, and termination. The initiation step involves decomposition of BP monomer into radicals at room temperature (Hamid Reza Seyyed Hosseinzadeh, 2013; Kuehn, Ege, & Gopp, 2005) (Figure 1.8).

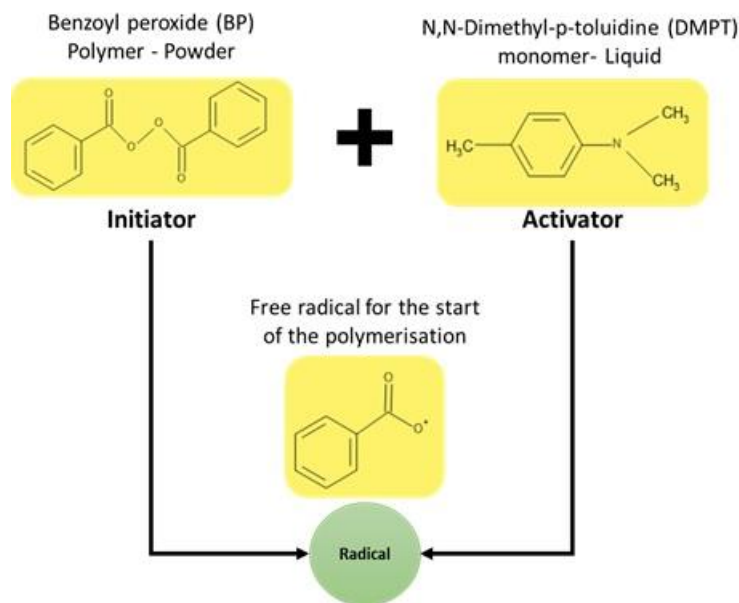


Figure 1.8 The initiation of the polymerisation of MMA: BP from the powder and DMPT from the liquid react to form radicals, starting the curing of bone cements. Adapted from 'The Acrylic Bone Cement in Arthroplasty' (Hamid Reza Seyyed Hosseinzadeh, 2013).

PMMA is currently the most commonly-used material, but it cannot degrade and may induce bone cement reactions such as hypotension or pulmonary embolism, due to cement leakage and the toxic monomers used (Qian, Dong, Yang, & Wang, 2012). Additionally, the long-term efficacy is also indefinable and over high strength may induce adjacent vertebral fracture (Boger, Bohner, Heini, Schwieger, & Schneider, 2008) and intervertebral disk degeneration.

This has been attributed to the load distribution in the spine due to PMMA's high Young's modulus in comparison to bone. After PMMA is administered at the fractured site, it does not integrate with the bone interface. It's been considered, monomer release from PMMA implantation might inhibit tissue repair and neovascularization (Qian et al., 2012). Stress breakage has also been found, between materials and peripheral bone, interface micro motion, vascular invasion and pulmonary embolism (Qian et al., 2012). The high heat generation (~80°C) as a result of PMMA polymerisation has been suggested to cause nerve damage at the treated fracture site. Due to the damaged nerves, patients lose the sensation of pain, resulting in rapid pain relief post the vertebroplasty procedure (Pawel Szulc, 2011).

PMMA cements are supplied to the surgeon as a powder and a liquid that must be mixed in the operating room prior to use (Kirsty Alexandra Ikrzycka Main, 2013). Hand mixing of powder and liquid components has been identified as producing PMMA cements with poor mechanical properties compared to mechanically/vacuum mixed cements (Wilkinson et al., 2000). There are concerns also about the exposure of methyl methacrylate during hand mixing; repeated exposure can lead to contact dermatitis and sensitisation (Borak, Fields, Andrews, & Pemberton, 2011).

Apart from thermal necrosis, other concerns using PMMA include

- 1) Debris from solidified bone cement; this is pronounced to be an outcome of monomer-mediated bone damage.

- 2) Volumetric shrinkage during end-polymerisation thus affecting the bone-cement interface.

- 3) Difference in stiffness of cement and the adjacent bone (Webb & Spencer, 2007). Studies have shown administration of PMMA at the fractured site, changes the load transfer in the adjacent vertebra, resulting in an increase in fracture risk of adjacent vertebrae (Alhashash, Shousha, Barakat, & Boehm, 2019). A frequent complication of vertebro- and kyphoplasty (50% of cases) is PMMA leakage (Alhashash et al., 2019). The leakage into the epidural space or the central canal may induce neurological deficits.

Cotton et al (1996) performed a study to determine whether the percentage of vertebral lesion filling and the leakage of methyl methacrylate have any clinical significance at follow-up (Cotten et al., 1996). A more recent study carried out in 268 patients (56 males and 212 females) from January 2015 to March 2019, presented the cement leakage rate at 32.5%. The most common cement leakage type was intradiscal leakage, followed with peri-vertebral soft tissue leakage, vein leakage and spinal canal leakage (T.-y. Zhang, Zhang, Xue, Zhang, & Jiang, 2020).

Different cement brands for commercial use have been developed with varying

properties due to their formulation. For the purpose of this project the most well-known and commonly used cement brand Simplex™ P will be used.

1.4.1.6 Composite Cements

Alternative bone composites; Cortoss® and Comp06® are inspired by dental composite materials that address PMMA's limitations, mentioned above. Dental composites are made of dimethacrylate monomers such as Bisphenol A Glycidyl Methacrylate (Bis-GMA), Urethane Dimethacrylate (UDMA) and Triethylene Glycol Dimethacrylate (TEGDMA) together with inorganic fillers usually supplied as a premixed paste that is cured by light activated free radical polymerization (Pratap, Gupta, Bhardwaj, & Nag, 2019). However, for bone cement applications, light cure is unsuitable due to the large volume of material and inaccessibility of the implant sites. Cortoss® and Comp06® are pre-mixed, dual pastes chemically curing alternatives to PMMA cements that are now frequently used in vertebroplasty.

These composite bone cements are more similar to dental composites than PMMA cements as they contain a mixture of dimethacrylate monomers and silica fillers more commonly found in dental composites. In addition Cortoss® contains the calcium containing phase, whilst Comp06® contains HA (Kirsty Alexandra Ikrzycka Main, 2013). Cortoss® and Comp06® already contain calcium-containing phases. Inclusion of calcium phosphates, into dental composites, aid in secondary reactions or release re-mineralising ions (Meyer, Amaechi, Fabritius,

& Enax, 2018). The release of re-mineralising ions could be useful for the localised treatment of osteoporosis. Although the usage of antibacterial components in PMMA cements is relatively common, they are still quite a new addition to composites.

1.5 Complications and failure of bone composite due to limitations in PMMA and other commercial products

Prior vertebral fractures, increases the risk of new vertebral fractures (Pawel Szulc, 2011). Subsequent fractures are a risk of 2%–23% in kyphoplasty and up to 52% in vertebroplasty, and often occur within 2 months after a vertebroplasty procedure (Jang et al., 2020). Adjacent fractures have been suggested to occur due to cement leakage within the intervertebral disc (Figure 1.9). This is possibly due to the difference between the stiffness of the vertebra undergoing the procedure and the adjacent vertebral body (J. H. Park, Kim, & Kim, 2016). Also during polymerisation of the cement the high temperature (85 °C) (Pawel Szulc, 2011) may be responsible for damage to the surrounding tissue. Pain relief after vertebroplasty has been presumed to be due to chemical toxicity, and thermal necrosis of surrounding tissues and nerve endings (Z. Zhang et al., 2020).



Figure 1.9 Cement leakage into the Batson's paravertebral venous system. Reprinted from Case Reports in Surgery, volume 2013, Giorgio Lo Iacono,¹ Chiara Lo Nigro,¹ Fabio Cannizzaro,¹ Massimo Cajozzo,¹ and Giuseppe Modica¹, Asymptomatic Bone Cement Pulmonary Embolism after Vertebroplasty: Case Report ad Literature Review. Page 2. This article is licenced under a Creative Commons Attribution Non-commercial licence 3.0 licence

Another common problem post-procedure is bacterial infections. Bacteria have the ability to adhere to biomaterials surfaces (L.-C. Xu & Siedlecki, 2020). Infection occurrence after vertebroplasty are rare, but can result in serious complications causing an invasive surgical intervention associated with high mortality rate (33%) (Abdelrahman, Siam, Shawky, Ezzati, & Boehm, 2013). The most commonly used antibiotics are gentamicin and tobramycin (specific for gram-negative bacteria) and vancomycin (specific for gram-positive bacteria) (Bistolfi et al., 2011). However, due to antibacterial resistance, antibiotics are not ideal for bone cements.

1.6 Components of experimental bone composites

1.6.1 Monocalcium Phosphate Monohydrate (MCPM)

Metabolism of calcium phosphate in the human body is essential for bone growth and development. The amount of mineral content in bone contributes to the elastic modulus of the bone matrix, increasing mineral concentration results in an increase in elastic modulus (Abou Neel et al., 2016).

Up to 70% of bone mass is calcium phosphate based mineral, commonly known as HA (Hughes, Robinson, Bassett, Cox, & Grover, 2019). The HA in teeth varies from empirically obtained HA, and HA found in bones, since the HA form found in dental substrates, is often calcium deficient due to fluorine substitutions (Abou Neel et al., 2016).

The incorporation of various calcium phosphates in composites such as amorphous calcium phosphate (ACP), dicalcium phosphate anhydride (DCPA), tetra calcium phosphate (TetCP), and MCPM has been studied (Habracken, Habibovic, Epple, & Bohner, 2016). Their incorporation can result in release of mineral content which decreases the composite's mechanical strength. Figure 1.10 is an image of MCPM particles taken via a scanning electron microscope (SEM).

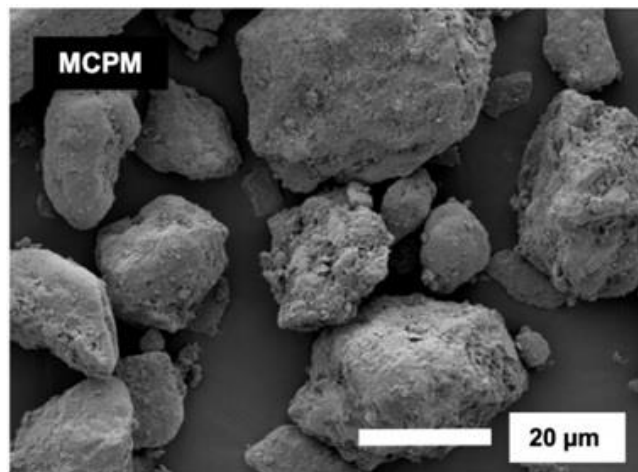


Figure 1.10 SEM images of MCPM particles. Retrieved from Kangwankai et al. (2017), licensed under CC BY 4.0

In general, the higher the calcium to phosphate ratio, the lower the solubility in water. At physiologic pH, the solubility of calcium phosphate species decreases in the order MCPM > dicalcium phosphate dihydrate(DCPD) = DCPA > Octacalcium phosphate (OCP)>beta-tricalcium phosphate (β -TCP)>HA (Wang & Nancollas, 2008).

The range in solubility allows calcium phosphates to dissolve, be transported and precipitate when necessary (Dorozhkin, 2011). Consequently, the right amounts of calcium phosphates used in the bone cement will precipitate on the surface of the bone composite overtime, since a composite with similar topography to bone is desired.

It has been demonstrated that a material that encourages apatite precipitation on its surface may potentially promote the remineralisation of demineralised dentine (Gandolfi et al., 2011).

An earlier study has shown that immersion of dental composites consisting of MCPM and tricalcium phosphate (TCP)

in simulated body fluid (SBF) encouraged the formation of calcium deficient HA (Abou Neel et al., 2016).

Other remineralising composites are tricalcium phosphate (TCP) and tri strontium phosphate (TSrp). β -TCP is a basic calcium phosphate which reacts with an acidic phosphate such as MCPM (Huan & Chang, 2009). The combination of these two provides a source of calcium and phosphate ions which encourage bone bonding. "Beta-Tricalcium phosphate (β -TCP) ceramics are known to be biocompatible and osteoconductive" (Bansal et al., 2009). In addition β -TCP has been used in different types of bone substitution bioceramics previously (Eliaz & Metoki, 2017).

For the purpose of this study to keep the experimental bone composite components minimal and efficient the only phosphate used was MCPM.

1.6.2 Polylysine (PLS)

As previously mentioned in section 1.5 the incorporation of antibiotics is limiting. PLS (Figure 1.11) has never been used in a commercial bone composite before and will be incorporated in the experimental bone composite for this study. PLS is widely used as an antibacterial agent in food and approved by Food and Drug Administration (FDA).

PLS has a function to prevent microorganisms from proliferating by ionic adsorption. It has a wide antibacterial spectrum and has an obvious lethal effect on Gram-positive and Gram-negative bacteria (Profod). Cationic PLS has been described to disrupt the cell membrane by interacting with the negatively charged cell membrane resulting in stripping the lipopolysaccharides and permeability of the cell membrane (Tan et al., 2019).

The most common antibacterial used in commercial bone cements is gentamicin. It is used against a wide range of human bacterial infections, mostly Gram-negative bacteria including *Pseudomonas*, *Proteus*, *Serratia*, and the Gram-positive *Staphylococcus*" (C. Chen, Chen, Wu, & Chen, 2014).

The use of antibiotic loaded bone cement is not yet widely accepted, due to the risk of antibacterial resistance. PLS is of interest as it is a natural antimicrobial that is biodegradable and innocuous.

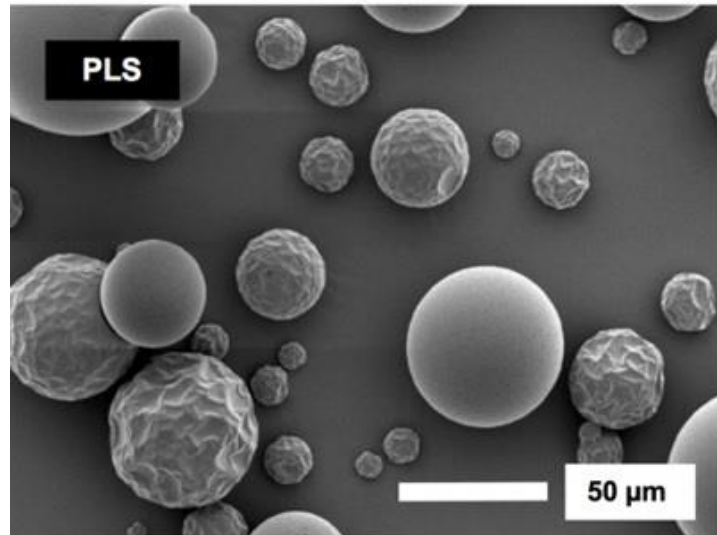


Figure 1.11 SEM images of PLS particles. Retrieved from Kangwankai et al. (2017), licensed under CC BY 4.0

Alkhouri et al demonstrated composites with PLS, penetrated porous dentine which encouraged adhesion, sealing and interlocking (Alkhouri, 2019). Furthermore, this would enable hydrophobic components of the composite to penetrate the demineralised tooth structure. This may be particularly useful in osteoporotic bone (heavily porous), to promote interlocking and prevent fibrous tissue formation.

1.6.3 Glass Fillers

Fillers reinforce the resin matrix and control the volume shrinkage during polymerisation (Ferracane, 2008). Current dental composites referred to as hybrid composites contain two types of fillers that are blended together, fine and micro fine particles. They overcome several problems, that are exhibited by bigger fillers; difficult to polish and retaining surface smoothness. Furthermore, smaller fillers by themselves are not ideal for load (Mitra, Wu, & Holmes, 2003). A similar idea for bone composites is being developed for this study where two different sized fillers are used.

Panpisut (2017) investigated the effects of different glass filler size (0.7 or 7 μm) on strength at early time (24 hours) and found reducing the glass filler sized improved solid-like behaviour of composite paste and strength (P. Panpisut, 2017).

Figure 1.12 represents the 2 glass fillers used for the bone composite prepared in this project.

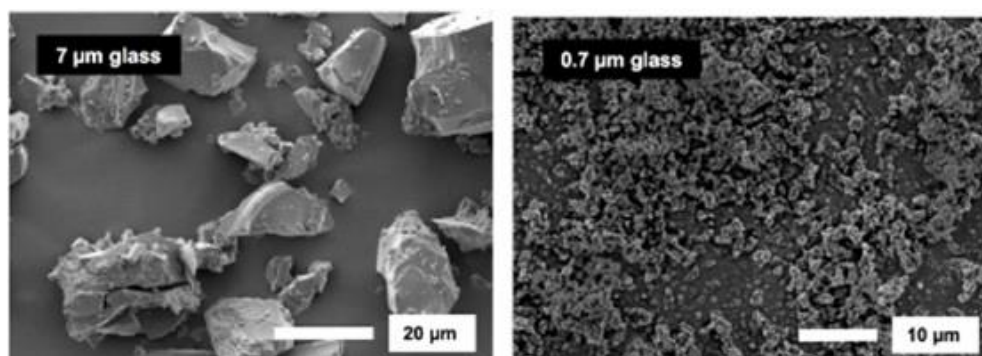


Figure 1.12 SEM images of glass filler particles, 7 μm and 0.7 μm . Retrieved from Kangwankai et al. (2017), licensed under CC BY 4.0

1.6.4 Organic Polymer Matrix

Formerly, Bis-GMA (Figure 1.13) was the main base monomer in resin-based restorative materials (Bowen & Marjenhoff, 1992). Since it is very viscous and may compromise the clinical handling, the resin matrix is mixed with diluent methacrylates, such as TEGDMA (Figure 1.14) (Peutzfeldt, 1997).

An alternative matrix resin, UDMA (Figure 1.15) has become popular in recent years. It comprises of reactive carbon double bonds on both endings that can undergo addition polymerisation initiated by free-radical initiators (John M. Powers, 2012). In comparison to Bis-GMA, UDMA has lower viscosity and has a highly flexible urethane linkage. These properties of UDMA may improve the mechanical properties and durability of resin composites (Anusavice, Phillips, Shen, & Rawls, 2013).

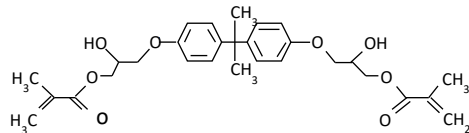


Figure 1.13 Chemical structure of Bis-GMA

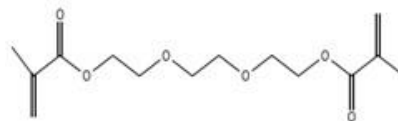


Figure 1.14 Chemical structure of TEGDMA

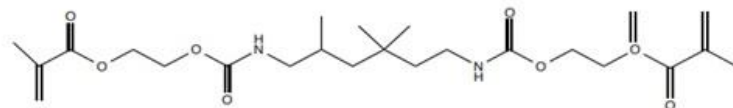


Figure 1.15 Chemical structure of UDMA

1.6.5 Flexible Diluent Monomer

Polypropylene-glycol-dimethacrylate (PPGDMA) (Figure 1.16) has low viscosity and it has not been used in a commercial material before. According to Main (2013) PPGDMA has better cure rate, conversion (free monomer remaining) and modulus; but with a small compromise on strength in comparison to TEGDMA. It is thought that PPGDMA could be a good candidate material for incorporation in commercially competitive bone cement materials (Kirsty Alexandra Iskrzycka Main, 2013). It was found that PPGDMA, combined with UDMA and hydroxyethylmethacrylate (HEMA) monomers, and silane treated silica glass particles could produce materials that cured more extensively than existing bone cements (Kirsty Alexandra Iskrzycka Main, 2013).

Panpisut (2017) investigated the effect of increasing PPGDMA on strength of the composites. The modulus of elasticity of the composites containing low level of PPGDMA was too high compared with cancellous bone but it was found one could optimise this by increasing the level of PPGDMA (P. Panpisut, 2017).

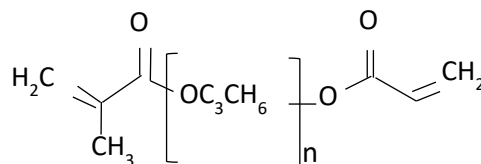


Figure 1.16 Chemical structure of PPGDMA

1.6.6 Adhesion promoting monomer

4-Methacryloxyethyl trimellitic anhydride (4-META) (Figure 1.17) comprises an anhydride group that reacts with water to form two carboxylic groups affixed to an aromatic group providing acidic properties and wettability. The hydrophobic aromatic group will neutralise the acidity and hydrophilicity of the carboxyl groups. 4-META has been demonstrated to form a chemical bond with calcium in HA improving adhesion to enamel and dentine (Van Landuyt et al., 2007). Thus it may also improve the adhesion to HA in bone.

HEMA (Figure 1.18) is another adhesion promoter; HEMA applied to dentinal substrates enhances monomer diffusion and entanglement with dentinal components, and facilitates the formation of a "hybrid" layer (Van Meerbeek, Yoshihara, Van Landuyt, Yoshida, & Peumans, 2020).

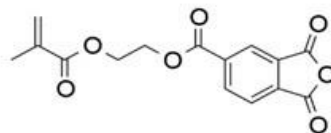


Figure 1.17 Chemical structure of 4-META

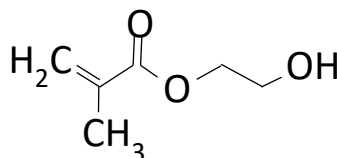


Figure 1.18 Chemical structure of HEMA

1.6.7 Initiator/Activator systems

Some dental materials consist of an initiator such as camphorquinone (CQ) which absorbs light resulting in the generation of free radicals to initiate polymerisation. The free radicals then combine with an organic amine that can be, dimethylaminoethyl methacrylate (DMAEMA)(Price & Rueggeberg, 2019) . Light cannot be used to cure composite for vertebroplasty thus a chemically cured system is required.

PMMA cements have a chemical initiator system usually incorporating; BP initiator (Figure 1.19) and DMPT accelerator. The BP radicals are stabilised by the DMPT accelerator; following mixing, the polymer beads in some PMMA cements can dissolve in the monomer. A solid bulk is formed via chemically induced free radical polymerization of the monomer liquid. DMPT is toxic, therefore NTG-GMA (Figure 1.20) can be used as an alternative monomer for the experimental bone composites (A. M. Khan, Walters, & Young, 2014).

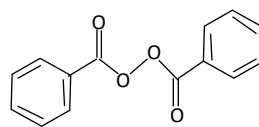


Figure 1.19 Chemical structure of BP

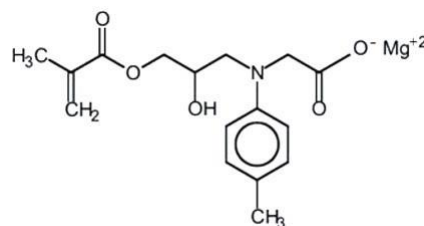


Figure 1.20 Chemical structure of NTG-GMA

1.7 Osteoconductive bone cement/composite

Bone cements that can stimulate cell attachment, migration or growth are considered as osteoconductive materials (Gao, Peng, Feng, & Shuai, 2017). PMMA is the most common cement of choice, however it is a bioinert material (Palmer et al., 2016), unlike calcium phosphate cements. Calcium phosphate cements are known for directing stem cell differentiation in orthopaedic applications (Y. Xu, Chen, Hellwarth, & Bao, 2019).

Bone cements that release minerals similar to bone (HA) are likely to create a bone like environment cells are familiar with. The release of HA on the surface of bone cements at the fractured site results in a micro-topographical surface. This has known to encourage osteoconduction by providing features that allow integrins known as fibrins to become entangled and attach (Şahin, 2018). Similarly the adhesion of cells on to the bone cement will require these mediated adhesion molecules(Gutiérrez-Prieto et al., 2019). Upon cell attachment, platelets are activated, which produce a density rich environment of cytokines and growth factors that further guide leukocytes and osteogenic cells during the healing process. Cells that reach the solid surface will initiate matrix synthesis by secreting the first collagenous matrix of the cement line directly on the implant surface. This new bone formation stage is generally considered as a separate and distinct phenomenon and is followed by remodelling of the bone (Kuzyk & Schemitsch, 2011). Further according to bone bonding theory of Davies helps one understand calcium phosphates surfaces readily adsorb proteins, which can increase fibrinogen bonding leading to platelet adhesion, followed by platelet activation which then may accelerate healing (Davies, 2007). These steps are

vital since cell survival requires a specific environment to further differentiate in to specific cells. Osteoblasts adhesion on biomaterials involves interaction with biological molecules within the environment, which further helps the cells proliferate, migrate and potentially differentiate (Gutiérrez-Prieto et al., 2019).

As a result with the right cells in the treated site, the ideal bone cement will potentially encourage self-healing to enable new bone formation (Palmer et al., 2016). This process is known as osteogenesis, another desired outcome of bone cements at fractured sites.

Fracture healing is influenced by several factors including, age, gender and disease. Fracture healing is decreased in patients with osteoporosis (Giannoudis, Tzioupis, Almalki, & Buckley, 2007) thus a bone composite that can aid remineralisation and cell attachment as oppose to an inert bone cement will be superior.

1.8 Regulatory Approval of Bone Composite

Medical devices may be classified in to Class I, IIa, IIb and III based on the risk upon application. A dental composite is usually classified as a class IIa medical device (MHRA, 2017). A dental composite similar to the bone composites in this work with MCPM and PLS is currently being assessed by a notified body for Conformité Européenne (CE) marking. Currently the dental composite similar in composition to the bone composite in this study is classified as IIa. Since the modified dental composite in this study has a different purpose (application within the body) this means the modified bone composite will need to go through an independent process for regulatory approval.

However since the dental composite has potential for remineralisation and antibacterial action, it may be considered as biological effects, thus it may shift the classification to III. If this is approved as a class III device it may become easier to apply for regulatory approval for a similar bone composite.

1.9 Statement of the Problem

Total fractures in the European Union plus Sweden alone are estimated to increase from 2.7 million in 2017 to 3.3 million in 2030; a 23% increase. The resulting annual fracture-related costs (€37.5 billion in 2017) are expected to increase by 27% (Borgström et al., 2020). Thus better management of the condition is required.

Current minimally invasive treatments which use PMMA causes problems such as cement leakage leading to poor fixation and complications in distant organs (Alexandru & So, 2012). Current bone composites like Cortoss[®] and Comp06[®] have partially addressed concerns over PMMA however neither materials match the mechanical properties of the vertebra nor do they bond well to the living bone. These materials also have limited or no antibacterial action to prevent post-operative infection.

Previous studies have worked on bone composites containing MCPM with TCP, where these components encouraged apatite precipitation. Similar composites, with MCPM but no TCP have been formulated for the purpose of this project. Polylysine has shown a wide antimicrobial spectrum and it is FDA approved as a food preservative, thus the incorporation of polylysine in a calcium bone composite may be of interest. Therefore, continuing with the incorporation of MCPM and incorporation of PLS will be considered in this study.

The aim of this study was to develop bone composite containing calcium phosphate as a remineralising agent and PLS as an antibacterial agent to overcome limitations of currently available materials.

It is anticipated that:

1) The experimental bone composites in its paste form should exhibit rheological properties suitable for injection. Chemically activated experimental bone composites can be developed and polymerisation time can be controlled by the addition of chemically activated initiator. Furthermore, the polymerisation kinetics should be optimised and compete with the commercially available bone composites (Chapter 3).

2) The novel remineralising and antibacterial releasing bone composites can be developed by the addition of remineralising agents (MCPM) and polylysine (PLS). The addition of remineralising agents should promote surface apatite precipitation. Furthermore, the addition of PLS should enable antibacterial PLS release from the composite. In addition, the experimental bone composites should exhibit high strength at early time. Elastic modulus of the composites should be comparable to that of cancellous bone. The addition of MCPM into bone composites should enable surface apatite formation for on the composite surfaces. (Chapter 4).

3) The experimental bone composite should be compatible with cells and prove to be cytocompatible ix-ovo (chapter 5 and 6).

Materials and Methods

This chapter summarises all the materials and protocols used for each section during the project. A summary of the methods used in each experiment specific to the chapter can be found at the start of each chapter.

2.1 Materials

Commercial materials, monomers examined in this thesis are provided in Table 2.1 and Table 2.2 respectively.

Monomers were handled with the correct personal protection equipment including latex gloves, safety glasses and a certified laboratory coat. The transfer of viscous monomers was carried out using a plastic spatula. Transfer of diluent monomers was with glass pipettes. All weighing of monomers and fillers was carried out on an OHAUS Pioneer Series of analytical and precision balance accurate to 4 decimal places. After weighing, all monomers and fillers, they were mixed together using a Speed Mixer™ DAC 150.1 FVZ (Synergy Devices Ltd) in disposable jars and lids.

2.1.1 Commercial Materials

Table 2.1 presents the 2 commercial bone cement/composites and their components. Simplex™ P consists of monomer liquid and powder supplied separately and mixed just before delivery in the body (chemical cure following mixing). Cortoss® arrives pre-mixed in a double barrelled syringe. Chemical cure occurs following mixing.

Table 2.1: Description of commercial materials used for this project with component information from manufacturer.

Name	Supplier	Components	
		Monomers	Fillers
Simplex™ P	Stryker	<ul style="list-style-type: none"> • MMA 	<ul style="list-style-type: none"> • Poly(styrene) • Barium sulphate
Cortoss®	Orthovita	<ul style="list-style-type: none"> • BisGMA • BisEMA • TEGDMA 	<ul style="list-style-type: none"> • Silane treated silica glass, • Combeite

2.1.2 Monomers

Table 2.2: Monomer details including molecular weight and manufacturer information

Name	Abbreviation	Type of monomer	Supplier	Product code	Molecular weight (g/mol)
Poly (propylene glycol)425 dimethacrylate	PPGD MA	Diluent monomer	Polysciences Inc	626208	600
Urethane dimethacrylate	UDMA	Bulk monomer	DMG, Hamburg, Germany	03072014	479
Hydroxyethylmethacrylate	HEMA	Adhesion promoter	DMG, Hamburg, Germany	100220	130
4-Methacryloxyethyl trimellitic anhydride	4-META	Adhesion promoter	Polysciences Inc	656649	304

2.1.3 Remineralisation agent and antibacterial agent

Table 2.3 shows the remineralising agent and antibacterial agent used in experimental composite.

Table 2.3 Remineralising agent and antibacterial agent with manufacture details

Name	Abbreviation	Supplier	Product code	Molecular weight (g/mol)
Monocalcium phosphate	MCPM	Himed	MCP-B26	234
Polylysine	PLS	Handary	0204	30,000-70,000

2.1.4 Fillers

Table 2.4 shows the glass fillers used, 0.7 μm and 7.0 μm in the powder phase at a ratio 4:5.

Table 2.4 Details of two glass fillers used in this project as fillers and information of manufacturer.

Size (μm)	Supplier	Product code
0.7	DMG, Hamburg, Germany	688344
7.0	DMG, Hamburg, Germany	680326

2.1.5 Initiator, Activator

Initiator, Benzoyl Peroxide (BP) and activator, N-(2-hydroxy-3-((2-methyl-1-oxo-2-propenyl) oxy) propyl)-N-tolyl glycine (NTGGMA) are presented in Table 2.5.

Table 2.5 Details of initiator, activator used in this project and details from manufacturer.

	Abbreviation	Supplier	Product code	Molecular weight (g/mol)
Initiator	BP	Polyscience Inc	593397	243
Activator	NTGGMA	Esschem Europe	850-30	329

2.2 Methods

2.2.1 Commercial material samples preparation

2.2.1.1 SimplexTM P (PMMA)

PMMA was hand mixed in a 2:1 powder to liquid ratio according to manufacturer's instructions. Powder and liquid were mixed using the centrifuge mixer (SpeedMixerTM, Germany) at 1400 rotations per minute (rpm) for 7 seconds.

2.2.1.2 Cortoss®

1 hour (h) prior to using the double barrel syringe containing Cortoss®, the material was removed from the fridge (4°C) to allow it to match room temperature (20 °C). Mixing of paste occurred in the automatic mixing tip. The time taken to reach the end of the tip was 5 seconds.

2.2.2 Experimental Composite Preparation

The required amounts of monomers were weighed using a four-figure analytical balance and mixed in a light protecting amber bottle using a magnetic stirrer (Figure 2.2 A) bar for 30 minutes at room temperature. This was carried out in pairs; both amber bottles included, PPGDMA and HEMA. One amber bottle contained BP (initiator) and 4-META while the second amber bottle N-(2-hydroxy-3-((2-methyl-1-oxo-2-propenyl) oxy) propyl)-N-tolyl glycine (NTGGMA) (activator). The adhesion promoter 4-META precipitates with NTGGMA and was therefore dissolved in the initiator paste (BP) only. Once all the components were dissolved, UDMA was added. The monomers were then left to mix at 300-500 rpm overnight before storing at 4°C.

2.2.3 Filler (Powder) Phase

Fillers were stored in air tight containers to prevent moisture getting in. For each given amount of fillers, MCPM or PLS required, initiator and activator pastes were prepared in pairs. Monomers were added to the fillers ensuring 3:1 powder to liquid weight ratio. Monomers and fillers combined were mixed at 1700 rpm for 2 minutes using a centrifuge mixer (SpeedMixer™, Germany).

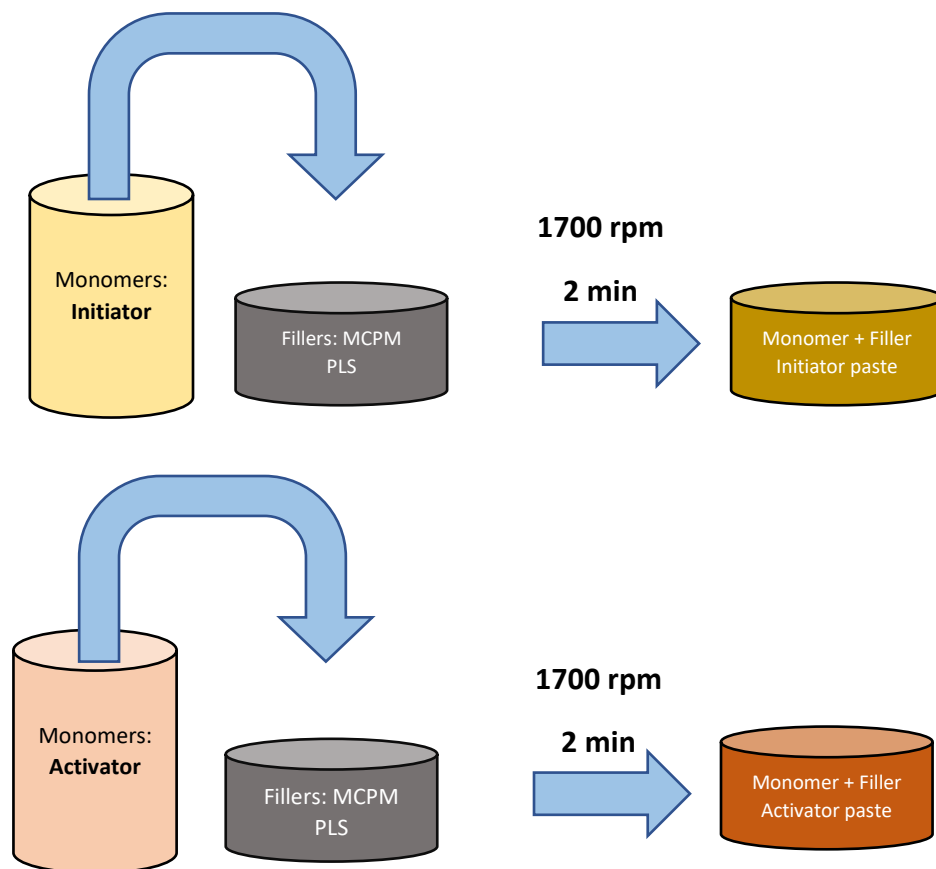


Figure 2.1 Illustrating the incorporation of monomers (liquid) within fillers (powder).

2.2.4 Paste Mixing and Syringe Filling

A sealed lid for the tip of the syringe (Figure 2.2 B) was secured to prevent paste from escaping when filling the double barrel syringe (Sulzer Chemteck, UK) (Figure 2.2 C).

The initiator and activator pastes were added to the double barrel syringe slowly using a metal spatula avoiding any trapped air bubbles. Before sealing with a rubber stopper, the double barrel syringe was held on top of a vibrating jig to allow any trapped air to escape. The double barrel syringe was stored in the fridge (4°C).

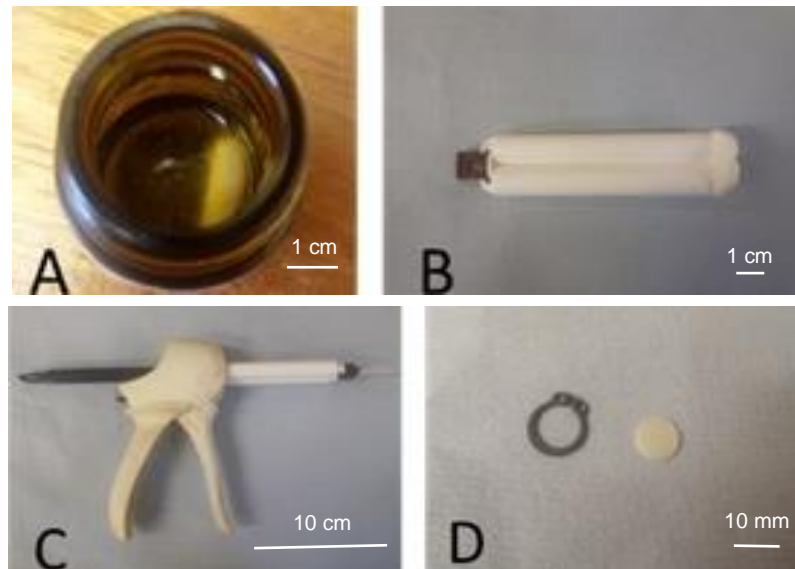


Figure 2.2 Preparation of experimental bone composite A=The monomer phase with magnetic mixer, B= Double barrel syringe with activator and initiator, C=Double barrel syringe dispensing gun, D= 10mm mould with experimental bone composite disc.

2.2.5 Fourier Transform Infrared Spectroscopy (FTIR)

Fourier Transform-Infrared Spectroscopy (FTIR) is used to identify degree of conversion of methacrylates (Izabela M. Barszczewska-Rybarek, 2012) FTIR allows real time monitoring of not only the degree of conversion but also the rate of polymerisation. The method of FTIR used in this project was based on that of Young et al (Young, Rafeeka, & Howlett, 2004).

2.2.5.1 FTIR Background

FTIR was chosen to be used for measuring the polymerisation rate and degree of conversion. A brief explanation of its underlying principles will be discussed in this section. This method utilises information following vibrational changes in molecular bonds after absorbance of incident infrared radiation. When infrared radiation is absorbed by a molecule or atom, energy is gained and transitions between energy levels occur. Bonds between atoms vibrate at higher amplitudes when infrared radiation is absorbed. Different bonds have varying lengths and will absorb different wavelengths of radiation (Larkin, 2018a).

2.2.5.2 FTIR Instrumentation

The aim of the FTIR is to define the wavelengths of infrared radiation that are absorbed by the material and deduce the type of bonds existing between the atoms of the molecules. According to Beer Lambert law the amount of light absorbed at a specific wavelength can be distinguished by finding the ratio of incident radiation to radiation that has been absorbed/transmitted (Beer Lambert law). Attenuated total reflectance (ATR) is the method used to find the intensity of radiation interacting with the sample. The material under investigation is placed on a diamond which has a high refractive index.

Radiation from the source has a real component that is totally internally reflected and an imaginary component (at 90° to the real part) that probes the surface of the sample in contact with the crystal (0.5 – 5 μm) (Larkin, 2018b). The wavelengths absorbed are absorbed by the Michelson interferometer. Figure 2.3

shows the experimental set up of a Michelson interferometer. The beam splitter splits the light from the sample. Half the signal is sent to a moving mirror while the other half is sent to a fixed mirror. The reflected signal from the moving mirror and fixed mirror arrive at the detector through a lens. The path varies depending on the position of the moving mirror. The interference of the two beams at the detector gives an interferogram of intensity as a function of time. The computer uses Fourier transform and the Beer Lambert law to convert this interferogram into a plot of Absorbance as a function of wavelength. Since all the wavelengths of the source reach the detector simultaneously; a full spectrum can be found rapidly thus making FTIR spectroscopy appropriate for real-time monitoring of polymerisation. FTIR spectra (Figure 2.4) can give qualitative and quantitative information about a material.

FTIR peaks at different positions in the spectrum give information about the chemical groups present whilst their absorbance is proportional to amounts of each bond type.

This is useful when polymerisation is monitored in real time, since the relative heights of the peaks correspond to the methacrylate groups, concluding how many groups have polymerised.

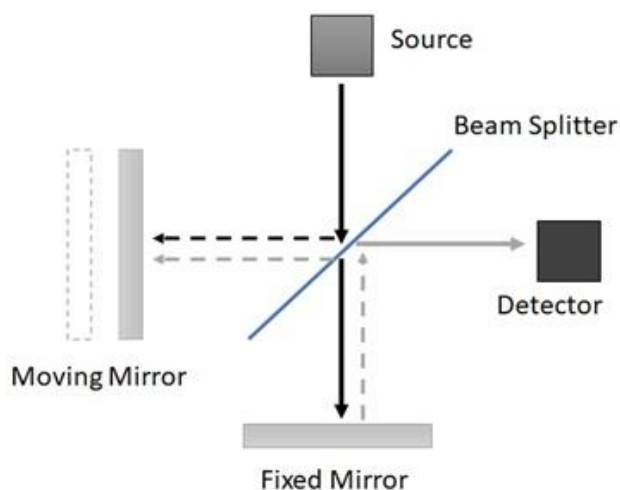


Figure 2.3 Schematic of Michelson Interferometer, representing the light source splitting between the moving and fixed mirror, reaching the detector with a different path depending on the position of the moving mirror.

2.2.5.3 Curing Profile and Degree of Conversion

Spectra were obtained using a 2000 FTIR spectrometer (Perkin-Elmer, UK) and Timebase software. Each experimental formulation was mixed using a double barrel syringe, while PMMA was mixed using the centrifuge (SpeedMixer™, Germany) for 47 seconds at 1700rpm. These were placed in turn on to the controlled golden gate diamond ATR attachment (Specac, UK) within a 1 mm thick 10 mm diameter mould ring and covered with an acetate sheet to avoid surface oxygen inhibiting the polymerisation process.

The experimental formulation was left to polymerise over 1 hour at 20 °C. For each formulation, the FTIR analyses was run 3 times. Spectra of the lower surface of the specimen were recorded with a resolution of 4 cm⁻¹, every 4 second for 1 hour. Different spectra were obtained to ensure methacrylate polymerisation was the only process causing spectral changes. Inhibition time,

half-life, reaction rate and monomer conversion were calculated via change in the height of the absorbance at peak 1320 cm^{-1} (C-O). Monomer conversion (M_C) was estimated using Equation 2.1.

$$M_C = \frac{100(h_o - h_t)}{h_o} \quad \text{Equation 2.1}$$

Where h_o and h_t were taken as peak absorbance at 1320 cm^{-1} above the background level (1335 cm^{-1}) initially and after a time (t) (Leung et al., 2005) (Figure 2.4). Final peak height and conversion C were obtained via extrapolation of data versus inverse time to zero.

The final degree of monomer conversion was calculated by linear extrapolation versus inverse time to zero.

Rate of polymerisation (R_p) was calculated using equation 2.2.

$$R_p = \frac{dD_c}{dt} \quad \text{Equation 2.2}$$

Where the change in monomer conversion (ΔD_c) is the change of monomer conversion over time t .

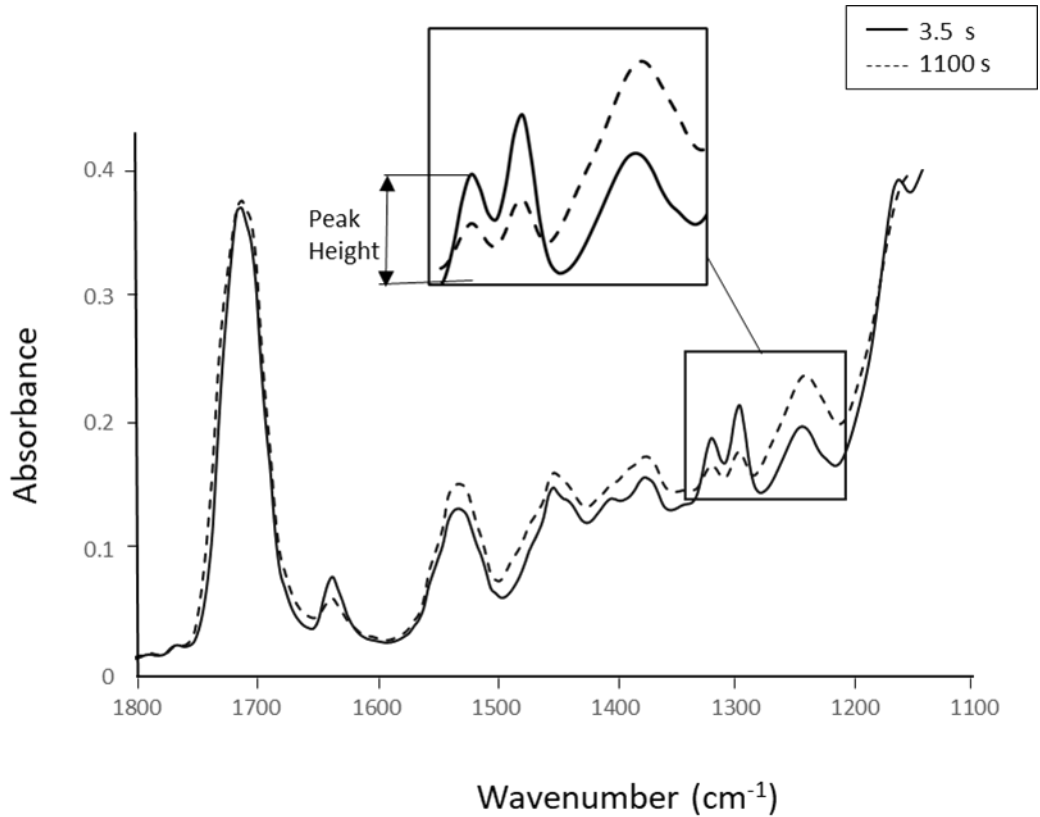


Figure 2.4 FTIR spectra of a curing experimental bone composite consisting of 3.5 % BP and 2.1 % NTGGMA (Levels of initiator and activator after mixing in monomer phase) at 20 °C. Inset shows change in absorbance used to determine cure profile. The 1320 cm^{-1} peak is used to measure peak height corresponding to C-O bond in the polymerising methacrylate group. Peaks corresponding to methacrylate groups are changing-implying one reaction (polymerisation) is occurring.

2.2.5.4 Polymerisation Equations

An equation for the rate of initiation (Equation 2.3), R_i can be obtained by assuming the initiation rate is proportional to the concentrations of initiator and activator and the rate initiation constant (52, 250).

$$R_i = 2\zeta k_d [I][A] \quad \text{Equation 2.3}$$

Where ζ is the initiator efficiency (number of collisions between radicals and monomer molecules resulting in the formation of a free radical).

[I] and [A] are the concentration of initiator and activator in the monomer respectively.

k_d is the initiation rate constant.

Equations for rates of propagation (R_p), inhibition (R_x) and termination (R_t) can also be derived from the free radical polymerisation reaction mechanism. These are presented in Equation 2.4, Equation 2.5 and Equation 2.6.

$$R_p = k_p [M][M_n^*] \quad \text{Equation 2.4}$$

$$R_x = k_x [X][M_n^*] \quad \text{Equation 2.5}$$

$$R_t = 2k_t [M_n^*]^2 \quad \text{Equation 2.6}$$

Where k_p , k_x and k_t are reaction rate constants for propagation, inhibition and termination respectively. $[M_n^*]$ is the total concentration of polymer and monomer radicals.

[X] and [M] are the concentration of inhibitor and monomer respectively.

Applying the stationary state/ steady state assumption, the rate of change of monomer and polymer free radicals (M_n^*) is 0. This leads to Equation 2.7.

$$-\frac{d[M_n^*]}{dt} = -R_i + R_t + R_x = 0 \quad \text{Equation 2.7}$$

Inserting rates of inhibition and termination (equation 2.5 and 2.6) into Equation 2.7 gives:

$$-\frac{d[M_n^*]}{dt} = -R_i + 2k_t[M_n^*]^2 + k_x[X][M_n^*] = 0 \quad \text{Equation 2.8}$$

Where $-R_i$ = rate of initiation, $2k_t[M_n^*]^2$ = rate of termination. $k_x[X][M_n^*]$ = rate of inhibition.

From the inhibition step, the rate of change of inhibitor becomes:

$$-\frac{d[X]}{dt} = k_x[X][M_n^*] \quad \text{Equation 2.9}$$

During early time points when the inhibition period is progressing, rate of termination can be ignored (Term B-Equation 2.8). Equation 2.8 and Equation 2.9 can then be combined to give rate of change of inhibitor concentration (Odián, 2004) .

$$-\frac{d[X]}{dt} = k_x[X] \frac{R_i}{k_x[X]} \quad \text{Equation 2.10}$$

Rate of initiation would stay constant if it was assumed that the concentration of initiators would be high enough. Thus, integration of Equation 2.10 gives;

$$[X] = [X_0] - R_i t \quad \text{Equation 2.11}$$

Where, X_0 is the initial concentration of inhibitors.

Setting $[X] = 0$ at the inhibition time (t_i).

Inhibition time can be given by Equation 2.12.

$$t_i = \frac{[X_0]}{R_i} = \frac{[X_0]}{2k_d[I][A]} \quad \text{Equation 2.12}$$

Where t_i ; inhibition time.

Re-ordering Equation 2.8 (neglecting term $k_x [X][M_n^*]$) gives $R_i = R_t$. R_i and R_t values gives;

$$2\delta k_d [I][A] = 2k_t [M_n^*] \quad \text{Equation 2.13}$$

It can also be presented as $[M_n^*]$:

$$[M_n^*] = \sqrt{\frac{\delta k_d [I][A]}{k_t}} \quad \text{Equation 2.14}$$

Placing $[M_n^*]$ from Equation 2.14 into rate of propagation Equation 2.4.

$$R_p = k_p [M][M_n^*] = k_m [M] \sqrt{\frac{\delta k_d [I][A]}{k_t}} \quad \text{Equation 2.15}$$

Rate of reaction at half-life (R_{t50}) is calculated from the reaction extent and presented as:

$$R_{t50} = \frac{d[M]}{dt} = \frac{d\xi C_f}{dt} = \frac{0.5 C_f}{t_{50} - t_i} \quad \text{Equation 2.16}$$

Where R_{t50} is the rate of reaction at half-life, C_f is the fraction of monomer conversion, ξ is the reaction extent. t_i and t_{50} are the inhibition and half-life. Half-life can be calculated from the above reaction extent and inhibition time. It is given by Equation 2.17.

$$t_{50} = \frac{0.5 C_f}{R_p} + t_i = \frac{0.5 C_f \sqrt{2k_t}}{k_p [M] \sqrt{2\delta k_d [I][A]}} + \frac{[X_0]}{2\delta k_d [I][A]} \quad \text{Equation 2.17}$$

2.2.6 Heat Rise

Discovery differential scanning calorimetry (DSC) (TA Instruments, Waters LtdTM, USA) was used to assess heat during the chemical cure of the experimental bone composite and the commercial PMMA (SimplexTM P).

The instrument operating parameters required approximately 300ml min⁻¹ base purge (for furnace heat regulation), and 50 ml min⁻¹ cell (sample chamber) purge of Nitrogen gas whilst running idle. The heating regime was programmed to run the following experiment parameters; a) To apply an equilibrium for 1 minute at 37°C followed by b) Isotherm at 37°C for 100 minutes in order to be able to capture thermal change as soon as samples were placed in sample cell.

Samples of PMMA (2.2.1.1) and experimental bone composite (2.2.2) were prepared and added 15-30 seconds after initial mixing into TzeroTM aluminium pans and then the weight of the sample was determined. The TzeroTM aluminium pan containing the sample was then subsequently crimped with a TzeroTM aluminium lid. The aforementioned program was simultaneously started as soon as the sample preparation had been completed. This was immediately followed by the placement of the crimped sample into the sample position within the cell.

The resulting thermal plot tracked the temperature and heat flow of the sample as a function of time. Changes in the thermal characteristics of the sample were determined relative to a reference TzeroTM aluminium pan and lid placed in the reference position adjacent to the sample. Due to the time lag, it was expected that an endotherm event would result shortly after the lid of the cell was opened in order to accommodate sample placement. Any exothermic heat flow and

temperature differentials which occurred due to polymerisation were expected to occur immediately following the endotherm.

The analysis of changes in temperature and heat flow of samples during the polymerisation step were conducted using the quantitative tools available within the software (TA instruments, Waters Ltd™, USA).

2.2.7 Composite Disc preparation

Pastes were prepared as described in section 2.2.2. Double barrel syringes were taken out of the fridge (4 °C) and kept at room temperature (20 °C) for 1 hour before preparing the discs. Paste was injected in 10 mm diameter and 1 mm thick moulds (Springmasters, UK) (Figure 2.2 D) at room temperature. The activator and initiator monomer pastes from separate barrels were mixed in the automatic mixing tip of the double barrel syringe. The mixed paste in the moulds were sealed top and bottom with acetate sheet and left over night at 20 °C to set. Number of discs of each formulation was test dependent (see below). Simplex™ P discs were prepared as described in section 2.2.1.1.

2.2.7.1 Sterilisation for in-vitro and in-ovo

Discs were sterilised using UV light (BonMay ®) exposure of 20 minutes on each side at 20 °C. 3 specimen discs were used per formulation per cell assay.

2.2.8 Mechanical Testing

In this project, biaxial flexural strength (BFS) and, Young's modulus (YM) were used to quantify the mechanical properties of the composite bone cements.

2.2.8.1 Biaxial Flexural Testing

Biaxial flexural testing was used to characterise the mechanical properties of the formulations. Composite materials are well known to be quasi-brittle which means the compressive strength of composite materials will be higher than the tensile strength (Borst, 2002). As a result failure is determined by the tensile strength of the material rather than the compressive forces (Havaladar, Pilli, & Putti, 2014). Determining the flexural strength includes various experimental methods. Below, some explanation on the background of flexural testing will be included, the advantages and limitations of biaxial testing compared to other flexural tests and finally the reasons for selecting the biaxial flexural test used for this project.

2.2.8.2 Biaxial Flexural Testing background

Under the ISO 5833-2008 (ISO for Implants for surgery — Acrylic resin cements), four point bending has been employed to determine the flexural strength of acrylic bone cements. Biaxial flexural testing has been used for the determination of flexural strength in many bone and dental cement materials (Boyd, Towler, Wren, & Clarkin, 2008; L. Chen, Yu, Wang, & Li, 2011; Chung, Yap, Chandra, & Lim, 2004; I. Mehdawi et al., 2009; Palin, Fleming, Burke, Marquis, & Randall, 2003). The comparison of various testing methods has

been a subject of much debate and research (Ban & Anusavice, 1990; Chung et al., 2004; Marquis, Palin, Fleming, Burke, & Randall, 2003). Uniaxial testing consists of simple stress state where stress alters linearly throughout the thickness of the material, where stress is uniaxial and the maximum tensile stress is on the bottom edge. 3-point bending has maximum stress occurring at one point while in 4-point bend test, a region of uniform tensile stress between the loading points is present. In biaxial testing the maximum stress is focussed on a small area on the underside of the specimen. The maximum stress acts across a larger volume in 4-point in comparison to 3-point bending and both are larger than biaxial testing.

Increasing volume space for maximum stress will increase the chance of inconsistent results (Kutz, 2002) thus making 3 and 4-point bending less reproducible than biaxial testing. With flexural beam testing, specimens required need to be larger thus resulting in the use of more material which increases cost. Specimens for beam testing are difficult to manufacture, which increases the possibility of error. The main drawback of beam bending flexural test is the false edge failure due to manufacturing flaws at the edge of beam specimens where maximum shear stress is subjected. Specimens prepared for biaxial testing, do not suffer from edge failures, they are easier to prepare and can be smaller. In the literature, one of the arguments for using biaxial testing is that for dental materials, biaxial flexure is more representative of occlusal stress state (Palin, Fleming, & Marquis, 2005).

This project is investigating materials for bone repair in osteoporotic vertebroplasty. In vertebroplasty the bone composite material is primarily in compression. For this project ball-on-ring biaxial method is used. Some of the assumptions behind the equation for biaxial strength include that the specimen is assumed to be 'thin', that is, the specimen is assumed to be thin enough that it is in a state of plane stress with no through thickness stresses developing. As a result the maths is significantly simplified and an analytical solution for the strength can be found. Commonly a 'thin' assumption requires the ratio of the radius to the thickness to go above 20. This aspect ratio is only four, in this project, so the values of strength found will be an overestimate of the true strength (Morrell, 1999). Therefore values of strength found via this method are suitable for comparison between different formulations tested in this way with this specimen geometry. However, they cannot be compared with values of flexural strength obtained from different specimen geometry or different test methods like 3-point bend tests. The biaxial method may not be ideal in terms of geometry, however in comparison to the 3-point and 4-point bending test; the justifications for this method such as increased reliability and reproducibility, ease of specimen manufacture, ability to use moulds that are cheap and disposable are enough.

2.2.8.3 Poisson's Ratio

Poisson's ratio measures the in-plane deformation relative to out of plane deformation. In biaxial testing when bending stress is applied to a material, it will expand and contract out of the plane of loading. The Young's modulus of the material is calculated using the applied load and the measured deflection. Therefore any Poisson's extension or contraction has to be considered and the

Poisson's ratio incorporated in the equation. Polymeric materials display viscoelastic behaviour (Gargallo, 2009). Their properties are time dependent (Nakayama, Hall, Grenoble, & Katz, 1974); and their stiffness is reliant on the strain rate; thus as the stiffness varies with time so does the Poisson's ratio. In the biaxial test for this project, the cross-head speed is 1mm/min thus strain rates are low. It is ideal to use a value for Poisson's ratio similar to that determined by low strain rate testing therefore Poisson's ratio of 0.3 has been used in this project.

2.2.8.4 Biaxial flexural strength test

Discs were prepared as described in section 2.2.7. Biaxial flexural strength was measured using a "ball on ring jig" with universal testing machine (Shimadzu AGSX, Japan) at a crosshead speed of 1 mm/min. The thickness of each sample was measured using a digital vernier calliper. The failure stress was recorded and BFS calculated using Equation 2.18.

$$\sigma_{\max} = \frac{P}{t^2} \left[(1 + \nu) \left(0.4851n \left(\frac{a}{t} \right) + 0.52 \right) + 0.48 \right] \quad \text{Equation 2.18}$$

Where:

σ is biaxial flexural strength (MPa), P is Maximum load (KN), a is support radius (mm), t is average thickness of specimen (mm) and ν is Poisson's ratio (0.3).

2.2.8.5 Young's modulus (YM)

A force versus displacement graph was used to calculate the Young's modulus using Equation 2.19 and 2.20.

$$E = \left(\frac{\Delta P}{\Delta W_c} \right) \times \left(\frac{\beta_c a^2}{t^3} \right) \quad \text{Equation 2.19}$$

$$\beta_c = -0.642 - 0.19m^{-3} + (0.5687 + 3.254m^{-3})x(1 - v^2) + [-0.3973 + 11.0513m^{-3} + (0.5223 - 7.8535 m^{-3}) (1 - v^2)]t^3 \quad \text{Equation 2.20}$$

Where E is elastic modulus of the specimen (MPa), $\Delta P / \Delta W_c$ = rate of change of load with regards to central deflection or gradient of force versus displacement curve (N/mm²), β_c is central deflection function, α is support radius (mm), t is ratio of support radius to the radius of disc, m is number of equally spaced supports, P is applied load (N) and ν is Poisson's ratio (0.3) (88).

2.2.9 In-vitro Studies With Experimental Bone Composite Discs

Assays were carried out on bone marrow derived sheep mesenchymal stem cells (MSCs) and MG63 cells. MSCs are the most investigated stem cell types. MSCs are isolated from the early-stage mesoderm and ectoderm, and they are pluripotent (Ullah, Subbarao, & Rho, 2015). MSCs have excellent proliferation and differentiation potential both in vivo and in vitro, and they can differentiate into any cell type, including osteoblasts (Gao et al., 2017). Due to sheep's similarity to humans, their low cost in comparison to other animals, they are usually used in orthopaedic research, particularly osteoporotic sheep

models (Music, Futrega, & Doran, 2018). Thus for the purpose of this project initial studies with these cells prior to animal studies was ideal before moving in to animal studies. For the purpose of this project it was thus reasonable to start initial studies with sheep stem cells that are multipotent progenitors with the potential to differentiate in to many specialised cells (Hughes, Chipara, Hall, Williams, & Grover, 2020).

MG63 cells are osteoblast cells derived from an osteosarcoma (Wilkesmann et al., 2020) and they are commonly used in bone tissue engineering.

The use of 2 different cell lines can demonstrate diverse or similar responses to a biomaterial. The environment where the bone composite is intended to be injected will also be exposed to an environment with different cell types. Native cells such as osteoblasts and potential stem cells.

A bioactive material allows for cell adhesion, affecting the stability and lifetime of the composite or can encourage tissue regeneration (Gutiérrez-Prieto et al., 2019).

2.2.9.1 Bone Marrow Derived Sheep MSCs

Sheep MSCs were cultured under standard conditions (37°C, 95% air, 5% carbon dioxide (CO₂), 95% relative humidity) in Dulbecco's Modified Eagle's Medium (DMEM), with 1000 mg glucose/L, L-glutamine, (Sodium Bicarbonate) NaHCO₃ and pyridoxine, hydrochloric acid (HCl) (SIGMA-ALDRICH), supplemented with 10% foetal calf serum and 1% penicillin /streptomycin. Passage number 2-3 was used for cytocompatibility studies.

2.2.9.2 MG63 Cells

MG63 (European Collection of Cell Cultures at the Health Protection Agency, Salisbury, UK) cells were cultured under standard conditions (37°C, 95% air, 5% CO₂, 95% relative humidity) in DMEM, with (Gibco®, Life Technologies Ltd., Paisley, UK) supplemented with 10% foetal bovine serum (FBS), 1% penicillin 1% of streptomycin at 37 °C.

2.2.10 In-ovo Chick Embryo Chorioallantoic Membrane assay (CAM)

This assay is a potential substitution for animal experimentation, where the material specimen under investigation is implanted on the extraembryonic membrane of the developing chick embryo. The in-ovo CAM assay is a low cost model, allowing quick screening of a large number of samples in a short time. The chick embryo is not considered a living animal from fertilisation until day 17. The stages of the developing embryo have been named by Hamilton and Hamburger as embryo development day (EDD)(I. Moreno-Jiménez, Kanczler, Hulsart-Billstrom, Inglis, & Oreffo, 2017). It is not innervated and experiments are terminated before the development of centres in the brain associated with pain perception thus no administrative procedure for obtaining ethics committee approval for animal testing is required (Inés Moreno-Jiménez et al., 2016). The CAM is found between the allantois and the eggshell. The egg shell is known to contribute to mineralisation as the chick embryo develops, as well as gas and waste exchange through the capillaries which form attachments to the egg shell at EDD 14. (I. Moreno-Jiménez et al., 2017). In this project specimen discs of varying formulations were implanted and integration of the material with the developing chick was assessed.

2.2.10.1 Preparation of CAM

Fertilised eggs were placed in an incubator under constant humidity at 37 °C. Chick eggs were incubated for a total of 14 days. At embryonic day (ED) 3, 2 ml of albumin was removed via needle syringe from the side of the egg. The hole was sealed with a tape and the egg was windowed (Figure 2.5). The removal of albumin detaches the CAM from the shell itself and the underlying CAM vessels

(I. Moreno-Jiménez et al., 2017). The window was sealed using sellotape to preserve amore physiological environment with the chick embryos staged according to Hamburger and Hamilton (Hamburger & Hamilton, 1951). Blood vessels in the CAM were scratched with a sharp blade until little bleeding was noticed and disc implants were placed on top. Discs were implanted at ED 7 followed by disc harvesting and humane euthanization of the chick embryo at ED 14. Implant discs were prepared and sterilised as described in section 2.7, 2.7.1 respectively.

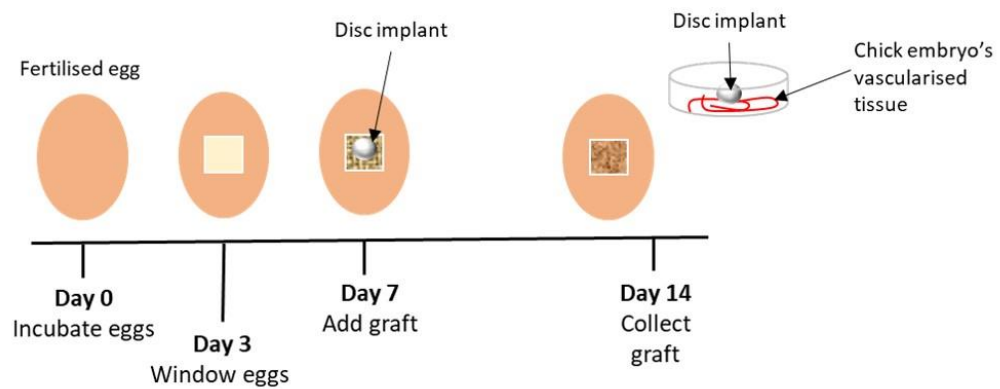


Figure 2.5 Time line presentation of CAM model

2.2.11 Scanning Electron Microscope

Scanning electron microscopy (SEM) was carried out using JSM-5410LV Scanning Microscope (Jeol, USA) INCA software.

SEM uses focused beam of electrons to create images of a materials surface. Electron beams pass through a high voltage, accelerating the beams. The accelerated beam passes through a sequence of gaps and electromagnetic lenses to produce a thin beam of electrons. Finally, the beam passes a scan coil, which scans the surface of the material and an image is obtained on the computer. The benefits of using SEM in this project meant the surface of specimen discs could be observed without the function of an objective lens unlike an optical microscope. As a result the magnification can be controlled over a range of about 6 orders of magnitude from 10 to 3,000,000 times. The specimens do have to be dried, and of a particular size. Images obtained are in grey however the detail and morphology is easily assessed.

All specimens used for SEM imaging in this project were mounted on stubs using double sided adhesive stickers. Discs were then coated with gold-palladium for imaging using sputter coating machine (Polaron E5000, East Sussex, UK) for 90 seconds at 20 mA. The SEM (Phillip XL-30, Eindhoven) instrument was operated with primary beam energy of 5kV and a current of approximately 200mA.

2.2.11.1 In-vitro Sample Preparation for SEM

For SEM imaging after each time point cells were fixed with 2.5% glutaraldehyde (Agar Scientific, UK) for 24 hours at 4 °C. They were then dehydrated at room temperature at (20 °C) in increasing concentrations of ethanol for 15 minutes each at 20 % ethanol, 50 %, 70 %, 90 % and 100%. Samples were finally dried by immersing in hexamethyldisilazane (TAAB Ltd, UK) in foil cups for 3 minutes with subsequent removal. Discs were left to air dry in a fume hood for an hour.

The discs and cells were sputter coated and analysed on SEM. Specimens were then coated with gold-palladium for imaging using sputter coating machine (Polaron E5000, east Susses, UK) for 90 seconds at 20 mA. The SEM (Phillip XL-30, Eindhoven) instrument was operated with primary beam energy of 5kV and a current of approximately 200 mA.

2.2.11.2 In-ovo Sample Preparation for SEM

Discs with tissue were fixed with 4 % Paraformaldehyde (PFA) overnight at 4 °C. They were then dehydrated and followed the rest of the same protocol as 2.2.11.1.

2.2.12 Antibody Staining

2.2.12.1 In-vitro

For antibody staining of cells, cells were washed 2 times in PBS at 37 °C and fixed in 4% formaldehyde in phosphate buffer saline (PBS) for 10 minutes at room temperature (20 °C). Cells were washed again 2 times with PBS for 1 and 5 minutes respectively. Cells were permeabilised with 0.5% Triton X-100 in PBS at

room temperature (20 °C) for 5-10 minutes. Cells were stained with 1:40 concentration of methanolic phalloidin (stains cells in actin) in PBS in the dark for 20 minutes. Hoechst stain (stains cell nucleus) was added to cells at concentration of 1:1000 in PBS and incubated for 10 minutes. Cells were imaged using a fluorescence microscope (Leica Microsystems, UK Milton Keynes, Buckinghamshire, UK).

2.2.12.2 *In-Ovo*

Discs with fixed tissue from the CAM assay were washed with PBS and fixed with 4% PFA overnight at 4°C. They were run through increasing sucrose concentrations (10, 20 and 30% in de-ionised water (dH₂O)) of which each change was left overnight at 4°C. Samples were rinsed with PBS and treated with blocking/permeabilisation solution 10% normal donkey serum (NDS)/0.5% (v/v) Triton X solution for 2 hours at room temperature. Primary antibodies were added and left to incubate overnight at 4 °C. Samples were rinsed 3 times for 5 minutes each with PBS plus 0.1% Tween 20 (PBST). Secondary antibodies were added, ZO-1, FLk-1, Pro Collagen 1 and Vimentin with Hoechst. Samples were left overnight at 4°C and rinsed the following day 3 times for 5 minutes each with PBST and store in PBS at 4°C. For imaging Ziess axio observer was used with the software Zen.

2.3 Statistical analysis

Data were analysed using Microsoft Excel Tools v. 16.46 for Mac (Windows, Ca, USA) and subsequently exported onto statistical software package SPSS v. 27 (IBM, Armonk, NY) where statistical inference tests were carried out. When data followed a normal distribution, parametric tests were conducted, to compare means across different groups in one-level (one-way ANOVA), or repeated measures across different time points (repeated measures ANOVA). When data did not follow a normal distribution, non-parametric Kruskal-Wallis H test was used. Post-hoc tests included Bonferroni or Games-Howell when data were heteroscedastic. All statistical inference tests were conducted at a significance level of 5% ($p < 0.05$).

Kinetics of Composite Formulation Settings

3.1 Abstract

The aim of this chapter was to evaluate how the varying levels of initiator, BP (3.5%, 3%, 2.5%, 2%, 1.5%, 1%, 0.5%) and activator, NTGGMA (2.1%, 1.8%, 1.5%, 1.2%, 0.9%, 0.6%, 0.3%) components of the experimental bone composite paste influenced conversion time. Additionally, the difference in temperature rise between an experimental bone composite formulation and the commercial PMMA (Simplex™ P) are compared.

FTIR allowed real time analysis of polymerisation and from this further information about inhibition time, half-life and final monomer conversion for different formulations were obtained and compared to a commercial PMMA product, (Simplex™ P).

The curing profiles and levels of conversion showed easily manageable manipulation by changing the levels of BP and NTGGMA and improved profiles in comparison to commercial products.

In conclusion the experimental formulations can be optimised easily to ensure desired setting kinetics.

3.2 Introduction

In previous studies experimental bone composites with a high polymerisation rate were developed by Main (2013) and Khan (2015). Final monomer conversion was achieved rapidly after inhibition time resulting in snap setting. This characteristic could be favourable because cement dissolution or wash out from the fractured site can be prevented.

Khan (2015) replaced DMPT with NTGGMA which resulted in increased monomer conversion of the experimental bone composites. Also Walters et al. (2016) demonstrated by replacing TEGDMA with a longer chain, higher molecular weight but lower crosslinking density-PPGDMA also increased monomer conversion (Walters, 2016).

Khan (2015) found that varying concentrations of BP and NTGGMA also influenced the mechanical properties of the experimental bone composites thus during mechanical tests the levels of BP and NTGGMA were kept consistent at 1.5% and 1% respectively in chapter 4. While Panpisut (2017) found this restriction a limitation as the inhibition time was far too short.

In this chapter levels of BP and NTGGMA were varied around 1.5% and 1% to see how much this influenced the experimental bone composite's delay time and final degree of conversion. Further the preferred final combination of BP and NTGGMA in the experimental bone composite was compared to two commercial products; Simplex™ P (PMMA) and Cortoss®.

3.3 Aims

This chapter aims to identify a formulation that can polymerise at an optimal rate for a vertebroplasty procedure, without risk of uncured monomers within the final material. Comparison with the commercial products; Simplex™ P and Cortoss® will be carried out to identify advantages or areas that can be manipulated by influencing inhibition time to improve the experimental bone composite without compromising monomer conversion. The monomer conversion of the experimental bone composite should be more than the current commercial products.

The shape of curing profile and level of cures will be established and the inhibition time (t_i) and time to 50% reaction (t_{50}) are to be quantified using FTIR.

3.4 Objectives

- From polymerisation equations (section 2.4.1.3), inhibition time will be calculated to see if it is proportional to the inverse square root of BP and NTGGMA wt % (Equation 2.11) which has been shown by Khan (2015).
- Reaction rate will be assessed with decreasing levels of BP and NTGGMA wt% (Equation 2.14).
- Observe final monomer conversion with increasing levels of BP and NTGGMA wt%.
- Inhibition time will be compared for experimental formulation in comparison to PMMA (Simplex™ P) and Cortoss®.
- Rate of reaction will be compared for experimental formulation in comparison to PMMA (Simplex™ P) and Cortoss®.
- Final monomer conversion for 2.5% BP and 1.5% NTGGMA will be compared with PMMA (Simplex™ P) and Cortoss®.
- Temperature change will be assessed during conversion for the commercial PMMA and the experimental bone composite formulations.

3.5 Materials and Methods

In this chapter formulations with varying levels of initiator and activator were assessed. The filler phase comprised of glass fillers 7 μm and 0.7 μm at ratio 4:5. The powder to liquid ratio was 3 to 1. Formulations were further refined and assessed compared to commercials.

Table 3.1 shows the BP and NTGGMA combinations in the first set assessed on the FTIR and Table 3.2 shows the combinations assessed in the second set.

Table 3.1 : Levels of BP and NTGGMA before mixing in composite monomer phase. Pastes were prepared using: UDMA (7.5 g), PPGDMA (2 g), HEMA (0.25 g). 4-META (0.3 g) was added in the initiator phase only.

Composition		BP2.5 (wt %)	BP1 (wt %)	BP0.5 (wt %)
Initiator	BP	0.5	1.0	2.5
Activator	NTGGMA	0.3	0.6	1.5

Table 3.2 Levels of BP and NTGGMA before mixing in composite monomer phase. Pastes were prepared using: UDMA (7.5 g), PPGDMA (2 g), HEMA (0.25 g). 4-META (0.3 g) was added in the initiator phase only.

Monomer Composition		BP3.5 (wt %)	BP3 (wt %)	BP2.5 (wt %)	BP2 (wt %)	BP1.5 (wt %)
Initiator	BP	1.5	2	2.5	3	3.5
Activator	NTGGMA	0.9	1.2	1.5	1.8	2.1

The curing profiles and degree of conversion were determined via FTIR (n=3) using intensity of spectral peaks identified as being involved in free radical polymerisation (see chapter 2; Materials and Methods).

3.6 Results

3.6.1 Monomer Conversion of Experimental Bone Composite

Figure 3.1 represents the degree of conversion during 1 hour of first three experimental composite formulas with increasing amounts of BP and NTGGMA

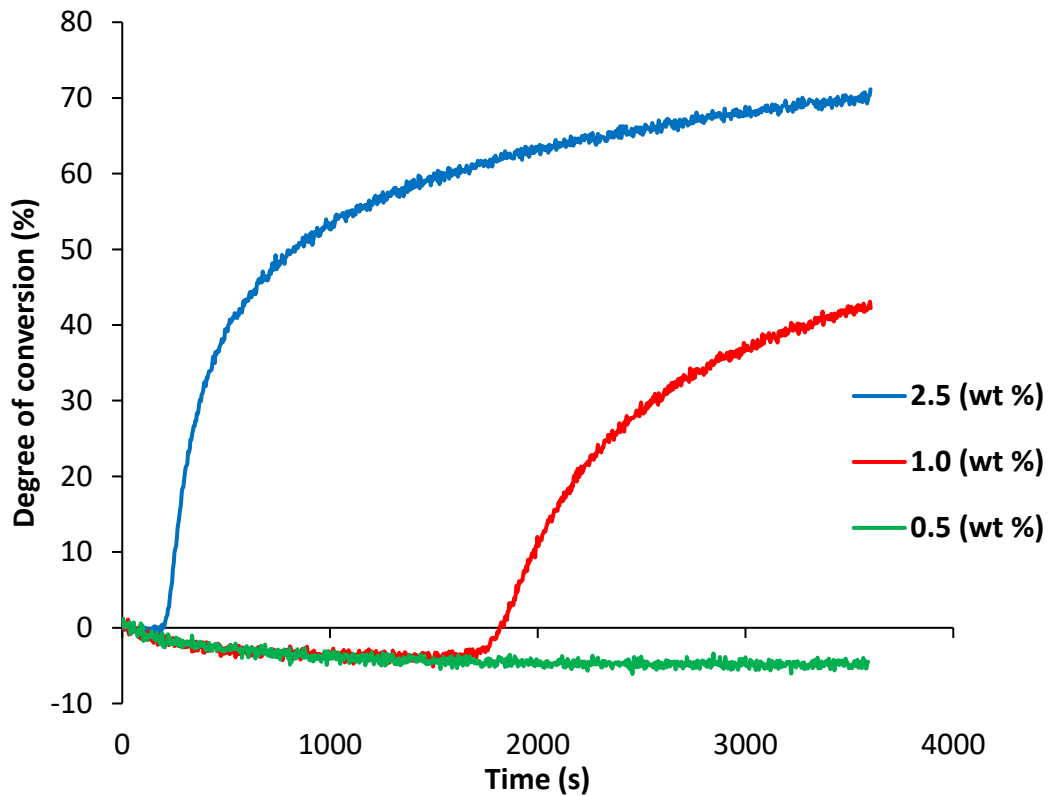


Figure 3.1 Monomer conversion (%) versus time (seconds) over 1 hour from mixing with increasing levels of BP (indicated on graph) in the initiator paste. Activator NTGGMA levels are 3/5 of BP wt%

Figure 3.2 represents the degree of conversion during 10 minutes of the second set of five experimental composite formulas (BP3.5-BP1.5) with increasing amounts of BP and NTGGMA.

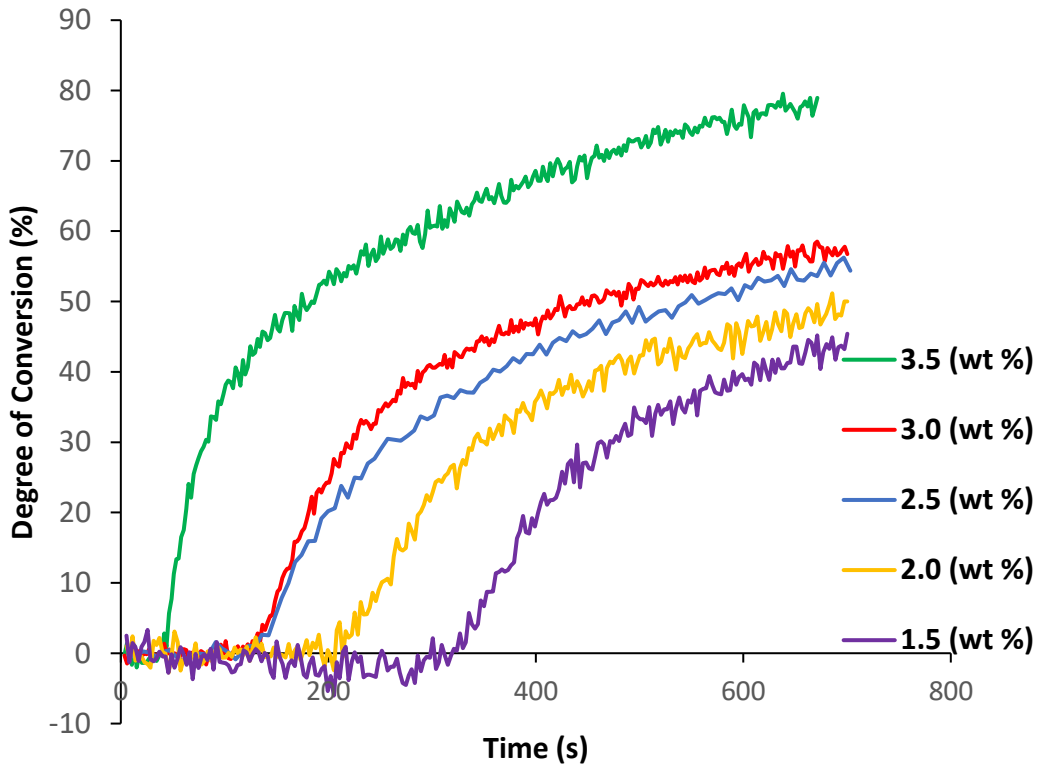


Figure 3.2 Monomer conversion (%) versus time (seconds) over 10 minutes with increasing levels of BP (indicated on graph). Activator NTGGMA levels are 3/5 of BP wt%

Final monomer conversion values calculated at 1 hour and by extrapolation to infinite time for 3 initial trial experimental bone composite formulations are given in Figure 3.3.

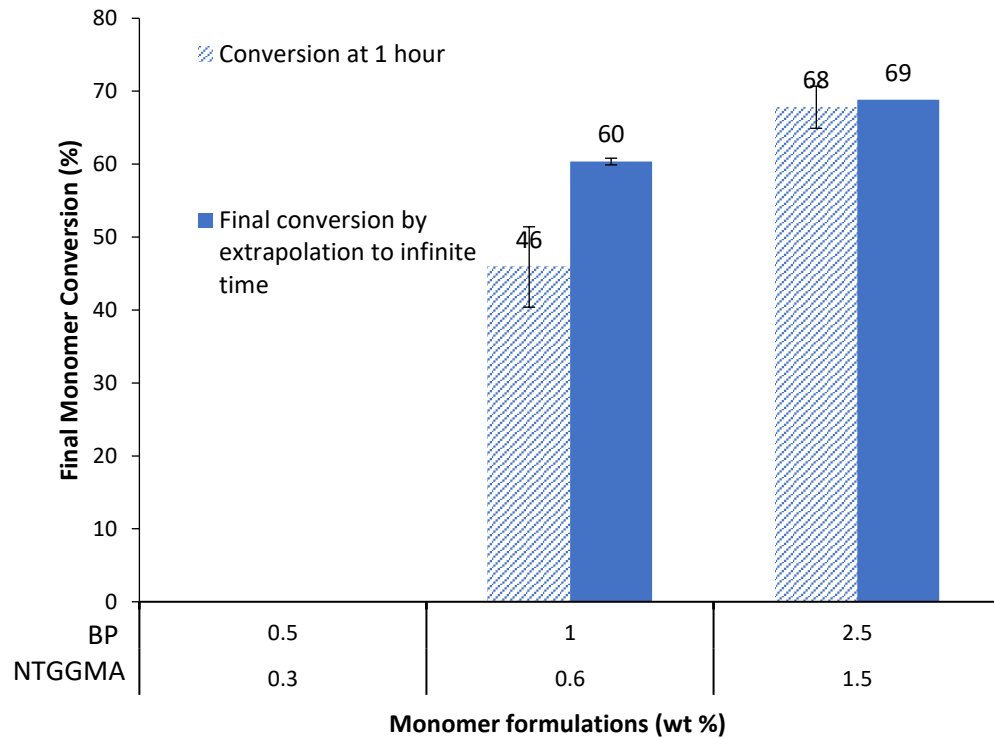


Figure 3.3 Final Monomer conversion values at 1 hour compared with final conversion values determined by extrapolation to infinite time. (Error bars = 95 % CI, n=3).

Final monomer conversion values after 10 minutes and calculated by extrapolation to infinite time for the 5 varying experimental bone composite formulations (BP3.5-BP1.5) are given in Figure 3.4.

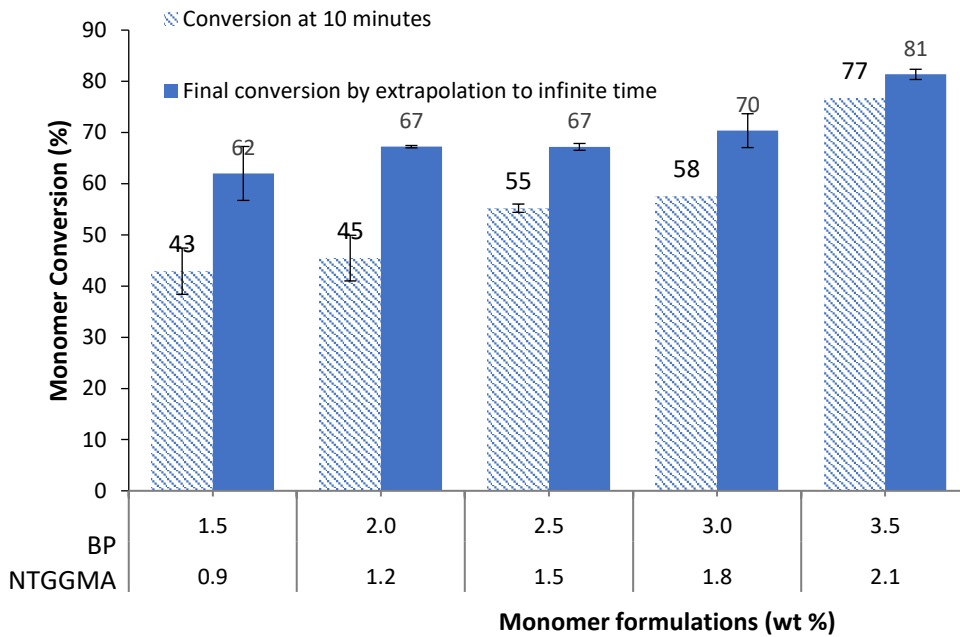


Figure 3.4 Final Monomer conversion values at 10 minutes compared with final values determined by extrapolation to infinite time. (Error bars = 95 % CI, n=3).

3.6.2 Inhibition Time and Half-life of Experimental Composites

Tables 3.3 and 3.4 show the inhibition time and half-life values for the 2 sets of composites with varying levels of BP and NTGGMA

Table 3.3 Inhibition time (t_i) and half-life ($t_{0.5}$) of experimental formulation with varying levels of initiator (BP) and activator (NTGGMA). BP and NTGGMA ratio was kept consistent at 5:3. FTIR analysis as performed at room temperature of 24 °C. Formulation contains fixed levels of monomers 70 %, UDMA 20 % PPGDMA. Monomer content was fixed at 25 % (PLR 3:1) (Error bars = 95 % CI, n=3).

Initiator (BP) (wt%)	Inhibition time (t_i) (s)	Half-life (t_{50}) (s)
0.5	N/A	N/A
1.0	1846 (± 11)	2467 (± 74)
2.5	218 (± 12)	441 (± 11)

Table 3.4 Inhibition time (t_i) and half-life(t_{50}) of experimental formulations with varying levels of initiator (BP) and activator (NTGGMA) further refined. BP and NTGGMA ratio was kept consistent at 5:3. FTIR analysis as performed at room temperature of 24 °C. Formulation contains fixed levels of monomers 70 %, UDMA 20 % PPGDMA. Monomer content was fixed at 25 % (PLR 3:1) (Error bars = 95 % CI, n=3).

Initiator (BP) (wt%)	Inhibition time (t_i) (s)	Half-life (t_{50}) (s)
1.5	308 (± 103)	591 (± 46)
2	257 (± 61)	450 (± 103)
2.5	125 (± 9)	266 (± 19)
3	133 (± 5)	251 (± 5)
3.5	43 (± 0.6)	109 (± 22)

Figure 3.5 represents the linear regression for the 2 sets of composites with varying levels of BP and NTGGMA. Table 3.5 and 3.6 show the gradients.

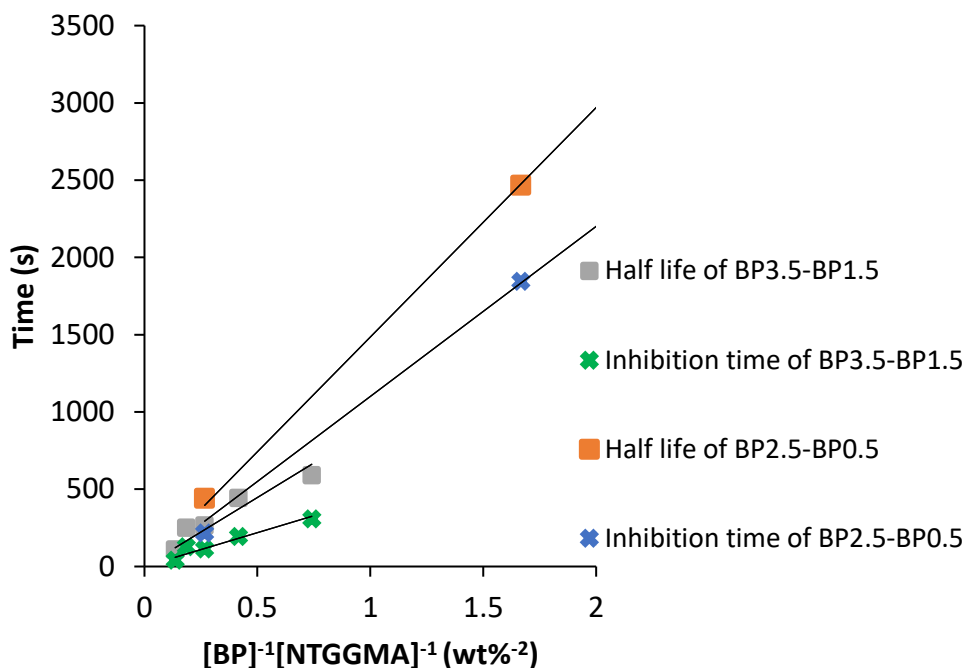


Figure 3.5 Linear regression analysis of half-life and inhibition time versus inverse concentration of BP and NTGGMA of the two batches. Data fits for high concentration, however there is significant curvature if there is low concentration.

Table 3.5 Gradients of the half-life time and inhibition time versus inverse BP and NTGGMA wt % with lower concentrations (BP concentrations from 2.5 to 0.5) (Error bars = 95%, CI, n=3)

Y (s)	X (wt% ⁻²)	Gradient (s.wt% ²)	R ²
Inhibition time	$[BP]^{-1}[NTGGMA]^{-1}$	1100	0.99
Half-life	$[BP]^{-1}[NTGGMA]^{-1}$	1484	0.99

Table 3.6 Gradients of the half-life time and inhibition time versus inverse BP and NTGGMA wt % (BP concentrations from 3.5 to 1.5) (Error bars = 95%, CI, n=3).

Y (s)	X (wt% ⁻²)	Gradient (s.wt% ²)	R ²
Inhibition time	$[BP]^{-1}[NTGGMA]^{-1}$	438	0.98
Half-life	$[BP]^{-1}[NTGGMA]^{-1}$	893	0.97

3.6.3 Rate of Polymerisation

The rate of reaction for the second set of experimental bone composites over 10 minutes is given in Figure 3.6.

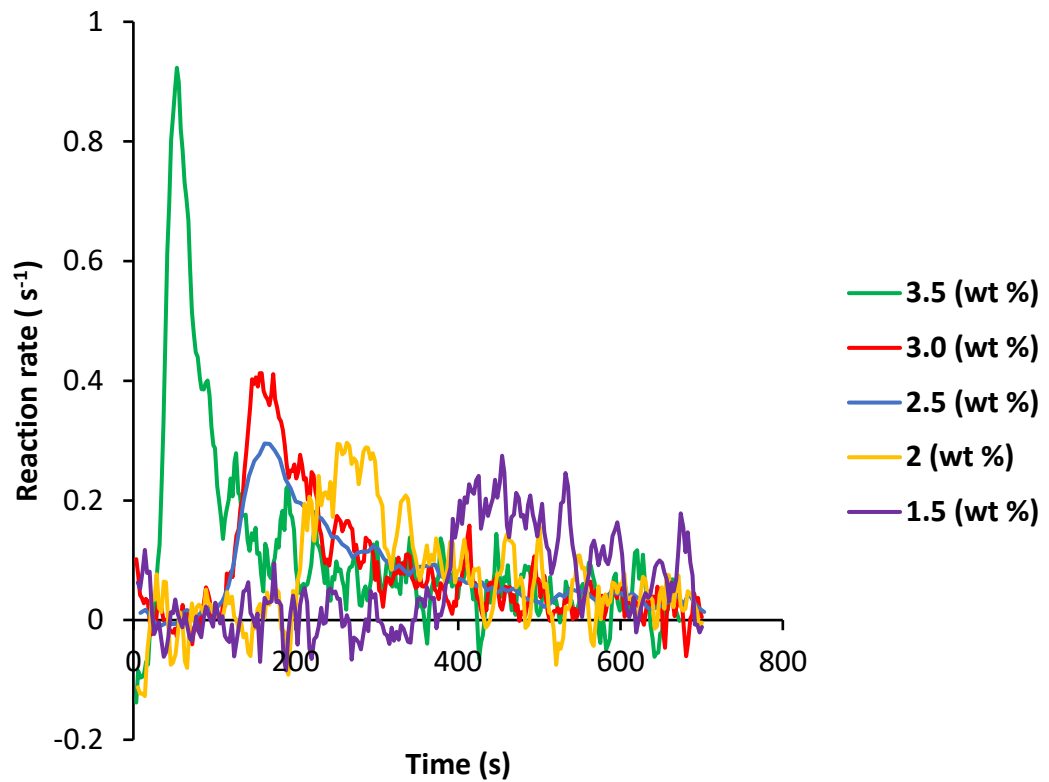


Figure 3.6 Rate of reaction (s^{-1}) of varying BP levels before mixing in composite paste from 1.5 to 3.5 wt %. BP, NTGGMA was kept at a consistent ratio of 5:3.

3.6.4 Monomer Conversion Comparison with Commercial Products

Figure 3.7 represents the degree of conversion for the experimental bone composite consisting of 2.5 % BP and 1.5 % NTGGMA, Cortoss[®] and PMMA.

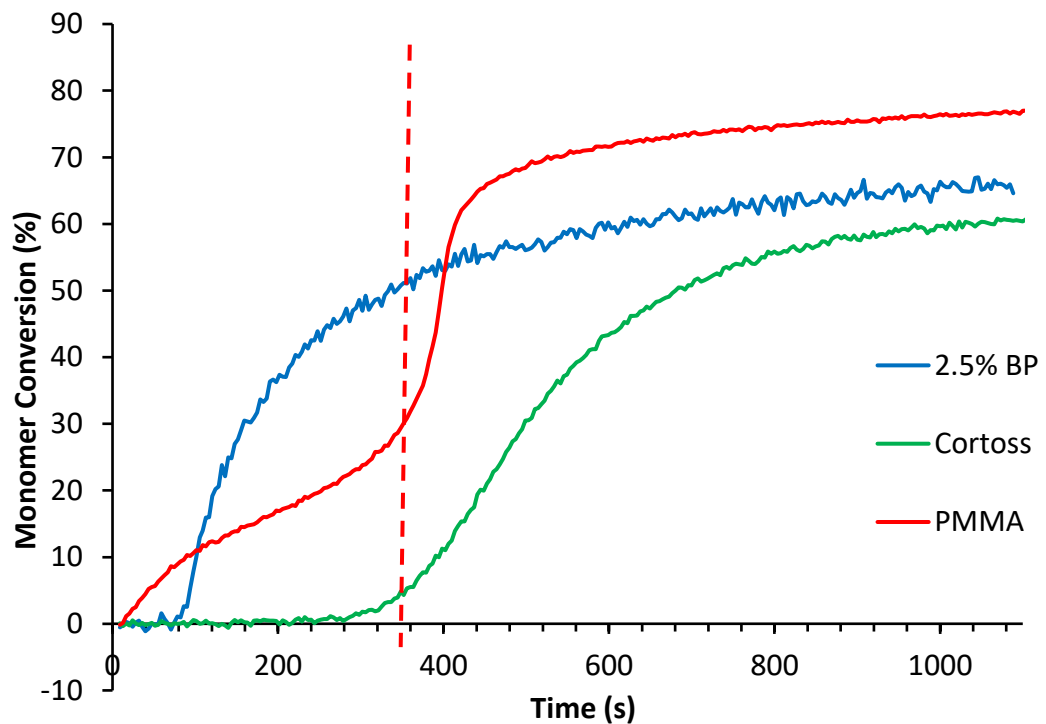


Figure 3.7 Monomer conversion of composite formulations with 2.5 % BP and 1.5 % NTGGMA compared with the commercial bone composite SimplexTM P (PMMA) and Cortoss[®]. PMMA data was collected by Dr. Piyapong Panpisut.

Figure 3.8 Demonstrates how the final amount of monomer reacted was calculated from extrapolation of data versus inverse time to zero for the experimental bone composite containing of 2.5% BP and 1.5% NTGGMA, Cortoss® and PMMA. The final conversion values are presented in Table 3.7.

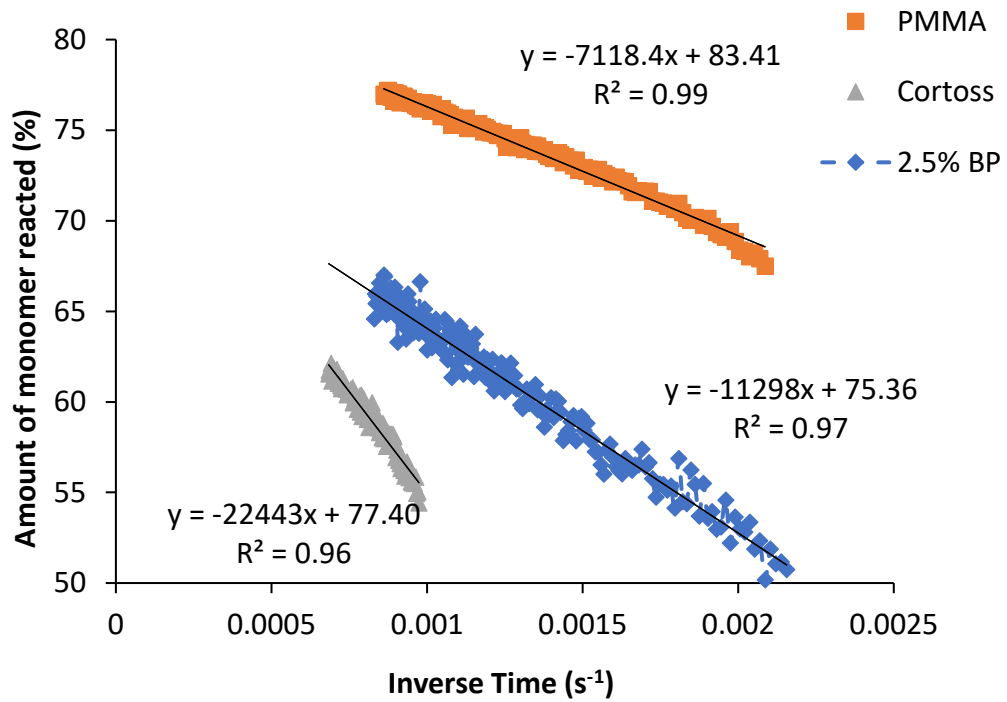


Figure 3.8 Percentage of monomer reacted vs inverse time (s^{-1}), for the formulation with 2.5 BP and 1.5 NTGGMA in initiator and activator paste respectively (%), Cortoss® and Simplex™ P (PMMA).

Table 3.7 Percentage final conversion for 2.5 % BP and 1.5 % NTGGMA formulation, Cortoss® and PMMA. (Data range employed, shown in Figure 3.8).

Bone composite/cement	Final conversion (%)	R ²
2.5 % BP	75	0.97
Cortoss®	77	0.96
PMMA	83	0.99

3.6.5 Inhibition Time and Half-life Comparison with Commercial Products

Inhibition time and half-life for experimental bone composite consisting of 2.5% BP and 1.5% NTGGMA, Cortoss[®] and PMMA are given in Table 3.8. Half-life is the time at which half of the final conversion is achieved. Cortoss[®] took the longest at 498 seconds (~8 minutes) while PMMA achieved half of final conversion at 105 seconds (1.75 minutes).

Table 3.8 Inhibition time (t_i) and half-life (t_{50}) of 2.5 % BP and 1.5 % NTGGMA formulation, Cortoss and PMMA (SimplexTM P) (n=3)

Monomer	Inhibition time (t_i) (s)	Half-life (t_{50}) (s)
2.5 % BP	125	266
Cortoss [®]	348	498
PMMA	359	105

Figure 3.9 represents the inhibition time for experimental bone composite consisting of 2.5% BP and 1.5% NTGGMA, Cortoss[®] and PMMA.

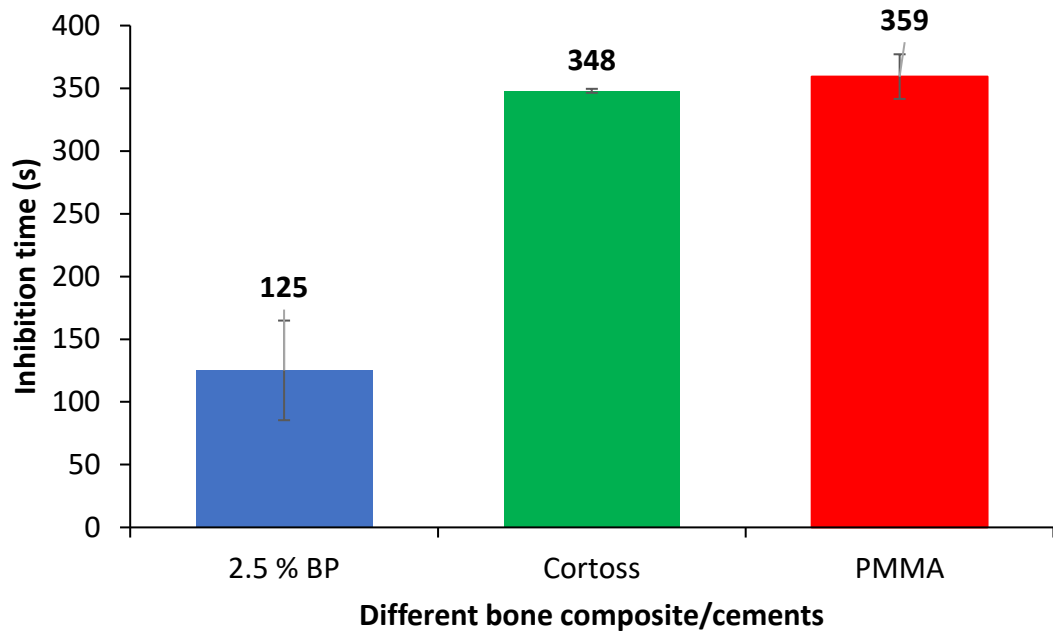


Figure 3.9 Inhibition time for 2.5 % BP and 1.5 % NTGGMA formulation, Cortoss[®] and Simplex[™] P (PMMA) (Error bars = 95 % CI, n=3). Significant difference between 2.5% BP and Cortoss and between 2.5% BP and PMMA ($p>0.001$).

3.6.6 Rate of Polymerisation Comparison with Commercial Products

The rate of reaction for the experimental bone composite consisting of 2.5% BP and 1.5% NTGGMA, Cortoss[®] and PMMA are presented in Figure 3.10. PMMA has a higher rate of reaction although it was later in comparison to the formulation consisting of 2.5% BP. PMMA has the highest mean maximum rate of reaction at 0.7 %/s at approximately 398 seconds (6-7 minutes). Cortoss[®] has a very slow rate of reaction and with the lowest mean maximum rate of reaction at 0.2%/s. This is not ideal since a lower rate of reaction increases the chance of the bone cement leaking from the administered site. The experimental bone composite's mean maximum rate of reaction was 0.5 %/s at 101 seconds (1.7 minutes).

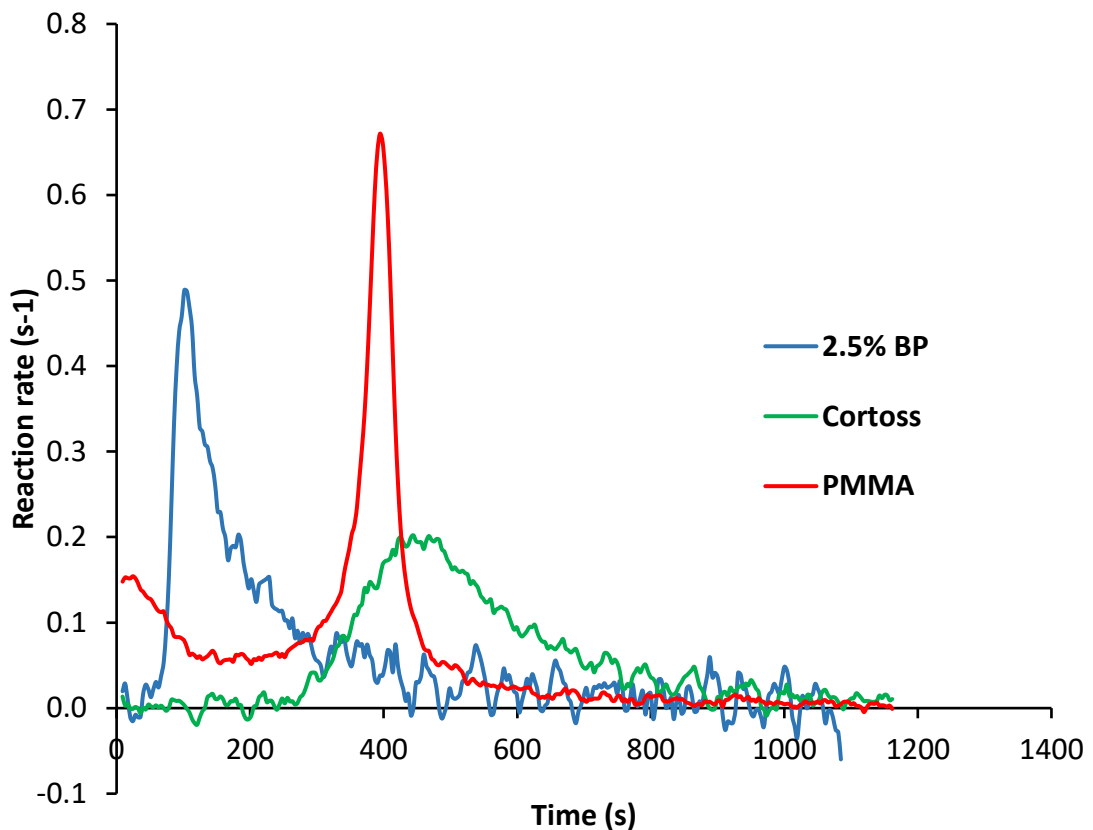


Figure 3.10 Rate of reaction (s^{-1}) of 2.5 % BP and 1.5 % NTGGMA formulation, Cortoss[®] and PMMA ($n=3$)

3.6.7 Temperature Rise Comparison of Preferred Formulation versus PMMA (Simplex™ P)

Figure 3.11 shows the temperature rise after activation of experimental bone (0.7 °C) composite and PMMA (6 °C).

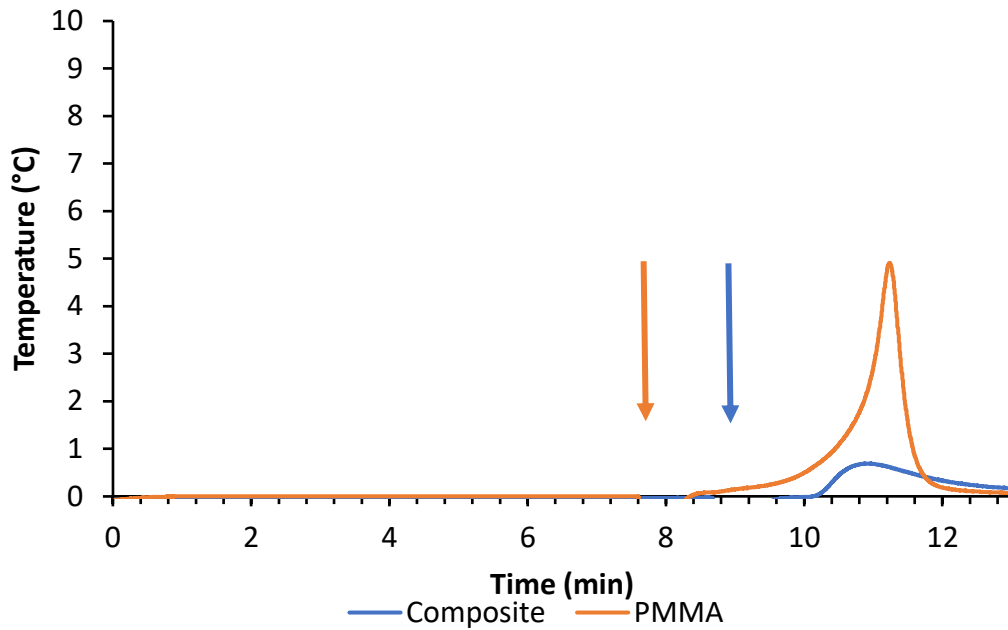


Figure 3.11 Heat rise of experimental composite (volume of composite ~44.7 cc. (2.5 % BP and 1.5 % NTGGMA) and Simplex™ P (PMMA) (volume of PMMA ~45.3 cc). Arrows indicate the time point at which the experimental composite and PMMA were added to the DSC chamber.

Table 3.9 presents the normalised enthalpy for the experimental bone composite and PMMA. PMMA dissipates more heat - 116 J/g - per unit weight (per gram) of sample to effect a greater change in temperature (6 °C), compared to the composite sample - 21 J/g - giving a 0.7°C temperature change.

Table 3.9 Comparison of enthalpy between commercial PMMA and Composite

Bone cement	Enthalpy (J/g)
Composite	21.7
PMMA	116.3

3.7 Discussion

3.7.1 Monomer Conversion of Experimental Bone Composite

The bone cement's setting time can be influenced by many external factors. Storage temperature, humidity, mixing conditions, mixing speed and handling of the cement can all influence setting time. In addition to this, operating room environments can vary. Hence all this can add up to very unpredictable set and working times in an otherwise very controlled surgical technique.

One method of controlling such influences is eliminating the method of surgeons having to manually mix the bone cement. The experimental bone composites do not require manual mixing. They are administered using a double barrel syringe directly at the site of interest. This administering method makes the procedure more efficient and less stressful for the surgeons.

It has been found that monomers can leak out from the required site during the inhibition time and after cure when less than 100% conversion is achieved. Uncured monomers are a problem. Until now no total conversion during polymerisation occurs in composites. There is a general consensus apart from a few exceptions, that uncured resin composite restorative materials are cytotoxic (Geurtsen, 1998a; Gupta, Saxena, Pant, & Pant, 2012). Very little information with respect to biological interaction between composite resin components in bone material and various tissues is available. MMA is an example of one such monomer that has

been reported to cause abnormalities or lesions in several organs (Gosavi, Gosavi, & Alla, 2010).

Also one must note that many dental materials are cured via light and the bone material is cured chemically. The clinical goal is to maximise the degree of monomer conversion via chemical cure and subsequently inhibit the elution of any unreacted components after treatment (Pomrink, DiCicco, Clineff, & Erbe, 2003). The level of monomer conversion should be more than in current products to reduce possible toxicity. If dimethacrylates monomers reach at least 50% conversion, it is enough due to cross linking resulting in 100% monomer reacted. This is not the case with the commercial bone cement Simplex™ P (PMMA) due to methacrylate monomers that do not cross link.

Decreasing BP and NTGGMA of 2.5% and 1.5% respectively by a little more than a half, delays monomer conversion by 30 minutes. Hence the final conversion for composite consisting of 1 wt% BP and 0.6 wt% NTGGMA, is not complete even after an hour (Figure 3.1) as the composite was still reacting. The FTIR analyses on the conversion was run for 1 hour where BP2.5 and BP1 showed final conversion at approximately 68% and respectively 46%. Composite consisting of 0.5 wt% BP and 0.3 wt% NTGGMA showed no conversion confirming the levels of BP and NTGGMA used in this amount are too low.

BP and NTGGMA in the second batch with 5 different formulation revealed final conversion by extrapolation to infinite time was not too different between BP levels in the first batch of 3 wt%, 2.5 wt% and 2 wt%, with monomer conversions at 70%, 67% and 67% respectively. BP amount at 3.5 % had monomer conversion at 81%.

Panpisut (2017) found increasing phosphates decreased the final monomer conversion of light cured paste. In bone composite Panpisut showed monomer conversion to increase by 5% upon increasing MCPM from 0-5 wt% or decreasing MCPM from 10 to 5 wt%. Earlier findings revealed, using TEGDMA instead of PPGDMA, decreased final monomer conversion (Kirsty Alexandra Ikrzycka Main, 2013) (M. A. Khan, 2015) (Walters, 2016). Due to TEGDMA having a lower molecular weight in comparison to PPGDMA's (P. Panpisut, 2017).

The experimental bone composites have dimethacrylates, which only require 50% conversion to bond all the monomer molecules together and prevent monomer leaching. The remaining 50% methacrylate groups cross-link the polymer chains. As the cross-linking reaction is slower than joining of monomers, 50% conversion of methacrylate groups is often a critical level at which monomer leaching declines (Piyaphong Panpisut et al., 2019). The monomer conversion over time desired by surgeons varies depending on their experience. The formulations allow for controlling the level of conversion by changing the levels of BP and NTGGMA, however further tests are required to see to what extent the remaining

components in the formulations influence the monomer conversion. The higher the final conversion for a methacrylate the lower the risk of leaching unconverted monomers. Signifying formulations with dimethacrylates will pose less toxicity to patients.

3.7.2 Inhibition Time and Half-life of Experimental Composite

Inhibition time translated to a clinical setting is the time the surgeon has to administer the composite to the fractured site i.e. working time. Sufficient working time allows adequate time for the surgeon to work with the material. If inhibition time is prolonged, risk of uncured monomers can leak, from the required site of application, leading to toxicity.

It can be shown that inhibition time is inversely proportional to BP and NTGGMA, assuming all the inhibitors have reacted before any polymerisation occurs, as observed in the linear regression in Figure 3.5. Half-life of the reaction showed a similar reliance on BP and NTGGMA levels. The half-life is therefore dominated by the inhibition period. Raising BP levels increases the concentration of free radicals. In turn, more free radicals mean more frequent molecular collisions (Collision theory).

Panpisut (2017) suggested the optimisation of BP and NTGGMA levels to allow inhibition time of the composite to be around 4-8 minutes. In this study, the combination of 1.5% BP and 1% NTGGMA resulted in 5 minutes of inhibition time.

Any combination higher is deemed too fast and lower amounts result in prolonged inhibition time. This is not a desired outcome in a clinical setting. Levels of 2.5% of BP in the 2 different batches show slightly different results, suggesting the presence of inhibitors influencing the reaction. Inhibitors can be found in monomers; a fresh batch will have active inhibitors where as an older batch of monomer will have used up inhibitors. Inhibition time is less in the second batch however final conversion is the same. This inhibition time for the first batch of 2.5% BP (218 seconds) is closer to 2.0% BP inhibition time (257 seconds) in the second batch, suggesting the difference in between the batches is most likely due to old inhibitors.

3.7.3 Rate of Polymerisation

Increasing levels of BP shows the higher the rate of reaction, with decreasing levels of BP the rate of reactions is lower and delayed (Figure 3.6). The highest combination of BP and NTGGMA had the highest rate of reaction after 1.5 minutes while the rest of the reducing levels of BP and NTGGMA displayed lower reaction rates at delayed times. A composite with high rate of reaction means the composite will polymerise immediately upon administration at the fractured site. Therefore reducing the risk of leakage or wash out by physiological fluid (Yu et al., 2013). Slow setting calcium phosphate cements often demonstrate a reduction in strength due to washout (F. Chen, Song, & Liu, 2015), leading to complications such as pulmonary cement embolism.

Ultimately an ideal composite should have a fast rate of reaction with controllable inhibition time. Main (2013) demonstrated, however that it can be difficult to

disentangle rate of reaction and inhibition time; increase in inhibition time results in slower rate of reaction.

3.7.4 Monomer Conversion Comparison with Commercial Products

The clinical goal is to maximise the degree of monomer via chemical cure and subsequently inhibit the elution of any unreacted components after treatment

Unreacted monomers are known to leak out of PMMA cement during induction time and after cure when less than 100% conversion is achieved. Uncured monomers are a problem. Until now no total conversion during polymerisation occurs in composites. There is a general consensus apart from a few exceptions, that resin composite restorative materials are cytotoxic (Geurtsen, 1998b, 2000). Most of the data is from dental research as most of the components are used in dental materials and very little information with respect to biological interaction between resin components in bone material and various tissues is available. Resin-based dental restorative materials are extensively used in bone fixtures. MMA is an example of one such monomer that has been reported to cause abnormalities or lesions in several organs (Gosavi et al., 2010).

Final monomer conversion was higher for PMMA (Figure 3.7). PMMA's conversion profile shows a kink during conversion unlike Cortoss[®] and the experimental bone composite. Cortoss[®] consists of Bis-GMA while the main monomer in the experimental composite is UDMA. However it has been shown

UDMA has higher conversion in comparison to Bis-GMA (Gajewski, Pfeifer, Fróes-Salgado, Boaro, & Braga, 2012). In addition Bis-GMA based composites have been found to have about 65% conversion (Lu, Trujillo-Lemon, Ge, & Stansbury, 2010). The difference in the conversion values could be due to UDMA's flexible backbone consisting of weaker hydrogen bonding given by the urethane groups (Gajewski et al., 2012; Gonçalves, Pfeifer, Stansbury, Newman, & Braga). In addition Bis-GMA is very hindered, due to the presence of strong hydrogen bond interaction within Bis-GMA (Lemon, Jones, & Stansbury, 2007).

The data for PMMA is not representative of the actual final conversion since the initial recordings are not due to polymerisation. The early recordings are actually due to the polymer dissolving in the monomer. Commencing the mix, the polymer does not make contact with the diamond on the FTIR, as the polymer dissolves the contact becomes better and this appears as if the MMA is polymerising. The point of inflexion is where the polymerisation starts. This is showing the polymer is expanding and while it is occupying space the polymerisation is delayed. Initial time of reaction starts after the polymer stops expanding at approximately 5-6 minutes.

PMMA has monomethacrylates, which require 100% conversion to prevent monomer release. The experimental bone composites have dimethacrylates, which only require 50% conversion and the remaining 50% monomers cross-link.

In this study PMMA only went up to 80%. This can be explained by the glass transition (T_g) temperature of PMMA of 105°C (Ashby, 2004).

During polymerisation of PMMA the glass transition temperature keeps increasing due to reduction of monomers. When the glass transition temperature matches room temperature the mixture will change from a highly viscous paste to glass. This will result in the reaction rate slowing substantially because the molecules move less readily. It would be ideal to know what ratio of polymethyl methacrylate to methyl methacrylate gives glass transition temperatures close to body temperature. The proportion of solid PMMA to liquid MMA initially was 2 to 1. Therefore when 80% of MMA is polymerised, the mixture will be 2.8 : 0.2, polymer : monomer which is equivalent to 6.7% monomer. As this study was carried out at room temperature, the final monomer content should be less at body temperature thus the final conversion would also be higher than 80%.

The higher the final conversion the lower the risk of leaching unconverted monomers. Further studies with varying levels of other components should be assessed to see how much monomer conversion is affected.

3.7.5 Inhibition Time and Half-life Comparison with Commercial Products

Inhibition time was longer for Cortoss[®] 348 seconds (5-6 minutes) in comparison to the experimental bone composite 125 seconds (2 minutes) (Table 3.8). Cortoss[®] working time have been studied in the group prior by Main (2013) who found the working time to be approximately 2-3 minutes. Khan (2015) also found Cortoss[®] working time around 4 minutes and Panpisut found it to be approximately 3 minutes.

Inhibition time for PMMA isn't applicable for the same reasons mentioned in section 3.7.4 due to monomer and polymer dissolving initially. According to

Dunne et al for calcium phosphate cements the initial setting time is 3-8 minutes at which the cement must be injected prior to this (O'Hara, Buchanan, & Dunne, 2014).

Khan (2015) previously demonstrated, inhibition time was inversely proportional to concentration of BP and NTGGMA. Thus increasing these components can increase inhibition time in comparison to commercial or vice versa. According to Panpisut (2017) the levels of BP and NTGGMA here 2.5% and 1.5% are too high. Inhibition time doesn't need to be as long as commercial PMMA since the experimental bone composite is directly injected at the fractured site via a double barrel, preloaded syringe, thus it does not require as much working time as bone cement such as PMMA. Average working time of PMMA (Simplex™ P) is 10-12 minutes (Stryker, 2021). The working time (period which the cement can be manipulated) is generally recommended for 5-8 minutes. Use of mechanical introduction tools, i.e. syringes can increase this time by 1 to 1.5 minutes (Rajesh Kumar Ranjan, 2017).

This study proves the experimental bone composite's inhibition time can be manipulated in comparison to the commercial cements. Inhibition time can be increased from 125 seconds (2 minutes) to 257 seconds (4 minutes) by decreasing BP from 2.5% to 2% and NTGGMA from 1.5% to 1.2%. However it is important to remember, decreasing initiator and activator also influences final monomer conversion.

3.7.6 Rate of Polymerisation Comparison with Commercial Products

Low rate of reaction increases the chance of the bone cement or composite leaking from the administered site. The experimental bone composite's rate of reaction is lower than PMMA but higher than Cortoss[®]. This could be due to Cortoss[®] monomer; Bis-GMA's intermolecular hydrogen bonding in conjunction with the high molecular weight monomer, causing low double bond conversion (Izabela Maria Barszczewska-Rybarek, 2019).

The experimental composite consists of mono-methacrylates. Theoretically, the degree of conversion of PMMA is a direct measurement of the number of monomers polymerised. Since all of the monomers in the experimental bone composites are dimethacrylate unlike PMMA, the experimentally derived degree of conversion is not indicative of the number that have reacted (Zafar, 2020).

Unlike PMMA, the composite consists of dimethacrylates which allows cross-linking. Upon initiator and activator mixing, the free radical reaction starts a chain reaction, joining single monomer molecules together in long linear polymer chains.

Ideally a bone cement with a high reaction rate would be desired to prevent leakage from the administered site, but training would be required for surgeons if bone fixtures were to set quickly. In addition high conversion is desired to decrease toxicity and to increase mechanical properties. Panpisut (2017) was able to demonstrate how temperature could be used to

control the rate of polymerisation. He found inhibition time to slightly increase upon ageing, possibly due to loss of initiator or activator.

3.7.7 Temperature Rise Comparison of Preferred Formulation versus PMMA (Simplex™ P)

Damage to bone due to the exothermic polymerisation of PMMA remains a concern. PMMA is known to have a rise in temperature at the interface with bone, which often leads to a fibrous capsule around the cement bulk. (McMahon et al., 2012) A recent study was carried out by Armand et al where temperature after cement injection was measured and found the temperature to rise after 12 minutes (Farvardin, Nejad, Pozin, Armand, & Asme, 2019). While the study was carried out on the proximal femur and temperature rise was 10°C, the timing and temperature in the experiment above was also after 10 minutes and at 5°C. However temperature cannot be compared directly since it is governed by the amount of material.

PMMA is known to increase in temperature upon activation and literature has shown many times PMMA's rise in temperature. This has been shown in the study where PMMA appears to have a higher rise in temperature in comparison to the experimental composite. While the experimental bone composite (volume ~44.7 cc) showed a temperature rise of approximately 1°C in temperature the PMMA (volume ~45.3 cc) displays a higher rise in temperature 6°C. Heat generation is proportional to the fraction of polymerisation and concentration of monomer per unit volume. If powder content is increased or final conversion is doubled, this will increase the heat generation. In a clinical setting

The amount of composite that may be used is increased therefore the heat generation also increases.

There's a greater heat output overall generated from PMMA when it undergoes setting in comparison to the same volume of composite. Studies thus far have not been conducted to correlate the changes in release of components with temperature in particular antibiotics. The process of polymerisation of the cement is an exothermic reaction, with temperatures up to 60°C – 80°C thus any incorporation of antibacterial agent must be chemically and thermally stable. This shouldn't be an issue for the experimental bone composite (Phull, Yazdi, Ghert, & Towler, 2021).

3.8 Conclusions

- Monomer conversion increased with increasing levels of BP and NTGGMA wt%.
- Inhibition time was proportional to the inverse square root of BP and NTGGMA wt% (Equation 2.11).
- Reaction rate decreased with decreasing levels of BP and NTGGMA wt%.
- Monomer conversion for 2.5 % BP and 1.5 % NTGGMA was higher than PMMA (Simplex™ P) but lower than Cortoss®.
- Inhibition time was shorter of experimental formulation in comparison to Cortoss®.
- Rate of reaction was higher of PMMA (Simplex™ P) than experimental bone composite and Cortoss®.
- Temperature rise during conversion for the commercial PMMA was higher than the experimental bone composite formulations.

Mechanical and Dimensional Properties of Optimised Formulations

4.1 Abstract

MCPM and PLS were incorporated in to the experimental bone composite (UDMA (7.5 g), PPGDMA (2 g), HEMA (0.25 g). 4-META (0.3 g) was added in the initiator phase only) to contribute towards mineralisation and antibacterial properties.

The aim of this chapter was to assess how MCPM (4 vs 8 wt%) and PLS (5 vs 2 wt%) in the filler phase influenced the mechanical and chemical properties of the experimental bone composite.

Experimental bone composites were prepared as discs and immersed in deionised water or simulated body fluid (SBF) over a period of 3 months. Discs were weighed in air versus water to calculate their mass and volume change in water. Additionally, pH change was monitored. Biaxial flexural strength and Youngs modulus was determined at 24 hours, 7 days, 1 month and 3 months. SEM was used to observe visual changes on the disc surfaces to investigate mineralisation.

Mass increased initially but after 2 weeks it plateaued for a further 2 weeks for all formulations. Volume increased after 2 weeks but then decreased for a further 2 weeks for all formulations. 8% MCPM and 5% PLS combination showed highest increase in mass and volume change, followed by 8% MCPM 2% PLS, 4%

MCPM and 5% PLS and least increase in mass and volume change in 4%. MCPM 2% PLS. Alongside this pH decreased for all combinations with the highest ion concentration due to 8% MCPM and 5% PLS combination. The strength of the discs and the Youngs modulus decreased for all combinations. Remineralisation occurred on the surface of all discs, however after 1 month discs with 8% MCPM displayed mineralisation visually very similar to hydroxyapatite like minerals.

In conclusion higher combinations of MCPM and PLS showed greater effect on mass and volume change as well as pH, strength and Youngs modulus. Remineralisation was also most notable with higher levels of MCPM.

4.2 Introduction

In chapter 3 the conversion profiles were established for varying levels of BP and NTGGMA combinations and compared with two commercial bone cements; Cortoss[®] and Simplex[™] P (PMMA). The setting phase is dependent on the amount of BP and NTGGMA and after setting MCPM and PLS contribute to mineralisation and antibacterial properties.

In this chapter, combinations of formulations were used with varying levels of MCPM (8 or 4 %) and PLS (5 or 2 %) in the filler phase. Incorporation of calcium phosphate (CaP), specifically MCPM has potential to promote self-healing of the fractured spine, much like the dental fillers for decayed tooth structures (Idris Mehdawi et al., 2009).

High mass and volume increase is due to water sorption whilst a decline may indicate MCPM and PLS release. Aljabo (2015) demonstrated mass and volume change results were strongly influenced by calcium phosphate addition. A previous study showed increasing levels of PLS encouraged water sorption too (Liaqat, 2015). In addition a decrease in pH could be an indication of proton release from MCPM.

Aljabo (2016) showed apatite precipitation on dental composites to be proportional to time and calcium phosphate content. Previous studies have shown MCPM with β -TCP can form brushite and phosphoric acid upon reacting with water.

The brushite may transform in to calcium deficient hydroxyapatite(Rocha et al., 2018). BFS has been found to decrease with increasing amounts of calcium phosphates and PLS (Liaqat, 2015) due to their water sorption properties. After after 3 months, however strength can level with the final BFS comparable to commercial bone cements (Kirsty Alexandra Ikrzycka Main, 2013).

This chapter investigates how the different combinations of MCPM and PLS affect the dimensional and mechanical properties of the experimental bone composite.

4.3 Aims

This chapter aims to look at the individual and combined effects of MCPM and PLS on the mechanical and chemical properties of the experimental bone composite over a certain period of time.

4.4 Objectives

With increasing MCPM (from 4 to 8 wt%) and PLS (from 2 to 5 wt%) of the powder phase:

- Mass and volume change will be assessed over time (24 hours, 3 days, 1 week, 2 weeks, 3 weeks and 1 month).
- pH change will be assessed over time.
- SBF will be assessed over 1 month.
- Mineralisation on disc surface after storage in SBF for 1 month will be observed.

4.5 Materials and Methods

Table 4.1 presents the 4 formulations with varying amounts of MCPM and PLS added to the monomer phase (UDMA (7.5 g), PPGDMA (2 g), HEMA (0.25 g). 4-META (0.3 g) was added in the initiator phase only).

Table 4.1 MCPM and PLS percentages added to initiator and activator paste fillers in formulations 1-4. (Monomer phase: UDMA (7.5 g), PPGDMA (2 g), HEMA (0.25 g). 4-META (0.3 g) was added in the initiator phase only. 2.5 % BP and 1.5 % NTGGMA. Glass filler: 7 μ m and 0.7 μ m ratio 4:5. PLR 3:1)

Formulation	Amount (wt% of filler)	
	MCPM	PLS
1	4	2
2	4	5
3	8	2
4	8	5

4.5.1 Discs for Gravimetric and Volumetric and pH Analysis

Discs were prepared as described in section 2.7. Discs were immersed in 10 ml deionised water within a sterile tube. Tubes were incubated at 37 °C for 3 hours, 24 hours, 3 days, 7 days and 1 month. At each time point, discs were removed from the original solution, their surface carefully dried by contact with absorbent tissue and weighed using a four digital balance with a density kit (OHAUS Pioneer, UK). Discs were also weighed in 1% sodium dodecyl sulphate solution. After weighing, discs were placed in fresh 10 ml of de-ionised water and incubated until the next time point. The percentage mass (M) and volume change (V) were determined using Equation 4.1 and Equation 4.2 respectively.

Furthermore, density (ρ_t) of each disc was determined using specimen mass in air and in water (Archimedes principle) (Equation 4.3) (Ambard & Mueninghoff, 2006).

$$M = \frac{100(M_t - M_0)}{M_0} \quad \text{Equation 4.1}$$

$$V = \frac{100(V_t - V_0)}{V_0} \quad \text{Equation 4.2}$$

$$\rho_t = \left[\frac{M_t}{M_t - M_w} \right] \times \rho_w \quad \text{Equation 4.3}$$

After each time point the pH was measured using a calibrated pH metre (Orion star A111, Thermo Scientific). The concentration of hydrogen ions in deionised water was calculated using Equation 4.5.

$$pH = -\log_{10} [H^+] \quad \text{Equation 4.4}$$

$$H^+ = 10^{-pH} \text{ mol/l} \quad \text{Equation 4.5}$$

The cumulative concentration of Hydrogen ions released from the discs was estimated using Equation 4.6.

$$[H^+] \text{ release} = \Sigma([H^+]_s - [H^+]_{dw}) \quad \text{Equation 4.6}$$

Where $[H^+]_s$ is the concentration of acid in the water in which the sample was stored, $[H^+]_{dw}$ is acid level found in deionised water and \sum indicates the sum over all solutions in which the sample was stored up to time t .

4.5.2 Discs for Biaxial Flexural Strength Test and Youngs Modulus

For the biaxial flexural strength test and Youngs Modulus each disc was immersed in 10 ml of simulated body fluid (SBF) at 37 °C in a 50 ml self-standing centrifuge tube. SBF was prepared according to ISO for implants for surgery. In vitro evaluation for apatite-forming ability of implant materials (ISO 23317:2012). 5 different time points were chosen; 0 hours, 24 hours, 7 days, 1 month and 3 months. 6 specimen discs were used for each time point of each formulation. Specimens with defects detected visually with the eye on the surface were excluded.

4.5.3 Discs for SEM

Surface of discs was assessed for calcium phosphate layer formation. Three discs of each formulation were incubated in 10 ml SBF at different time points; 0 hours, 24 hours, 7 days, 1 month and 3 months for 37 °C. Discs were sputter coated as described in methods chapter section 2.2.11.

4.5.4 Factorial Analysis

Factorial analysis for the two variables (each at high and low levels) was used to assess effect of MCPM (8 wt% versus 4 wt%) and PLS (2 wt% versus 5 wt%)

on mass change, volume change, pH change, biaxial flexural strength, Young's modulus.

4.6 Results

4.6.1 Mass and Volume change

Mass change plotted against square root of time shown in Figure 4.1. Formulations consisting of high low combinations of MCPM and PLS with fixed amount of monomers, fillers and initiator and activators. At first there was a fast mass increase in all the formulations for the first 24 hours. All formulations display a gradual increase in mass change. Formulations with higher levels of MCPM at 8% show bigger increase in mass change in comparison to formulations with lower levels of MCPM at 4%. Repeated measures ANOVA showed that time has indeed a significant impact on the mean mass change ($p < 0.001$) as the formulation ($p = 0.011$), while the interaction effect between the formulation and the time did not ($p > 0.05$).

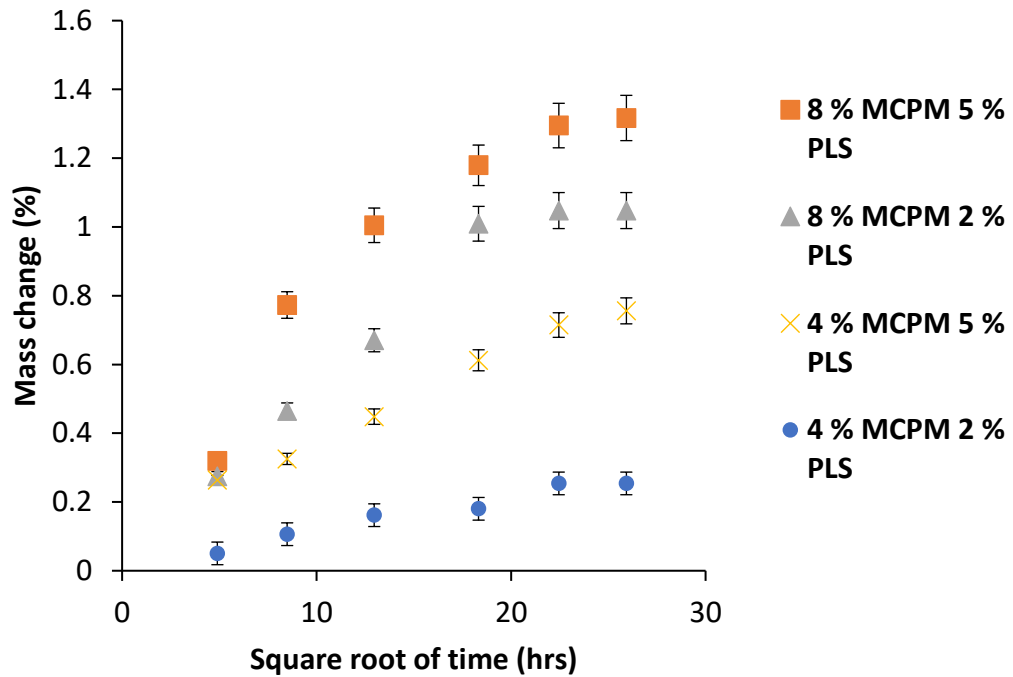


Figure 4.1 Mass change plotted against the square root of time. Samples have varying levels of MCPM and PLS and were kept in distilled water. (Error bars = 95 % CI n=3). Significant differences found, 8% MCPM 2 % PLS vs 4 % MCPM 4 % PLS (Games-Howell, $p=0.006$)

Volume change over a month in deionised water for experimental composites plotted versus square root of time is presented in Figure 4.2. The volume increase with 8 % MCPM and 5 % PLS was highest ~3 %. The maximum change in volume can be seen in the initial 24 hours, followed by a decline between 2 and 4 weeks. Repeated measures ANOVA showed that time has indeed a significant impact on the mean volume change ($p=0.001$), while the interaction effect between the formulation and the time did not ($p>0.05$).

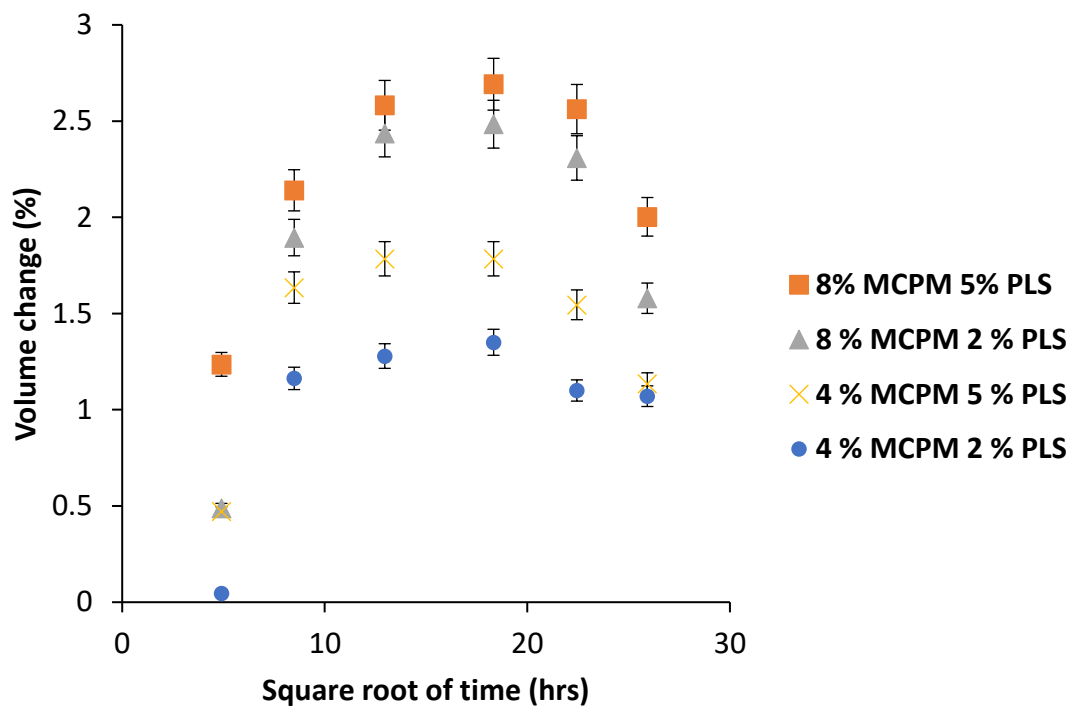


Figure 4.2 Volume change (%) of discs with varying levels of MCPM and PLS in distilled water plotted against square root of time (hrs). (Error bars = 95 % CI n=3). There was no significant differences found between the different formulations ($p>0.05$).

Factorial analysis of mass change and volume change after 1 month is presented in Figure 4.3. With increasing levels of MCPM, mass increases by 190%. With increasing levels of PLS mass change increases by 89%. When MCPM and PLS are both high or low the mass change is on average reduced by 24%. (B) Volume change after 1 month; with increasing levels of MCPM volume change increases by 65%. With increased levels of PLS volume change decreases by 11% but there is an interaction effect showing MCPM and PLS both high or low, increases volume change by 26%.

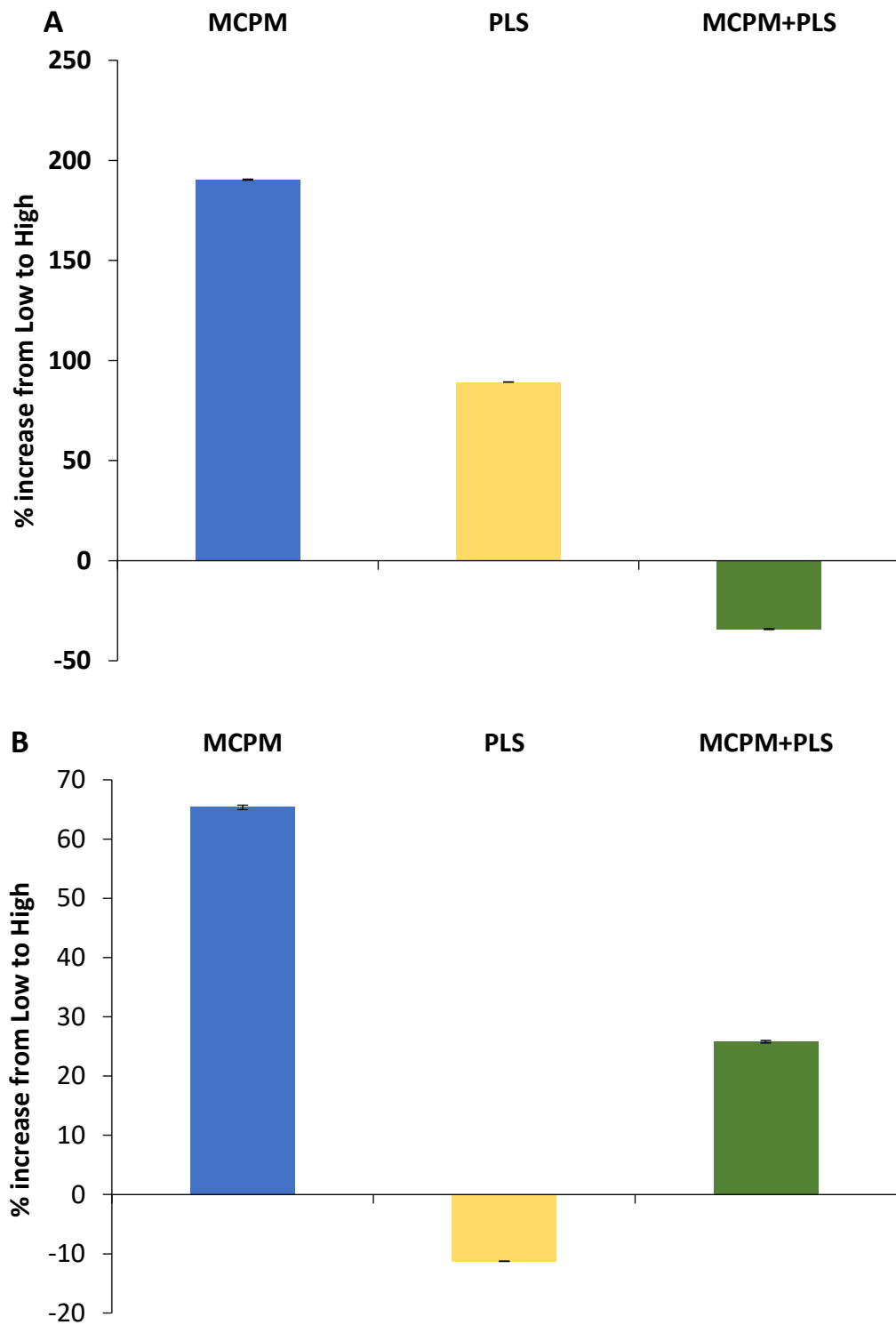


Figure 4.3 Factorial analysis of (A) Mass change and (B) Volume change of formulation discs after submersion in distilled water at 37 °C after 1 month with increasing levels of MCPM and PLS. (Error bars = 95 % CI n=6).

4.6.2 Potential of hydrogen (pH) change

pH measurements across 12 weeks of the deionised water in which the discs were submerged at each time point are provided in Figure 4.4. Fresh deionised water was added to discs at each time point. Initial pH readings were ~5, dropping down to less than ~4 pH for the last storage solution. Formulations with 8 % MCPM had lower pH at all time points in comparison to the formulations with 4% MCPM. Repeated measures ANOVA showed that time has a significant impact on the mean pH ($p < 0.001$), as did the formulation used ($p < 0.001$) and the interaction effect between the formulation and time point ($p < 0.001$).

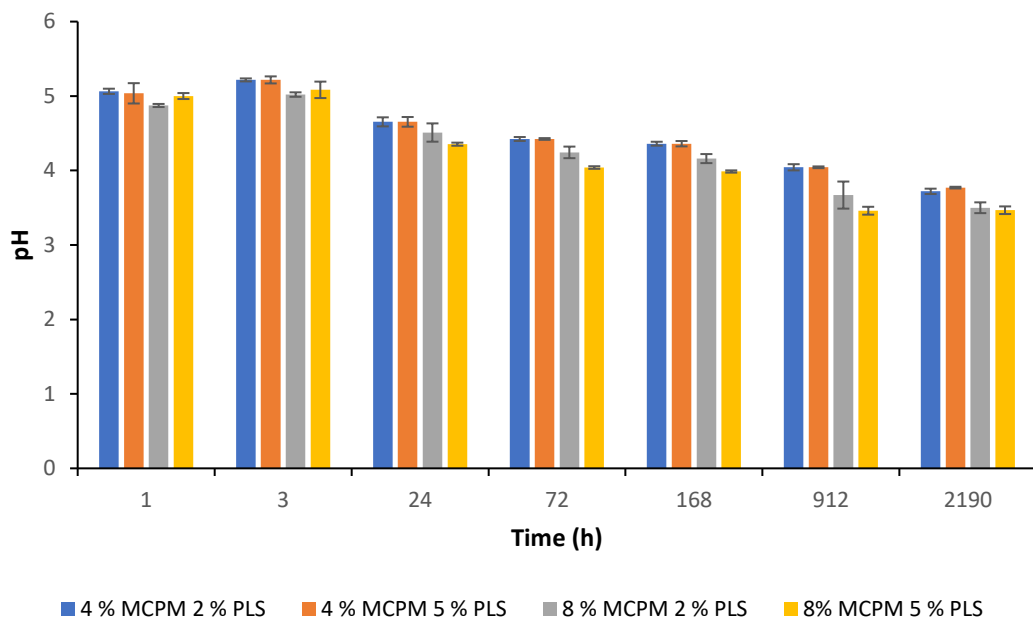


Figure 4.4 pH of deionised water in which discs with varying levels of MCPM and PLS were placed for a period of 12 weeks. (Error bars = 95 % CI $n=6$). Significant differences found: 8%MCPM 5%PLS vs. 4% MCPM 5%PLS (Games-Howell, $p=0.001$), 8% MCPM 5% PLS vs. 4% MCPM 2% PLS (Games-Howell, $p=0.001$), 8% MCPM 2 %PLS vs. 4% MCPM 5% PLS (Games-Howell, $p=0.022$), 8% MCPM 2% PLS vs. 4% MCPM 2% PLS (Games-Howell, $p=0.013$).

Factorial analysis of pH data at 12 weeks is shown in Figure 4.5. With increasing levels of MCPM, pH decreased by 6%. With increasing levels of PLS, pH increased by 0.3%. With MCPM and PLS both low or high on average pH increased by 0.3%. With MCPM and PLS both low or high on average pH decreased by 1% compared with when one was high and the other low.

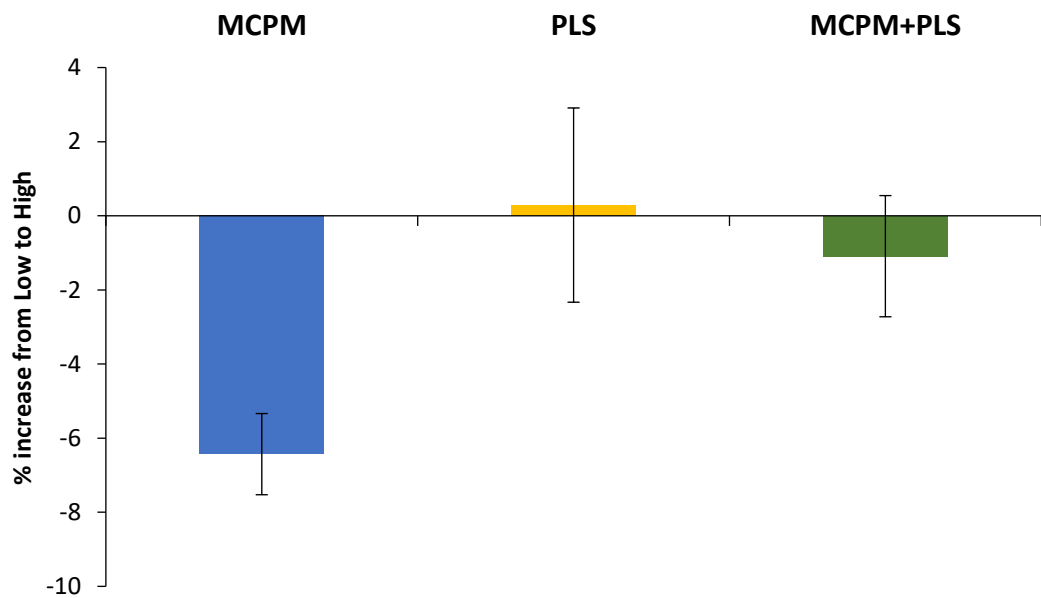


Figure 4.5 Factorial analysis for pH of deionised water in which discs were submerged in after 12 weeks. (Error bars = 95 % CI n=6).

Hydrogen ion concentration in the deionised water in which the discs were immersed in over a 12 week time period plotted against the square root of time presents a linear plot for all the formulations (Figure 4.6). Formulations with higher levels of MCPM at 8% and high levels of PLS at 5% give a steeper gradient (Table 4.2).

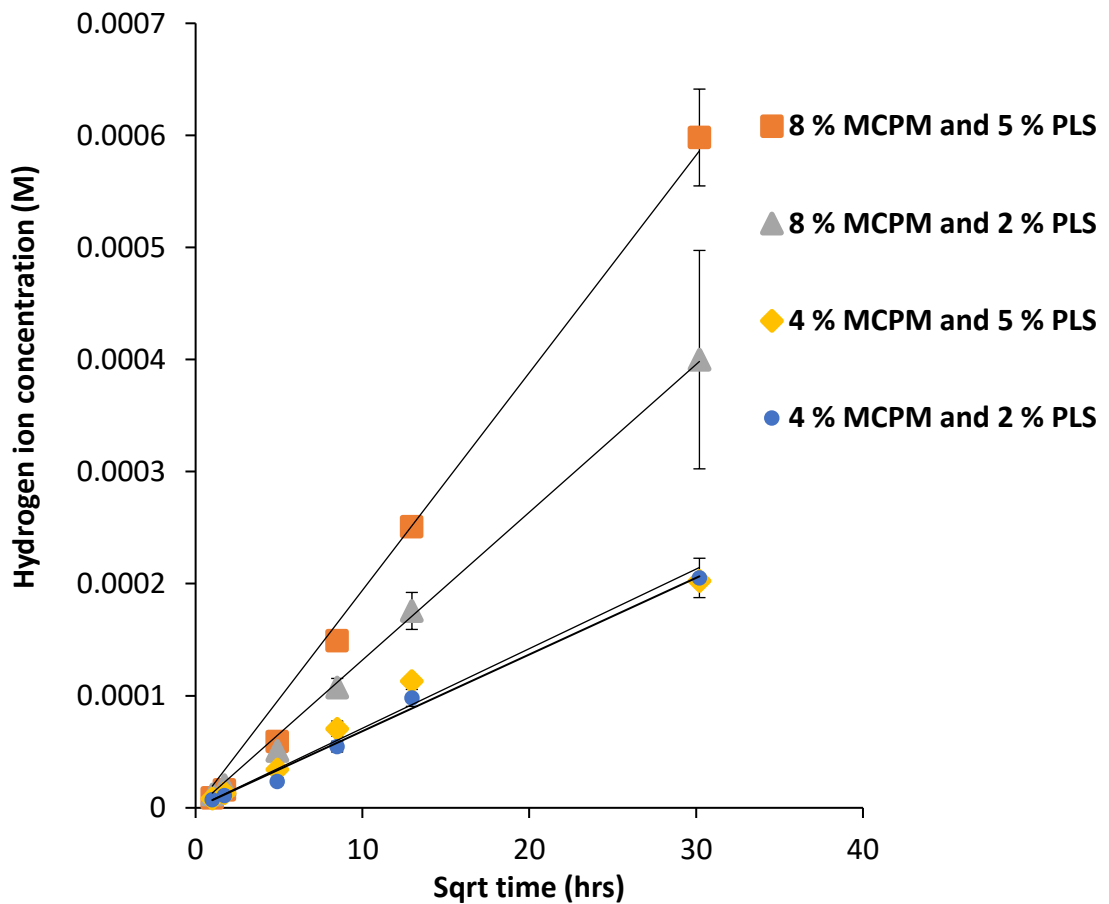


Figure 4.6 Hydrogen ion concentration of deionised water in which discs with varying levels of MCPM and PLS were placed in for 12 weeks versus square root of time (hrs). (Error bars = 95 % CI n=6).

Table 4.2 Gradient and R^2 for hydrogen ion concentration ($H^+ = 10^{-pH}$) versus Sqrt time (hrs).

Components (wt %)		Gradient	R^2
MCPM	PLS		
4	2	1×10^{-5}	0.99
4	5	1×10^{-5}	0.99
8	2	1×10^{-5}	0.99
8	5	2×10^{-5}	0.99

4.6.3 Biaxial Flexural Strength (BFS)

Figure 4.7 shows composites with high versus low levels of MCPM (8% and 4%) and PLS (5% and 2%) ultimate strength after 24 hours, 7 days, 1 month and 3 months in SBF storage. Formulation discs with 4 % MCPM and 2 % PLS had the highest strength at early times of 131 MPa at 24 hours. In comparison the lowest strength was 110 MPa for the formulation discs with 8% MCPM and 5% PLS. At 3 months formulation with high PLS and 8 versus 4% MCPM had strength of 70 MPa and 84 MPa respectively. Discs with low PLS and 8 versus 4% MCPM had strength of 94 MPa and 76 MPa. Thus discs with lower levels of PLS had on average higher ultimate strength after 3 months. Since data did not follow a normal distribution, the Kruskal Wallis H Test (non-parametric) was used. Significant differences were found among the different formulations when the following time points were considered – BFS at 0 hours (KW; $p=0.006$), 24 hours (KW; $p=0.021$); 7 days (KW; $p=0.006$); 1 month (KW; $p=0.001$) and 3 months (KW; $p=0.001$).

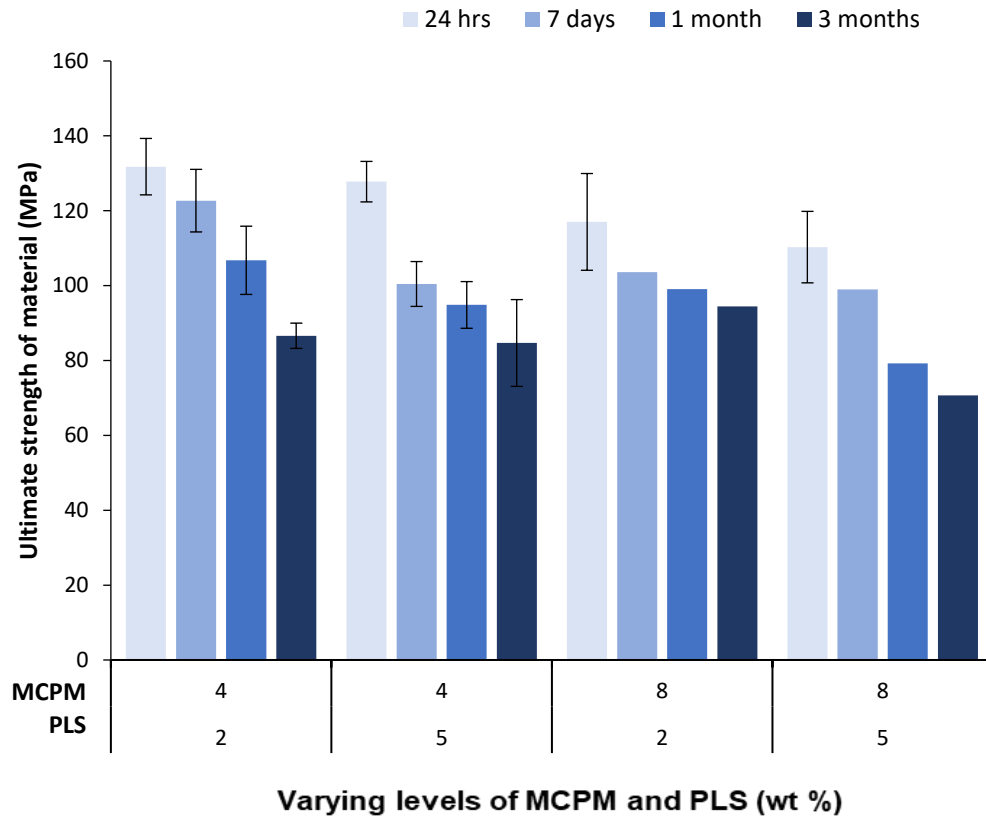


Figure 4.7 BFS of composite formulation with varying levels of MCPM wt % and PLS wt % at different time points; 24 hours to 3 months. (Error bars = 95 % CI n=6). At 0 hours, the significant differences found were: 8% MCPM 5% PLS vs. 4% MCPM 2% PLS ($p=0.022$), 8% MCPM 5% PLS vs. 8% MCPM 2% PLS ($p=0.001$), 8% MCPM 2% PLS vs. 4% MCPM 5% PLS ($p=0.041$). At 24 hours, the significant differences found were: 8% MCPM 5% PLS vs. 4% MCPM 5% PLS ($p=0.025$), 8% MCPM 5% PLS vs. 4% MCPM 2% PLS ($p=0.006$). At 7 days the significant differences found were: 8% MCPM 5% PLS vs. 4% MCPM 2% PLS ($p=0.001$), 4% MCPM 5% PLS vs. 4% MCPM 2% PLS ($p=0.011$), 8% MCPM 2% PLS vs. 4% MCPM 2% PLS ($p=0.014$). At 1 month, the significant differences found were: 8% MCPM 5% PLS vs. 4% MCPM 5% PLS ($p=0.037$), 8% MCPM 5% PLS vs. 8% MCPM 2% PLS ($p=0.006$), 8% MCPM 5% PLS vs. 4% MCPM 2% PLS ($p<0.001$). At 3 months, the significant differences found were: 8% MCPM 5% PLS vs. 4% MCPM 5% PLS ($p=0.05$), 8% MCPM 2% PLS vs. 4% MCPM 5% PLS ($p=0.05$), 8% MCPM 5% PLS vs. 8% MCPM 2% PLS ($p<0.001$), 8% MCPM 5% PLS vs. 4% MCPM 2% PLS ($p<0.014$).

Factorial analysis, Figure 4.8 shows at 24 hours with increasing levels of MCPM, ultimate strength decreased by 13%. With increasing levels of PLS, ultimate strength decreased by 4% .

The interaction effect was only 1%. After 7 days, higher PLS decreased ultimate strength by 11 %, however the interaction effect increased strength by 8%. After 1 month PLS decreased ultimate strength by 16% more than MCPM which decreased strength by 12% with the interaction effect decreasing strength by 5%. By 3 months PLS itself decreased strength by 14% in comparison to MCPM which decreased strength by 4%. Variables interaction decreased strength by 12%.

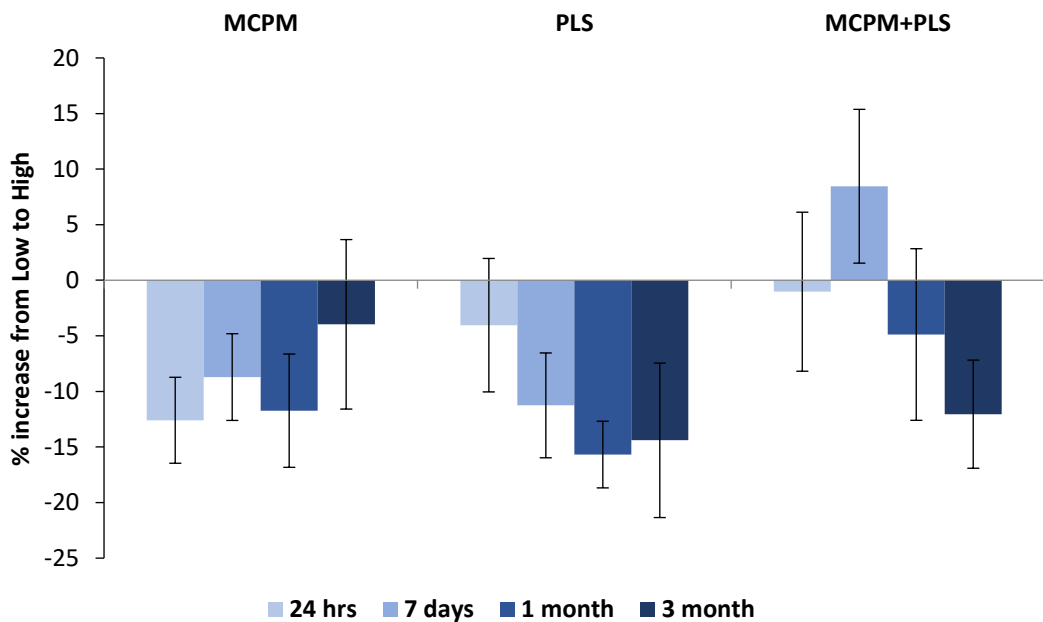


Figure 4.8 Factorial analysis for ultimate strength of discs (MPa) with varying levels of MCPM and PLS for each time point (Error bars = 95 % CI n=6)

4.6.4 Youngs Modulus (YM)

Figure 4.9 shows the YM of the composite discs with high and low levels of MCPM (8% and 4%) and PLS (5% and 2%) at 4 time intervals, 24 hours, 7 days, 1 month and 3 months. Formulation discs with 4 % MCPM and 2 % PLS at every time interval had the highest YM value, but the last time point; 3.7 GPa at 24 hours in comparison to the highest formulation discs with 8 % MCPM and 5 % PLS with the YM value at 3 GPa. While all the formulations show a decrease in the YM value, the lowest formulation combination (4MCPM 2PLS) showed a more abrupt drop at 3 months. At 3 months, formulations with high PLS and 8 versus 4% MCPM of 1.7 GPa and 2.3 GPa respectively. Discs with low PLS and 8 versus 4% MCPM have YM of 2.4 and 2.3

GPa. Thus discs with higher MCPM and PLS cause the YM to decrease. Since data did not follow a normal distribution, the Kruskal Wallis H Test (non-parametric) was used. Significant differences were found among the different formulations when the following time points were considered – at 24 hours (KW; $p=0.013$); 7 days (KW; $p=0.008$); 1 month (KW; $p=0.001$) and 3 months (KW; $p=0.039$).

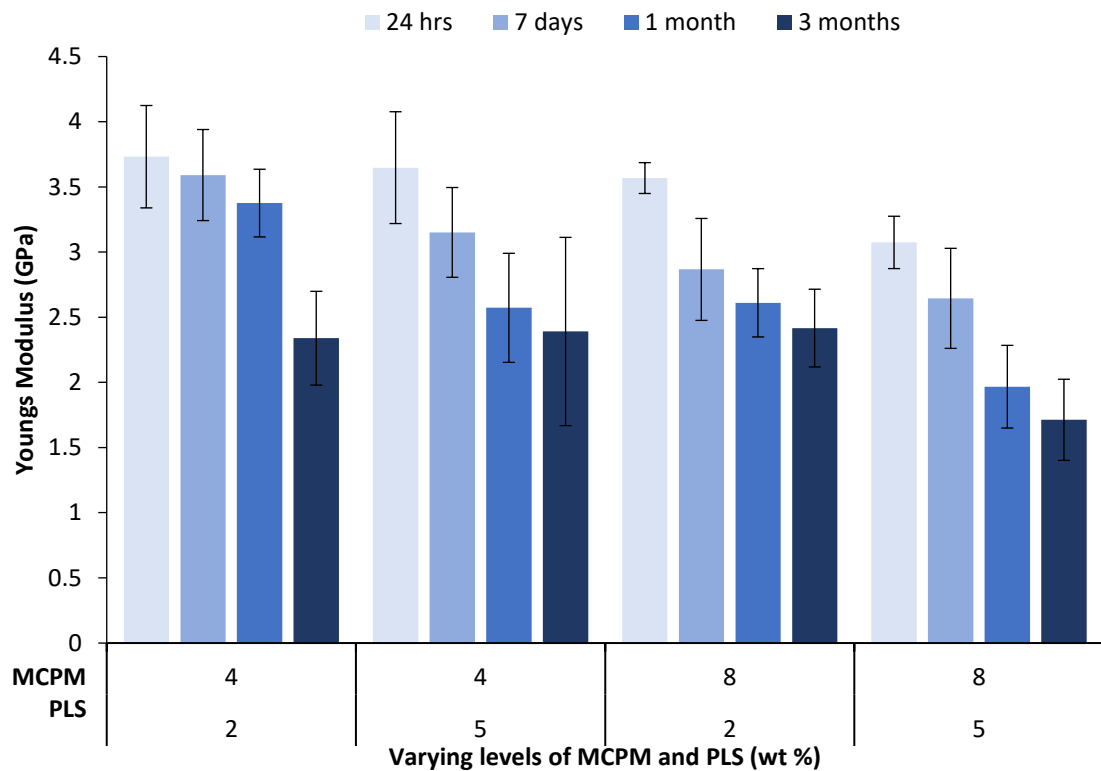


Figure 4.9 Youngs Modulus of composite formulations with varying levels of MCPM wt. % and PLS wt. % at different time points; 24 hours to 3 months. (Error bars = 95 % CI n=6). At 24 hours, the significant differences were found: 8% MCPM 5% PLS vs. 4% MCPM 5% PLS ($p=0.009$), 8% MCPM 5% PLS vs. 4% MCPM 2% PLS ($p=0.005$), 8% MCPM 5% PLS vs. 8% MCPM 2% PLS ($p=0.010$). At 7 days, the significant differences found were: 8% MCPM 5% PLS vs. 4% MCPM 2% PLS ($p=0.001$), 8% MCPM 2% PLS vs. 4% MCPM 2% PLS ($p=0.020$). At 1 month, the significant differences found were: 4% MCPM 5% PLS vs. 4% MCPM 2% PLS ($p=0.018$), 8% MCPM 2% PLS vs. 4% MCPM 2% PLS ($p=0.027$), 8% MCPM 5% PLS vs. 4% MCPM 2% PLS ($p<0.001$). At 3 months, the significant differences found were: 8% MCPM 5% PLS vs. 4% MCPM 5% PLS ($p=0.030$), 8% MCPM 5% PLS vs. 4% MCPM 2% PLS ($p=0.020$), 8% MCPM 5% PLS vs. 8% MCPM 2% PLS ($p=0.011$).

Factorial analysis of the mean YM after 3 months is presented in Figure 4.10. With increased levels of MCPM the YM decreased by 11%. With increasing levels of PLS the YM decreases by 15%. The interaction effect with increasing levels of MCPM and PLS the BFS decreases by 14%.

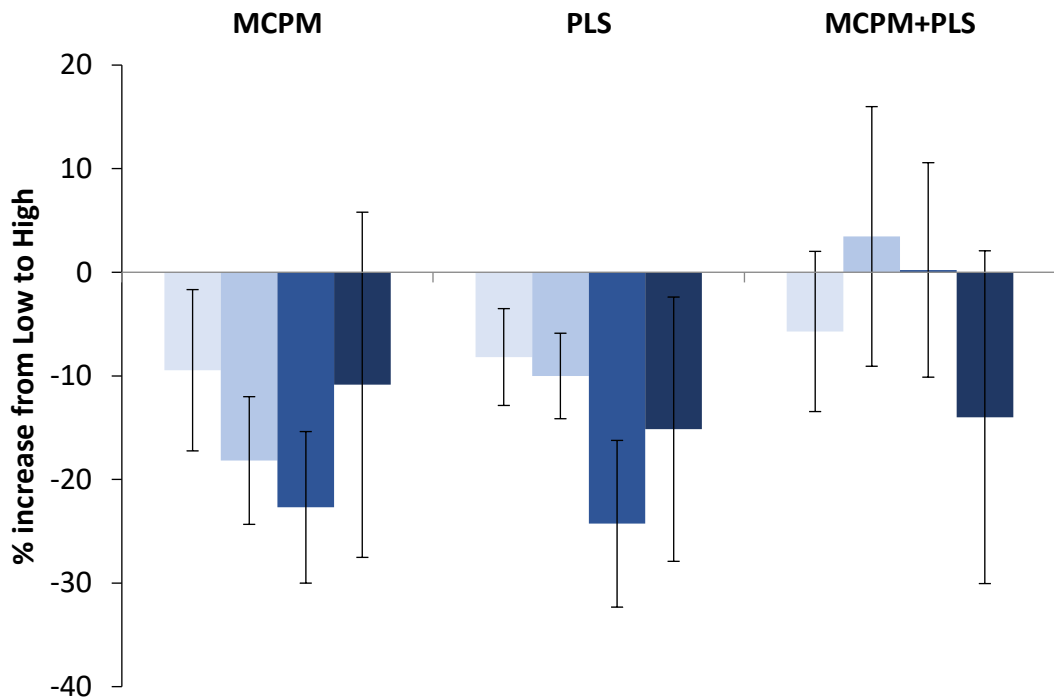


Figure 4.10 Factorial analysis of mean Youngs Modulus (GPa) with varying levels of MCPM and PLS for each time point. (Error bars = 95 % CI n=6).

4.6.5 Remineralisation on Disc Surface

Discs imaged at time 0 showed almost plain and smooth disc surfaces. An example of a formulation disc's image prior to any manipulation is presented in Figure 4.11.

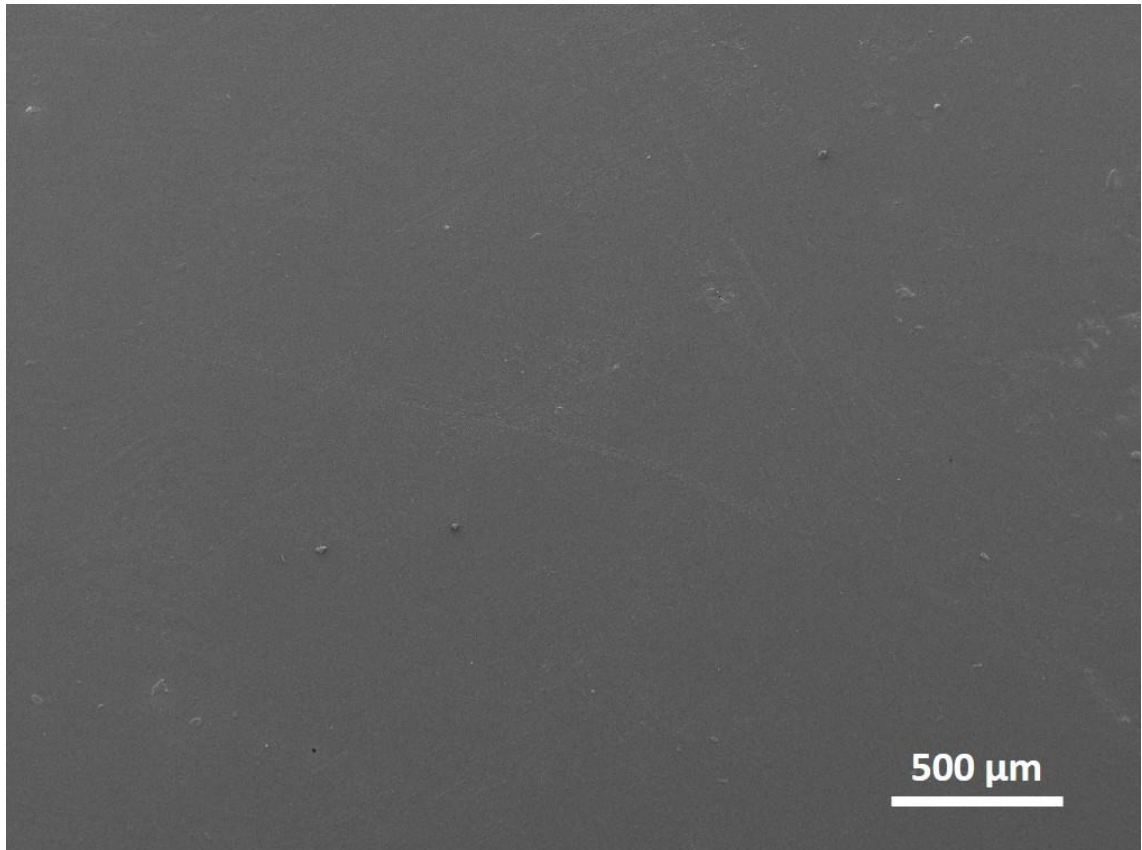


Figure 4.11 Representation of surface discs at low magnification at time 0, prior to immersing discs in SBF.

All formulation discs showed new-found precipitate on the surfaces in very small areas of the discs. After 24 hours, Figure 4.12 presents each formulation disc's surfaces with precipitate. The lowest levels of MCPM and PLS does not show much precipitate (D), however some precipitate is evident. The SEM image for formulation disc 4% MCPM and 5% PLS shows a cracked layer which indicates the surface of the disc was covered with precipitate (C). However, it was a very small area of the disc.

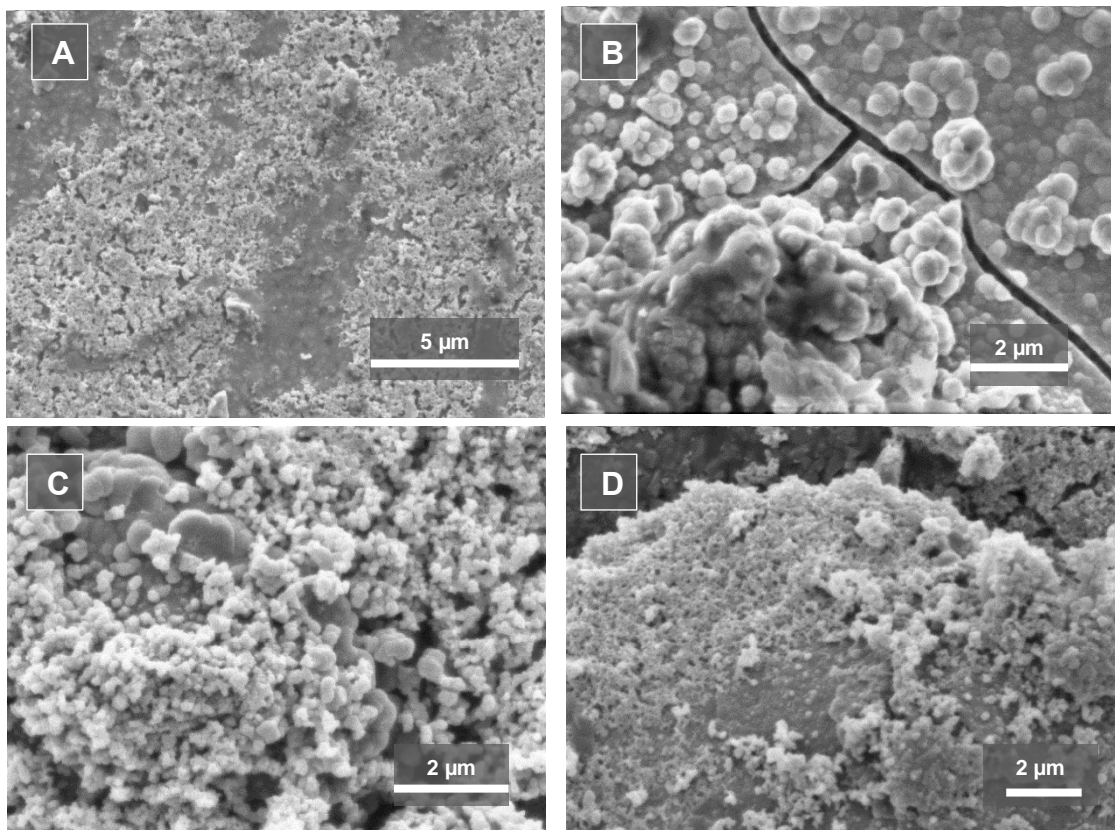


Figure 4.12 High magnification SEM images of specimen's surfaces of each formulation after 24 hours of incubation in SBF at magnification (A) 4 % MCPM 2 % PLS, (B) 4 % MCPM 5 % PLS, (C) 8 % MCPM 2 % PLS and (D) 8 % MCPM 5 % PLS.

SEM images of disc surfaces collected 7 days after incubation in SBF are presented in Figure 4.13 at low magnification. Lighter grey circular cluster like precipitations across the disc surfaces can be seen. Formulation 8 % MCPM and 5 % PLS has circular clusters across the disc surface (A) while the lowest formulation combination of 4 % MCPM and 2 % PLS appears to have random spread of precipitate (D).

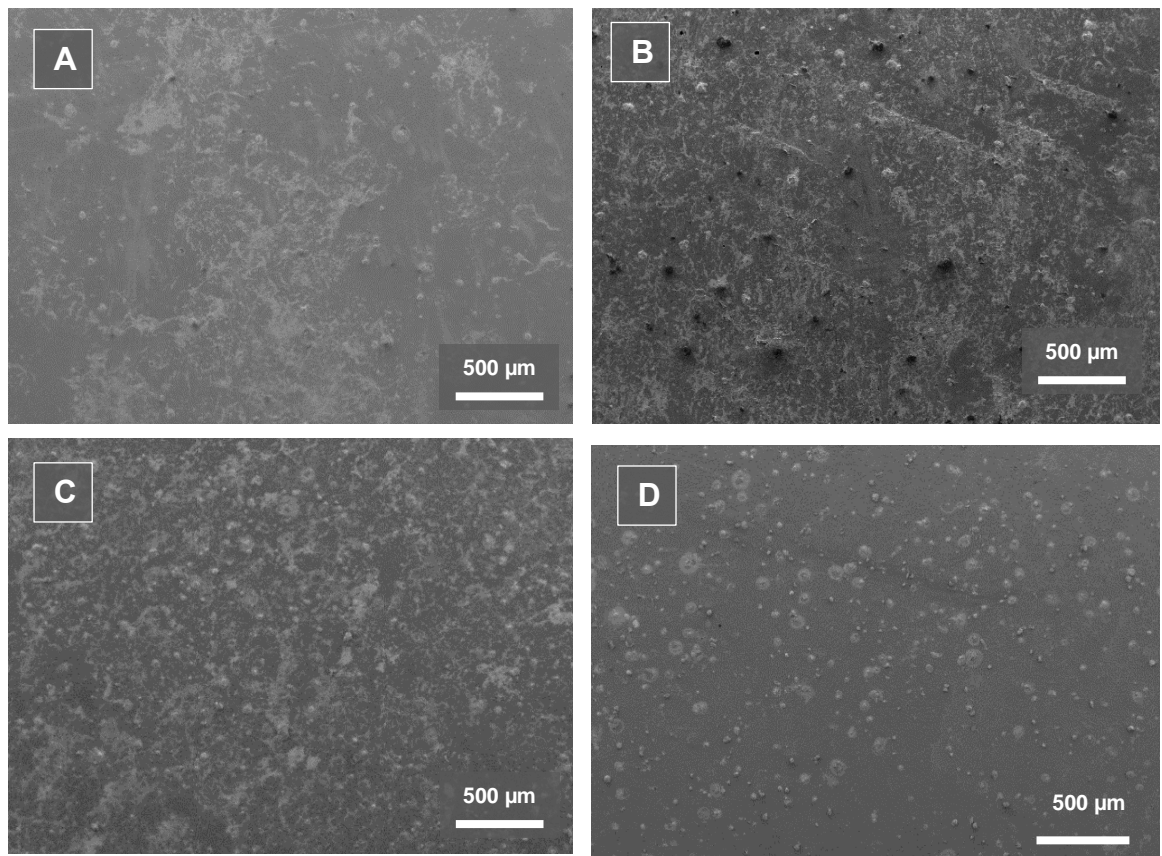


Figure 4.13 Low magnification SEM images of specimen's surfaces of each formulation after 7 days of incubation in SBF (A) 4 % MCPM 2 % PLS, (B) 4 % MCPM 5 % PLS, (C) 8 % MCPM 2 % PLS and (D) 8 % MCPM 5 % PLS.

A closer look at the precipitate on the disc surfaces for each formulation can be seen in Figure 4.14. For each formulation the clusters are formed by spheres clustering together in all the formulation disc surfaces. Formulations with the lowest combination of 4 % MCPM and 2 % PLS appears to have a thin layer that isn't as clustered (D) as the other formulation discs.

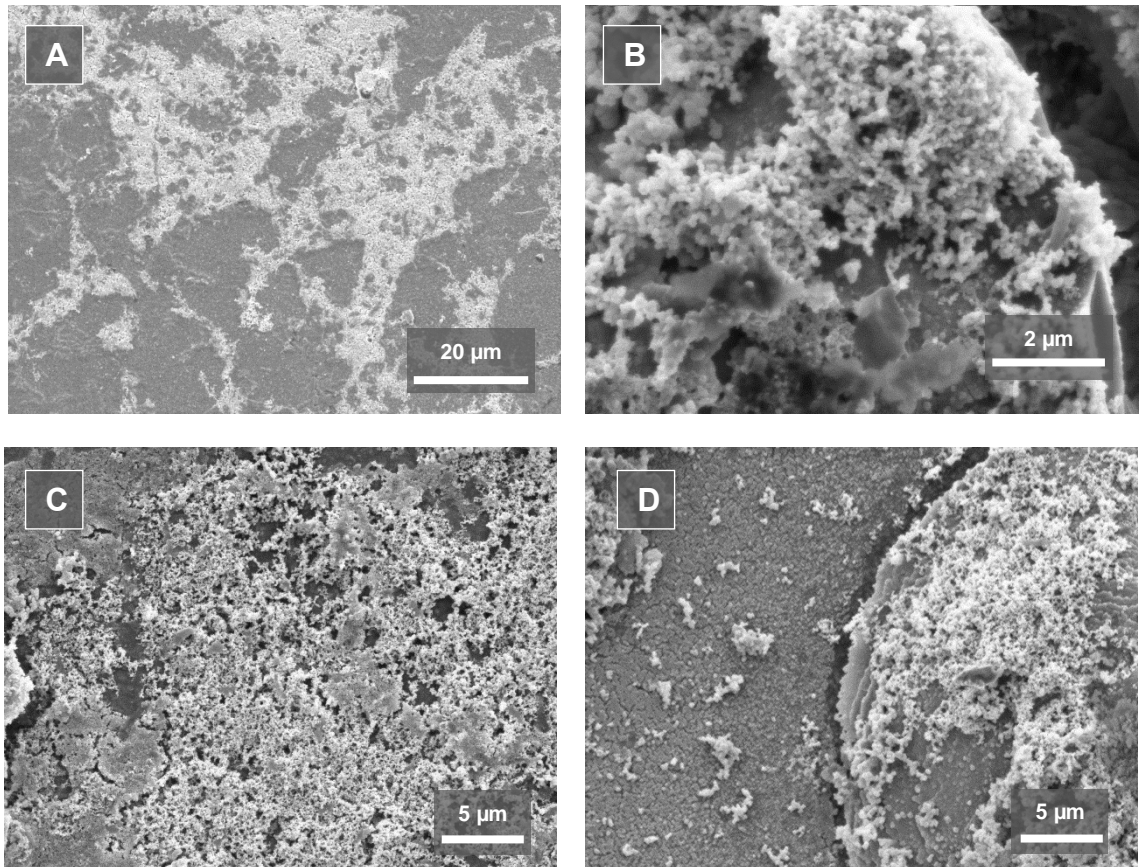


Figure 4.14 High magnification SEM images of specimen's surfaces of each formulation after 7 days of incubation in SBF at magnification (A)4% MCPM 2% PLS, (B) 4 % MCPM 5 % PLS, (C)8 % MCPM2 % PLS and (D) 8% MCPM 5% PLS.

Figure 4.15 presents the SEM images of formulation disc surfaces with precipitate at 1 month. By 1 month it can be seen that the precipitate morphology is different amongst the formulations. The highest formulation combination of 8 % MCPM and 5 % PLS has a thick layer of precipitate (A).

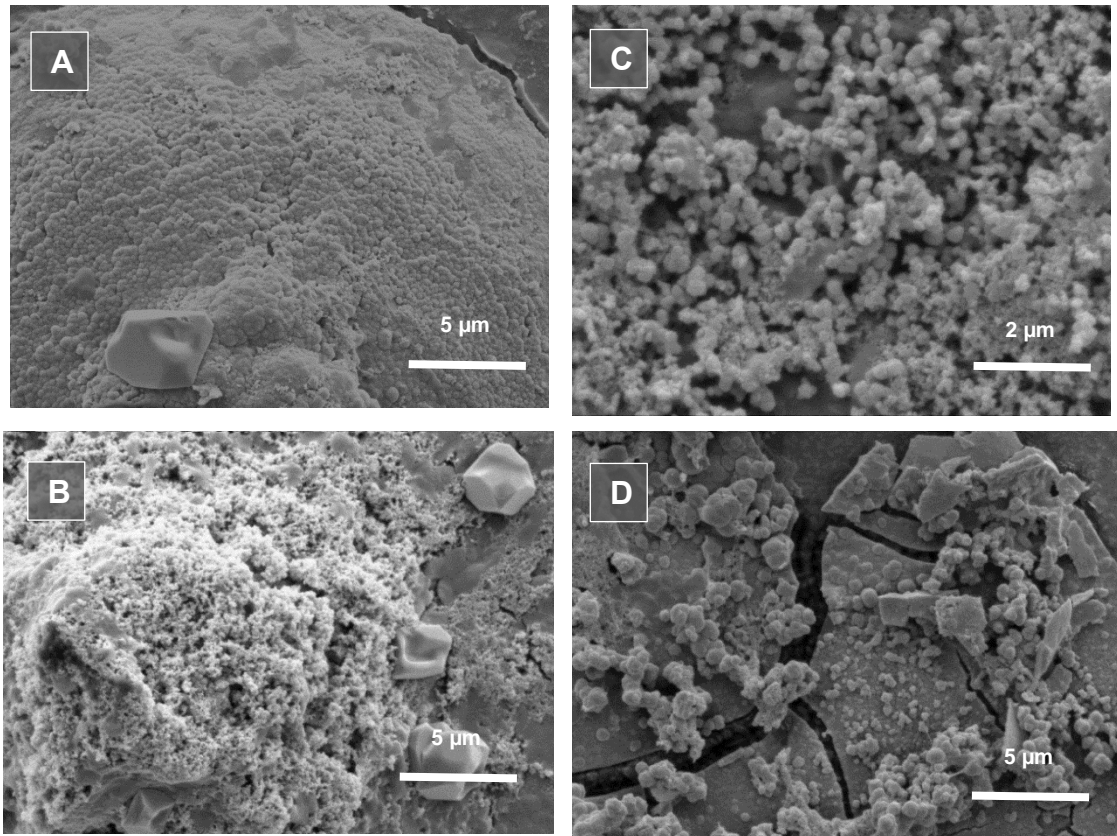


Figure 4.15 High magnification SEM images of specimen's surfaces of each formulation after 1 month of incubation in SBF (A)4% MCPM 2 % PLS, (B) 4 % MCPM 5 % PLS, (C) 8% MCPM 2 % PLS and (D)8 % MCPM 5 % PLS.

4.7 Discussion

4.7.1 Mass and Volume Change

Water sorption in a material is dependent on the composite's hydrophilicity. In literature most resin composites have exhibited water sorption in aqueous solution to some degree. Water sorption can lead to the release of un-reacted monomers from the composite material, resulting in cytotoxic effects (Hegde, Bhat, & Nagesh, 2012). Furthermore un-reacted monomers can cause plasticisation and expansion of the polymer matrix (Wei et al., 2013), resulting in a decline in mechanical properties (Ito et al., 2005).

In this study MCPM has been used as a remineralising agent and it seems to promote water uptake. It was observed, mass increase for 8 % MCPM and 5 % PLS was highest but after a month the mass change and volume change plateaued. This can be explained by the material absorbing water initially when placed in an aqueous solution, resulting in the expansion of the composite. For all the formulations volume change was double the mass change, suggesting the expansion of the material is due to water sorption. After 2 weeks the mass increased but the volume remained constant, implying the water may have been replacing the calcium phosphates which were released. It was assumed the experimental discs did not have any pores and water expands the material, thus the overall volume will be the original volume combined with the volume of water.

Alkhouri (2019) also showed MCPM and PLS to increase water sorption and solubility, mass and volume change and H⁺ release (Alkhouri, 2019).

Other factors that influence water sorption includes the length of chains between cross-links; the lower the cross-link density the higher the water sorption (Izabela Maria Barszczewska-Rybarek, 2019; J.-G. Park et al., 2009; J. Park, Eslick, Ye, Misra, & Spencer, 2011; I. Sideridou, Tserki, & Papanastasiou, 2003). Water-sorption is also influenced by the hydrophilicity of the resin matrix (I. D. Sideridou, Karabela, & Vouvoudi, 2008). While this study only looked at the comparison of high and low values of MCPM in the material, it would be interesting to see the difference in water sorption with different levels of monomers and adhesion promoters such as HEMA.

Water sorption to some degree is useful when materials are known to shrink due to polymerisation. It was found that polymerisation shrinkage deformation can be compensated by hygroscopic expansion in dental materials (Izabela Maria Barszczewska-Rybarek, 2019). This may be the case with bone composite also.

4.7.2 Potential of Hydrogen (pH) Change

Calcium phosphates with high solubility easily change the local pH and ion concentration. This in turn influences protein adhesion to the material. This is vital since protein adhesion causes cell adhesion and determines the bone regeneration efficiency (Bodhak, Bose, & Bandyopadhyay, 2009; Hu et al., 2007; Jeong, Kim, Shim, Hwang, & Heo, 2019). In addition the release of calcium and phosphorus ions influence the activity of osteoblasts and osteoclasts to facilitate bone regeneration (Gustavsson, Ginebra, Planell, & Engel, 2012).

This study shows the experimental bone composite is capable of reducing its surrounding pH levels. Alkhouri (2019) also showed, dental composites with high levels of PLS and MCPM, resulted in significant release of H⁺ from cured discs.

The acid phosphates dissolve in water, releasing phosphate anions which form the acid-phosphate resulting in low pH (Şahin, 2018). As the pH decreases the calcium phosphates become more soluble and release higher levels of Ca²⁺ cations.

Low pH can dissolve hydroxyapatite and it can also prove to be toxic for cells. However in the body due to the homeostatic buffer system this can be easily managed as the study above shows there is not a sudden decrease in pH. It is important to note that various biological systems change their surrounding pH based on their activity.

The pH around macrophages and osteoclasts can reduce pH to 5 by excreting lactic acid, while serum surrounding osteoblasts pH can go up as high as 8.5 due to the excretion of ammonia (Driessens, Wolke, & Jansen, 2012).

Bioactivity of apatite forming calcium phosphates is dependent on the alkaline microenvironment rich in calcium and phosphate ion in ratio similar to the bone extracellular matrix. Thus the right pH environment is vital (Driessens et al., 2012).

The study allows better understanding of the relationship between the amounts of calcium phosphate and PLS and pH. To further understand the pH decrease it would be interesting to assess the PLS release in future experiments.

4.7.3 Biaxial Flexural Strength (BFS)

Each spinal segment is subjected to multiple loads and forces such as compression, tension, shear and torsion. Loads on the spine are exerted from weight of body segments as well as from the weights being handled. The pattern of injury to the spine is dependent on the type and size of forces existent at time of injury.

Flexural strength is the ability of a material to resist deformation under load (Hodgkinson, 2010). Thus adequate flexural strength is required for bone cement that is used to treat osteoporotic fractures.

Biologically active restorative materials are being developed to stimulate the repair of tooth structures through the release of calcium phosphates (Schumacher, Antonucci, O'Donnell, & Skrtic, 2007). However in calcium phosphate composites, the filler is weakened and bone composites exhibit similar problems. Furthermore the addition of antibacterial agents can also reduce strength. PLS is hydrophilic (W. Zhang, Li, Tang, & Zhai, 2020), so it increases water sorption, which results in increasing the mobility of polymer chains leading to a decrease in stiffness and strength.

The experimental bone composite's levels of remineralising agents and PLS were varied to identify the optimum strength for providing support as a bone fixture. In this study higher levels of MCPM and PLS reduce the ultimate strength of the material. However the difference in strength is relatively small from the varying levels of MCPM and PLS. High level MCPM 8% and low level PLS 2 % exhibited better mechanical properties after 3 months compared to the other formulations, despite water absorption being high for this formulation in comparison to the combined lower formulations. Literature has shown dental materials to have lower mechanical properties with the incorporation of antibacterial agents (Imazato, 2003; Kramer, Garcia-Godoy, & Frankenberger, 2005; Leung et al., 2005; I. Mehdawi et al., 2009; X. Xu & Burgess, 2003). MCPM and PLS are both soluble in water consequently the reason behind the decrease in composite's strength. The addition of antibacterial agents is important in the bone cement as it will discourage infection at the site of fixation. It's inevitable the inclusion of MCPM and PLS will compromise strength, however quantities that will not significantly influence the mechanical properties of the bone composite can be considered.

4.7.4 Youngs Modulus (YM)

33% of patients who have had treatment for a fractured vertebra will have further vertebral fractures within 6 months and there is higher risk at the adjacent vertebrae (Alexandru & So, 2012). The exact reason is unknown, but there could be reason to suggest it could be due to leakage or high differences in modulus. It has been proposed that bone fixtures may well act as load transfer devices. Thus decreasing the cement's stiffness may provide effective load transfer

(Kayanja, Togawa, & Lieberman, 2005). Baroud et al showed that after injecting PMMA cement, the stiffness of augmented cancellous bone was increased by 8.5 times, which could alter the local load transfer of the spinal segment (Baroud, Bohner, Heini, & Steffen, 2004).

PMMA cements are far from satisfactory in terms of mechanical properties; the modulus of PMMA is up to an order of magnitude higher than cancellous bone (Jaeblo, 2010; Lopez, Unosson, Engqvist, & Persson, 2011; Saha & Pal, 1984) meaning that cement deflection on loading will be very different from surrounding bone. This could cause damage to weak low density bone (Kirsty Alexandra Iskrzycka Main, 2013). PMMA for vertebroplasty has greater stiffness than vertebral cancellous bone, causing higher incidences of fracture of neighbouring vertebral bodies (Arora, Chan, Gupta, & Diwan, 2013; Beck & Boger, 2009).

In this study, results showed that the modulus gradually declined over the 3 month period, with the final values for 8 % MCPM and PLS 5 %, 8% MCPM and PLS 2%, 4 % MCPM and PLS 5 % and 4 % MCPM and 2 % PLS at 1.7 GPa, 2.4 GPa, 2.3 GPa and 2.3 GPa respectively. According to literature, cortical bone's YM is 17 GPa and cancellous bone is 350 MPa. Previous tests of YM of PMMA and Cortoss[®] gave values of 1.6 GPa and 3.4 GPa respectively (Kirsty Alexandra Iskrzycka Main, 2013). A lower YM for bone fixation would be ideal because it will have similar deformable properties to bone.

An ideal bone cement would have a Young's modulus which is low enough to resemble that of the cancellous bone to spread the load across the bone and material, while also maintaining necessary yield strength (σ_y) to withstand the axial stresses reinforced by the spine (Lopez, Hoess, et al., 2011).

4.7.5 Remineralisation on Disc Surface

The precipitate on the disc surface imaged by SEM is similar in appearance to other apatite studies (Aljabo, Abou Neel, Knowles, & Young, 2016; P. Feng, Wei, Shuai, & Peng, 2014). Previous works have shown that the MCPM usually dissolves from the surface of reactive filler composites in the first 24 hrs after placement in water (Idris Mehdawi et al., 2009). Explaining the solution's decrease in pH in this study. As the pH of the solution decreases, the solubility of apatite increases.

The SEM images show a higher level of MCPM results in a thicker layer of apatite precipitate after 3 months. Phosphoric acid may interact with PLS to form a complex that promotes apatite precipitation from SBF. Remineralisation is beneficial for bone composite since it will encourage integration.

An ideal bone composite will exhibit osseointegration by triggering a specific biological response, resulting in the formation of a bond between the host tissue and biomaterial.

The superficial carbonated HA is chemically equivalent to the mineral phase in bone. Studies have demonstrated that for a bond with host tissues to occur, this layer of carbonated HA must form, the same topography between both phases resulting in interfacial bonding (Eliaz & Metoki, 2017). The HA formation on the surface of the various bone composites were not quantified, statistically analysed and compared in this study, thus the method is limited. Future experiments require Energy Dispersive Spectroscopy (EDAX) analysis to identify and quantify the presence of elements on the surface of the discs.

4.8 Conclusions

Increasing MCPM (from 4 to 8 wt%) and PLS (from 2 to 5 wt%) of the powder showed:

- Increased water sorption due to their hydrophilic properties.
- Decreased in pH over time.
- Decreased strength and modulus over time, after storage in SBF for 1 month.
- Increased mineralisation on disc surface after storage in SBF for 1 month.

Different Cell Viability In-vitro with Optimised Formulation Discs

5.1 Abstract

The aim of this chapter was to optimise and assess reproducible cell studies for the experimental bone composites with varying levels of MCPM and PLS. Bone marrow derived sheep mesenchymal stem cells (MSCs) and human osteoblast-like cells (MG63) were exposed to disc extracts. Additionally, sheep mesenchymal cells were imaged via SEM and confocal microscopy on the surfaces of the experimental bone composites.

Data showed cells to respond to the varying levels of MCPM and PLS. Increasing MCPM and PLS concentration decreased activity in bone marrow derived sheep MSCs and MG63 cells. Bone marrow derived sheep MSCs were visible on all disc surfaces of all formulations.

In conclusion disc extracts of composite discs with increasing levels of MCPM and PLS appeared unfavourable to the metabolic activity of the cells. However, cells were observed on all discs, thus further assays are required to confirm the data that was collected and compliment this study.

5.2 Introduction

In this chapter, increasing MCPM (from 4 to 8 wt%) and PLS (from 2 to 5 wt%) of the powder phase were used to assess cell toxicity via alamar blue and cell morphology on the disc surface.

The ideal bone composite will play a crucial role in bone repair, thus it is important the composite comprises of appropriate biological properties, such as being non-toxic and not eliciting inflammatory or immune responses. In addition, they should have good biocompatibility and bioactivity. The bone composite should not merely fill the fractured site but integrate with the bone and encourage the bone to self-heal.

One of the disadvantages of the widely used bone cement, PMMA is its poor osteointegration and minimal bone attachment (Oryan, Alidadi, Bigham-Sadegh, & Moshiri, 2018). A successful interface between native bone and bone cement/composite is necessary to aid cell adhesion, proliferation and differentiation, further enabling the formation of new bone tissue integrated with the cement/composite. (Gao et al., 2017).

MSCs have differentiation potential (Gao et al., 2017), and in this chapter increasing levels of PLS concentration were added to the bone derived sheep MSCs to assess cell activity. Indicating what the threshold levels of PLS would be when adding to the experimental bone composite.

A hostile bone cement/composite will prevent cell adhesion, thus bone derived sheep MSCs were seeded on to the experimental bone composite discs and the morphology of cells was evaluated.

In chapter 4, it was observed, the immersion of experimental bone composite discs in de-ionised water resulted in a decrease in pH. In addition results in chapter 4 showed remineralisation, suggesting the release of MCPM. To assess cell activity in response to the releasing components from the discs, experimental bone composite discs with MCPM (from 4 to 8 wt%) and PLS (from 2 to 5 wt%) were immersed in cell culture medium and this was added to the cells.

Furthermore increasing concentration of PLS, MCPM and HCl was added to MG63 cells to assess cell activity. MG63 cells were also exposed to experimental bone composite discs with MCPM (from 4 to 8 wt%) and PLS (from 2 to 5 wt%) immersed in cell culture medium, to assess cell activity.

5.3 Aims

The aim of this chapter was to assess the individual and combined effects of MCPM and PLS on cellular activity, to finally determine the optimum formulation combination the cells thrived in.

5.4 Objectives

- Assess if increasing MCPM (from 4 to 8 wt%) and PLS (from 2 to 5 wt%) of the powder phase will have significant effect on cell spreading on the disc surfaces.
- Assess if increasing PLS concentration has any effect on sMSC activity.
- Assess if increasing MCPM (from 4 to 8 wt%) and PLS (from 2 to 5 wt%) of the powder phase will have significant effect on sMSC activity.
- Assess if increasing concentrations of HCl, PLS and MCPM will have any effect on MG63 cell activity.
- Assess if increasing MCPM (from 4 to 8 wt%) and PLS (from 2 to 5 wt%) of the powder phase will have significant effect MG63 cell activity

5.5 Materials and Methods

Table 5.1 presents the 4 formulations with varying amounts of MCPM and PLS added to the monomer phase.

Table 5.1 MCPM and PLS percentages added to initiator and activator paste fillers in formulations 1-4 (Monomer phase: UDMA (7.5 g), PPGDMA (2 g), HEMA (0.25 g). 4-META (0.3 g) was added in the initiator phase only. 2.5 % BP and 1.5 % NTGGMA. Glass filler: 7 μ m and 0.7 μ m ratio 4:5. PLR 3:1).

Formulation	Amount (wt %)	
	MCPM	PLS
1	4	2
2	4	5
3	8	2
4	8	5

5.5.1 Experimental Bone Composite Discs

For in-vitro work, discs were prepared with paste injected in 10 mm diameter and 1 mm thick moulds (Springmasters, UK) at room temperature. Discs were sterilised using ultra-violet (UV) light (BonMay®) exposure of 20 minutes on each side. 3 specimen discs were used per formulation per in-vitro assay explained in section 2.7 and sterilised as suggested in 2.7.1.

5.5.2 Bone Marrow Derived Sheep MSCs

5.5.2.1 Assessing PLS Concentration on Bone Marrow Derived Sheep MSCs

To assess the effect of different concentrations of PLS cells were seeded in a 96 well plate at 30,000 cells/cm². After 24 hours a serial dilution of PLS was serially diluted in cell culture medium DMEM, (1% penicillin and streptomycin (Gibco)). Concentration of PLS ranged from 3200 mM to 0.32 mM. Cells were left to incubate with PLS for a further 24 hours in a 37°C incubator with 5% CO₂ in air.

To assess cell activity, the medium was replaced by 10% v/v Alamar blue and incubated for 4 hours according to manufacturer's instructions. Fluorescence of the subsequently removed medium was measured using Fluroskan Ascent plate reader (Labsystems, Helsinki, Finland) and corrected for background.

5.5.2.2 Cell Morphology Assessment

Discs were prepared as described in section 2.7 and sterilised as suggested in 2.7.1. Cells were seeded at 30,000/cm² for attachment. Cells were suspended in a 50 µl drop on to the disc surface and incubated at 37°C, 95% air, 5% CO₂, 95% relative humidity for 1 hour in a 24 well plate. DMEM was added up to 1 ml and cells were incubated again at 37°C, 95% air, 5% CO₂, 95% relative humidity for 24 hours.

5.5.2.3 Influence of Disc Extract on Sheep Mesenchymal Stem Cell Activity

Discs were prepared as described in section 2.7 and sterilised as suggested in 2.7.1. 3 discs from each sample was conditioned in 600µl DMEM in 50 ml self-standing centrifuge tube according to ISO for Biological evaluation of medical devices-Part 12: Sample preparation and reference materials) (ISO 10993-12) for 24 hours at 37°C at 100 rpm. Medium extract in which discs were incubated was added to cells. Medium extract from 2 different time points were used; 24 hours and 7 days (including the initial 24 hour time period). Before exposing cells to disc extract media, cells were seeded in to a 96 well plate 24 hours prior. Bone marrow derived sheep MSCs were seeded at a density of 30,000 cells/cm² in 96 well plates (n= 6 per 2 specimens, time-point and assay). After an initial 24 hours seeding period, cell culture medium was replaced with 100µL of the disc's composite extract for 24 hours.

Cell activity was then assessed using resazurin (Alamar Blue® Invitrogen).

Absorbance readings were collected at 570nm excitation and 585nm emission on (Tecan Infinite M200).

5.5.3 MG63 Cells

Most in vitro studies assessing biomaterials use immortalised cells instead of MSC cells. They are easier to obtain and can grow in vitro several many passages. MG63 cells are examples of osteosarcoma cell lines that are widely used to understand osteogenic cell behaviour on biomaterials. They can also undergo osteoblastic differentiation in response to osteogenic chemical cues (Vohra, Hennessy, Sawyer, Zhuo, & Bellis, 2008). Thus MG63 cells were also used to compare cell response with MSC cells.

5.5.3.1 Assessing PLS and MCPM vs HCl Concentration on MG63 Cells

PLS was serially diluted in DMEM, with (Gibco®, Life Technologies Ltd., Paisley, UK) and sterilised using a filter 0.22 µm (Millipore) and subsequently serially diluted. In replicates of 3, 100 µl were added to a 96 well plate, giving concentration from 10 mM down to 0.001 mM.

5.5.3.2 Disc extract toxicity on MG63 cells

Discs were prepared as described in section 2.7 and sterilised as suggested in 2.7.1. Discs from each sample were conditioned in 600µl DMEM for 24 hours at 37°C at 100 rpm according to ISO for Biological evaluation of medical devices — Part 12: Sample preparation and reference materials (ISO 10993-12).

Medium in which discs had been incubated was added to cells. Medium containing extracts from 2 different storage times were used; 24 hours and 7 days. Before exposing cells to disc extract media, cells were seeded in to a 96 well plate following the same protocol as bone marrow derived sheep MSCs in section 2.12.1.2.

5.5.4 Factorial Analysis

Factorial analysis for the two variables (each at high and low levels) was used to assess effect of MCPM (8 wt% versus 4 wt%) and PLS (2 wt% versus 5 wt%) on metabolic activity of bone marrow derived sheep MSCs exposed to disc extract 24 hours and 7 day incubation, Metabolic activity of MG63 cells after 24 hour incubation with disc extracts of varying formulations for 24 hours and 7 days.

5.6 Results

5.6.1 Sheep Mesenchymal Stem Cell: Morphology on Disc Surfaces

SEM images of disc surfaces, 24 hours post seeding bone marrow derived sheep MSCs on are presented in Figure 5.6. All formulation discs had cells present on their disc surfaces. The edges of the discs generally had less cells but these were still found to be flat and spread (A). Cells appeared flat and spread with long filopodia connecting to other cells across most of the surface of the discs irrespective of experimental formulations (B) with many areas consisting of several overlapping layers of cells (C). Most of the PMMA disc surface looked very much similar to the edge of the discs where cells were difficult to notice, possibly due to a thinner spread layer. Features of cells were noticeable on PMMA disc surface unlike the experimental formulations.

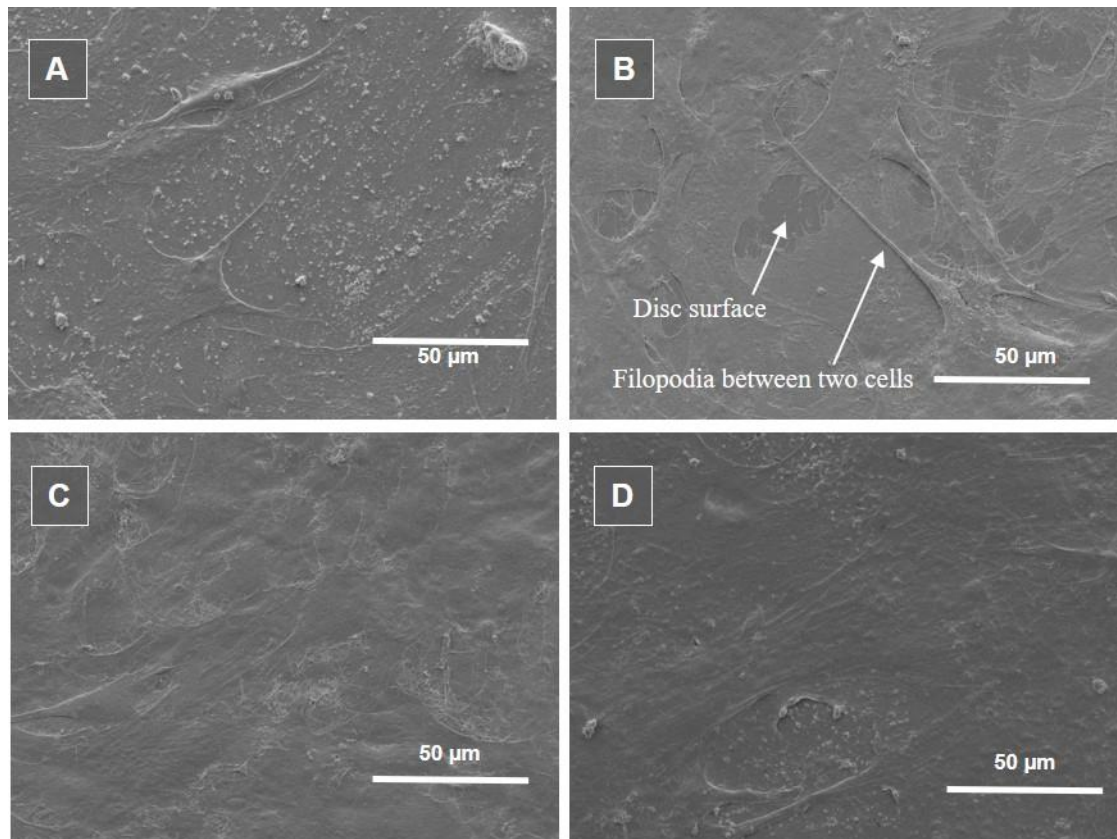


Figure 5.1 SEM images of disc surface of formulation disc with MCPM and PLS (A) 8% MCPM 5% PLS, edge of disc. (B) 8% MCPM 2 % PLS and (C) 4% MCPM 5% PLS. random location near centre of discs. (D) PMMA after 24 hours of seeding bone marrow derived sheep MSCs

Figure 5.7 and 5.8 represent types of grey clusters spread on the cell surface on areas of the disc surface from low to high magnification after 24 hours. Most discs in all formulations with combinations of MCPM and PLS had 1 or two grey clusters. Figure 5.7 A and 5.8 A show a lighter grey region of the discs in comparison to the rest of the disc surface. Higher magnification of the grey disc area presents a cluster of precipitate on the cell surfaces in Figure 5.7 B and 5.8 B. Figure 5.7 C shows a cluster of precipitate covering the cell structures and Figure 5.8 C shows different sizes of precipitate on different areas of the cell.

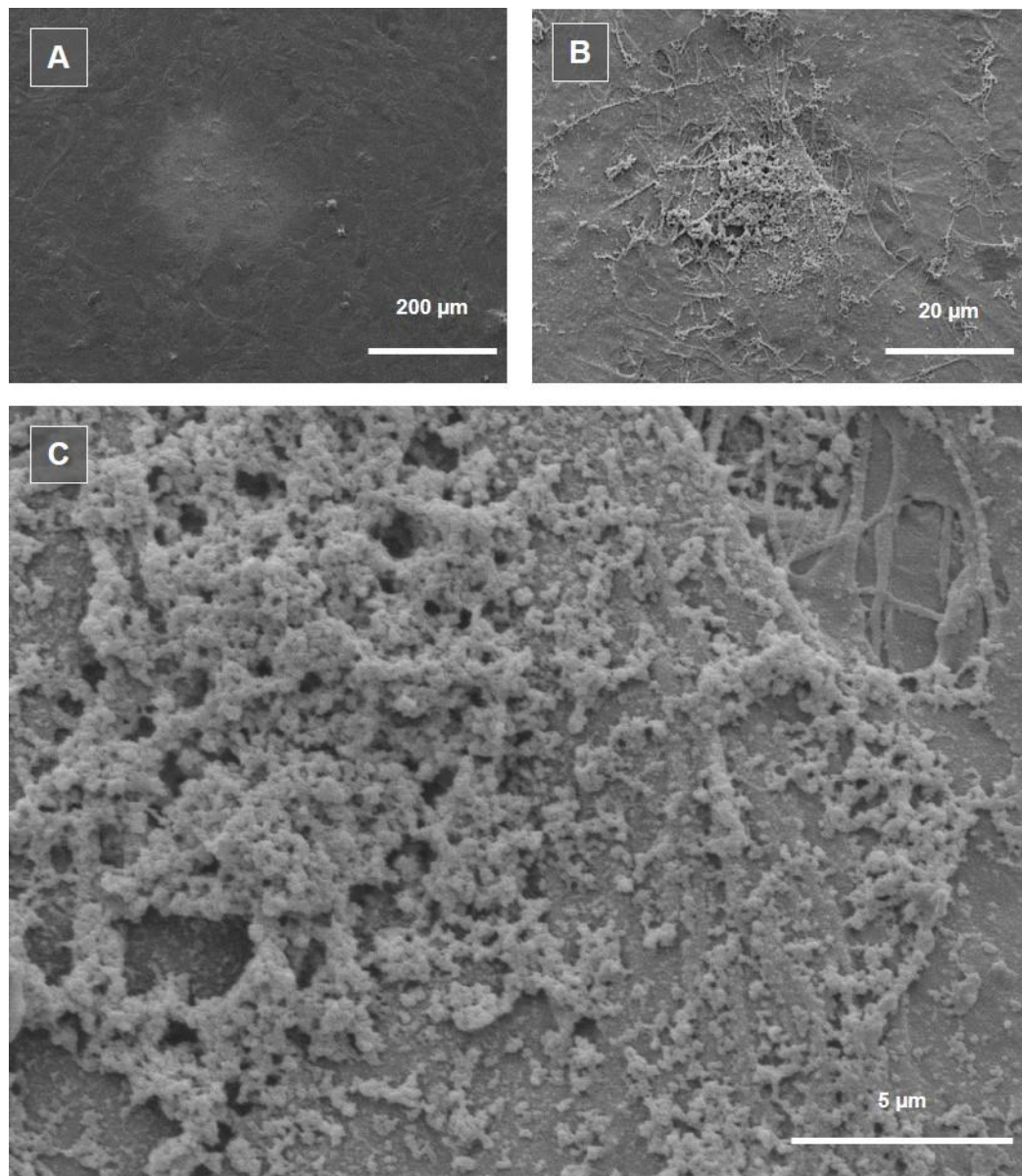


Figure 5.2 SEM images of cells on disc surfaces, formulation 8% MCPM and 2 % PLS; increasing magnification from low to high (A-C) after 24 hours of seeding bone marrow derived sheep MSCs.

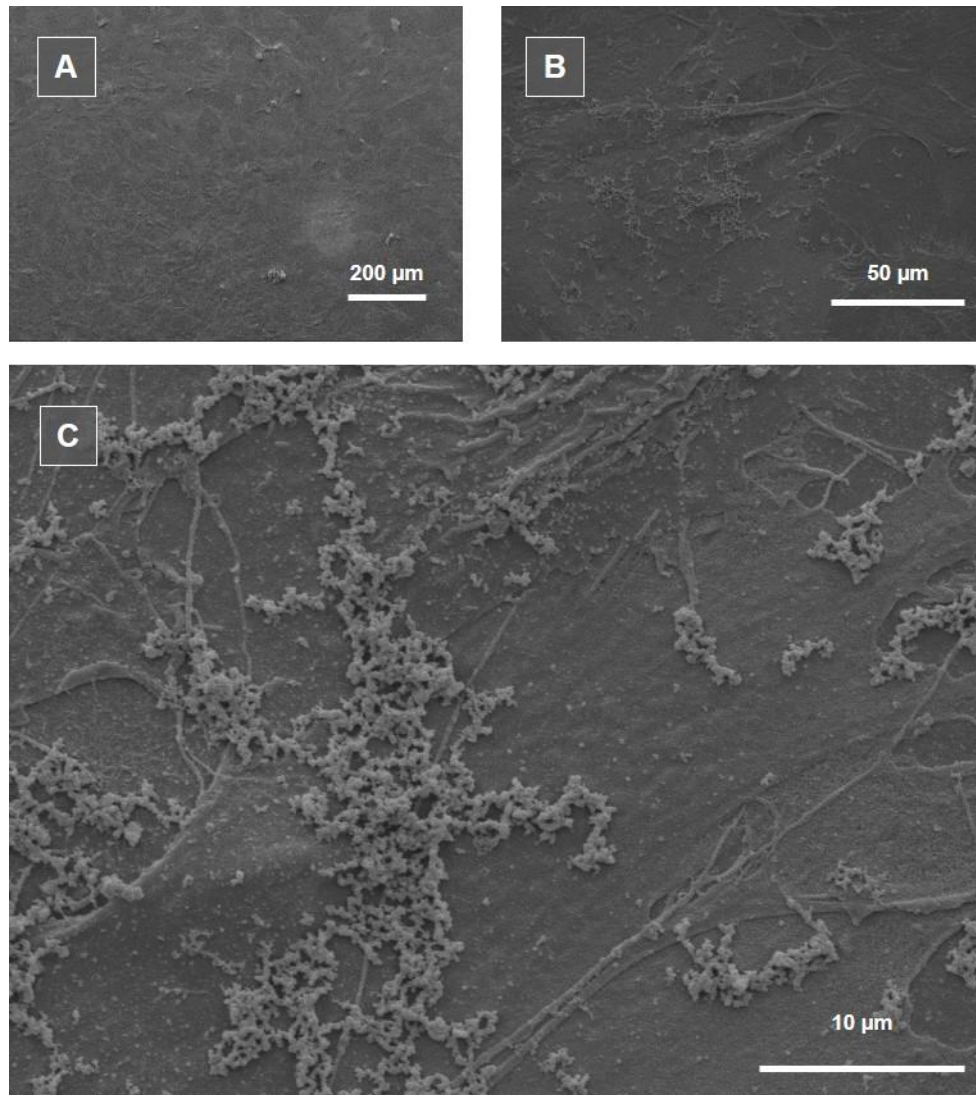


Figure 5.3 SEM images of cell surfaces on disc surfaces, formulation 4% MCPM and 5% PLS; increasing magnification from low to high (A-C) after 24 hours of seeding bone marrow derived sheep MSCs.

SEM images of disc surfaces post 3 days of seeding bone marrow derived sheep MSCs on formulation discs are presented in Figure 5.9. All formulation discs showed cells present on their disc surfaces with a spread and flat morphology with less filopodia in comparison to cells on disc surfaces after 24 hours (A). Cell morphology on the commercial PMMA's disc surface did not appear to show clear cell structures indicating their presence (B).

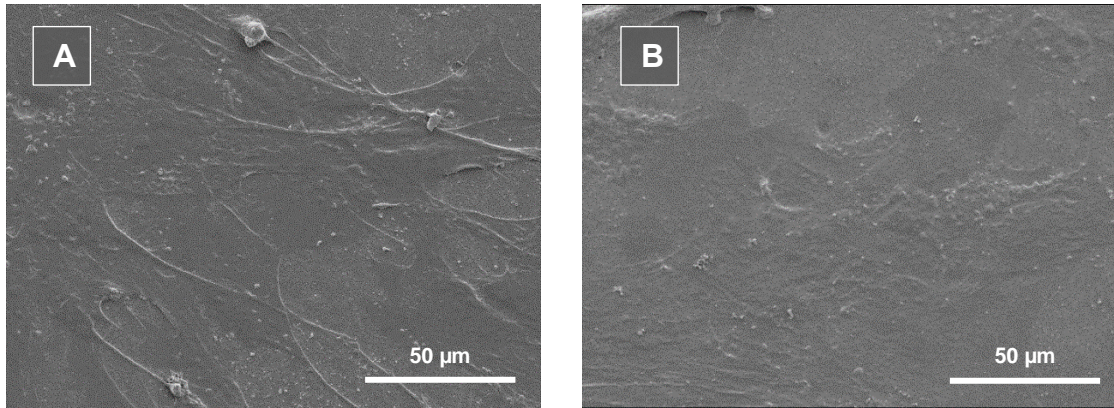


Figure 5.4 SEM images of disc surfaces after 3 days of seeding bone marrow derived sheep MSCs experimental composite (A) 4% MCPM 2% PLS and commercial (B) PMMA.

Images of bone marrow derived sheep MSCs stained with Hoechst for the nuclei (blue) and cell actin (green) and on disc surfaces after 24 hours are given in Figure 5.10. Cells were present but in isolation around the edges of the disc surfaces (A) for most of the formulation discs and in some areas of the discs cells were found in clusters with stretched morphologies (B). The centre of the discs often had an abundance of cells overlapping each other (C). Cells on the PMMA disc surface were spread in clusters across the surface but most cells present were in isolation (D).

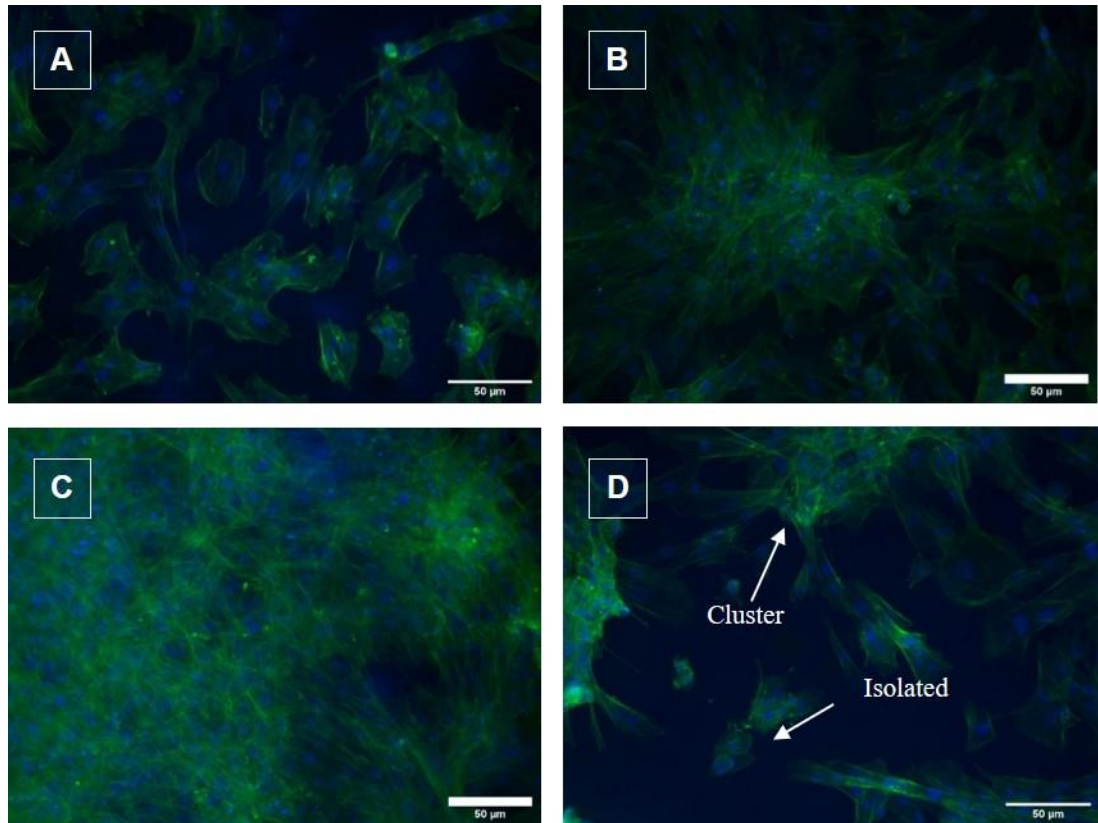


Figure 5.5 Confocal microscopy images of experimental bone composite with 4% MCPM and 5% PLS. Blue is the Hoechst staining (cell nucleus) and green staining is phalloidin (cell's actin). (A) Edge of disc, (B-C) Areas near the centre of disc (D) Near centre of PMMA disc after 24 hours of seeding bone marrow derived sheep MSCs.

5.6.2 Bone Marrow Derived Sheep MSCs: Effect of Disc Extract Solution

Figure 5.3 show the cell metabolic activity of bone marrow derived sheep MSCs in the presence of disc extract collected after 24 hours and 7 days. Extract from discs collected after 24 hours from samples with 5% PLS appeared to slightly lower metabolic activity of cells after 24 hours exposure with them in comparison from those with 2% PLS. Overall all the 24 hour extracts reduced the cell metabolic activity by approximately 20%. 7 day extracts reduced overall metabolic activity by approximately 50%. Repeated measures ANOVA showed a significant difference within time points ($p<0.001$) and between concentrations ($p<0.001$). Interaction between the different time points and the material used was also significant at $p<0.001$. Bonferroni post-hoc tests showed that the control formulation was significantly different to the rest ($p<0.001$), while PMMA was different also to the 4% MCPM, 2% PLS formulation (Bonferroni, $p=0.049$). The 8% MCPM 2% PLS was also significantly different to the 8% MCPM and 5% PLS ($p=0.002$).

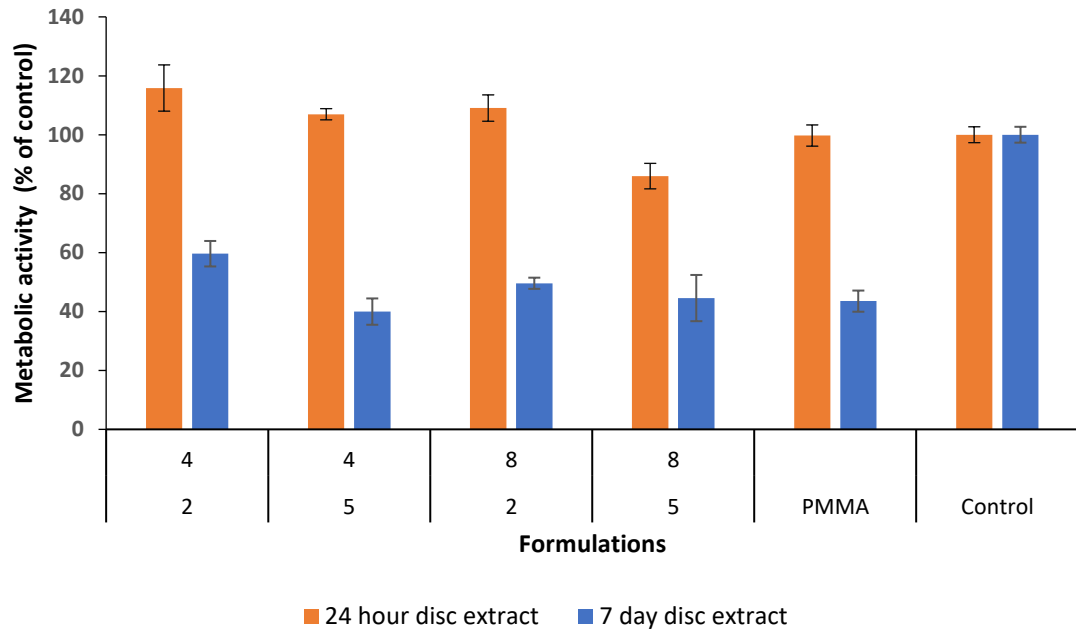


Figure 5.6 Metabolic activity of bone marrow derived sheep MSCs assessed via Alamar blue. Fluorescence following exposure to disc extracts from formulations and a commercial cement after 24 hours and 7 days (including the first 24 hours). (Error bars = 95 % CI n=6). Bonferroni, ($P < 0.05$).

Factorial analysis of the metabolic activity of bone marrow derived sheep MSCs exposed to disc extract is given in Figure 5.4. With increasing levels of MCPM the metabolic activity of cells decreased by 7% after 24 hours and after 7 days the metabolic activity of cells decreased by 3%. With increasing levels of PLS the metabolic activity of the cells decreased by 12% after 24 hours and by 14% after 7 days. With combined increasing levels of MCPM and PLS the cell metabolic activity decreased by 6% after 24 hours and increased by 10% after 7 days.

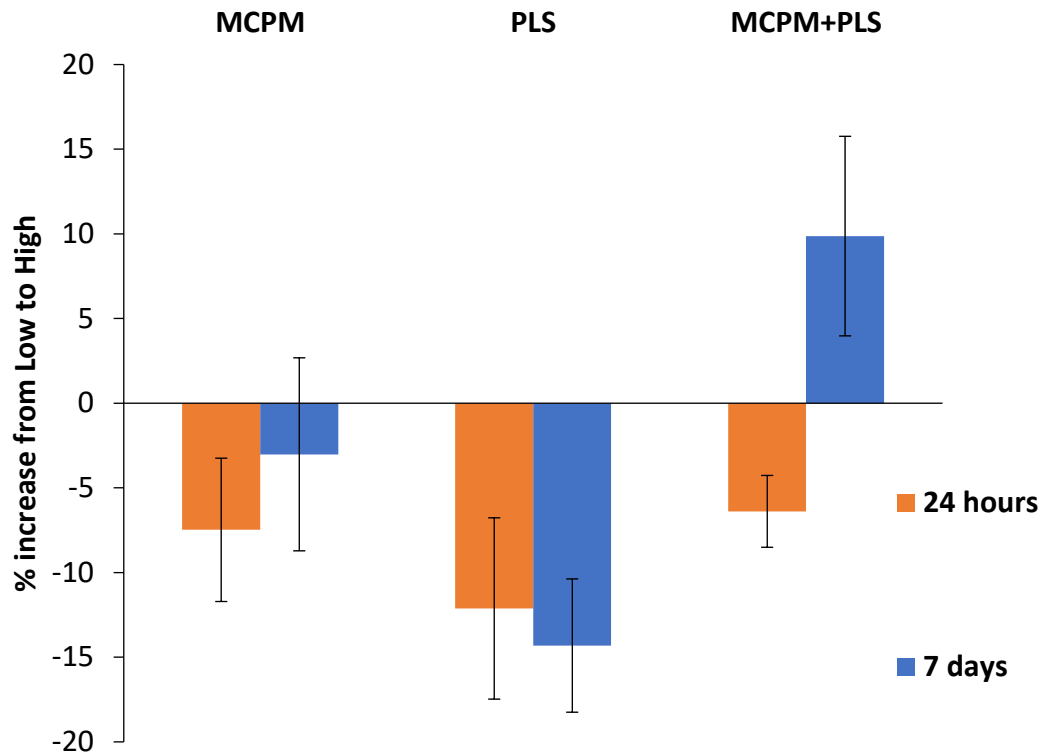


Figure 5.7 Factorial analysis for metabolic activity of bone marrow derived sheep MSCs exposed to disc extract of varying levels of MCPM and PLS after 24 hours and 7 day incubation. (Error bars = 95 % CI n=6).

Disc's extract solution from each formulation after 24 hours was photographed (Figure 5.5). Cell culture media 24 hours with discs containing higher (5 wt%) versus lower (2 wt%) levels of PLS, peach versus the original pink colour respectively. All disc extract solutions after 24 hours showed cloudiness but those that had contained formulations with higher levels of MCPM were more so.



Figure 5.8 Disc extract solutions after 24 hours sample storage at 37 °C.

5.6.3 Bone Marrow Derived Sheep MSCs: Polylysine Toxicity

To understand better which components may influence cell activity, PLS was added individually to assess cell activity. Figure 5.1 presents sheep mesenchymal cell metabolic activity before and after exposure to PLS at different concentration for 24 hours. Concentrations of PLS of 32 mM to 0.32 mM caused a gradual increase in cell metabolic activity but still low in comparison to control. Considering the repeated measures ANOVA, within-subjects, a significant difference was found for the different time points ($p < 0.001$). Between-subjects, concentration was also significant at $p = 0.01$. Bonferroni post-hoc tests revealed the control group was significantly different to 0.32 mM ($p = 0.02$), 3.2 mM ($p = 0.02$), 32 mM ($p = 0.028$), 320 mM ($p = 0.02$) and 3200 mM ($p = 0.02$). However, the concentrations were similar between them ($p > 0.05$).

Figure 5.2 is a photograph of a 96 well plate with serially diluted PLS from 3200 mM to 0.32 mM.

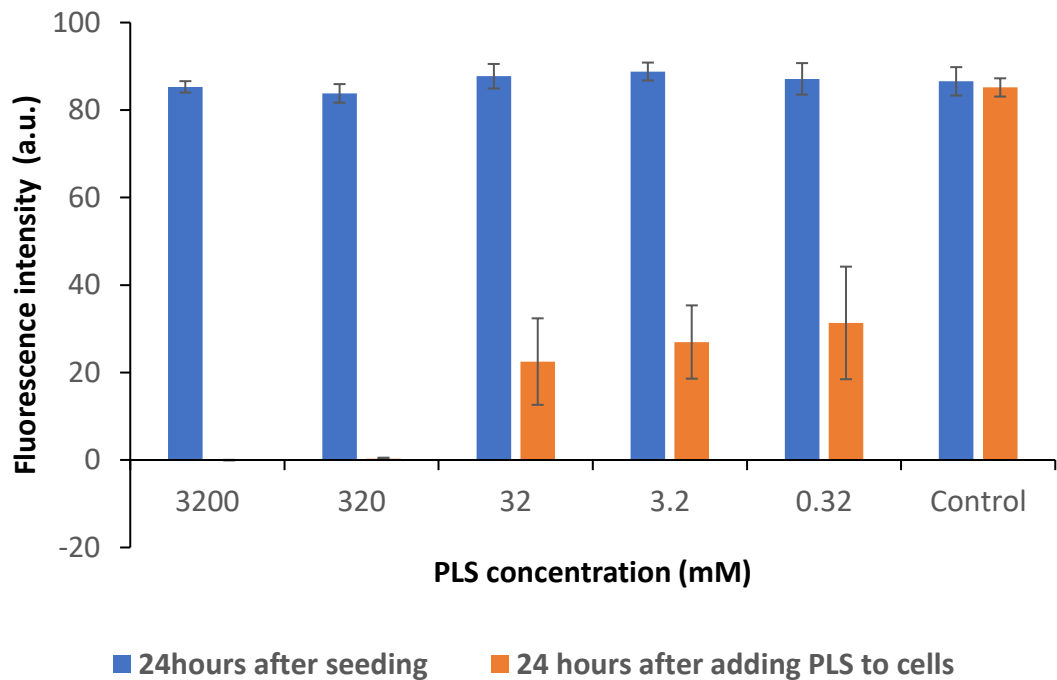


Figure 5.9 Fluorescence intensity versus bone marrow derived sheep MSCs exposure to increasing concentration of PLS (3200 mM to 0.32 mM) after 24 hours. Metabolic activity was assessed used Alamar blue. Control was cells exposed to cell culture media. (Error bars = 95 % CI n=3). Brackets indicate significant differences among groups, Bonferroni, ($P < 0.05$).

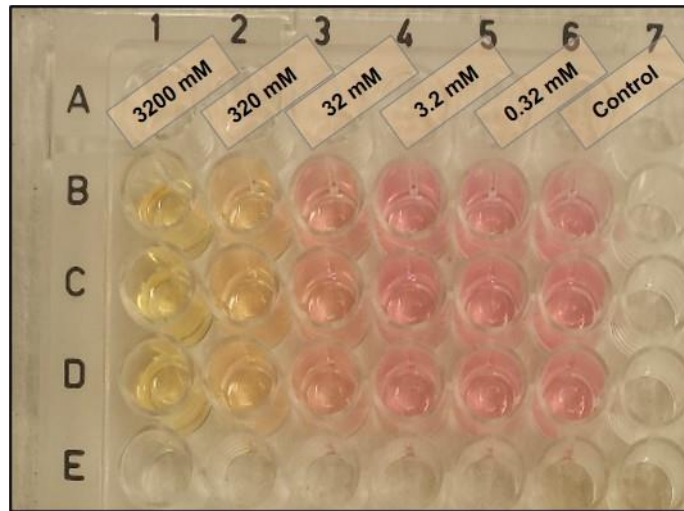


Figure 5.10 Visual indication of DMEM colour change due to the different amounts of PLS concentration in a 96 well plate in replicates of 3. PLS concentrations decreasing from wells 1 to 7.

5.6.4 MG63 cells: Effect of Disc Extract Solution

Figure 5.12 presents the metabolic activity of MG63 cells after 24 hour exposure to disc extracts from formulations with varying levels of MCPM and PLS and a control with no MCPM and PLS. The mean metabolic activity (%) was significantly different across the different materials, as confirmed by one-way ANOVA ($p < 0.001$). Bonferroni revealed the control group was significantly different to all ($p < 0.001$), while PMMA was significantly different to 4% MCPM 2% PLS ($p < 0.001$), 4% MCPM 5% PLS ($p < 0.001$), 8% MCPM 2% PLS ($p = 0.017$) and 8% MCPM 5% PLS ($p < 0.001$). 4MCPM 2% PLS was found to be significantly different to 4% MCPM 5% PLS ($p = 0.020$) and 8% MCPM 5% PLS ($p < 0.001$). 4% MCPM 5% PLS was also significantly different to 8% MCPM and 2% PLS ($p = 0.001$). 8% MCPM 2% PLS was significantly different to 8% MCPM 5% PLS ($p < 0.001$).

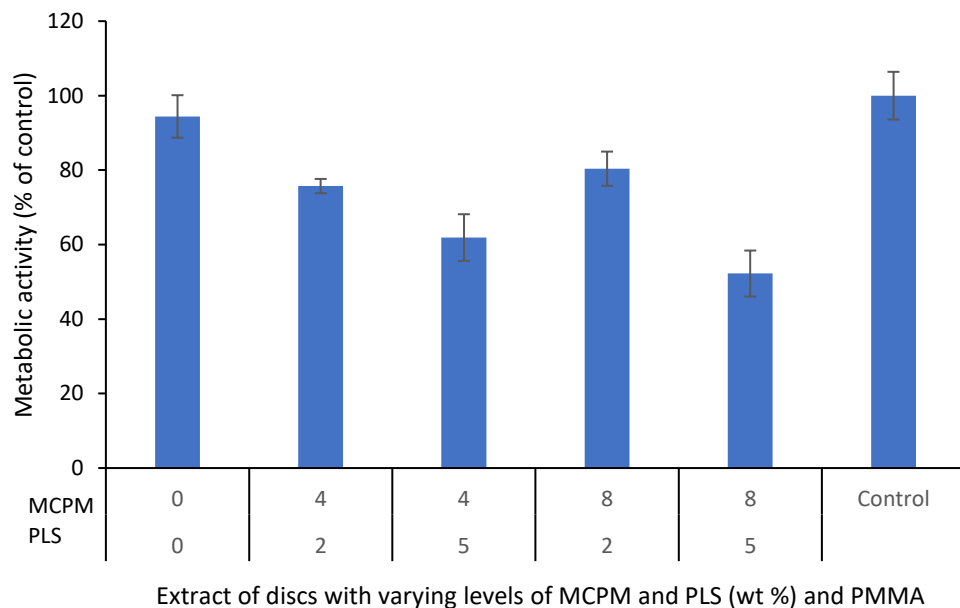


Figure 5.11 Metabolic activity of MG63 cells assessed after 24 hour exposure to disc extracts of experimental bone composite with varying levels of MCPM and PLS (Error bars = 95 % CI n=9). Bonferroni ($P < 0.05$).

Factorial analysis of the metabolic activity of MG63 cells exposed to disc extract after 24 hours, is given in Figure 5.13. With increasing levels of MCPM in the composite fillers the metabolic activity of cells in composite extracts increased by 2%. With increasing levels of PLS the metabolic activity of cells decreased by 17%. With increasing levels of PLS the metabolic activity of cells decreased by 17%. With combined increasing levels of MCPM and PLS the cell metabolic activity decreased by 12%.

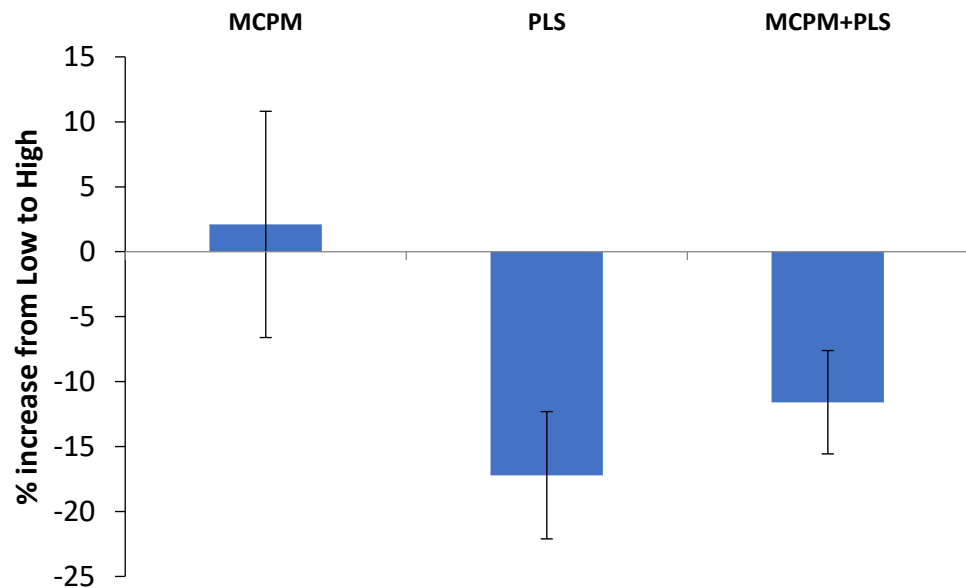


Figure 5.12 Factorial analysis of MG63 cells exposed to disc extract of varying MCPM and PLS formulation after 24 hour (Error bars = 95 % CI n=3).

Figure 5.14 is showing the cell metabolic activity of MG63 cells to disc extract with varying levels of MCPM and PLS and commercial PMMA, collected after 24 hours and 7 days. 24 hours extract with 5% PLS showed lower metabolic activity in comparison to 2% PLS extract. 7 day extract showed a further reduction in metabolic activity with 5% PLS showing lower metabolic activity in comparison to 2% PLS extract. Extract from PMMA had no effect on metabolic activity after 24 hours and 7 days. The metabolic activity (% of control) was found to be significantly different for the two studied time points ($p < 0.001$), and the interaction between the different materials and the time points ($p < 0.001$). Means were also different between-subjects, considering the different materials ($p < 0.001$). Control was not different to PMMA ($p > 0.05$), nor was the 8% MCPM and 5% PLS when compared to the 4% MCPM 5% PLS ($p > 0.05$), or the 8% MCPM 2% PLS compared to the 4% MCPM 2% PLS. All other groups were significantly different to each other at $p < 0.001$.

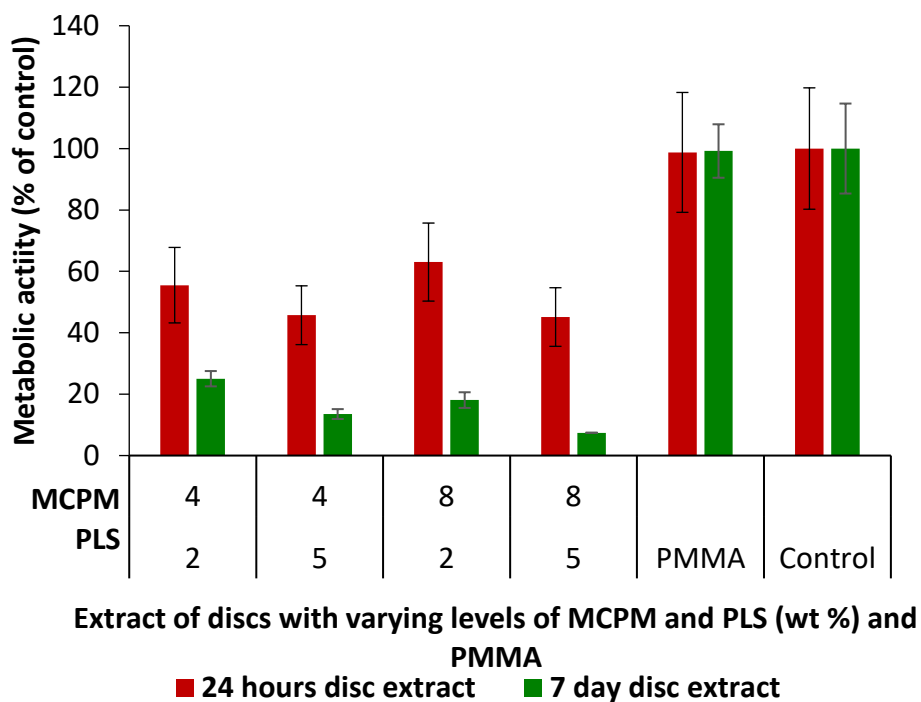


Figure 5.13 Metabolic activity of MG63 cells after 24 hour incubation with disc extracts of varying formulations for 24 hours and 7 days. Metabolic activity was assessed using Alamar blue and absorbance was measured. (Error bars = 95 % CI n=9).

Factorial analysis of the metabolic activity of M63 cells exposed to disc extract is given in Figure 5.15. With increasing levels of MCPM the metabolic activity of cells increased by 14% after 24 hours and after 7 days the metabolic activity of the cells decreased by 36 %. With increasing levels of PLS the metabolic activity of cells decreased by 14% after 24 hours and by 43% after 7 days. With increasing levels of PLS the metabolic activity of cells decreased by 14% after 24 hours and by 43% after 7 days. With combined increasing levels of MCPM and PLS the cell metabolic activity decreased by 11% after 24 hours and increased by 20% after 7 days.

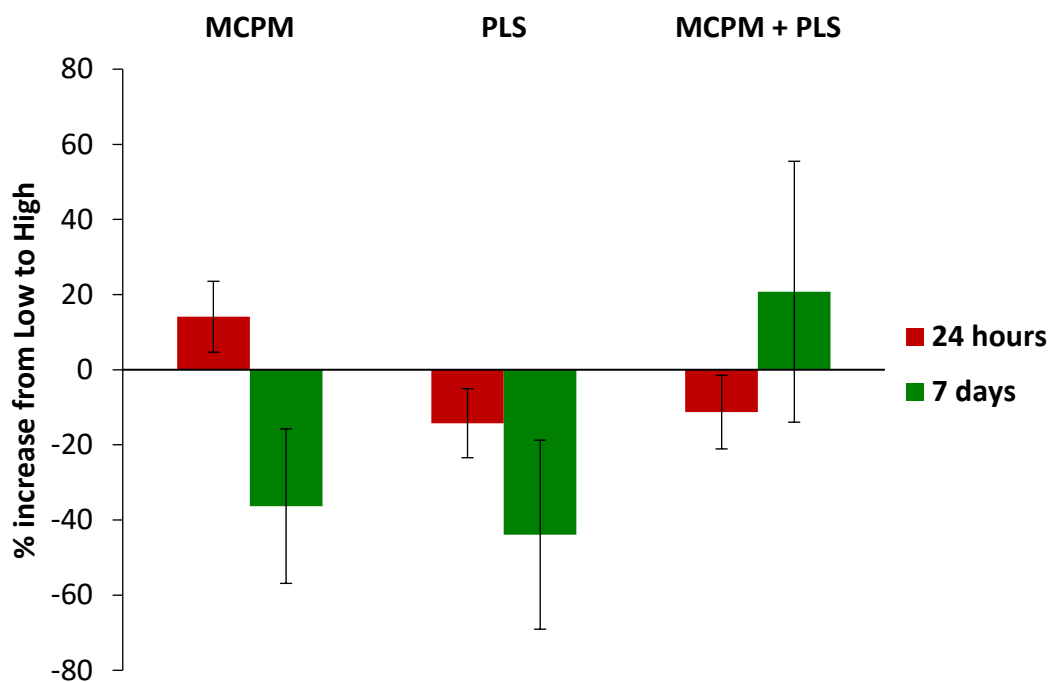


Figure 5.14 Factorial analysis of MG63 cells exposed to disc extract of varying MCPM and PLS formulation after 24 hour incubation and) after 7 days incubation. (Error bars = 95 % CI n=3).

5.6.5 MG63 cells: Polylysine, Monocalcium phosphate and Hydrochloric Acid Toxicity

MG63 cells were exposed to increasing concentrations of individual components of the experimental bone composite and hydrochloric acid (HCl). Figure 5.11 presents MG63 cell metabolic activity after exposure to HCl, PLS and MCPM at different concentration for 24 hours. With increasing concentrations of HCl a gradual effect can be seen on the cell's metabolic activity. PLS and MCPM display a sharp effect from 10 mM to 1 mM and 1m to 0.1 mM respectively. The medians for the metabolic activity (%), within the same concentrations, were dependent upon the additive (HCL, PLS or MCPM). Thus, differences between the additives were found for the following concentrations: 10 mM (Kruskal-Wallis, $p=0.027$), 1 mM ($p=0.026$), 0.1 mM ($p=0.027$) and 0.01 mM ($p=0.027$). Considering 0.001 mM and control (DMEM), no differences were found between the materials (KW, $p>0.05$). Pairwise comparisons, adjusted by the Bonferroni method, were significant at $p=0.043$ for all significant comparisons.

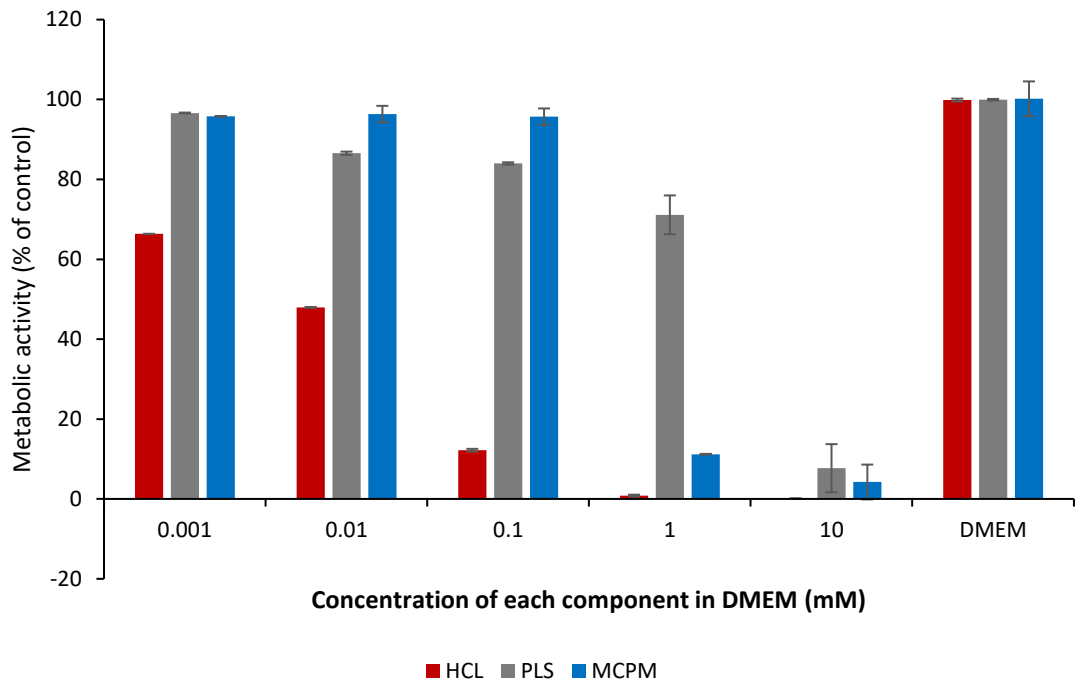


Figure 5.15 Metabolic activity of MG63 cells against decreasing concentrations of HCl, PLS and MCPM after 24 hour incubation. Metabolic activity was assessed using Alamar blue. Flouresence was measured (a.u.) (Error bars = 95 % CI n=3). Kruskal-Wallis $P<0.05$, Bonferroni ($P<0.05$).

5.7 Discussion

5.7.1 Sheep Mesenchymal Stem Cell: Morphology on Disc Surfaces

For a material to integrate and have osteoconductive properties it is vital the surrounding cells are able to attach to the material. When a new biomaterial is placed, mesenchymal stem cells are recruited from the bone marrow to the material. Here the cells bind and differentiate into bone forming cells (osteoblasts) (Vohra et al., 2008).

It was predicted high levels of MCPM and PLS combined would hinder sheep mesenchymal cell activity and cell spreading on the disc surfaces. Despite the decrease in metabolic activity of the cells after exposure to the disc extract, this study was able to demonstrate the presence and spread of cells on the disc surfaces. PMMA, a material that's already used commercially was able to allow cell attachment as well as the experimental bone composite with varying levels of MCPM and PLS combinations.

Disc surfaces for all formulations discs showed presence of flat and spread cells and upon higher magnification nodules could be identified on top of the cells. Normally bone cells lay down the extracellular matrix, collagen I which then could mineralise bone-like apatite (Jones, 2006) similar to what was observed on the discs in chapter 4. Further examination with EDAX can provide information on elements on the disc surfaces and on cells. This may be difficult if element levels are low such as the nodules present on the cells.

The wettability of a material also influences cell spreading. Formulation levels and combinations can influence this property of the material thus affecting cell response. A water contact angle test would allow assessment and information on how much this influences the materials surface. A recent study quantified the SBF contact angle of a biomaterial surface which showed the composite with HA on its surface became more hydrophilic, enhancing the surface wettability (Ho et al., 2020). Bone composite that has potential to release apatite such as HA may increase the success of composite-tissue integration. In this study SEM observation revealed cell density on all formulation discs was high. Cells are all spread on all formulation discs as well as images showing filopodia on cells, implying the formulation discs facilitate cell adhesion and spreading thus promoting cell growth. While the differences in MCPM levels were different by a half, the high or low levels may be crucial in the process of cell attachment, growth and further interactions between the biomaterial and cells in the fractured site. According to Anselme et al (Anselme, 2000; Anselme, Ponche, & Bigerelle, 2010; Rabel et al., 2020) this is important; the quality of the initial phase of interaction between the cells and the biomaterial surface affects the quality of the second phase. The initial phase involves cell docking on to the surface and then locking on to the biomaterial (Khalili & Ahmad, 2015). It must also be noted the cell adhesion process is slightly different in a static medium culture and a dynamic in vivo process (where docking and locking will occur). In this study a static medium culture process was assessed where the cell adhesion was reliant on electrostatic interaction between the cells and experimental bone composite and integrin bonding followed by focal adhesion (Khalili & Ahmad, 2015). Focal adhesion is evident as the results showed cell spreading.

Typically osteoblasts attach and spread on an implant surface followed by the proliferation and subsequent differentiation. These steps lead to direct contact between the bone and the biomaterial surface. Since these were bone marrow derived sheep MSCs and not developed bone cells such as osteoblasts, it would be sensible to assess the same factors osteoblasts. In addition further studies using specific human mesenchymal stem cells assessing differentiation potential upon contact with the material would be required.

Studies in literature have shown implants that don't have smooth surfaces, encouraging osteoblast-triggered hard tissue integration (Wennerberg & Albrektsson, 2009). The bone composite in this study initially is smooth as seen in chapter 4 Figure 4.11 . Over time the surface topography changes as seen in Figures 4.15 due to remineralisation which should encourage cell interaction.

Zhao et al demonstrated MG63 cells to attach and spread on composite surfaces, however a 24 hour of passivation was carried out to ensure release and removal of any harmful products (Zhao et al., 2010). However this step was not needed for the bone derived sheep MSC cells.

Studies with MSCs and chemobrionic calcium phosphates scaffold have demonstrated upregulations of osteogenic markers including runt-related transcription factor 2 (RUNX2), transcription factor SP7 (SP7), collagen type 1 alpha 1 (COL1A1), and bone gamma-carboxyglutamic acid-containing protein (BGLAP) (Hughes et al., 2020). Similar biomarkers should be investigated with cells exposed to the experimental bone discs.

Material stiffness can influence cell behaviour, increasing stiffness has improved specific cell behaviours such as cell migration and proliferation (Cheema, 2013). PMMA is known to have a higher modulus than that of the normal vertebral body, resulting in higher stiffness (Jiang et al., 2015). Future work can look at this and use this technique to see cell interaction with different pastes with different modulus and cell behaviour towards mineralisation of collagen from experimental bone composite.

5.7.2 Bone Marrow Derived Sheep MSCs: Effect of Disc Extract Solution

Once cells attach to a biomaterial, cells begin to proliferate and spread. The cell adhesion process is involved in stimulating signals that further differentiate and encourage cell migration and cell survival (Khalili & Ahmad, 2015). Thus it is important to understand the environment around the cells and how it influences their behaviour after attachment.

Disc extract solution visually show how the components change the pH of the cell culture medium; higher levels of PLS at 5% caused the cell culture medium to be less pink and more peach. This is reflective in the cell activity; cells exposed to cell culture medium with higher levels of PLS showed lower metabolic activity.

The initial exposure in 24 hours of cells to the disc extract has little effect on cell activity, however 7 day's extract, decreases cell activity. In chapter 4 discs with a combination of 8% MCPM with 5% PLS in the filler phase have exhibited acidity in deionised water.

It is possible the acidic environment for the cell culture medium is responsible for the decrease in cell activity. However the levels of MCPM are not as effective as the levels of PLS in decreasing pH. In the factorial analysis from this study we can see that interaction of MCPM and PLS seem to increase cell activity. Increasing levels of PLS in dental composites showed similar results where increasing PLS concentrations may induced cytotoxic effects to MSCs (Alkhoury, 2019). However discs in this study were not stored in any media for 24 hours prior to exposure to cells unlike previous studies.

While alamar blue is able to give results that show differences in the composite formulations after several repeated experiments, the method is an indirect method to assess cellular activity. It relies on a metabolic pathway that can be affected by individual cells intracellular activity.

A direct cell viability assay would complement the above study would be to determine the ratio of live and dead cells. This assay will not give information on whether cell death occurred due to apoptosis or necrosis, but it will give quantifiable results based on cells that were able to withstand disc extract conditions or not.

5.7.3 Bone Marrow Derived Sheep MSCs: Polylysine Toxicity

In this study PLS has shown to create an acidic environment around the disc, thus looking at how PLS was directly influencing cell activity was of interest. PLS is generally used for promoting attachment of cells and proteins to solid surfaces to enable growth. In this study, concentrations of 3200 mM to 320 mM prevented cell metabolic activity. Conversely concentrations of 32 mM to 0.32 mM PLS had less effect on cell metabolic activity however these were still too low to claim safe levels of PLS for the cells. Percentage of viable cells equal to or more than 70% compared to control would be considered safe levels of PLS according to literature (Assad & Jackson, 2019).

Previous studies have suggested PLS (M. A. Khan, 2015) to buffer the acidic effect of MCPM in SBF and de-ionised water. However according to this study, PLS appears to change the cell culture medium from pink to yellow, suggesting a change of pH. With decreasing concentration of PLS, the cell culture medium's colour was closer to pink. All PLS concentrations investigated lowered metabolic activity by more than 50 %.

The most common components of a cell culture media are glucose and sodium bicarbonate to maintain the correct pH with phenol red. The sodium bicarbonate reacts with the hydrogen ions generated by CO₂ to neutralise the acidic conditions. For cells to perform optimally and grow, pH is critical in influencing mesenchymal cell behaviour (Wuertz, Godburn, Neidlinger-Wilke, Urban, & Iatridis, 2008).

PLS decreasing pH may therefore be the cause of reduced cell metabolic activity. If this experiment was to be repeated, a serial dilution of PLS would be carried out until metabolic activity levels were close to the control to identify the critical point. To further assess if it is pH that influenced the activity of cells and not PLS itself, other components such as N-2-hydroxyethylpiperazine-N-ethanesulfonic acid (HEPES) can be added to increase buffering capacity.

The experimental bone composite's function is to provide a healthy environment after it is injected at the site of fracture to encourage healing. 2-Dimensional (2D) cell cultures are not reflective of fracture sites where blood pH levels are accurately controlled along with a constant flow of ions, proteins and nutrients being exchanged. Here cell-extracellular environment interactions are not representative of the fracture site with the bone composite.

A previous study examining the effects of the same PLS used in this study, on human mesenchymal stem cells found low concentrations promoted adhesion, spread, proliferation and chondrogenic differentiation while a high concentration proved to be toxic (Lu, Guo, Kawazoe, Tateishi, & Chen, 2009). A certain level of PLS is therefore potentially beneficial for cells. This study looked at very high concentrations of PLS in the cell culture medium. Cells in the fracture site may be initially exposed to high levels of PLS and later small amounts over a period of time. Previous studies of PLS release have shown a linear relationship between percentage of polylysine release and the square root of time in an experimental bone composite (M. A. Khan, 2015), representing a diffusion controlled process.

In addition this has also been shown by Panpisut (2017) and Alkhouri (2019), where a burst release from formulations was found particularly with discs with higher powder to liquid ratio.

Diffusion rate of a component from experimental bone composite can be affected by several factors (temperature, concentration difference, diffusion distance and diffusing material). Fick's first law states that diffusion is proportional to concentration gradient and it is a time dependant process (Alkhouri, 2019). Based on this the difference between the concentration between the experimental bone composite and the fractured sight will encourage the experimental bone to release more PLS.

It would be reasonable to carry out PLS release studies to see the amount of PLS released over a period of time giving an indication of how much PLS would be in contact with the cells.

5.7.4 MG63 cells: Effect of disc extract solution

It was predicted MG63 cell activity would respond to disc extract the same way as sheep mesenchymal cells activity. However disc extract of 7 days for all formulations resulted in cell activity below 20% as a percentage of control whereas sheep mesenchymal stem cell activity was approximately half of control. A similar trend can be seen where disc extracts with higher levels of PLS at 5% reduced cell activity more than disc extracts with PLS at 2%.

The release of methacrylate monomers together with compounds of the polymerisation system from dental composites has been considered as a source of a wide variety of adverse biological reactions, including local and systemic toxicity, pulp reactions, allergic and estrogenic effects. These effects have been extensively reviewed in the literature (Bakopoulou, Papadopoulos, & Garefis, 2009). However in this study the disc extract solution from the control composite appears to have little effect on reducing cell metabolic activity of the cells.

In comparison to bone marrow derived sheep MSCs, disc extracts appear to reduce activity of the MG63 cells much more. In comparison to bone marrow derived sheep MSCs, disc extract of 7 days appears to reduce activity of the MG63 cells a lot more, for all formulation disc extracts the metabolic activity as a percentage of control was below 20% (Figure 5.13) amongst MG63 cells. Whereas the metabolic activity of the sheep mesenchymal stem cells for all formulations after 7 days was above 40% (Figure 5.6).

A study carried out by Vohra looked at the MSC and osteosarcoma cells and found both cells to bind to HA covered biomaterials via different mechanisms. MG63 cells demonstrated maximal binding to fibronectin-coated HA, while MSCs alternatively preferred HA-coated with collagen-1. Further interestingly the binding of MG63 was via 2 integrins ($\alpha 5$ and αv) in comparison to MSC which was via 1 integrin (αv). They also found the osteosarcoma cells were unable to spread on the HA coated material whereas MSC cells spread very well (Vohra et al., 2008). The study looked at a direct comparison between the 2 different cell lines, although the focus was on binding and not proliferation. The results from this project also looks at the 2 different cell line's response to the disc extract demonstrating the cell response was better amongst MSC cells in comparison to the MG63 cells. The mechanisms are not known as to how the cells respond to the disc extracts and what it is in the formulations that may hinder activity but it is something that could be studied further.

A study carried out by Debnath et al showed PLS to have cytotoxic effect on 4 types of cancer cells (K562, A549, U937 and B16F10 cancer cells). Concentrations of polylysine from 20-40 mg/kg were used, which are much higher in comparison to the levels of PLS used in the disc extract. (Debnath, Karan, Debnath, Dash, & Chatterjee, 2017). It is possible PLS extract from the disc extracts have target specific cell activity inhibition against MG63 cells.

The results for this study need better understanding and detailed testing including, cell markers, cell progenitors, antibodies markers. Thus the data for this particular study for now can be represented as observational.

The disc extract effect on cell activity has exhibited results to allow further investigation in interaction with cells, laying the ground work for future studies.

5.7.5 MG63 Cells: Polylysine, Monocalcium phosphate and Hydrochloric Acid Toxicity

PLS and MCPM appear to have critical points at which they significantly reduce metabolic activity of MG63 cells. PLS and MCPM display a sharp effect from 10 mM to 1 mM and 1m to 0.1 mM respectively. MCPM is known to release phosphoric acid decreasing pH (Alkhouri, 2019) potentially creating a toxic environment for the cells. Similar to the PLS which was observed in section 5.6.1 where increasing levels of PLS decreased pH reduced bone derived sheep MSCs activity.

A study was conducted investigating the effect of calcium ion concentration in culture medium on the promotion of osteogenesis by MG63 osteoblast-like cells. After 14 days, alkaline phosphatase activity of cells supplemented in high calcium ion concentration was down regulated and after 28 days calcium content of gelatin hydrogels was significantly higher in comparison to cells supplemented in standard calcium ion concentration (Takagishi et al., 2006). Suggesting calcium may enhance and aid cells in precipitation of minerals.

Further detailed studies are required to assess how MG63 cells are affected by varying levels of PLS and MCPM along with parallel studies to assess the different behaviour of cells in response to the disc extracts at different time points.

5.8 Conclusions

- PLS concentrations from 32000 mM to 0.32 mM were toxic to for bone marrow derived sheep MSCs under the examined conditions.
- Increasing MCPM (from 4 to 8 wt%) and PLS (from 2 to 5 wt%) of the powder phase had significant effect on bone marrow derived sheep MSCs activity.
- 5 wt% of PLS in fillers of experimental bone composites reduced cell metabolic activity more than 2 wt% of PLS.
- The experimental bone composite did not present itself to be t a hostile surface to bone marrow derived sheep MSCs
- MG63 cells were more sensitive to experimental bone composite extracts in comparison to the bone marrow derived sheep MSCs

CAM grafting In-ovo of Composite Discs

6.1 Abstract

The aim of this chapter was to evaluate chick embryo viability in the presence of the experimental bone composite and to establish whether the vascular network continued to grow normally.

Discs were prepared, grafted on to the chick CAM (chorioallantoic membrane), harvested after 14 days and health of vasculature in areas of contact with the composite and embryo survival was assessed by in vivo and ex-vivo imaging, scanning electron microscopy and immunofluorescence staining. The first set of discs consisted of individual levels of MCPM (4 and 16 wt%), and PLS (2 and 10 wt%). Second set also consisted of individual levels of MCPM (8 wt%) and PLS (5 wt%) based on the formulations described in chapter 4. The discs were implanted as a whole and in quarters in the chick embryo. Final set included discs with combined formulations (8 wt % MCPM + 5 % PLS, 8 wt% MCPM + 2 wt % PLS, 4 wt% MCPM + 5 wt% PLS, + 4 wt % MCPM + 2 wt %) similar to those in the chapter 4.

Data showed all the chick's membrane in contact with the experimental bone composite discs, appeared to have healthy vascularisation. Discs consisting of MCPM, showed apatite precipitation. The experimental bone composite material showed strong adherence to the membrane, while PMMA discs easily detached upon harvest.

In conclusion discs were not harmful or toxic to the developing chick embryo.

6.2 Introduction

Chapter 5 looked at initial compatibility assays, which are common for biomaterial's preclinical testing. However 3-Dimensional (3D) cell culture systems provide a better model of *in vivo* conditions compared to 2D cell cultures. A 3D cell culture will represent a more precise microenvironment of bone cells for this study, however, 3D cell culture assays at present lack reproducibility, are time consuming and expensive. Furthermore, it does not inform on the potential of the biomaterial to become vascularised. The CAM model is an inexpensive alternative to other animal models which allows for a quick and initial evaluation of material biocompatibility and vascularisation. The CAM is a highly vascularised tissue, and can be observed *in vivo* under a microscope, allowing assessment of how disc implants influence the growth of blood vessels (I. Moreno-Jiménez et al., 2017).

The site of fracture is influenced by physical constraint which also affect signal transduction, influencing gene expression and cellular behaviour (Edmondson, Broglie, Adcock, & Yang, 2014), this a continuous dynamic process which the CAM model can mimic unlike a static *in vitro* cell culture system. CAM assays have been used for bone tissue engineering purposes with composite materials such as, bioactive glass nanoparticles. Vargas et al examined the biocompatibility and bone mineralization potential of 45S5 Bioglass using an *ex ovo* approach, where the authors used the embryo survival rate as an indicator of biocompatibility (Vargas et al., 2009).

In this chapter, discs implants consisting of MCPM and PLS as well as the commercial Simplex P™ PMMA were grafted onto the CAM. The biocompatibility and bone mineralisation potential of the experimental bone composites was examined after 1 week *in-ovo*. Disc implants included either MCPM (4, 8 or 16 wt%), PLS (2, 5 or 10 wt%) or neither. Discs were also cut in to quarters to assess if any unreacted monomers within the experimental bone composite were toxic to the developing chick embryo. Disc implants with combined levels, of MCPM (8 or 4 wt%) and PLS (5 or 2 wt%) similar to the formulations used in chapters 4 and 5 were CAM-grafted, and, compared with the commercial PMMA. The CAM's central section is completely developed by day 8 where disc implants can be sustained, thus the discs were implanted at day 7. The embryo is fully enveloped by the CAM at day 12 and the blood vessels are highly angiogenic (Deryugina & Quigley, 2008). An ideal bone composite will have the mechanical strength to withstand load as well as providing a suitable environment for blood vessel formation for bone growth, as well as the ability to stimulate osteogenic proteins to stimulate surrounding cells and induce differentiation of cells as well as mineralisation and calcification of new bone (Gao et al., 2017). This study observed the vascularisation around the disc implants and the disc implants' ability to remineralise.

6.3 Aims

This chapter aims to assess if high levels of PLS and MCPM in the experimental composite discs or Simplex™ P (PMMA) have any toxic effect on the developing chick embryos and how they influence vasculature. Discs will be implanted in to the CAM, and harvested 7 days later to be observed via SEM and immunofluorescence staining.

6.4 Objectives

Assess if increasing MCPM (from 0 to 4 % to 8 % to 16 % wt) and PLS (from 0 to 2 % to 5 % to 10% wt) individually or combined in the disc versus commercial PMMA:

- Has any effect on the chick embryo.
- Has any effect on vasculature of embryo membrane around the implant
- Increases mineralisation on the disc surfaces
- Show cell migration on to the disc surfaces

6.5 Materials and Methods

Disc preparation and sterilisation along with the CAM graft protocol is described in chapter 2. The disc size used for implants were 8mm in diameter.

6.5.1 MCPM and PLS Added Individually in Disc Implants

Table 6.1 presents the 5 formulations used for the disc implants. Low levels of PLS (2 %) and high levels of PLS (10 %) were used and the same was done with MCPM, low at 4 % and high at 16 %.

Table 6.1 MCPM and PLS percentages added to initiator versus activator paste fillers in 5 formulations (Monomer phase: UDMA (7.5 g), PPGDMA (2 g), HEMA (0.25 g). 4-META (0.3 g) was added in the initiator phase only. 2.5 % BP and 1.5 % NTGGMA. Glass filler: 7 µm and 0.7 µm ratio 4:5.. PLR 3:1).

Formulation	MCPM (wt %)	PLS (wt %)
2P	0	2
10P	0	10
4M	4	0
16M	16	0
0PM	0	0

6.5.2 MCPM 8 wt% and PLS 5 wt% Added Individually in Disc Implants

Table 6.2 shows the levels of PLS and MCPM used individually for in disc implant formulations. These amounts were selected on the basis of the combined composite formulations discussed in the previous chapters; the highest amounts were used to see if these levels were toxic to the chick embryo and how they may influence vascularisation within the CAM and around the disc implants.

Table 6.2 Intermediate levels of MCPM and PLS percentages added to initiator versus activator paste fillers in 5 formulations (Monomer phase: UDMA (7.5 g), PPGDMA (2 g), HEMA (0.25 g). 4-META (0.3 g) was added in the initiator phase only. 2.5 % BP and 1.5 % NTGGMA. Glass filler: 7 μ m and 0.7 μ m ratio 4:5.. PLR 3:1).

Formulation	MCPM (wt %)	PLS (wt %)
5P	0	5
8M	8	0
0PM	0	0

Discs were cut in to quarters (Figure 6.1B) using a low speed hand piece (Figure 6.1A). These set of discs were added to the CAM as full round discs and in quarters.

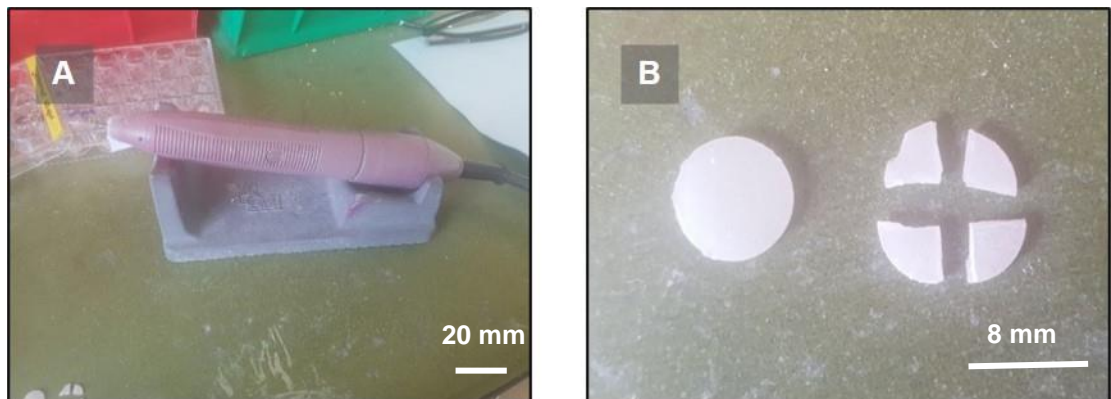


Figure 6.1 (A) Low speed hand piece used to cut the discs in quarters. (B) Discs before and after cutting.

Figure 6.2 shows that a whole disc of the experimental bone composite remained in place and the embryo was alive, as indicated by the healthy vasculature 7 days after CAM-grafting (ED 14).



Figure 6.2 Whole disc of the experimental bone composite(0 wt % MCPM and 0 wt% PLS) photographed in ovo 7 days after CAM-grafting

Figure 6.3 represents how disc implants of the experimental bone composite cut in to quarters remained on the chorioallantoic membrane for 14 days.



Figure 6.3 Discs cut in quarters of experimental bone composite (0 wt% MCPM and 0 wt% PLS) photographed in-ovo at ED 7 after CAM-grafting.

6.5.3 Experimental Bone Composite Formulations Versus Commercial PMMA Bone Cement for Disc Implants

Table 6.3 presents the combined formulations used for the disc implants of the experimental bone composite. Full round discs were used for these set of discs.

Table 6.3 Combined levels of MCPM and PLS percentages added to initiator versus activator paste fillers in 5 formulations (Monomer phase: UDMA (7.5 g), PPGDMA (2 g), HEMA (0.25 g). 4-META (0.3 g) was added in the initiator phase only. 2.5 % BP and 1.5 % NTGGMA. Glass filler: 7 μ m and 0.7 μ m ratio 4:5.. PLR 3:1).

Formulation	MCPM (wt %)	PLS (wt %)
4M2P	4	2
4M5P	4	5
8M2P	8	2
8M5P	8	5

6.5.4 Vascular density, junctions and branches quantification

Microscope images of the discs were processed using the 'vessel-analysis' plug-in, in the ImageJ software (NIH). Images converted into binary images and the vascular density analysis function was applied. The software automatically calculates the vascular density normalised to the area of the disc. Junction and branching points were counted in each image using ImageJ 'counter' function by digitally selecting the number of junction and branching points seen in the vasculature on the disc implants.

6.6 Results

6.6.1 MCPM and PLS Added Individually in Formulations for Disc Implants

Figure 6.4 represents chick embryos from ED 7 to ED 14 with a disc of the experimental bone composite grafted onto the CAM. Baseline images were collected prior to adding implants. Some disc implants moved to the edges which became difficult to image at ED 14.

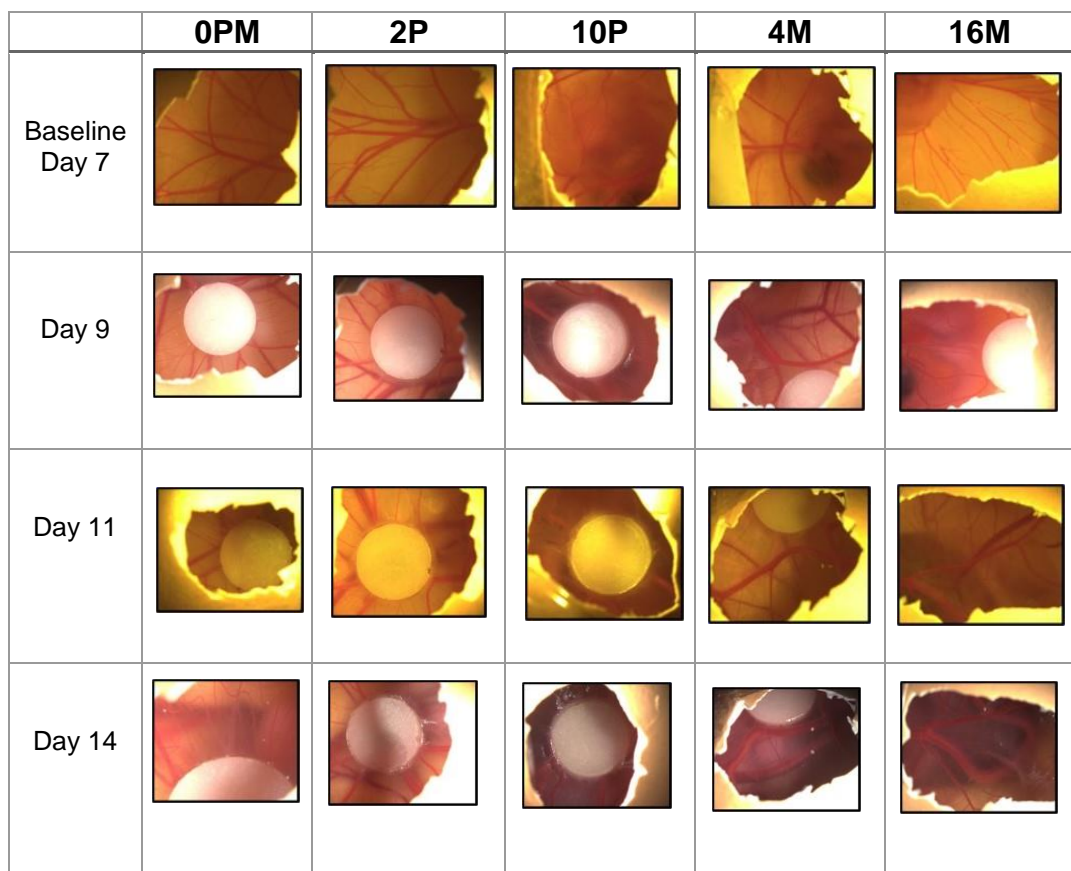


Figure 6.4 Macroscopic timeline from day 7 to 14 days of in-ovo features with disc implants (diameter 8mm) of the experimental bone composite with different formulations; 2 % PLS, 10 % PLS, 4 % MCPM and 16 % MCPM. (n=5).

Figure 6.5 shows the disc implants of the experimental bone composite on the CAM at ED 11. White cloudy areas are visible around discs. This was observed on all discs except discs with no MCPM and PLS during incubation. Healthy blood vessels could be seen around the discs.

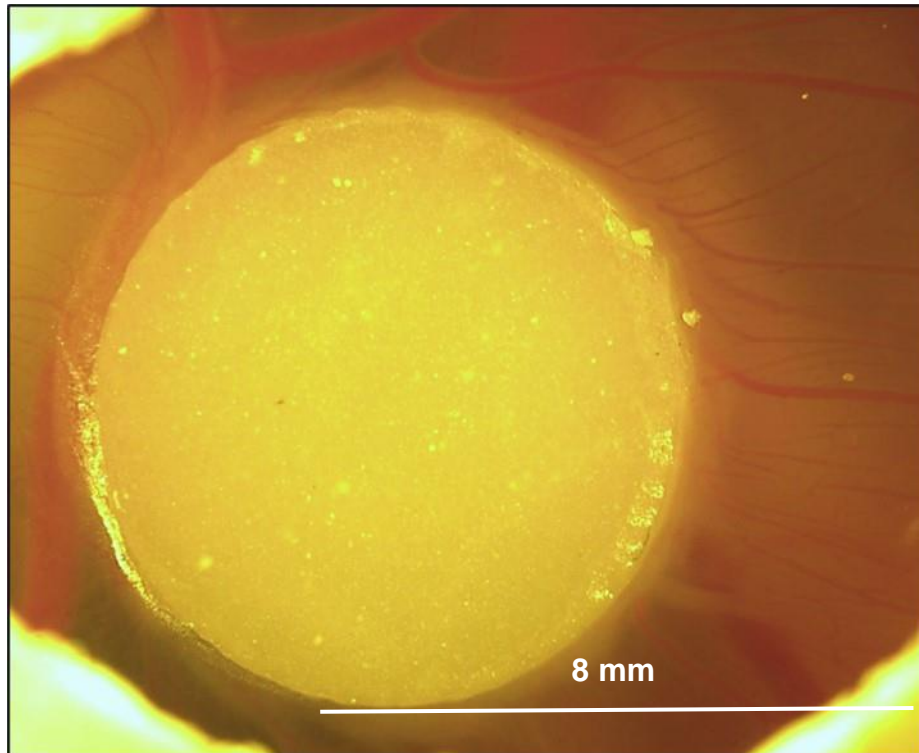


Figure 6.5 Disc implants of the experimental bone composite at ED 11 on the CAM.

The disc implants were collected at ED14 and imaged in Figure 6.6. Images of the disc side that was in contact with the CAM (A) and of the upper side (B) are shown. Most disc implants had the CAM adhering to both sides. This can be seen on 10P, 4M and 16M discs. The CAM side of the discs exhibited numerous healthy branching blood vessels. 3 discs with 16M were found submerged in the CAM and blood vessels were observed on both sides. Thicker blood vessels were most commonly found on discs with 10 % PLS and 4 % MCPM.

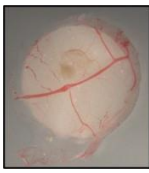
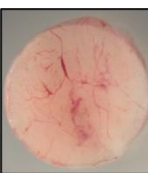

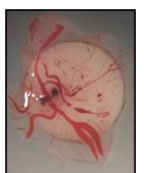
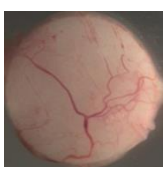
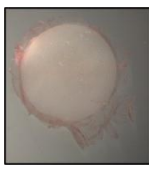
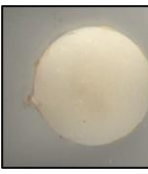


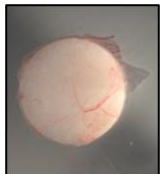
	0PM	2P	10P	4M	16M
MCPM (wt %)	0	0	0	4	16
PLS (wt %)	0	2	10	0	0
(A)					
(B)					

Figure 6.6 Disc implants (diameter 8mm) of the experimental bone composite with different formulations harvested 7 days after CAM-grafting; 0% PLS and MCPM, 2 % PLS, 10 % PLS, 4 % MCPM and 16 % MCPM. (A) Side placed on the CAM, (B) Upper side. (n=5)

Figure 6.7 represents the conversion of the disc images from their original image to binary form for each group. Figure 6.8 is the average quantification of the vascular density on the discs from each group.

For the first set of data (0 PM versus 2P versus 10 P versus 4M versus 16M), three separate ANOVAs were conducted to assess the differences between the groups in regard to vascular density, branching and junction. Figure 6.9 presents the quantification of the number of junction points and branching vessels on the disc surfaces for each group.

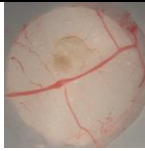
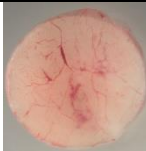

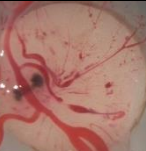
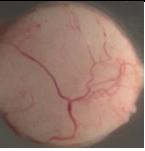
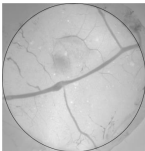
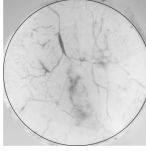
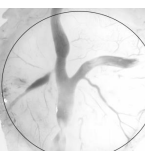
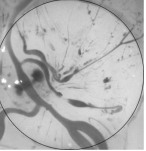
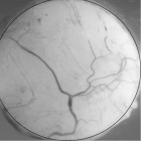
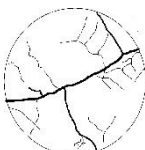
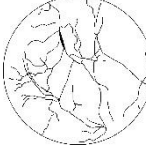



	0PM	2P	10P	4M	16M
MCPM (wt%)	0	0	0	4	16
PLS (wt%)	0	2	10	0	0
					
					
					

Figure 6.7 Microscope and binary images for disc implants (diameter 8mm) of the experimental bone composite with different formulations harvested 7 days after CAM-grafting; 0% PLS and MCPM, 2 % PLS, 10 % PLS, 4 % MCPM and 16 % MCPM. (n=3). See appendix for all images per group.

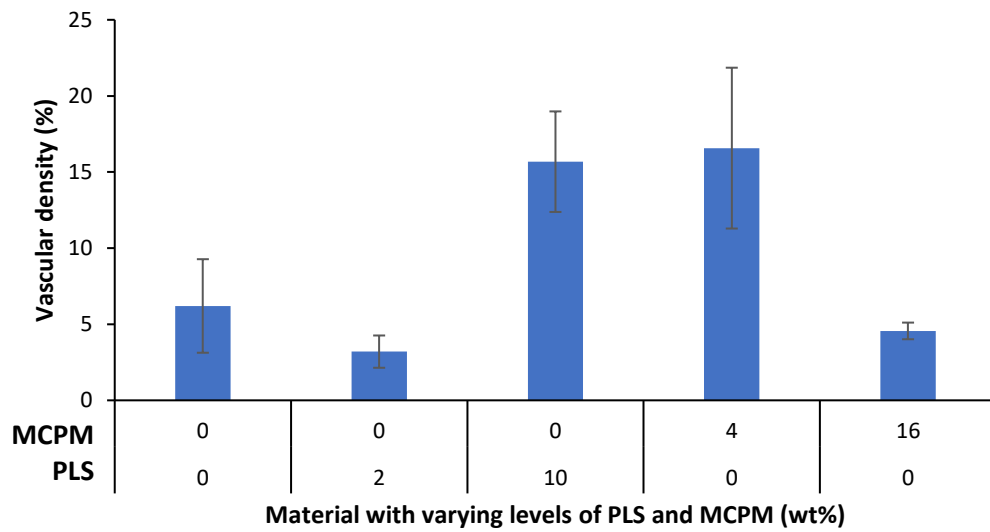


Figure 6.8 Vascular density (%) of disc implants of the experimental bone composite with different formulations harvested 7 days after CAM-grafting; 0% PLS and MCPM, 2 % PLS, 10 % PLS, 4 % MCPM and 16 % MCPM. Formatted to binary using image J. (n=3). No differences were found, ANOVA to test differences in Vascular Density means, $p=0.194$.

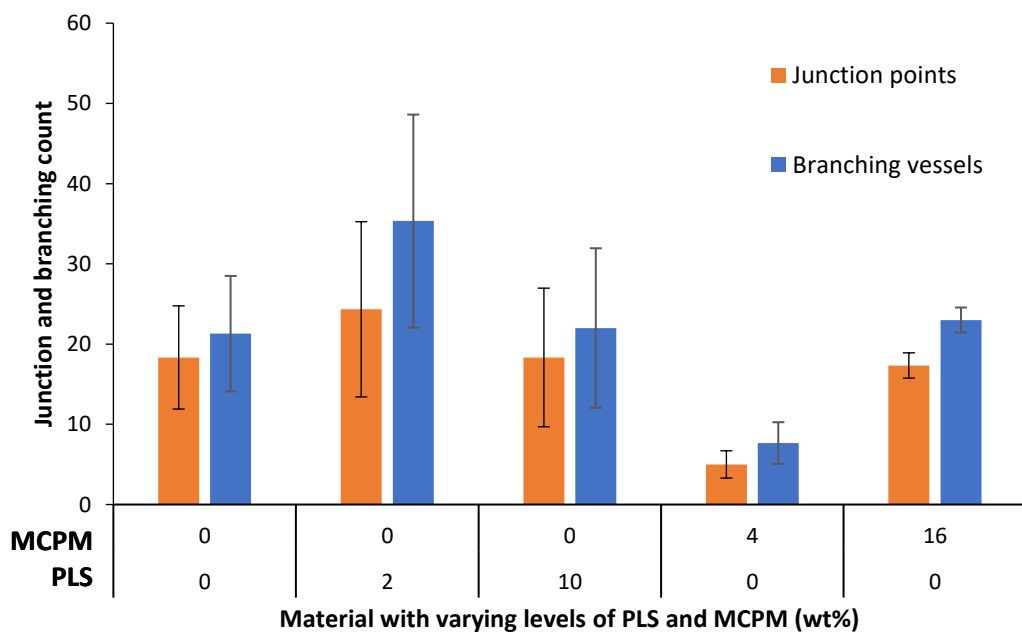


Figure 6.9 Junction points and branching vessel count on disc implants of the experimental bone composite with different formulations harvested 7 days after CAM-grafting; 0% PLS and MCPM, 2 % PLS, 10 % PLS, 4 % MCPM and 16 % MCPM.. (n=3). No differences were found, ANOVA to test differences in Branching means, $p=0.639$. ANOVA to test differences in Junction mean, $p=0.754$

The number of alive and dead chick embryos grafted with different disc implants is presented in Figure 6.7. Survival was similar in groups exposed to disc implants with 10 % PLS, 4 % MCPM and 16 % MCPM. In the group exposed to no MCPM and PLS 3 chick embryos survived and 2 died. These data show that neither PLS or MCPM affect chick embryo viability.

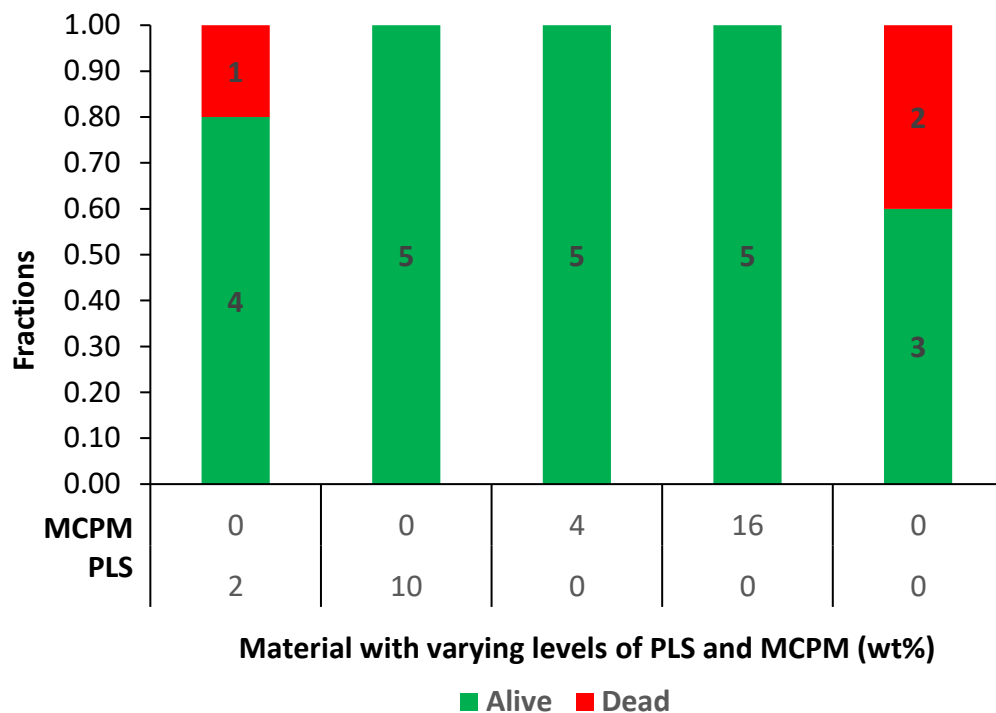


Figure 6.10 Graph representing the chick embryo's that survived out of 25 chicks at day 14 in different groups exposed to disc implants of experimental bone composite with different amounts of MCPM and PLS (wt. %). (n=5).

Figure 6.8 presents SEM images of the experimental bone composite surfaces that were in contact with the CAM. Discs with no MCPM or PLS showed generally a typical cell layer structure with cells junctions and healthy red blood cells (A). Discs with 2 % PLS were covered by epithelial looking cells; protruding particles/granular material which may be located between the CAM and the disc surface was observed (B). Discs with 10 % PLS showed healthy flat cells and healthy red blood cells (C). Disc with 4 % MCPM appears to have a precipitate layer that seems to have cracked. Cellular structure similar to macrophage along with healthy red blood cells can also be seen (D). Disc with 16 % MCPM shows extensive precipitate like apatite, which is characteristic of HA.

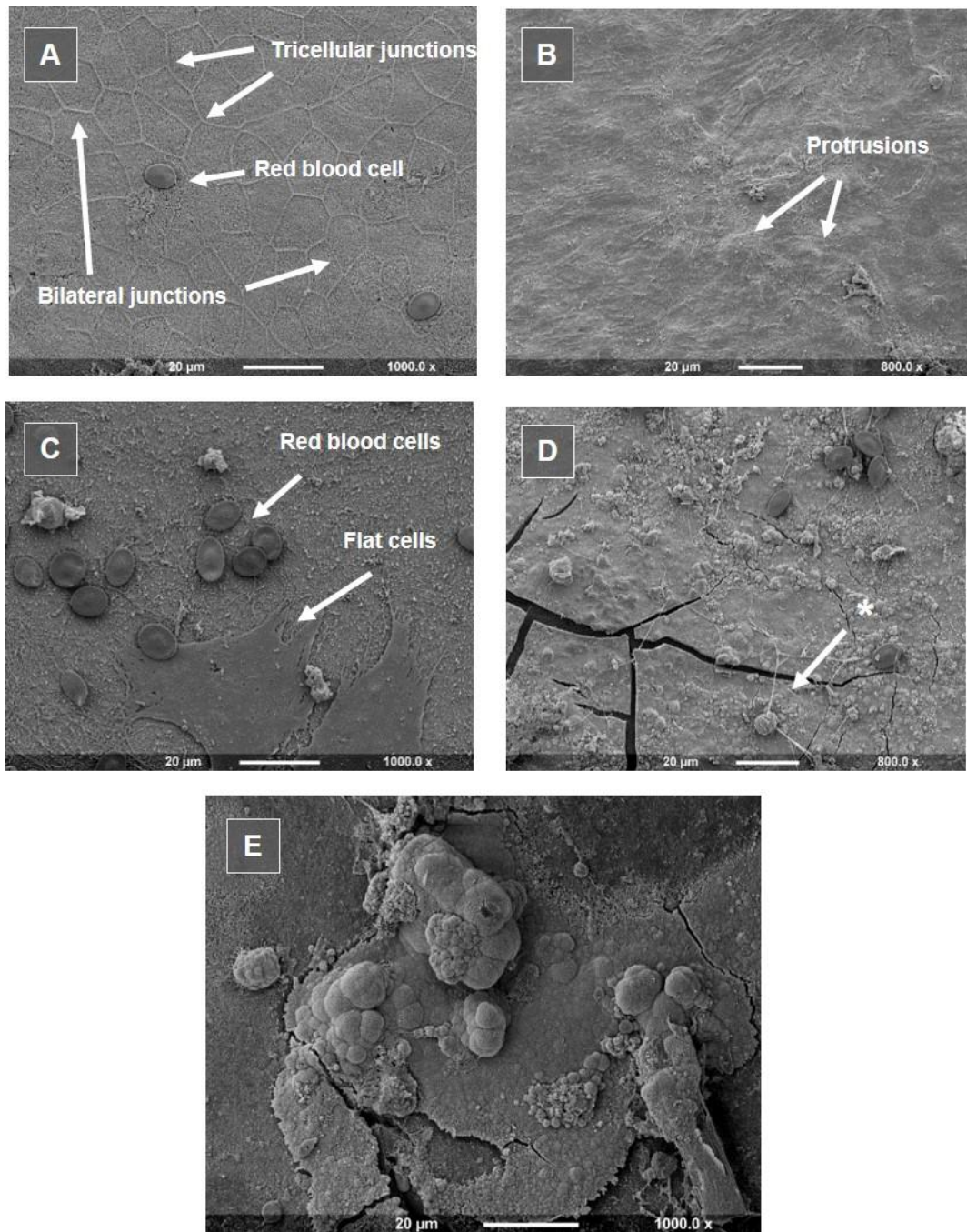


Figure 6.11 SEM images of tissue on adhering to the experimental bone composite surface on the CAM sides 7 days after CAM grafting. (A) Disc surface with 0 % MCPM and PLS. Arrows pointing at tight junctions and red blood cells. (B) Disc surface with 2 % PLS. Arrows pointing at particles are the cell layer. (C) Disc surface with 10 % PLS. Arrows pointing at red blood cells and flat unidentified cells. (D) Disc surface with 4 % MCPM *Suspected macrophage. (E) Disc surface with 16 % MCPM. (n=5).

A high magnification SEM image of the precipitate on the surface of the fixed disc implant with 16 % MCPM (Figure 6.9).

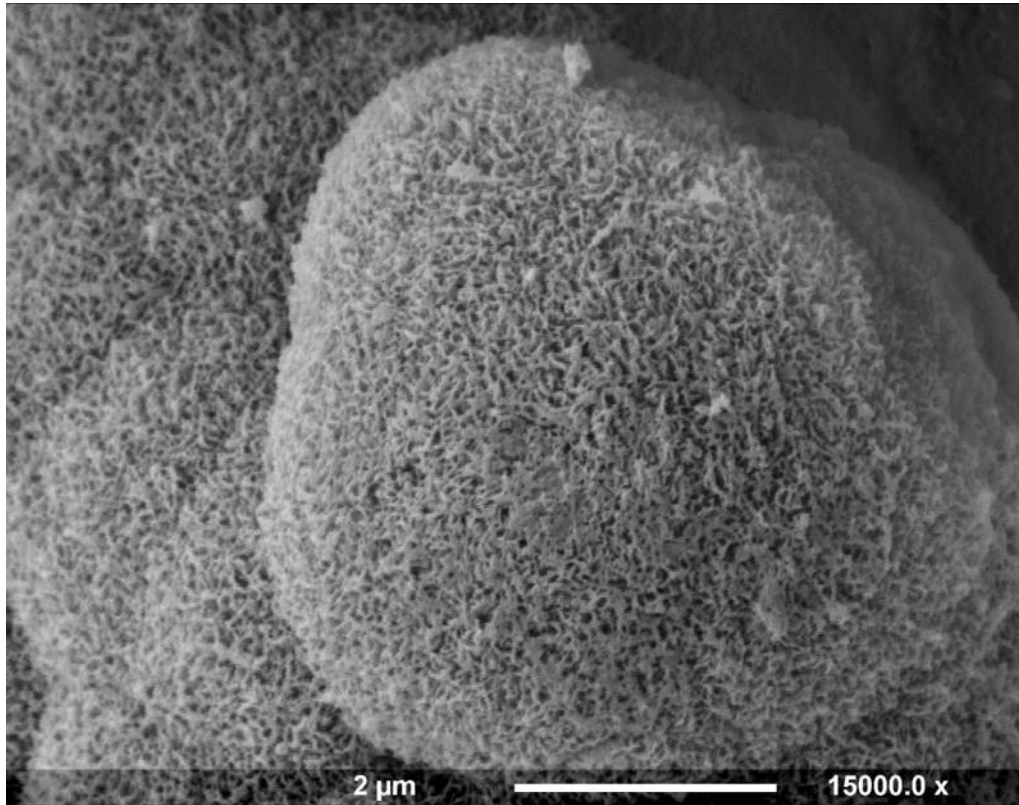


Figure 6.12 High magnification SEM image of precipitate on fixed tissue in contact with experimental bone composite disc with 16 % MCPM.

Figure 6.10 shows representative antibody reactivity observed in fixed tissue on all the disc implants stained with an antibody ZO-1 (green), which recognises tight junction protein 1, to detect epithelial cells, and with PC1 (red) to detect fibroblasts, nuclei are counter stained with Hoechst (blue).

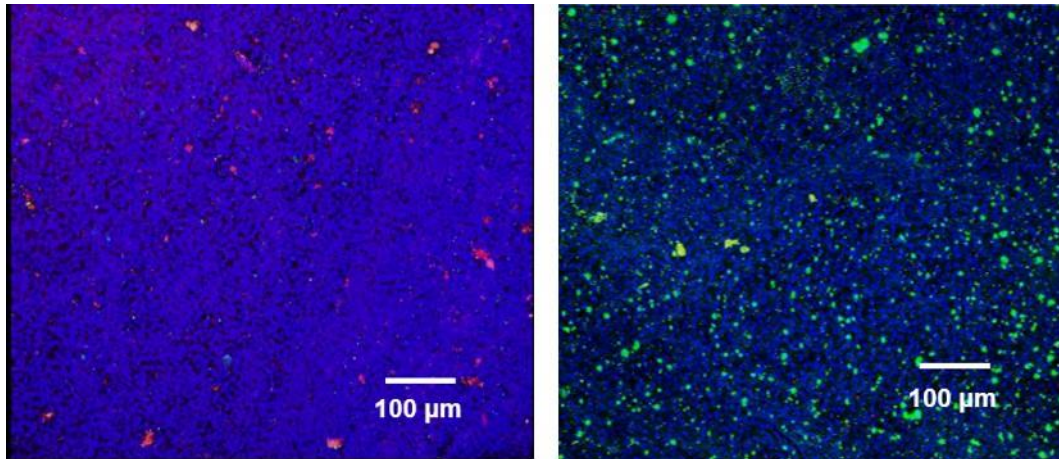


Figure 6.13 Antibody staining for epithelial cells (green), fibroblasts (red) and cell nucleus (blue) on experimental bone composite disc (0 wt% MCPCM and PLS) in contact with the CAM (N=3)

6.6.2 MCPM 8 wt% and PLS 5 wt% Added Individually in Disc Implants

Figure 6.11 shows images of disc implants of the experimental bone composite with only 5 % PLS, 8 % MCPM and discs with no MCPM and PLS, during incubation in the chick embryos at ED 9 and upon harvest at ED 14. Throughout the 14 days extremely rich vascular networks could be seen in all chick embryo's CAM with the disc implants. A membrane with numerous blood vessels was attached to the side of the disc which was in contact with the chorioallantoic membrane.


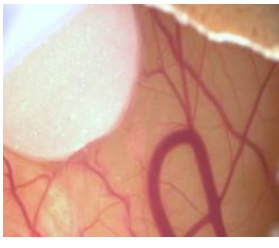
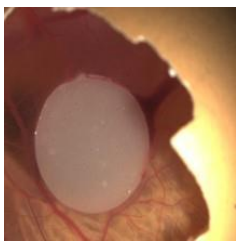
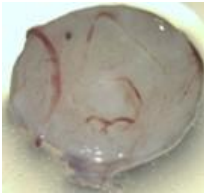
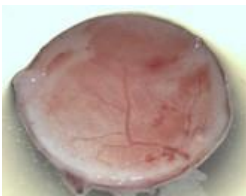

	5P	8M	0PM
MCPM (wt %)	0	8	0
PLS (wt %)	5	0	0
Day 9			
Day 14 Harvested disc implants			

Figure 6.14 Images of disc implants (diameter 8mm) of the experimental bone composite with 5 % PLS and 8 % MCPM at day 9 and after harvest (n=5).

Figure 6.15 represents the conversion of the disc images from their original image to binary form for each group. Figure 6.16 is the average quantification of the vascular density on the discs from each group. No differences were also found amongst 8 PM versus 5P versus 0PM).

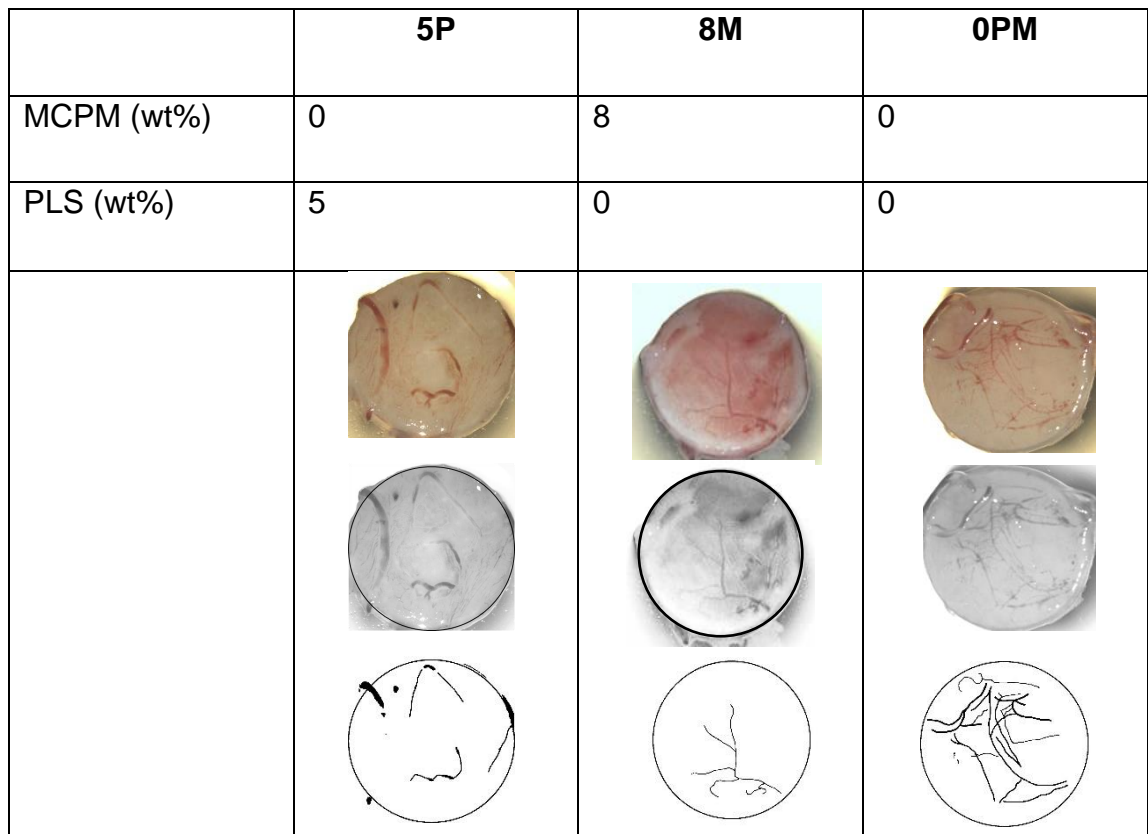


Figure 6.15 Microscope and binary images of disc implants (diameter 8mm) of the experimental bone composite with different formulations harvested 7 days after CAM-grafting; 5 % PLS, 8 % MCPM and 0% PLS and MCPM. (n=3). See appendix for all images per group.

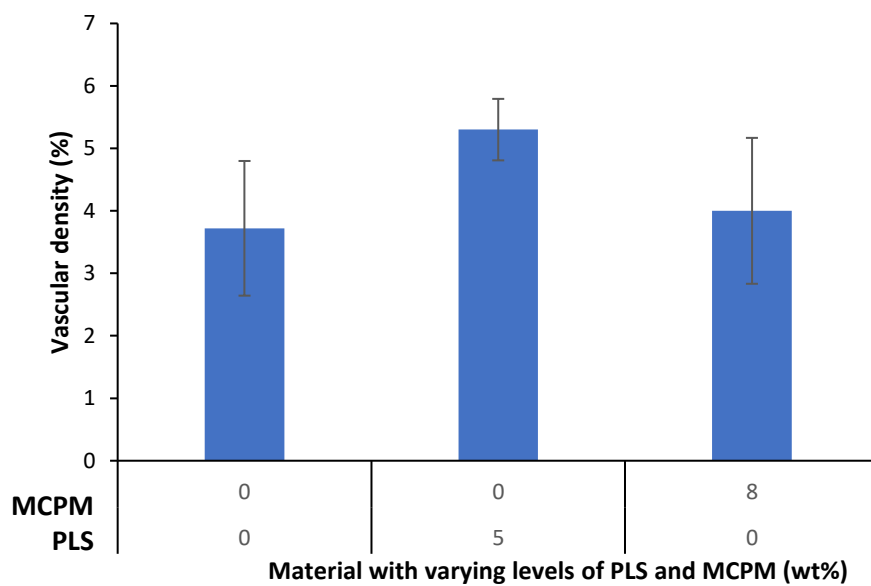


Figure 6.16 Vascular density (%) of disc implants of the experimental bone composite with different formulations harvested 7 days after CAM-grafting; 5 % PLS, 8 % MCPM and 0% PLS and MCPM. Formatted to binary using image J. (n=3). ANOVA to test differences in Vascular Density, $p=0.715$.

Figure 6.17 presents the quantification of the number of junction points and branching vessels on the disc surfaces for each group.

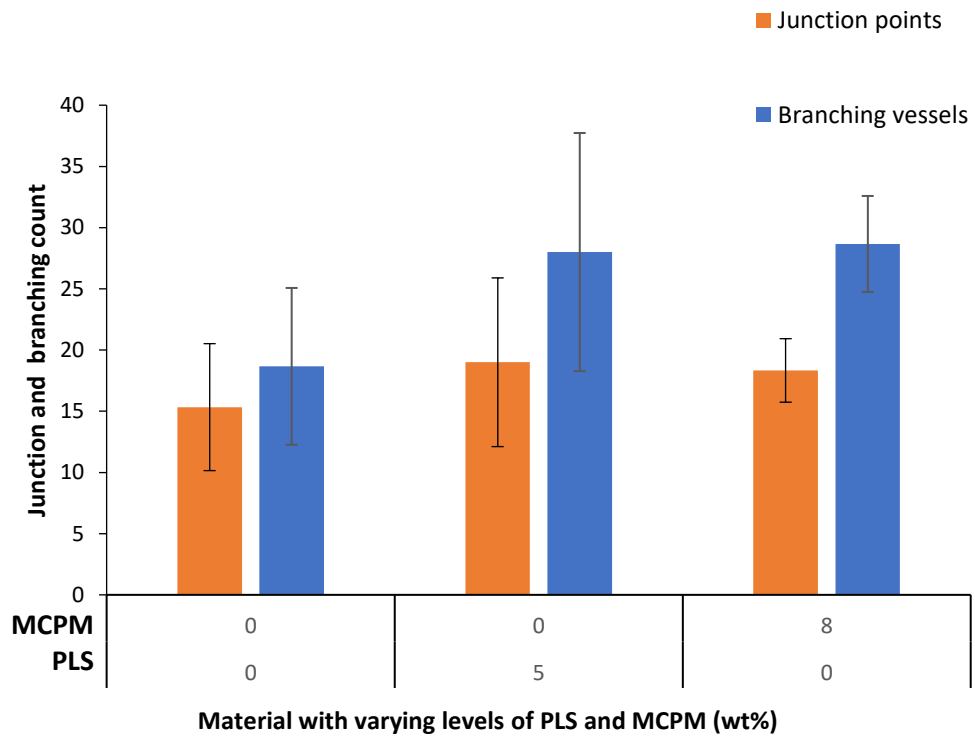


Figure 6.17 Junction points and branching vessel count on disc implants of the experimental bone composite with different formulations harvested 7 days after CAM-grafting; 5 % PLS, 8 % MCPM and 0% PLS and MCPM. Formatted to binary using image J. (n=3). ANOVA to test differences in Branching mean, $p=0.763$. ANOVA to test differences in Junction means, $p=0.938$.

The number of chick embryos that survived at time of harvest are presented in Figure 6.12. The lowest survival rate was observed in chick embryos which were exposed to 5 % PLS (3/5 chicks died). In the group where chick embryos were exposed to 8 % MCPM no chick died. In the group in which chick embryos were exposed to no MCPM and PLS. 1/5 chick died.

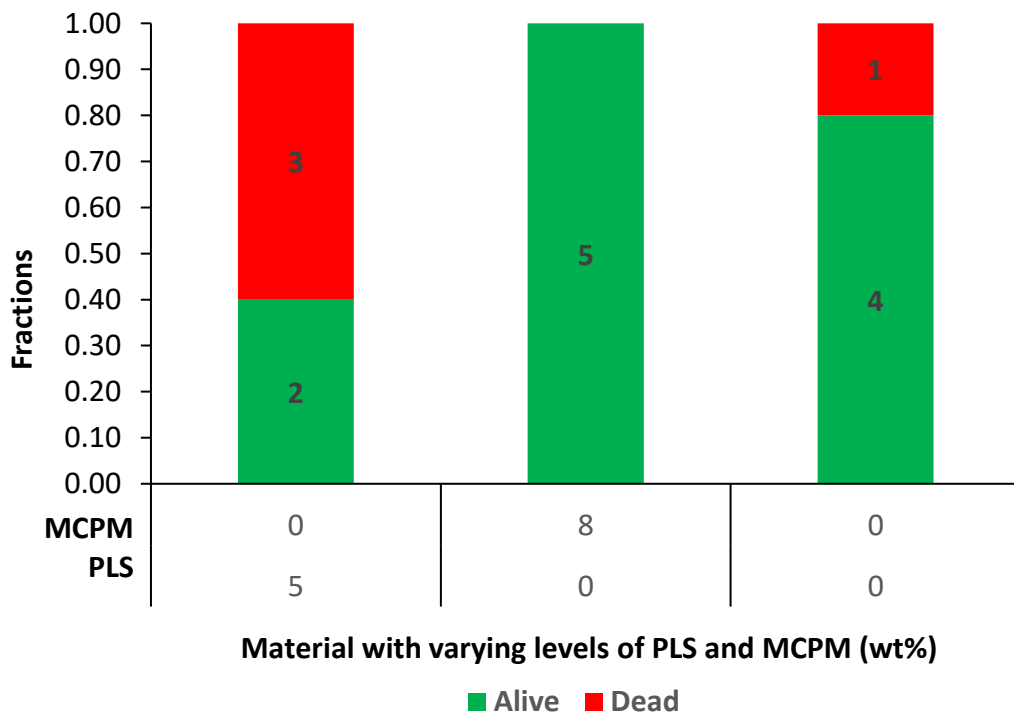


Figure 6.18 Graph representing the chick embryo's that survived out of 15 chicks at embryo day 14 in different groups exposed to disc implants of experimental bone composite with different amounts of MCPM and PLS (wt. %). (n=5).

Figure 6.13 presents disc implants of the experimental bone composite with only 5 % PLS and 8 % MCPM, placed after cutting in to quarters. Throughout the 14 days extremely rich vascular networks could be seen in all chick embryo's CAM, much like the chick embryos with the round disc implants. Harvesting the quarters required precision and delicate removal since they were easily lost. At ED 14, upon collecting the experimental composite pieces, it was noticed that the CAM surrounded the quarters holding them together in a group. All quarters were surrounded with the membrane which was rich in vasculature.

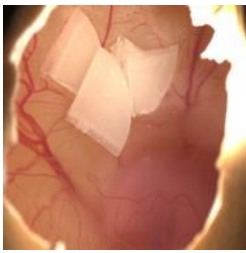
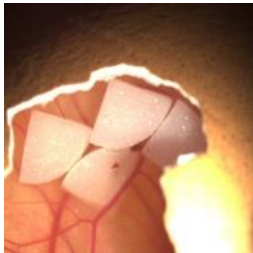
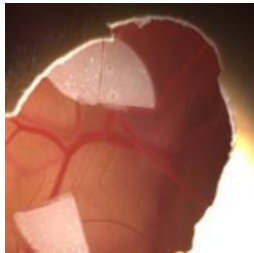
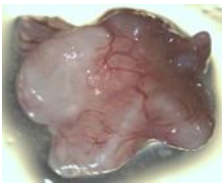
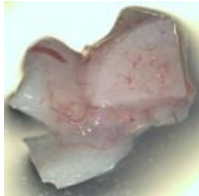
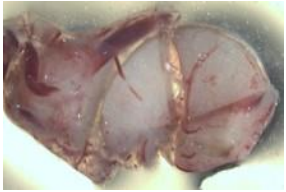
	5P	8M	0PM
MCPM (wt %)	0	8	0
PLS (wt %)	5	0	0
Day 9			
Day 14 Harvested disc implants			

Figure 6.19 Images of disc implants (diameter 8mm) cut in quarters with 5 % PLS and 8 % MCPM at day 9 and after harvest (n=5).

The number of chick embryos at time of harvest are shown in Figure 6.14. 3 chick embryos survived which were exposed to 5 % PLS (2 chicks died). In the groups where chick embryos were exposed to 8 % MCPM and the group with exposure to 0 % PLS and MCPM, 2 chicks died in each group.

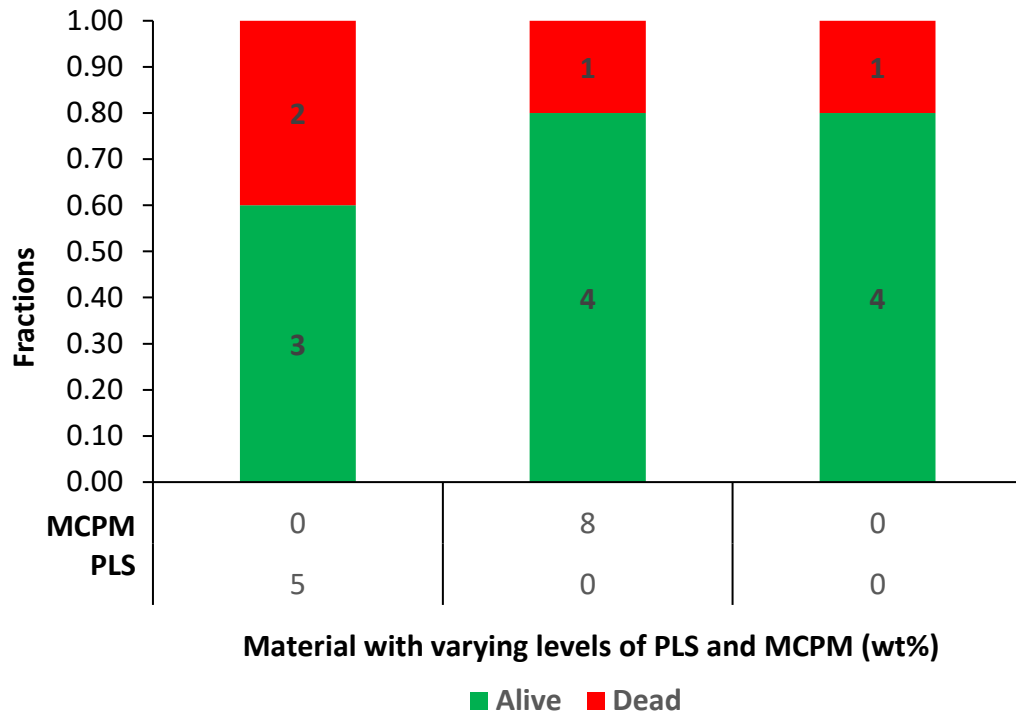


Figure 6.20 Graph representing the chick embryo's that survived out of 15 chicks at embryo day 14 in different groups exposed to disc implants in quarters of experimental bone composite with different amounts of MCPM and PLS (wt. %). (n=5).

6.6.3 Experimental Bone Composite Formulations Versus Commercial PMMA Bone Cement for Disc Implants

Figure 6.15 presents implants with varying levels of PLS and MCPM (wt %) and commercial PMMA on the CAM at ED 9 and upon harvest at embryo day 14. Throughout the 14 days extremely rich vascular networks could be seen in the CAM and around the discs. Membrane was attached to the side of the discs which was in contact with the CAM. All discs showed numerous blood vessels. PMMA was harvested easily and quickly since the CAM easily detached itself from the disc surface at ED 14.

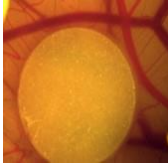
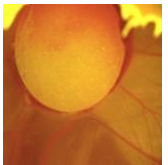
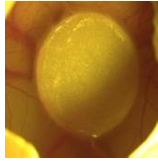
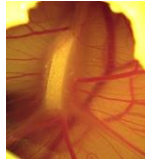
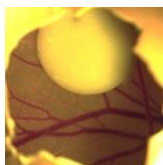



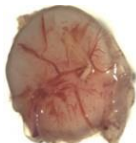

	4M2P	4M5P	8M2P	8M5P	PMMA
MCPM (wt %)	4	4	8	8	0
PLS (wt %)	2	5	2	5	0
Day 9					
Day 14 Harvested disc implants					

Figure 6.21 Disc implants (diameter 8mm) with varying levels of PLS and MCPM (wt %) and PMMA at embryo day 9 and embryo day 14.

Figure 6.22 represents the conversion of the disc images from their original image to binary form for each group. Figure 6.23 is the average quantification of the vascular density on the discs from each group. 4% MCPM 2% PLS versus PMMA, was significantly different.

The ANOVA was significantly different when the Junction means were considered, $p=0.046$. In the vascular . In the vascular density ($p=0.201$) and branching ($p=0.059$), the ANOVA was non-significant. For the junction means, Tukey's post-hoc detected a significant difference between 8% MCPM 5% PLS and PMMA ($p=0.049$).



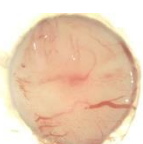
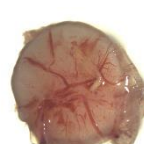




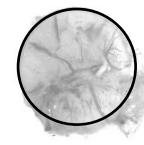
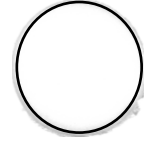
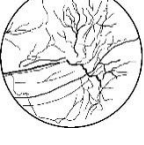
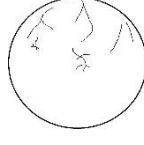


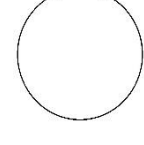
	4M2P	4M5P	8M2P	8M5P	PMMA
MCPM (wt%)	4	4	8	8	0
PLS (wt%)	2	5	2	5	0
					
					
					

Figure 6.22 Microscope and binary images of disc implants (diameter 8mm) of the experimental bone composite with different formulations harvested 7 days after CAM-grafting with varying levels of PLS and MCPM (wt %) and PMMA. ($n=3$). See appendix for all images per group.

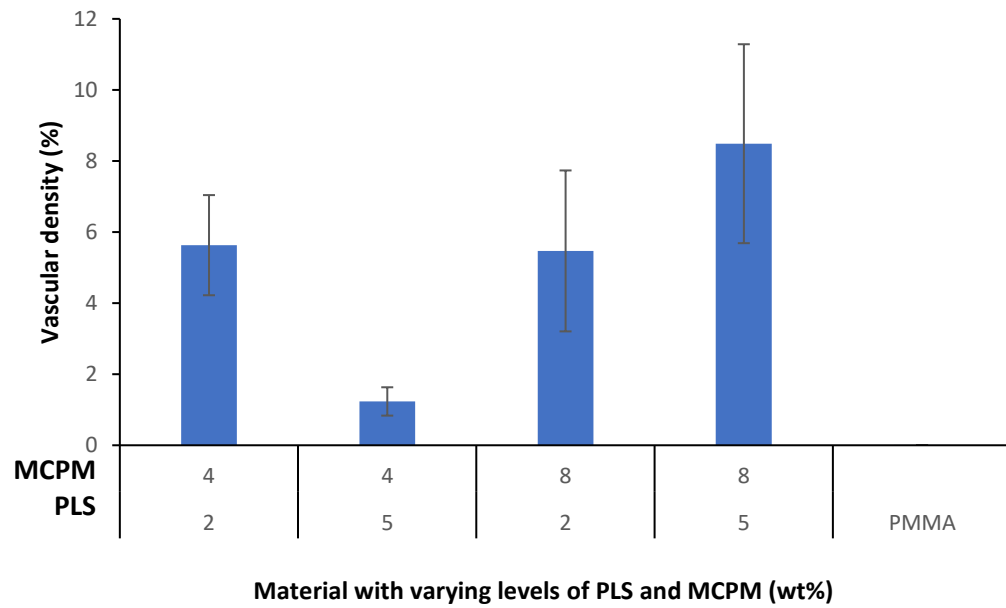


Figure 6.23 Vascular density (%) of disc implants of the experimental bone composite with different formulations harvested 7 days after CAM-grafting varying levels of PLS and MCPM (wt %) and PMMA. Formatted to binary using image J. (n=3). Add in caption nothing as observed for PMMA. (ANOVA $p=0.201$)

Figure 6.24 presents the quantification of the number of junction points and branching vessels on the disc surfaces for each group.

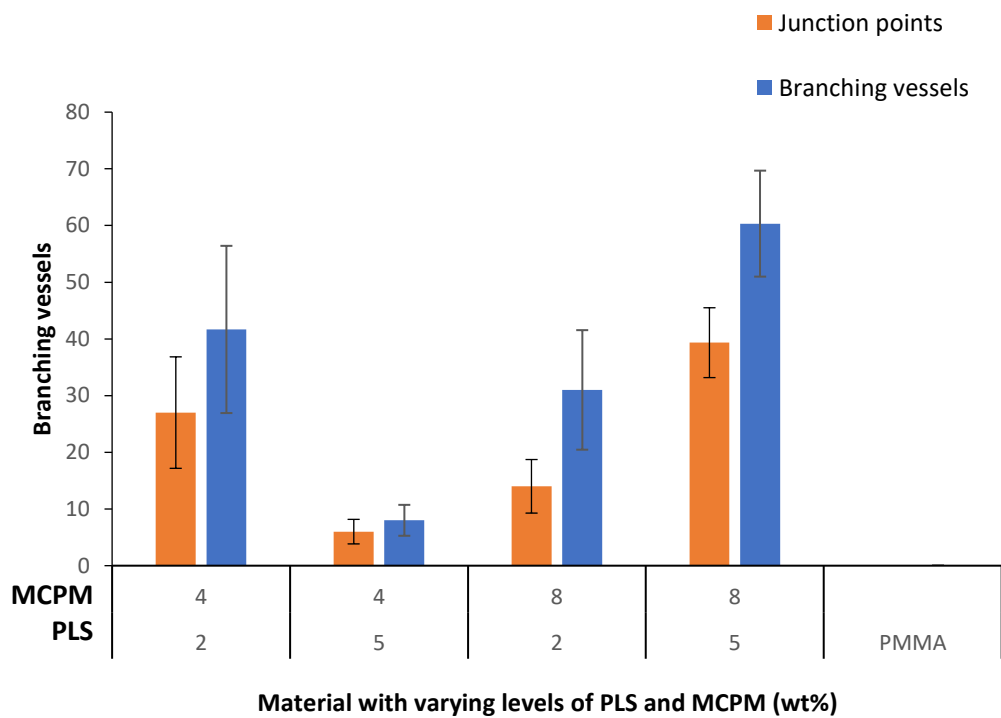


Figure 6.24 Junction points and branching vessel count on disc implants of the experimental bone composite with different formulations harvested 7 days after CAM-grafting varying levels of PLS and MCPM (wt %) and PMMA. Formatted to binary using image J. (n=3). Significant difference between 8% MCPM 5% PLS and PMMA (Branching ANOVA $p=0.059$), (Junction Tukey's post-hoc $p=0.049$)

The number of chick embryos at time of harvest are presented in Figure 6.16. 3 chick embryos survived in the group exposed to commercial PMMA. 3 chick embryos also survived in groups from 8 % MCPM and 5 % PLS, and 4 % MCPM and 2 % PLS. Groups exposed to 8 % MCPM and 2 % PLS and 4 % MCPM and 5 % PLS had 2 chick embryos survive.

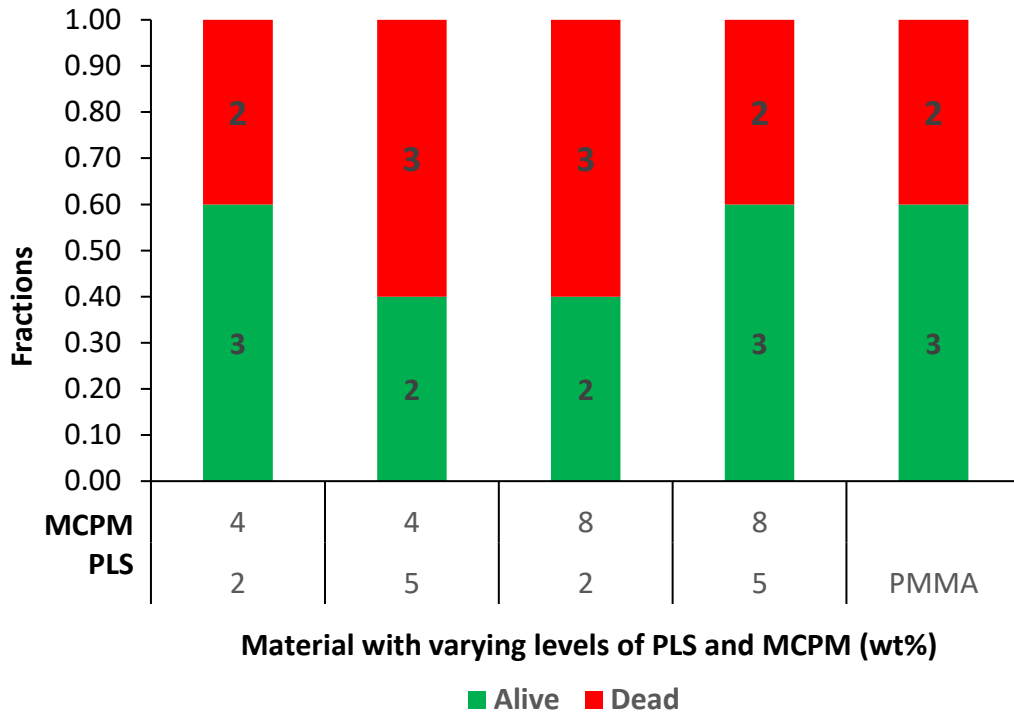


Figure 6.25 Graph representing the number of chick embryo's that survived out of 25 chicks at embryo day 14 in different groups exposed to disc implants of PMMA and experimental bone composite with different amounts of MCPM and PLS (wt. %). (n=5).

6.7 Discussion

6.7.1 MCPM and PLS Added Individually in Disc Implants

While 3D cell culture techniques have shown similar responses to *in vivo* experiments in comparison to 2D cultures, 3D cell cultures lack vasculature preventing the study of complex interactions that may be involved with a biomaterial (Edmondson et al., 2014).

The CAM assay allowed *in-vivo* visual evaluation of vascularisation of the disc implants over time *in vivo*. Angiogenic response around disc implants of the experimental bone composite, is observed by macroscopic evaluation within 2 days after grafting and is more extensive at ED 14, as indicated by the numerous blood vessels and capillary branching. Disc implants with the lowest quantity of PLS at 2 % were the lowest survival group while disc implants with higher quantities of PLS at 10 % and MCPM at 4 and 16 % had equally 100% survival rate. Chick survival does not appear to be related to the components or their amounts in the disc implants since chick death was also observed when disc with no MCPM and PLS were implanted. It is possible the formation of calcium phosphate layers on the disc may be reducing detrimental interactions between the material and the chick, thus supporting chick survival (Gupta et al., 2012). Monomers in previous studies have been a concern in terms of toxicity. The number of embryos should be increased for future studies to establish whether this difference is significant, but nonetheless it is clear that addition of MCPM or PLS does not negatively affect survival.

All discs, except discs with 0 % PLS and MCPM, grafted on the CAM were surrounded by a cloudy area by embryo day 9. It is not known whether it was components released from the disc or a protective layer made by the CAM. In previous chapters the release of components was observed, resulting in pH decrease and the visual colour change and cloudiness of the cell culture medium. The disc implants with no PLS and MCPM did not display cloudy areas, which means PLS and MCPM were released from the discs and the accumulation of components is observed. The cloudy areas were not as noticeable by ED 14 suggesting dispersion of components, and it did not seem to affect embryo viability. While it is not known how the CAM responds towards such components, chick embryos have been shown to develop several mechanisms, including material isolation and encapsulation of the material in amniotic fluid to prevent interaction with the graft (I. Moreno-Jiménez et al., 2017).

During chick development the mesodermal layer and the chorion fuse to establish the CAM. As the CAM expands it generates a rich vascular network providing interface for gas and waste exchange and in this case around the implanted disc (Ribatti, 2016). The disc grafting on the CAM did not hinder the growth of vasculature and this is essential around a biomaterial since the movement of nutrients is required for cells to grow and communicate. An ideal biomaterial encourages extensive vascularisation, aiding removal of waste, transport of nutrients and oxygen to the repairing tissue. Discs with high levels of PLS at 10% and low levels of MCPM at 4% showed higher vascular density. The increase in vascular density value can be seen due to the thicker blood vessels.

However the number of junctions and branching was highest with low levels of PLS at 2% and the lowest levels of branching and junctions was with low levels of MCPM at 4%. Increased levels of MCPM at 16% and discs with no MCPM and PLS were similar in vascular density, junction and branching count, suggesting the increased levels of MCPM may not influence angiogenesis. Kohli et al carried out a study looking at biomaterial's intrinsic angiogenic property based on different components within the materials such as fibrin. Kohli's study showed similar trends in vascular density and branching points however for 2 biomaterials they found after quantification of binary images that high vascular density did not show high branching points (reference (Kohli et al., 2020)). The biomaterials used in this study differ in formulations and have not been studied in a CAM model before and the formulation component's mechanism of action in angiogenesis is not understood, therefore further studies are needed in the future.

Vascularisation found on in the membrane upon contact with the experimental bone composite could be further assessed by quantifying angiogenesis by injecting a dye for vessel perfusion and biochemical assays to measure haemoglobin, in the area around the implant was placed (Osorio et al., 2019).

The CAM displayed strong adherence to the disc implants in all formulations of the experimental composite. The hydrophilic properties of PLS and MCPM in the material may be responsible for this adhesion.

SEM images for the disc implant with no MCPM and PLS indicate the presence of a layer of epithelial looking cells with bilateral and tricellular junctions. Their morphology resembles that of chicken yolk sac endodermal epithelial cells (E. A. Wong & Uni, 2021).

Histologically, the CAM consists of two epithelial sheets which restrict a thin layer of stroma and it is within the stroma that the blood vasculature and lymphatics are found (Nowak-Sliwinska, Segura, & Iruela-Arispe, 2014). The captured areas can be assumed as the stroma since red blood vessels are present.

Disc surfaces with 2 % PLS exhibited a layer of cells, further investigation is required to characterise the cells and protrusions seen on the surface. Disc implants with 10 % PLS seem to have 2 distinct cell types that that have yet to be confirmed amongst the epithelial cells, and deposition of extracellular matrix and a few red blood cells were observed. The cells present may have been induced specifically by the PLS or in generally the disc implants irrespective of the components. Depending on the induced response the levels of proteins and communication between cells will vary, which can influence the interaction between the biomaterial and the cells surrounding it. It is also possible the cells migrated from the CAM or the cells directly from the CAM adhered to the material.

Disc implants with low and high levels of MCPM, at 4 % and 10 % respectively exhibited precipitate on the disc surfaces. A particular notable feature in Figure 6.8D is the presence of a cell which resembles a macrophage due to the long ultrathin projections emanating from it, however this needs to be confirmed. It is unknown whether different composites evoke a different immune response. The chick immune system is not yet mature, but there is already a cellular response, macrophages/monocytes have been found in cellularised scaffolds as detected by the KUL01 antibody (New et al., 2017). While at ED 14, a fully developed immune system is not established, a few studies carried out by Valdes et al suggested an acute inflammatory response due to the presence of leukocytes and macrophages may exist (I. Moreno-Jiménez et al., 2017). The investigation of an immune response can give an indication of the biomaterials efficacy and safety. Disc implants consisting of 16 % MCPM showed extensive apatite precipitate, which requires further analysis so the elements can be confirmed. The morphological features are characteristic of HA which can encourage osseointegration of the material. Studies have shown HA also promotes cell growth and enhances cell adhesion (Ho et al., 2020). Study carried out by Anas (2016) showed very similar apatite precipitate in composites when placed in SBF (Aljabo et al., 2016). The CAM assay has been able to encourage precipitate of the same morphology on the experimental disc composites with high levels of MCPM in just 14 days. The egg shell is known to regulate the transport of calcium for mineralisation of the chick's skeleton. However Vargas was able to demonstrate in an ex ovo experiment that the CAM is capable of taking up mineral from an implant to compensate for the absence of the eggshell (Vargas et al., 2009). Thus it can be postulated that the implant discs with calcium phosphates

can contribute to the mineralisation of not only the disc surface but the chick skeleton also.

Antibody staining didn't show anything in particular further investigation into specific markers are required. It is well known for CAM assays the reagents compatible with avian species is limited, including antibodies (Nowak-Sliwinska et al., 2014).

From this study it is understood the disc implants are not toxic to the chick embryos but further tests are required to understand the interactions occurring at the cellular level.

6.7.2 MCPM 8 wt% and PLS 5 wt% Added Individually in Disc Implants

8 % MCPM and 5 % PLS was added individually to the disc implants to assess their effects on the developing chick embryo. Discs were also cut in to quarters to assess if any leaching or unreacted monomers affected the chick embryos. MCPM and PLS were used in the disc composites and both components in the cell studies showed higher acidity and reduced metabolic activity. This study allowed assessment of which component at its highest level may affect the developing chick embryo and the vascularisation. Vascularisation was evident around all the disc implants. Vascular density was not significantly different amongst formulations with 0 MCPM and PLS, 5% PLS and 8% MCPM. Junction and branching points showed similar trends to vascular density in all the formulations.

Disc implants cut in quarters were also surrounded by the membrane rich in vasculature and the membrane adhered well to the implant. Suggesting neither component independently is toxic to the developing chick embryo.

6.7.3 Experimental Bone Composite Formulations Versus Commercial PMMA Bone Cement for Disc Implants

Vertebral fractures to be treated with bone composites will incorporate both MCPM and PLS to encourage remineralisation and assist in antibacterial action. Combining both components have shown to have lower strength and increase acidity but it is not known how the material will affect an *in vivo* environment. This study looked at combined variations in comparison to the commercial PMMA and their effect on the developing chick embryo.

Developing chick embryos survived equally (2 out of 5) in groups exposed to bone composite implants with 8 % MCPM and 5 % PLS combined, 4 % MCPM and 2 % PLS and PMMA. PMMA was hypothesised to have toxic effects on the chick embryo, the chick embryo thrived until the end time point at day 14. However the CAM did not show strong adherence to the PMMA disc implant unlike the experimental bone composites, and was not surrounded by the CAM and its vasculature. It is not clear why there is less adhesion between the PMMA and the CAM in comparison to the composites but PMMA has been described to have no adhesive properties to bone surfaces and no bioactivity in other studies (Oryan et al., 2018).

Vascular density was highest for the highest formulation combination of 8%MCPM and 5% PLS. The lowest vascular density was for the formulation 4% MCPM and 5 % PLS. The results for this set are not a true reflection since the survival rate of the chicks from the group with the disc formulation 4%MCPM and 5% PLS and 4% MCPM and 2 % PLS was 2 out of 5 in comparison to the other groups.

The junction and branching points show similar trends to the vascular density. PMMA had now vascular density, junction or branching values since the CAM did not adhere to the material. Previous studies have shown materials derived from natural polymers with textured surfaces are more angiogenic than smooth, synthetic inert materials. Materials derived from natural polymers, with an enhanced textured surface are indicated as more angiogenic in contrast to smooth, synthetic inert materials (Marshall, Kanczler, & Oreffo, 2020).

An angiogenic response in the membrane occurs 72–96 h after stimulation in the form of an increased vessel density around the implant. However, when an angiostatic compound is tested, the vessels become less dense around the implant after 72–96 h, and eventually disappear (Ribatti, 2016). Vessels were present on the CAM under all the material implants.

The combined formulations suggest increasing levels of combined MCPM and PLS do not reduce vascular density or junction and branching points, thus higher combinations are not harmful to the blood vessels. Osteogenesis is a vascular-dependent process, which depends on the biomaterial's angiogenic

potential. Angiogenesis plays a vital role repair of critical bone defects (Liu et al., 2018).

Similarly in chapter 5, cells adhered better to the experimental bone composite and not so much on PMMA. Khan proposed that using NTGGMA as an activator enhanced cytocompatibility of experimental composites compared with DMPT (M. A. Khan, 2015). It is possible the different initiators in the PMMA (DMPT) and experimental bone composite (NTGGMA), may be influencing the membrane attraction.

Although this study mimics a continuous dynamic biological system better than a 2D cell culture it does not however mimic the clinical conditions because the disc implants are added after the material has reacted and set. Whereas the bone composite after injecting at the fractured site will undergo polymerisation and change from paste to solid. During this stage there are several factors that may influence cell behaviour. A study looking at the reason for fibrous tissue formation

around PMMA showed that local toxic tissue reaction occurred at the beginning of the process and PMMA has poor tissue compatibility which can cause severe local tissue changes (Kalteis et al., 2004). Furthermore the time period is a limiting factor in this study at ED 14.

6.8 Conclusion

Increasing MCPM (from 0 to 4 % to 8 % to 16 % wt) and PLS (from 0 to 2 % to 5 % to 10% wt) individually or combined in the disc versus commercial PMMA:

- Had no effect on the chick embryo
- Had no negative effect on vasculature of embryo membrane around the implant.
- Showed increased precipitation on disc surfaces with high levels of MCPM
- Showed cells on disc surfaces
- Showed membranes had stronger attraction to the discs with combined quantities of MCPM and PLS than the commercial PMMA

Conclusions and Further Work

7.1 Conclusions

The experimental bone composite in this study is easier to prepare than the most widely used commercially available cement, PMMA (Simplex™ P). The setting time can be optimised and manipulated easily and is comparable to the commercially available cement. Furthermore the experimental bone composite generates less heat in comparison to commercially available cement. The experimental bone has a closer mechanical match to bone than PMMA and the experimental bone composite also displays ability to remineralise, we've seen this in in-vitro and in-ovo. Cells were present, attached and active with the material, exhibiting angiogenic ability. Good bone integration and vasculature will mean good input of nutrients to fractured site, improving healing.

7.2 Further work

- **Assess water contact angle:**

Water contact angle measurements are used to ascertain whether a biomaterial's surface is hydrophilic or hydrophobic. Materials with a higher affinity for water means the water will spread across the material better and will not repel the polar water molecules thus also attracting proteins to the surface of the biomaterial. Hydrophilicity threshold is below 90 ° (Law, 2014). Materials exhibiting low values indicate high hydrophilicity, a desired characteristic of a bone composite material since this is one of the first parameters that affect adsorption of proteins (Paterlini et al., 2017). Varying the formulations and comparing them with commercial pastes, will give better understanding about which formulation combinations are best to achieve good hydrophilic properties for the bone composite.

- **Measuring PLS infiltration in to porous bone:**

Alkhoury (2019) showed penetration of PLS in to tooth tubules resulting in effective antibacterial delivery into deeper layers of caries affecting dentine (Alkhoury, 2019). An assay would need to be developed to study the penetration of PLS in to bone from the formulation paste. This will be of particular interest for osteoporotic bone, where the interior is extra porous. A composite paste that is able to infiltrate porous bone to provide support to the structure would be advantageous as well as exerting antibacterial action. Establishing an assay looking at how PLS penetrates porous bone would be the initial step.

- **Cell differentiation, Cell migration and co-culture studies:**

An ideal bone composite will encourage differentiation of stem cells into osteoblasts that will encourage bone repair. Further biological studies with the experimental bone composite should be investigated to see if cells are able to differentiate. Specific markers can be quantified to assessed.....

Further assessment of how the experimental bone composite induces cell migration to the material and how different cell types, such as osteoblasts and osteoclast interact around the experimental bone composite.

- **Antibacterial effect**

PLS is a novel component in the bone composite formulations. Antibacterial assessment of PLS should be investigated and its efficacy on bacteria at different concentrations. Particularly the inhibitory concentration, to help determine the minimum levels of PLS needed in the formulation to exert a sufficient antibacterial response to potential infections.

- **Carry out in-vivo studies:**

An *In-vivo* study is carried out prior to clinical trials. The lower femoral implantation procedure is a good model to assess the response of trabecular bone to an implant material.

- **Clinical Trials:**

An initial pilot study with a small subject group would need to be carried out to determine preliminary safety and performance information for the experimental bone composite.

Bibliography

- Abdelrahman, H., Siam, A. E., Shawky, A., Ezzati, A., & Boehm, H. (2013). Infection after vertebroplasty or kyphoplasty. A series of nine cases and review of literature. *Spine J*, 13(12), 1809-1817. doi:10.1016/j.spinee.2013.05.053
- Abou Neel, E. A., Aljabo, A., Strange, A., Ibrahim, S., Coathup, M., Young, A. M., . . . Mudera, V. (2016). Demineralization-rem mineralization dynamics in teeth and bone. *International journal of nanomedicine*, 11, 4743-4763. doi:10.2147/IJN.S107624
- Alexandru, D., & So, W. (2012). Evaluation and Management of Vertebral Compression Fractures. *The Permanente Journal*, 16(4), 46-51.
- Alhashash, M., Shousha, M., Barakat, A. S., & Boehm, H. (2019). Effects of Polymethylmethacrylate Cement Viscosity and Bone Porosity on Cement Leakage and New Vertebral Fractures After Percutaneous Vertebroplasty: A Prospective Study. *Global Spine Journal*, 9(7), 754-760. doi:10.1177/2192568219830327
- Aljabo, A., Abou Neel, E. A., Knowles, J. C., & Young, A. M. (2016). Development of dental composites with reactive fillers that promote precipitation of antibacterial-hydroxyapatite layers. *Materials Science and Engineering: C*, 60, 285-292. doi:<https://doi.org/10.1016/j.msec.2015.11.047>
- Alkhouri, N. (2019). *Optimising Novel Dental Composites for Paediatric Patients*. (Doctor of Philosophy), University College London,
- Ambard, A. J., & Mueninghoff, L. (2006). Calcium Phosphate Cement: Review of Mechanical and Biological Properties. *Journal of Prosthodontics*, 15(5), 321-328. doi:10.1111/j.1532-849X.2006.00129.x
- Anil, S., Venkatesan, J., Shim, M. S., Chalisserry, E. P., & Kim, S. K. (2017). 4 - Bone response to calcium phosphate coatings for dental implants. In A. Piattelli (Ed.), *Bone Response to Dental Implant Materials* (pp. 65-88): Woodhead Publishing.
- Anselme, K. (2000). Osteoblast adhesion on biomaterials. *Biomaterials*, 21(7), 667-681. doi:10.1016/s0142-9612(99)00242-2
- Anselme, K., Ponche, A., & Bigerelle, M. (2010). Relative influence of surface topography and surface chemistry on cell response to bone implant materials. Part 2: biological aspects. *Proc Inst Mech Eng H*, 224(12), 1487-1507. doi:10.1243/09544119jeim901
- Anusavice, K. J., Phillips, R. W., Shen, C., & Rawls, H. R. (2013). *Phillips' Science of Dental Materials* (12 ed.). Missouri: Elsevier/Saunders.
- Arora, M., Chan, E. K. S., Gupta, S., & Diwan, A. D. (2013). Polymethylmethacrylate bone cements and additives: A review of the literature. *World Journal of Orthopedics*, 4(2), 67-74. doi:10.5312/wjo.v4.i2.67
- Ashby, M. F. (2004). *Materials Selection in Mechanical Design* (3rd Edition ed.): Elsevier Science & Technology.
- Assad, M., & Jackson, N. (2019). Biocompatibility Evaluation of Orthopedic Biomaterials and Medical Devices: A Review of Safety and Efficacy Models. In R. Narayan (Ed.), *Encyclopedia of Biomedical Engineering* (pp. 281-309). Oxford: Elsevier.
- Bakopoulou, A., Papadopoulos, T., & Garefis, P. (2009). Molecular toxicology of substances released from resin-based dental restorative materials. *International journal of molecular sciences*, 10(9), 3861-3899. doi:10.3390/ijms10093861
- Ban, S., & Anusavice, K. J. (1990). INFLUENCE OF TEST METHOD ON FAILURE STRESS OF BRITTLE DENTAL MATERIALS. *J Dent Res*, 69(12), 1791-1799. doi:10.1177/00220345900690120201

- Bansal, S., Chauhan, V., Sharma, S., Maheshwari, R., Juyal, A., & Raghuvanshi, S. (2009). Evaluation of hydroxyapatite and beta-tricalcium phosphate mixed with bone marrow aspirate as a bone graft substitute for posterolateral spinal fusion. *Indian Journal of Orthopaedics*, 43(3), 234-239. doi:10.4103/0019-5413.49387
- Baroud, G., Bohner, M., Heini, P., & Steffen, T. (2004). Injection biomechanics of bone cements used in vertebroplasty. *Bio-Medical Materials and Engineering*, 14(4), 487-504.
- Baroud, G., Vant, C., & Wilcox, R. (2006). Long-term effects of vertebroplasty: adjacent vertebral fractures. *J Long Term Eff Med Implants*, 16(4), 265-280. doi:10.1615/jlongtermeffmedimplants.v16.i4.10
- Barszczewska-Rybarek, I. M. (2012). Quantitative determination of degree of conversion in photocured poly(urethane-dimethacrylate)s by Fourier transform infrared spectroscopy. *Journal of Applied Polymer Science*, 123(3), 1604-1611. doi:10.1002/app.34553
- Barszczewska-Rybarek, I. M. (2019). A Guide through the Dental Dimethacrylate Polymer Network Structural Characterization and Interpretation of Physico-Mechanical Properties. *Materials (Basel, Switzerland)*, 12(24), 4057. doi:10.3390/ma12244057
- Beck, S., & Boger, A. (2009). Evaluation of the particle release of porous PMMA cements during curing. *Acta Biomater*, 5(7), 2503-2507. doi:<http://dx.doi.org/10.1016/j.actbio.2009.04.002>
- Bistolfi, A., Massazza, G., Verné, E., Massè, A., Deledda, D., Ferraris, S., . . . Crova, M. (2011). Antibiotic-Loaded Cement in Orthopedic Surgery: A Review. *ISRN Orthopedics*, 2011, 290851. doi:10.5402/2011/290851
- Bodhak, S., Bose, S., & Bandyopadhyay, A. (2009). Role of Surface Charge and Wettability on Early Stage Mineralization and Bone Cell-Materials Interactions of Polarized Hydroxyapatite. *Acta Biomater*, 5, 2178-2188. doi:10.1016/j.actbio.2009.02.023
- Boger, A., Bohner, M., Heini, P., Schwieger, K., & Schneider, E. (2008). Performance of vertebral cancellous bone augmented with compliant PMMA under dynamic loads. *Acta Biomater*, 4(6), 1688-1693. doi:10.1016/j.actbio.2008.06.019
- Borak, J., Fields, C., Andrews, L. S., & Pemberton, M. A. (2011). Methyl methacrylate and respiratory sensitization: a critical review. *Critical reviews in toxicology*, 41(3), 230-268. doi:10.3109/10408444.2010.532768
- Borgström, F., Karlsson, L., Ortsäter, G., Norton, N., Halbout, P., Cooper, C., . . . for the International Osteoporosis, F. (2020). Fragility fractures in Europe: burden, management and opportunities. *Archives of Osteoporosis*, 15(1), 59. doi:10.1007/s11657-020-0706-y
- Borst, R. (2002). Fracture in quasi-brittle materials: A review of continuum damage-based approaches. *Engineering Fracture Mechanics*, 69, 95-112. doi:10.1016/S0013-7944(01)00082-0
- Boszczyk, B. M., Bierschneider, M., Panzer, S., Panzer, W., Harstall, R., Schmid, K., & Jaksche, H. (2006). Fluoroscopic radiation exposure of the kyphoplasty patient. *European spine journal : official publication of the European Spine Society, the European Spinal Deformity Society, and the European Section of the Cervical Spine Research Society*, 15(3), 347-355. doi:10.1007/s00586-005-0952-0
- Bowen, R. L., & Marjenhoff, W. A. (1992). Dental composites/glass ionomers: the materials. *Adv Dent Res*, 6, 44-49.
- Boyd, D., Towler, M. R., Wren, A., & Clarkin, O. M. (2008). Comparison of an experimental bone cement with surgical Simplex® P, Spineplex® and Cortoss®. *Journal of Materials Science: Materials in Medicine*, 19(4), 1745-1752. doi:10.1007/s10856-007-3363-4

- Cagli, S., Isik, H. S., & Zileli, M. (2010). Vertebroplasty and kyphoplasty under local anesthesia: review of 91 patients. *Turk Neurosurg*, *20*(4), 464-469. doi:10.5137/1019-5149.jtn.2954-10.0
- Cheema, U. (2013). 2 - Three-dimensional collagen biomatrix development and control. In V. Salih (Ed.), *Standardisation in Cell and Tissue Engineering* (pp. 18-33): Woodhead Publishing.
- Chen, C., Chen, Y., Wu, P., & Chen, B. (2014). Update on new medicinal applications of gentamicin: evidence-based review. *J Formos Med Assoc*, *113*(2), 72-82. doi:10.1016/j.jfma.2013.10.002
- Chen, F., Song, Z., & Liu, C. (2015). Fast setting and anti-washout injectable calcium–magnesium phosphate cement for minimally invasive treatment in bone defect. *J. Mater. Chem. B*, *3*. doi:10.1039/C5TB01453K
- Chen, L., Yu, Q. S., Wang, Y., & Li, H. (2011). BisGMA/TEGDMA dental composite containing high aspect-ratio hydroxyapatite nanofibers. *Dental Materials*, *27*(11), 1187-1195. doi:10.1016/j.dental.2011.08.403
- Choksi, P., Jepsen, K. J., & Clines, G. A. (2018). The challenges of diagnosing osteoporosis and the limitations of currently available tools. *Clinical Diabetes and Endocrinology*, *4*(1), 12. doi:10.1186/s40842-018-0062-7
- Chu, C., Liu, L., Rung, S., Wang, Y., Ma, Y., Hu, C., . . . Qu, Y. (2020). Modulation of foreign body reaction and macrophage phenotypes concerning microenvironment. *Journal of Biomedical Materials Research Part A*, *108*(1), 127-135. doi:<https://doi.org/10.1002/jbm.a.36798>
- Chung, S. M., Yap, A. U., Chandra, S. P., & Lim, C. T. (2004). Flexural strength of dental composite restoratives: comparison of biaxial and three-point bending test. *J Biomed Mater Res B Appl Biomater*, *71*(2), 278-283. doi:10.1002/jbm.b.30103
- Clarke, B. (2008). Normal bone anatomy and physiology. *Clinical journal of the American Society of Nephrology : CJASN*, *3* Suppl 3(Suppl 3), S131-S139. doi:10.2215/CJN.04151206
- Cotten, A., Dewatre, F., Cortet, B., Assaker, R., Leblond, D., Duquesnoy, B., . . . Clarisse, J. (1996). Percutaneous vertebroplasty for osteolytic metastases and myeloma: effects of the percentage of lesion filling and the leakage of methyl methacrylate at clinical follow-up. *Radiology*, *200*(2), 525-530. doi:10.1148/radiology.200.2.8685351
- Davies, J. E. (2007). Bone bonding at natural and biomaterial surfaces. *Biomaterials*, *28*(34), 5058-5067. doi:10.1016/j.biomaterials.2007.07.049
- Debnath, S., Karan, S., Debnath, M., Dash, J., & Chatterjee, T. K. (2017). Poly-L-Lysine Inhibits Tumor Angiogenesis and Induces Apoptosis in Ehrlich Ascites Carcinoma and in Sarcoma S-180 Tumor. *Asian Pacific journal of cancer prevention : APJCP*, *18*(8), 2255-2268. doi:10.22034/APJCP.2017.18.8.2255
- Denaro, V., Longo, U. G., Maffulli, N., & Denaro, L. (2009). Vertebroplasty and kyphoplasty. *Clinical Cases in Mineral and Bone Metabolism*, *6*(2), 125-130.
- Deryugina, E. I., & Quigley, J. P. (2008). Chapter 2. Chick embryo chorioallantoic membrane models to quantify angiogenesis induced by inflammatory and tumor cells or purified effector molecules. *Methods in enzymology*, *444*, 21-41. doi:10.1016/S0076-6879(08)02802-4
- Dorozhkin, S. V. (2011). Calcium orthophosphates: Occurrence, properties, biomineralization, pathological calcification and biomimetic applications. *Biomatter*, *1*(2), 121-164. doi:10.4161/biom.18790

- Driessens, F. C. M., Wolke, J., & Jansen, J. A. (2012). A new theoretical approach to calcium phosphates, aqueous solutions and bone remodeling. *Journal of the Australian Ceramic Society*, 48, 144-149.
- Edmondson, R., Broglie, J. J., Adcock, A. F., & Yang, L. (2014). Three-dimensional cell culture systems and their applications in drug discovery and cell-based biosensors. *Assay and drug development technologies*, 12(4), 207-218. doi:10.1089/adt.2014.573
- Eliasz, N., & Metoki, N. (2017). Calcium Phosphate Bioceramics: A Review of Their History, Structure, Properties, Coating Technologies and Biomedical Applications. *Materials (Basel, Switzerland)*, 10(4), 334. doi:10.3390/ma10040334
- Farvardin, A., Nejad, M. B., Pozin, M., Armand, M., & Asme. (2019). *A BIOMECHANICAL AND THERMAL ANALYSIS FOR BONE AUGMENTATION OF THE PROXIMAL FEMUR*. New York: Amer Soc Mechanical Engineers.
- Feng, P., Wei, P., Shuai, C., & Peng, S. (2014). Characterization of Mechanical and Biological Properties of 3-D Scaffolds Reinforced with Zinc Oxide for Bone Tissue Engineering. *PLoS ONE*, 9, e87755. doi:10.1371/journal.pone.0087755
- Feng, X., & McDonald, J. M. (2011). Disorders of bone remodeling. *Annual review of pathology*, 6, 121-145. doi:10.1146/annurev-pathol-011110-130203
- Ferracane, J. L. (2008). Buonocore Lecture. Placing dental composites--a stressful experience. *Oper Dent*, 33(3), 247-257. doi:10.2341/07-BL2
- Fribourg, D., Tang, C., Sra, P., Delamarter, R., & Bae, H. (2004). Incidence of subsequent vertebral fracture after kyphoplasty. *Spine (Phila Pa 1976)*, 29(20), 2270-2276; discussion 2277.
- Gajewski, V. E., Pfeifer, C. S., Fróes-Salgado, N. R., Boaro, L. C., & Braga, R. R. (2012). Monomers used in resin composites: degree of conversion, mechanical properties and water sorption/solubility. *Braz Dent J*, 23(5), 508-514. doi:10.1590/s0103-64402012000500007
- Gandolfi, M. G., Taddei, P., Siboni, F., Modena, E., De Stefano, E. D., & Prati, C. (2011). Biomimetic remineralization of human dentin using promising innovative calcium-silicate hybrid "smart" materials. *Dent Mater*, 27(11), 1055-1069. doi:10.1016/j.dental.2011.07.007
- Gao, C., Peng, S., Feng, P., & Shuai, C. (2017). Bone biomaterials and interactions with stem cells. *Bone Research*, 5(1), 17059. doi:10.1038/boneres.2017.59
- Gargallo, L., Radic, Deodato. (2009). Viscoelastic Behaviour of Polymers. In *Physicochemical Behavior and Supramolecular Organization of Polymers* (pp. 43-162). Dordrecht: Springer Netherlands.
- Genant, H. K., Jergas, M., Palermo, L., Nevitt, M., Valentin, R. S., Black, D., & Cummings, S. R. (1996). Comparison of semiquantitative visual and quantitative morphometric assessment of prevalent and incident vertebral fractures in osteoporosis. *Journal of Bone and Mineral Research*, 11(7), 984-996. doi:<https://doi.org/10.1002/jbmr.5650110716>
- Geurtsen, W. (1998a). Substances released from dental resin composites and glass ionomer cements. *Eur J Oral Sci*, 106(2 Pt 2), 687-695. doi:10.1046/j.0909-8836.1998.eos10602ii04.x
- Geurtsen, W. (1998b). Substances released from dental resin composites and glass ionomer cements. *Eur J Oral Sci*, 106(2 Pt 2), 687-695.
- Geurtsen, W. (2000). Biocompatibility of resin-modified filling materials. *Crit Rev Oral Biol Med*, 11(3), 333-355.

- Giannoudis, P., Tzioupis, C., Almalki, T., & Buckley, R. (2007). Fracture healing in osteoporotic fractures: Is it really different?: A basic science perspective. *Injury*, *38*(1, Supplement), S90-S99. doi:<https://doi.org/10.1016/j.injury.2007.02.014>
- Gonçalves, F., Pfeifer, C. C. S., Stansbury, J. W., Newman, S. M., & Braga, R. R. Influence of matrix composition on polymerization stress development of experimental composites. *Dental Materials*, *26*(7), 697-703. doi:10.1016/j.dental.2010.03.014
- Gosavi, S. S., Gosavi, S. Y., & Alla, R. K. (2010). Local and systemic effects of unpolymerised monomers. *Dental research journal*, *7*(2), 82-87.
- Gupta, S. K., Saxena, P., Pant, V. A., & Pant, A. B. (2012). Release and toxicity of dental resin composite. *Toxicology international*, *19*(3), 225-234. doi:10.4103/0971-6580.103652
- Gustavsson, J., Ginebra, M. P., Planell, J., & Engel, E. (2012). Osteoblast-like cellular response to dynamic changes in the ionic extracellular environment produced by calcium-deficient hydroxyapatite. *J Mater Sci Mater Med*, *23*(10), 2509-2520. doi:10.1007/s10856-012-4705-4
- Gutiérrez-Prieto, S. J., Perdomo-Lara, S. J., Diaz-Peraza, J. M., & Sequeda-Castañeda, L. G. (2019). Analysis of *In Vitro* Osteoblast Culture on Scaffolds for Future Bone Regeneration Purposes in Dentistry. *Advances in Pharmacological Sciences*, *2019*, 5420752. doi:10.1155/2019/5420752
- Habraken, W., Habibovic, P., Epple, M., & Bohner, M. (2016). Calcium phosphates in biomedical applications: materials for the future? *Materials Today*, *19*(2), 69-87. doi:<https://doi.org/10.1016/j.mattod.2015.10.008>
- Hamburger, V., & Hamilton, H. L. (1951). A series of normal stages in the development of the chick embryo. *Journal of Morphology*, *88*(1), 49-92. doi:<https://doi.org/10.1002/jmor.1050880104>
- Hamid Reza Seyyed Hosseinzadeh, M. E., Farivarabdollahzadeh Lahiji, Ali Sina Shahi, Aidin Masoudi and Sina Emami. (2013). *The Acrylic Bone Cement in Arthroplasty*. In P. P. Kinov (Ed.), *Intech*. Retrieved from <http://www.intechopen.com/books/arthroplasty-update/the-acrylic-bone-cement-in-arthroplasty> doi:10.5772/53252
- Härle, F., & Boudrieau, R. J. (2012). Chapter 2 - Maxillofacial bone healing. In F. J. M. Verstraete & M. J. Lommer (Eds.), *Oral and Maxillofacial Surgery in Dogs and Cats* (pp. 7-13). Oxford: W.B. Saunders.
- Havaldar, R., Pilli, S. C., & Putti, B. B. (2014). Insights into the effects of tensile and compressive loadings on human femur bone. *Advanced biomedical research*, *3*, 101-101. doi:10.4103/2277-9175.129375
- He, Z., Zhai, Q., Hu, M., Cao, C., Wang, J., Yang, H., & Li, B. (2015). Bone cements for percutaneous vertebroplasty and balloon kyphoplasty: Current status and future developments. *Journal of Orthopaedic Translation*, *3*(1), 1-11. doi:<https://doi.org/10.1016/j.jot.2014.11.002>
- Hegde, M., Bhat, G. T., & Nagesh, S. C. (2012). "Release of monomers from dental composite materials" - An in vitro study. *International Journal of Pharmacy and Pharmaceutical Sciences*, *4*, 500-504.
- Hernlund, E., Svedbom, A., Ivergård, M., Compston, J., Cooper, C., Stenmark, J., . . . Kanis, J. A. (2013). Osteoporosis in the European Union: medical management, epidemiology and economic burden: A report prepared in collaboration with the International Osteoporosis Foundation (IOF) and the European Federation of Pharmaceutical Industry Associations (EFPIA). *Archives of Osteoporosis*, *8*(1-2), 136. doi:10.1007/s11657-013-0136-1

- Ho, Y.-H., Man, K., Joshi, S. S., Pantawane, M. V., Wu, T.-C., Yang, Y., & Dahotre, N. B. (2020). In-vitro biomineralization and biocompatibility of friction stir additively manufactured AZ31B magnesium alloy-hydroxyapatite composites. *Bioactive Materials*, 5(4), 891-901. doi:<https://doi.org/10.1016/j.bioactmat.2020.06.009>
- Hodgkinson, J. M. (2010). *Mechanical Testing of Advanced Fibre Composites*: Woodhead Publishing, Ltd.
- Hu, Q., Tan, Z., Liu, Y., Tao, J., Cai, Y., Zhang, M., . . . Tang, R. (2007). Effect of Crystallinity of Calcium Phosphate Nanoparticles on Adhesion, Proliferation, and Differentiation of Bone Marrow Mesenchymal Stem Cells. *Journal of Materials Chemistry*, 17, 4690-4698. doi:10.1039/B710936A
- Huan, Z., & Chang, J. (2009). Novel bioactive composite bone cements based on the β -tricalcium phosphate–monocalcium phosphate monohydrate composite cement system. *Acta Biomater*, 5(4), 1253-1264. doi:<http://dx.doi.org/10.1016/j.actbio.2008.10.006>
- Hughes, E. A. B., Chipara, M., Hall, T. J., Williams, R. L., & Grover, L. M. (2020). Chemobrionic structures in tissue engineering: self-assembling calcium phosphate tubes as cellular scaffolds. *Biomaterials Science*, 8(3), 812-822. doi:10.1039/C9BM01010F
- Hughes, E. A. B., Robinson, T. E., Bassett, D. B., Cox, S. C., & Grover, L. M. (2019). Critical and diverse roles of phosphates in human bone formation. *Journal of Materials Chemistry B*, 7(47), 7460-7470. doi:10.1039/C9TB02011J
- Imazato, S. (2003). Antibacterial properties of resin composites and dentin bonding systems. *Dent Mater*, 19(6), 449-457.
- InstituteOfBoneHealth. (2015). Epidemiology. Retrieved from <https://www.osteoporosis.foundation/health-professionals/fragility-fractures/epidemiology>
- Iqbal, M. M. (2000). Osteoporosis: Epidemiology, Diagnosis, and Treatment. 93(1). http://www.medscape.com/viewarticle/410461_2
- Ito, S., Hashimoto, M., Wadgaonkar, B., Svizero, N. d., Carvalho, R., Yiu, C., . . . Pashley, D. (2005). Effect of resin hydrophilicity on water sorption and changes in modulus of elasticity. *Biomaterials*, 26, 6449-6459. doi:10.1016/j.biomaterials.2005.04.052
- Jaeblon, T. (2010). Polymethylmethacrylate: properties and contemporary uses in orthopaedics. *J Am Acad Orthop Surg*, 18(5), 297-305.
- Jang, H.-D., Kim, E.-H., Lee, J. C., Choi, S.-W., Kim, K., & Shin, B.-J. (2020). Current Concepts in the Management of Osteoporotic Vertebral Fractures: A Narrative Review. *Asian Spine J*, 14(6), 898-909. doi:10.31616/asj.2020.0594
- Jeong, J., Kim, J. H., Shim, J. H., Hwang, N. S., & Heo, C. Y. (2019). Bioactive calcium phosphate materials and applications in bone regeneration. *Biomaterials Research*, 23(1), 4. doi:10.1186/s40824-018-0149-3
- Ji, M.-X., & Yu, Q. (2015). Primary osteoporosis in postmenopausal women. *Chronic diseases and translational medicine*, 1(1), 9-13. doi:10.1016/j.cdtm.2015.02.006
- Jiang, H.-J., Xu, J., Qiu, Z.-Y., Ma, X.-L., Zhang, Z.-Q., Tan, X.-X., . . . Cui, F.-Z. (2015). Mechanical Properties and Cytocompatibility Improvement of Vertebroplasty PMMA Bone Cements by Incorporating Mineralized Collagen. *Materials*, 8(5), 2616-2634. doi:10.3390/ma8052616
- John M. Powers, R. L. S. (2012). *Craig's Restorative Dental Materials* (13th ed.). Philadelphia: Elsevier Mosby.
- Johnell, O., & Kanis, J. (2005). Epidemiology of osteoporotic fractures. *Osteoporosis International*, 16(2), S3-S7. doi:10.1007/s00198-004-1702-6

- Jones, J. R. (2006). Observing cell response to biomaterials. *Materials Today*, 9(12), 34-43. doi:[https://doi.org/10.1016/S1369-7021\(06\)71741-2](https://doi.org/10.1016/S1369-7021(06)71741-2)
- Kalteis, T., Lüring, C., Gugler, G., Zysk, S., Caro, W., Handel, M., & Grifka, J. (2004). [Acute tissue toxicity of PMMA bone cements]. *Z Orthop Ihre Grenzgeb*, 142(6), 666-672. doi:10.1055/s-2004-832317
- Kanis, J. A., Johnell, O., De Laet, C., Johansson, H., Oden, A., Delmas, P., . . . Tenenhouse, A. (2004). A meta-analysis of previous fracture and subsequent fracture risk. *Bone*, 35(2), 375-382. doi:<http://dx.doi.org/10.1016/j.bone.2004.03.024>
- Kayanja, M. M., Togawa, D., & Lieberman, I. H. (2005). Biomechanical changes after the augmentation of experimental osteoporotic vertebral compression fractures in the cadaveric thoracic spine. *Spine J*, 5(1), 55-63. doi:10.1016/j.spinee.2004.08.005
- Khalili, A. A., & Ahmad, M. R. (2015). A Review of Cell Adhesion Studies for Biomedical and Biological Applications. *International journal of molecular sciences*, 16(8), 18149-18184. doi:10.3390/ijms160818149
- Khan, A. M., Walters, N. J., & Young, A. M. (2014). *Fibre-reinforced injectable orthopedic composites with improved toughness and cell compatibility*. Paper presented at the Pioneering the future of biomaterials, Denver Colorado.
- Khan, M. A. (2015). *Development of Antibacterial and Remineralising Composite Bone Cements*. (Doctor of Philosophy), University College London, London.
- Kohli, N., Sawadkar, P., Ho, S., Sharma, V., Snow, M., Powell, S., . . . García-Gareta, E. (2020). Pre-screening the intrinsic angiogenic capacity of biomaterials in an optimised ex ovo chorioallantoic membrane model. *Journal of tissue engineering*, 11, 2041731420901621-2041731420901621. doi:10.1177/2041731420901621
- Kramer, N., Garcia-Godoy, F., & Frankenberger, R. (2005). Evaluation of resin composite materials. Part II: in vivo investigations. *Am J Dent*, 18(2), 75-81.
- Kuehn, K. D., Ege, W., & Gopp, U. (2005). Acrylic bone cements: composition and properties. *Orthop Clin North Am*, 36(1), 17-28, v. doi:10.1016/j.ocl.2004.06.010
- Kutz, M. (2002). *Handbook of Materials Selection*: John Wiley & Sons.
- Kuzyk, P. R., & Schemitsch, E. H. (2011). The basic science of peri-implant bone healing. *Indian journal of orthopaedics*, 45(2), 108-115. doi:10.4103/0019-5413.77129
- Larkin, P. J. (2018a). Chapter 2 - Basic Principles. In P. J. Larkin (Ed.), *Infrared and Raman Spectroscopy (Second Edition)* (pp. 7-28): Elsevier.
- Larkin, P. J. (2018b). Chapter 3 - Instrumentation and Sampling Methods. In P. J. Larkin (Ed.), *Infrared and Raman Spectroscopy (Second Edition)* (pp. 29-61): Elsevier.
- Law, K.-Y. (2014). Definitions for Hydrophilicity, Hydrophobicity, and Superhydrophobicity: Getting the Basics Right. *The Journal of Physical Chemistry Letters*, 5(4), 686-688. doi:10.1021/jz402762h
- Lemon, M. T., Jones, M. S., & Stansbury, J. W. (2007). Hydrogen bonding interactions in methacrylate monomers and polymers. *J Biomed Mater Res A*, 83(3), 734-746. doi:10.1002/jbm.a.31448
- Leung, D., Spratt, D. A., Pratten, J., Gulabivala, K., Mordan, N. J., & Young, A. M. (2005). Chlorhexidine-releasing methacrylate dental composite materials. *Biomaterials*, 26(34), 7145-7153. doi:10.1016/j.biomaterials.2005.05.014
- Liaqat, S. (2015). *Development of Antibacterial-releasing Dental Composites with high strength and dentine bonding*. (Doctor of Philosophy), University College London, London.
- Liu, X., Jakus, A. E., Kural, M., Qian, H., Engler, A., Ghaedi, M., . . . Niklason, L. E. (2018). Vascularization of Natural and Synthetic Bone Scaffolds. *Cell Transplantation*, 27(8), 1269-1280. doi:10.1177/0963689718782452

- Lopez, A., Hoess, A., Thersleff, T., Ott, M., Engqvist, H., & Persson, C. (2011). Low-modulus PMMA bone cement modified with castor oil. *Biomed Mater Eng*, 21(5-6), 323-332. doi:10.3233/bme-2012-0679
- Lopez, A., Unosson, E., Engqvist, H., & Persson, C. (2011). Direct and interactive effects of three variables on properties of PMMA bone cement for vertebral body augmentation. *J Mater Sci Mater Med*, 22(6), 1599-1606. doi:10.1007/s10856-011-4322-7
- Lu, H., Guo, L., Kawazoe, N., Tateishi, T., & Chen, G. (2009). Effects of poly(L-lysine), poly(acrylic acid) and poly(ethylene glycol) on the adhesion, proliferation and chondrogenic differentiation of human mesenchymal stem cells. *J Biomater Sci Polym Ed*, 20(5-6), 577-589. doi:10.1163/156856209x426402
- Lu, H., Trujillo-Lemon, M., Ge, J., & Stansbury, J. W. (2010). Dental resins based on dimer acid dimethacrylates: a route to high conversion with low polymerization shrinkage. *Compend Contin Educ Dent*, 31 Spec No 2, 1-4.
- Luo, X., Barbieri, D., Zhang, Y., Yan, Y., Bruijn, J. D., & Yuan, H. (2015). Strontium-Containing Apatite/Poly Lactide Composites Favoring Osteogenic Differentiation and in Vivo Bone Formation. *ACS Biomaterials Science & Engineering*, 1(2), 85-93. doi:10.1021/ab500005e
- Maggiano, I. S., Maggiano, C. M., Clement, J. G., Thomas, C. D. L., Carter, Y., & Cooper, D. M. L. (2016). Three-dimensional reconstruction of Haversian systems in human cortical bone using synchrotron radiation-based micro-CT: morphology and quantification of branching and transverse connections across age. *Journal of anatomy*, 228(5), 719-732. doi:10.1111/joa.12430
- Main, K. A. I. (2013). *Development of Composites for Bone Repair*. (Doctor of Philosophy), University College London,
- Main, K. A. I. (2013). *Development of Composites for Bone Repair*. (Doctor of Philosophy), University College London,
- Marquis, P. M., Palin, W. M., Fleming, G. J. P., Burke, F. J. T., & Randall, B. C. (2003). The relative reliability of biaxial and 3-point bend flexure testing of the strength of brittle light setting dental biomaterials. *J Dent Res*, 82, B37-B37.
- Marshall, K. M., Kanczler, J. M., & Oreffo, R. O. C. (2020). Evolving applications of the egg: chorioallantoic membrane assay and ex vivo organotypic culture of materials for bone tissue engineering. *Journal of tissue engineering*, 11, 2041731420942734. doi:10.1177/2041731420942734
- McMahon, S., Hawdon, G., Bare, J., Sim, Y., Bertollo, N., & Walsh, W. R. (2012). THERMAL NECROSIS AND PMMA – A CAUSE FOR CONCERN? *Orthopaedic Proceedings*, 94-B(SUPP_XXIII), 64-64. doi:10.1302/1358-992X.94BSUPP_XXIII.AOAoz2009-064
- Mehdawi, I., Abou Neel, E., Valappil, S., Palmer, G., Salih, V., Pratten, J., . . . Young, A. (2009). Development of remineralizing, antibacterial dental materials. *Acta Biomater*, 5, 2525-2539. doi:10.1016/j.actbio.2009.03.030
- Mehdawi, I., Neel, E. A., Valappil, S. P., Palmer, G., Salih, V., Pratten, J., . . . Young, A. M. (2009). Development of remineralizing, antibacterial dental materials. *Acta Biomater*, 5(7), 2525-2539. doi:10.1016/j.actbio.2009.03.030
- Meyer, F., Amaechi, B. T., Fabritius, H.-O., & Enax, J. (2018). Overview of Calcium Phosphates used in Biomimetic Oral Care. *The open dentistry journal*, 12, 406-423. doi:10.2174/1874210601812010406
- MHRA. (2017). An introductory guide to the medical device regulation (MDR) and the in vitro diagnostic medical device regulation (IVDR). In M. a. H. p. R. Agency (Ed.).
- Mitra, S. B., Wu, D., & Holmes, B. N. (2003). An application of nanotechnology in advanced dental materials. *J Am Dent Assoc*, 134(10), 1382-1390.

- Moreno-Jiménez, I., Hulsart-Billstrom, G., Lanham, S. A., Janeczek, A. A., Kontouli, N., Kanczler, J. M., . . . Oreffo, R. O. (2016). The chorioallantoic membrane (CAM) assay for the study of human bone regeneration: a refinement animal model for tissue engineering. *Scientific reports*, *6*, 32168-32168. doi:10.1038/srep32168
- Moreno-Jiménez, I., Kanczler, J. M., Hulsart-Billstrom, G., Inglis, S., & Oreffo, R. O. C. (2017). (*) The Chorioallantoic Membrane Assay for Biomaterial Testing in Tissue Engineering: A Short-Term In Vivo Preclinical Model. *Tissue Eng Part C Methods*, *23*(12), 938-952. doi:10.1089/ten.TEC.2017.0186
- Morrell, R. (1999). *Biaxial Flexural Strength Testing of Ceramic Materials*: Centre for Materials Measurement and Technology, National Physical Laboratory.
- Music, E., Futrega, K., & Doran, M. R. (2018). Sheep as a model for evaluating mesenchymal stem/stromal cell (MSC)-based chondral defect repair. *Osteoarthritis Cartilage*, *26*(6), 730-740. doi:10.1016/j.joca.2018.03.006
- Nakayama, W. T., Hall, D. R., Grenoble, D. E., & Katz, J. L. (1974). Elastic properties of dental resin restorative materials. *J Dent Res*, *53*(5), 1121-1126. doi:10.1177/00220345740530050901
- New, S. E. P., Ibrahim, A., Guasti, L., Zucchelli, E., Birchall, M., Bulstrode, N. W., . . . Ferretti, P. (2017). Towards reconstruction of epithelialized cartilages from autologous adipose tissue-derived stem cells. *Journal of Tissue Engineering and Regenerative Medicine*, *11*(11), 3078-3089. doi:<https://doi.org/10.1002/term.2211>
- Nowak-Sliwinska, P., Segura, T., & Iruela-Arispe, M. L. (2014). The chicken chorioallantoic membrane model in biology, medicine and bioengineering. *Angiogenesis*, *17*(4), 779-804. doi:10.1007/s10456-014-9440-7
- O'Hara, R., Buchanan, F., & Dunne, N. (2014). Injectable calcium phosphate cements for spinal bone repair. In P. Dubruel & S. V. Vlierberghe (Eds.), *Biomaterials for Bone Regeneration* (pp. 26-61): Woodhead Publishing.
- Odian, G. (2004). *Principles of Polymerization, 4th Edition*. New York: Wiley-Interscience.
- Oryan, A., Alidadi, S., Bigham-Sadegh, A., & Moshiri, A. (2018). Healing potentials of polymethylmethacrylate bone cement combined with platelet gel in the critical-sized radial bone defect of rats. *PLoS ONE*, *13*(4), e0194751-e0194751. doi:10.1371/journal.pone.0194751
- Osorio, M., Cañas, A., Puerta, J., Díaz, L., Naranjo, T., Ortiz, I., & Castro, C. (2019). Ex Vivo and In Vivo Biocompatibility Assessment (Blood and Tissue) of Three-Dimensional Bacterial Nanocellulose Biomaterials for Soft Tissue Implants. *Scientific reports*, *9*(1), 10553. doi:10.1038/s41598-019-46918-x
- Osterhoff, G., Morgan, E. F., Shefelbine, S. J., Karim, L., McNamara, L. M., & Augat, P. (2016). Bone mechanical properties and changes with osteoporosis. *Injury*, *47* Suppl 2(Suppl 2), S11-S20. doi:10.1016/S0020-1383(16)47003-8
- Palin, W. M., Fleming, G. J. P., Burke, F. J. T., Marquis, P. M., & Randall, R. C. (2003). Monomer conversion versus flexure strength of a novel dental composite. *J Dent*, *31*(5), 341-351. doi:10.1016/s0300-5712(03)00050-2
- Palin, W. M., Fleming, G. J. P., & Marquis, P. M. (2005). The reliability of standardized flexure strength testing procedures for a light-activated resin-based composite. *Dental Materials*, *21*(10), 911-919. doi:10.1016/j.dental.2005.01.005
- Palmer, I., Nelson, J., Schatton, W., Dunne, N. J., Buchanan, F., & Clarke, S. A. (2016). Biocompatibility of calcium phosphate bone cement with optimised mechanical properties: an in vivo study. *Journal of Materials Science: Materials in Medicine*, *27*(12), 191. doi:10.1007/s10856-016-5806-2
- Panpisut, P. (2017). *Development of a remineralising, antibacterial dental composite*. (MSc Dissertation), University College London,

- Panpisut, P., Khan, M. A., Main, K., Arshad, M., Xia, W., Petridis, H., & Young, A. M. (2019). Polymerization kinetics stability, volumetric changes, apatite precipitation, strontium release and fatigue of novel bone composites for vertebroplasty. *PLoS ONE*, *14*(3), e0207965. doi:10.1371/journal.pone.0207965
- Park, J.-G., Ye, Q., Topp, E. M., Lee, C. H., Kostoryz, E. L., Misra, A., & Spencer, P. (2009). Dynamic mechanical analysis and esterase degradation of dentin adhesives containing a branched methacrylate. *J Biomed Mater Res B Appl Biomater*, *91*(1), 61-70. doi:10.1002/jbm.b.31374
- Park, J., Eslick, J., Ye, Q., Misra, A., & Spencer, P. (2011). The influence of chemical structure on the properties in methacrylate-based dentin adhesives. *Dent Mater*, *27*(11), 1086-1093. doi:10.1016/j.dental.2011.07.011
- Park, J. H., Kim, H. S., & Kim, S. W. (2016). Cement Leakage into Adjacent Vertebral Body Following Percutaneous Vertebroplasty. *Korean Journal of Spine*, *13*(2), 74-76. doi:10.14245/kjs.2016.13.2.74
- Paterlini, T. T., Nogueira, L. F. B., Tovani, C. B., Cruz, M. A. E., Derradi, R., & Ramos, A. P. (2017). The role played by modified bioinspired surfaces in interfacial properties of biomaterials. *Biophysical reviews*, *9*(5), 683-698. doi:10.1007/s12551-017-0306-2
- Pawel Szulc, M. L. B. (2011). *Overview of osteoporosis: Epidemiology and clinical management*. Retrieved from http://www.osteofound.org/sites/default/files/PDFs/Vertebral%20Fracture%20Initiative/IOF_VFI-Part_I-Manuscript.pdf
- Peutzfeldt, A. (1997). Resin composites in dentistry: the monomer systems. *Eur J Oral Sci*, *105*(2), 97-116.
- Phull, S. S., Yazdi, A. R., Ghert, M., & Towler, M. R. (2021). Bone cement as a local chemotherapeutic drug delivery carrier in orthopedic oncology: A review. *Journal of Bone Oncology*, *26*, 100345. doi:<https://doi.org/10.1016/j.jbo.2020.100345>
- Pomrink, G. J., DiCicco, M. P., Clineff, T. D., & Erbe, E. M. (2003). Evaluation of the reaction kinetics of CORTOSS, a thermoset cortical bone void filler. *Biomaterials*, *24*(6), 1023-1031.
- Pratap, B., Gupta, R. K., Bhardwaj, B., & Nag, M. (2019). Resin based restorative dental materials: characteristics and future perspectives. *The Japanese dental science review*, *55*(1), 126-138. doi:10.1016/j.jdsr.2019.09.004
- Price, R. B., & Rueggeberg, F. A. (2019). 6 - Light Curing of Restorative Materials. In A. V. Ritter, L. W. Boushell, & R. Walter (Eds.), *Sturdevant's Art and Science of Operative Dentistry* (pp. 170-199). St. Louis: Elsevier.
- Profod. *Polylysine— A Natural Antimicrobial Agent*. Retrieved from: <http://www.profoodinternational.com/polylysin%20technical%20bulletin.pdf>
- Prost, S., Pesenti, S., Fuentes, S., Tropiano, P., & Blondel, B. (2020). Treatment of osteoporotic vertebral fractures. *Orthopaedics & Traumatology: Surgery & Research*, 102779. doi:<https://doi.org/10.1016/j.otsr.2020.102779>
- Qian, G., Dong, Y., Yang, W., & Wang, M. (2012). Injectable calcium phosphate cement and fibrin sealant recombined human bone morphogenetic protein-2 composite in vertebroplasty: an animal study. *Bosn J Basic Med Sci*, *12*(4), 231-235. doi:10.17305/bjbm.2012.2443
- Querido, W., Campos, A. P. C., Martins Ferreira, E. H., San Gil, R. A. S., Rossi, A. M., & Farina, M. (2014). Strontium ranelate changes the composition and crystal structure of the biological bone-like apatite produced in osteoblast cell cultures. *Cell and Tissue Research*, *357*(3), 793-801. doi:10.1007/s00441-014-1901-1

- Rabel, K., Kohal, R.-J., Steinberg, T., Tomakidi, P., Rolauffs, B., Adolfsson, E., . . . Altmann, B. (2020). Controlling osteoblast morphology and proliferation via surface microtopographies of implant biomaterials. *Scientific reports*, *10*(1), 12810. doi:10.1038/s41598-020-69685-6
- Rajesh Kumar Ranjan, M. K., Rakesh Kumar, Md Farman Ali. (2017). Bone cement. *International Journal of Orthopaedics Sciences*, *3*(4), 79-82. doi:10.22271/ortho.2017.v3.i4b.12
- Reznikov, N., Shahar, R., & Weiner, S. (2014). Bone hierarchical structure in three dimensions. *Acta Biomater*, *10*(9), 3815-3826. doi:<https://doi.org/10.1016/j.actbio.2014.05.024>
- Ribatti, D. (2016). The chick embryo chorioallantoic membrane (CAM). A multifaceted experimental model. *Mechanisms of Development*, *141*, 70-77. doi:<https://doi.org/10.1016/j.mod.2016.05.003>
- Rocha, D. N. d., Silva, M. H. P. d., Campos, J. B. d., Marçal, R. L. S. B., Mijares, D. Q., Coelho, P. G., & Cruz, L. R. (2018). Kinetics of conversion of brushite coatings to hydroxyapatite in alkaline solution. *Journal of Materials Research and Technology*, *7*(4), 479-486. doi:<https://doi.org/10.1016/j.jmrt.2018.02.002>
- Rosen, C. J. (2000). *The Epidemiology and Pathogenesis of Osteoporosis*. In A. B. Feingold KR, Boyce A, et al., editors. (Ed.).
- Saha, S., & Pal, S. (1984). Mechanical properties of bone cement: a review. *J Biomed Mater Res*, *18*(4), 435-462. doi:10.1002/jbm.820180411
- Şahin, E. (2018). *Calcium Phosphate Bone Cements*: IntechOpen.
- Santolini, E., Kanakaris, N. K., & Giannoudis, P. V. (2020). Sacral fractures: issues, challenges, solutions. *EFORT Open Reviews*, *5*(5), 299-311. doi:10.1302/2058-5241.5.190064
- Schumacher, G. E., Antonucci, J. M., O'Donnell, J. N. R., & Skrtic, D. (2007). The use of amorphous calcium phosphate composites as bioactive basing materials: Their effect on the strength of the composite/adhesive/dentin bond. *J Am Dent Assoc*, *138*(11), 1476-1484.
- Sideridou, I., Tserki, V., & Papanastasiou, G. (2003). Study of water sorption, solubility and modulus of elasticity of light-cured dimethacrylate-based dental resins. *Biomaterials*, *24*(4), 655-665. doi:10.1016/s0142-9612(02)00380-0
- Sideridou, I. D., Karabela, M. M., & Vouvoudi, E. (2008). Volumetric dimensional changes of dental light-cured dimethacrylate resins after sorption of water or ethanol. *Dent Mater*, *24*(8), 1131-1136. doi:10.1016/j.dental.2007.12.009
- Stryker. (2021). SpinePlex bone cement. *Information for healthcare professionals*. Retrieved from <https://www.stryker.com/us/en/interventional-spine/products/spineplex-cement.html#:~:text=SpinePlex%20bone%20cement%20is%20a,using%20the%20same%20proprietary%20process>.
- Takagishi, Y., Kawakami, T., Hara, Y., Shinkai, M., Takezawa, T., & Nagamune, T. (2006). Bone-like tissue formation by three-dimensional culture of MG63 osteosarcoma cells in gelatin hydrogels using calcium-enriched medium. *Tissue Engineering*, *12*(4), 927-937. doi:10.1089/ten.2006.12.927
- Tan, Z., Shi, Y., Xing, B., Hou, Y., Cui, J., & Jia, S. (2019). The antimicrobial effects and mechanism of ε-poly-lysine against *Staphylococcus aureus*. *Bioresources and Bioprocessing*, *6*(1), 11. doi:10.1186/s40643-019-0246-8
- Thormann, U., Ray, S., Sommer, U., ElKhassawna, T., Rehling, T., Hundgeburth, M., . . . Alt, V. (2013). Bone formation induced by strontium modified calcium phosphate cement in critical-size metaphyseal fracture defects in ovariectomized rats. *Biomaterials*, *34*(34), 8589-8598. doi:<https://doi.org/10.1016/j.biomaterials.2013.07.036>

- Tseng, Y.-Y., Yang, T.-C., Tu, P.-H., Lo, Y.-L., & Yang, S.-T. (2009). Repeated and Multiple New Vertebral Compression Fractures After Percutaneous Transpedicular Vertebroplasty. *34(18)*, 1917-1922. doi:10.1097/BRS.0b013e3181ac8f07
- Tu, K. N., Lie, J. D., Wan, C. K. V., Cameron, M., Austel, A. G., Nguyen, J. K., . . . Hyun, D. (2018). Osteoporosis: A Review of Treatment Options. *P & T: a peer-reviewed journal for formulary management*, *43(2)*, 92-104.
- Ullah, I., Subbarao, R. B., & Rho, G. J. (2015). Human mesenchymal stem cells - current trends and future prospective. *Bioscience reports*, *35(2)*, e00191. doi:10.1042/BSR20150025
- Vaishya, R., Chauhan, M., & Vaish, A. (2013). Bone cement. *Journal of Clinical Orthopaedics and Trauma*, *4(4)*, 157-163. doi:<http://dx.doi.org/10.1016/j.jcot.2013.11.005>
- Van Landuyt, K. L., Snauwaert, J., De Munck, J., Peumans, M., Yoshida, Y., Poitevin, A., . . . Van Meerbeek, B. (2007). Systematic review of the chemical composition of contemporary dental adhesives. *Biomaterials*, *28(26)*, 3757-3785.
- Van Meerbeek, B., Yoshihara, K., Van Landuyt, K., Yoshida, Y., & Peumans, M. (2020). From Buonocore's Pioneering Acid-Etch Technique to Self-Adhering Restoratives. A Status Perspective of Rapidly Advancing Dental Adhesive Technology. *J Adhes Dent*, *22(1)*, 7-34. doi:10.3290/j.jad.a43994
- Vargas, G. E., Mesones, R. V., Bretcanu, O., López, J. M. P., Boccaccini, A. R., & Gorustovich, A. (2009). Biocompatibility and bone mineralization potential of 45S5 Bioglass®-derived glass-ceramic scaffolds in chick embryos. *Acta Biomater*, *5(1)*, 374-380. doi:<https://doi.org/10.1016/j.actbio.2008.07.016>
- Vohra, S., Hennessy, K. M., Sawyer, A. A., Zhuo, Y., & Bellis, S. L. (2008). Comparison of mesenchymal stem cell and osteosarcoma cell adhesion to hydroxyapatite. *J Mater Sci Mater Med*, *19(12)*, 3567-3574. doi:10.1007/s10856-008-3525-z
- Wagh, A. S. (2016). Chapter 13 - Calcium Phosphate Cements. In A. S. Wagh (Ed.), *Chemically Bonded Phosphate Ceramics (Second Edition)* (pp. 165-178): Elsevier.
- Walters, N. J. (2016). *Remineralising composites with improved cytocompatibility and containing antimicrobial agents for conservative treatment of caries*. (Doctor of Philosophy), University College London,
- Wang, L., & Nancollas, G. H. (2008). Calcium orthophosphates: crystallization and dissolution. *Chem Rev*, *108(11)*, 4628-4669. doi:10.1021/cr0782574
- Warriner, A. H., Patkar, N. M., Curtis, J. R., Delzell, E., Gary, L., Kilgore, M., & Saag, K. (2011). Which fractures are most attributable to osteoporosis? *Journal of Clinical Epidemiology*, *64(1)*, 46-53. doi:10.1016/j.jclinepi.2010.07.007
- Webb, J. C., & Spencer, R. F. (2007). The role of polymethylmethacrylate bone cement in modern orthopaedic surgery. *J Bone Joint Surg Br*, *89(7)*, 851-857. doi:10.1302/0301-620x.89b7.19148
- Wegst, U. G. K., Bai, H., Saiz, E., Tomsia, A. P., & Ritchie, R. O. (2015). Bioinspired structural materials. *Nat Mater*, *14(1)*, 23-36. doi:10.1038/nmat4089
- Wei, H., Ren, J., Han, B., Xu, L., Han, L., & Jia, L. (2013). Stability of polydopamine and poly(DOPA) melanin-like films on the surface of polymer membranes under strongly acidic and alkaline conditions. *Colloids Surf B Biointerfaces*, *110*, 22-28. doi:10.1016/j.colsurfb.2013.04.008
- Wennerberg, A., & Albrektsson, T. (2009). Effects of titanium surface topography on bone integration: a systematic review. *Clinical Oral Implants Research*, *20(s4)*, 172-184. doi:<https://doi.org/10.1111/j.1600-0501.2009.01775.x>

- Whitney, E., & Alastra, A. J. (2020). Vertebral Fracture. In *StatPearls*. Treasure Island (FL): StatPearls Publishing
- Copyright © 2020, StatPearls Publishing LLC.
- Wilkesmann, S., Fellenberg, J., Nawaz, Q., Reible, B., Moghaddam, A., Boccaccini, A. R., & Westhauser, F. (2020). Primary osteoblasts, osteoblast precursor cells or osteoblast-like cell lines: Which human cell types are (most) suitable for characterizing 45S5-bioactive glass? *Journal of Biomedical Materials Research Part A*, *108*(3), 663-674. doi:<https://doi.org/10.1002/jbm.a.36846>
- Wilkinson, J. M., Eveleigh, R., Hamer, A. J., Milne, A., Miles, A. W., & Stockley, I. (2000). Effect of mixing technique on the properties of acrylic bone-cement: a comparison of syringe and bowl mixing systems. *J Arthroplasty*, *15*(5), 663-667. doi:10.1054/arth.2000.6620
- Williams, S. A., Chastek, B., Sundquist, K., Barrera-Sierra, S., Leader, D., Jr., Weiss, R. J., . . . Curtis, J. R. (2020). Economic burden of osteoporotic fractures in US managed care enrollees. *Am J Manag Care*, *26*(5), e142-e149. doi:10.37765/ajmc.2020.43156
- Wong, C. C., & McGirt, M. J. (2013). Vertebral compression fractures: a review of current management and multimodal therapy. *Journal of Multidisciplinary Healthcare*, *6*, 205-214. doi:10.2147/jmdh.s31659
- Wong, E. A., & Uni, Z. (2021). Centennial Review: The chicken yolk sac is a multifunctional organ. *Poultry Science*, *100*(3), 100821. doi:<https://doi.org/10.1016/j.psj.2020.11.004>
- Wu, X., Tang, Z., Wu, K., Bai, Y., Lin, X., Yang, H., . . . Yang, L. (2021). Strontium-calcium phosphate hybrid cement with enhanced osteogenic and angiogenic properties for vascularised bone regeneration. *J Mater Chem B*, *9*(30), 5982-5997. doi:10.1039/d1tb00439e
- Wuertz, K., Godburn, K., Neidlinger-Wilke, C., Urban, J., & Iatridis, J. C. (2008). Behavior of mesenchymal stem cells in the chemical microenvironment of the intervertebral disc. *Spine (Phila Pa 1976)*, *33*(17), 1843-1849. doi:10.1097/BRS.0b013e31817b8f53
- Xu, H. H. K., Wang, P., Wang, L., Bao, C., Chen, Q., Weir, M. D., . . . Reynolds, M. A. (2017). Calcium phosphate cements for bone engineering and their biological properties. *Bone Research*, *5*(1), 17056. doi:10.1038/boneres.2017.56
- Xu, L.-C., & Siedlecki, C. A. (2020). Chapter 2 - Bacterial cell–biomaterials interactions. In M. Mozafari (Ed.), *Handbook of Biomaterials Biocompatibility* (pp. 11-42): Woodhead Publishing.
- Xu, X., & Burgess, J. O. (2003). Compressive strength, fluoride release and recharge of fluoride-releasing materials. *Biomaterials*, *24*(14), 2451-2461.
- Xu, Y., Chen, C., Hellwarth, P. B., & Bao, X. (2019). Biomaterials for stem cell engineering and biomanufacturing. *Bioactive Materials*, *4*, 366-379. doi:10.1016/j.bioactmat.2019.11.002
- Yao, S., Lin, X., Xu, Y., Chen, Y., Qiu, P., Shao, C., . . . Tang, R. (2019). Osteoporotic Bone Recovery by a Highly Bone-Inductive Calcium Phosphate Polymer-Induced Liquid-Precursor. *Advanced Science*, *6*(19), 1900683. doi:<https://doi.org/10.1002/advs.201900683>
- Yoon, S.-P., Lee, S.-H., Ki, C.-H., Lee, Y.-T., Hong, S.-H., Lee, H.-M., & Moon, S.-H. (2014). Quality of life in patients with osteoporotic vertebral fractures. *Asian Spine J*, *8*(5), 653-658. doi:10.4184/asj.2014.8.5.653
- Young, A. M., Rafeeka, S. A., & Howlett, J. A. (2004). FTIR investigation of monomer polymerisation and polyacid neutralisation kinetics and mechanisms in various aesthetic dental restorative materials. *Biomaterials*, *25*(5), 823-833. doi:10.1016/S0142-9612(03)00599-4

- Yousefi, A.-M. (2019). A review of calcium phosphate cements and acrylic bone cements as injectable materials for bone repair and implant fixation. *Journal of Applied Biomaterials & Functional Materials*, 17(4), 2280800019872594. doi:10.1177/2280800019872594
- Yu, L., Li, Y., Zhao, K., Tang, Y., Cheng, Z., Chen, J., . . . Wu, Z. (2013). A novel injectable calcium phosphate cement-bioactive glass composite for bone regeneration. *PLoS ONE*, 8(4), e62570. doi:10.1371/journal.pone.0062570
- Zafar, M. S. (2020). Prosthodontic Applications of Polymethyl Methacrylate (PMMA): An Update. *Polymers (Basel)*, 12(10). doi:10.3390/polym12102299
- Zhang, T.-y., Zhang, P.-x., Xue, F., Zhang, D.-y., & Jiang, B.-g. (2020). Risk factors for cement leakage and nomogram for predicting the intradiscal cement leakage after the vertebra augmented surgery. *BMC Musculoskeletal Disorders*, 21(1), 792. doi:10.1186/s12891-020-03810-4
- Zhang, W., Li, J.-X., Tang, R.-C., & Zhai, A.-D. (2020). Hydrophilic and antibacterial surface functionalization of polyamide fabric by coating with polylysine biomolecule. *Progress in Organic Coatings*, 142, 105571. doi:<https://doi.org/10.1016/j.porgcoat.2020.105571>
- Zhang, Z., Jiao, F., Feng, Y., Xie, C., Qin, F., Zhang, S., . . . Tang, W. (2020). Evaluation of the analgesic effect of vertebral cancellous bone infiltration anaesthesia during vertebroplasty. *Journal of Orthopaedic Surgery and Research*, 15(1), 342. doi:10.1186/s13018-020-01872-7
- Zhao, X., Olsen, I., Li, H., Gellynck, K., Buxton, P. G., Knowles, J. C., . . . Young, A. M. (2010). Reactive calcium-phosphate-containing poly(ester-co-ether) methacrylate bone adhesives: Chemical, mechanical and biological considerations. *Acta Biomater*, 6(3), 845-855. doi:<https://doi.org/10.1016/j.actbio.2009.09.020>

Appendix A

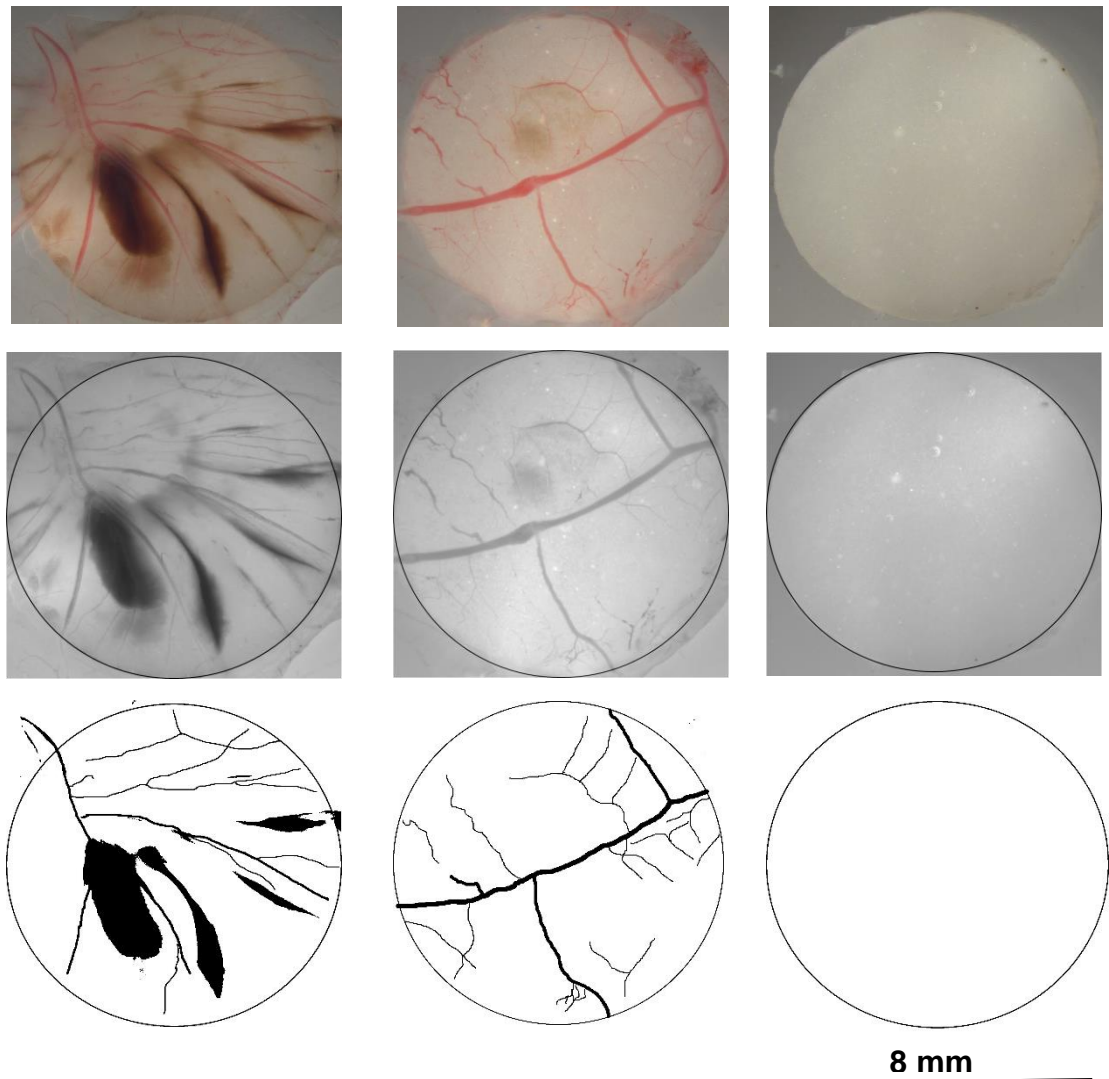


Figure 8.1 Image of disc implants with 0 % PLS and MCPM of the experimental bone composite harvested 7 days, grey scaled and in binary format via image J ($n=3$).

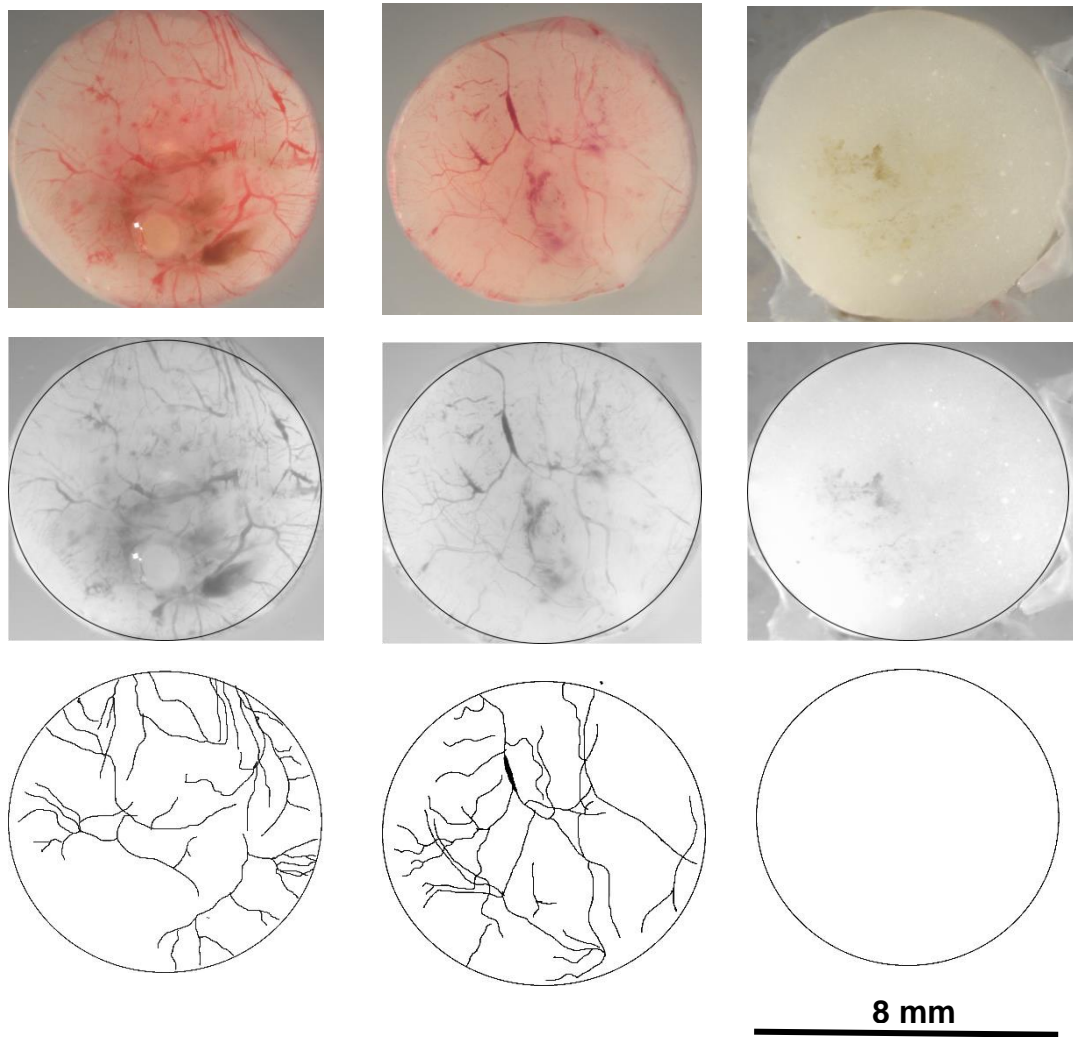


Figure 8.2 Image of disc implants with 2% PLS of the experimental bone composite harvested 7 days, grey scaled and in binary format via image J (n=3).

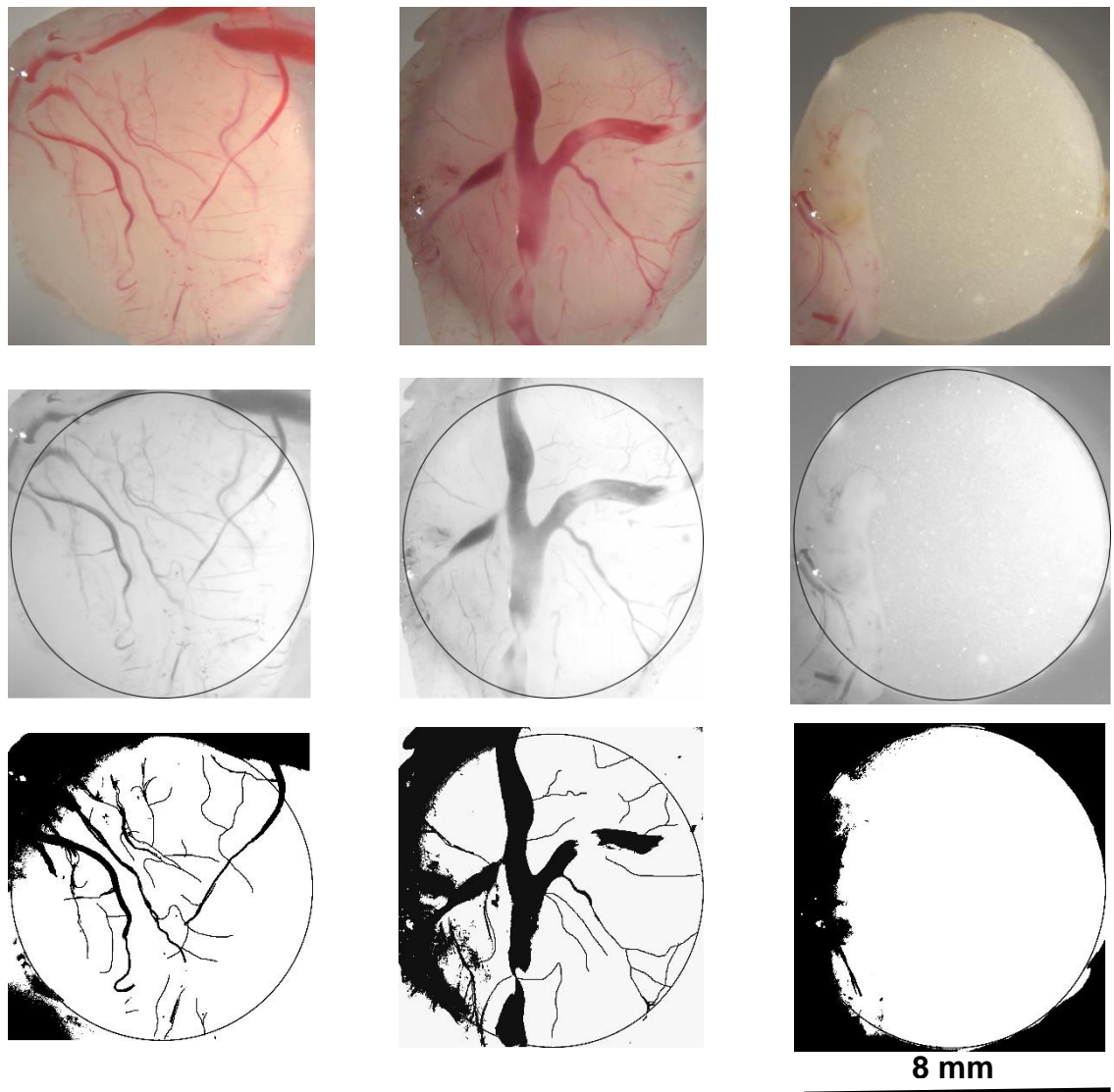


Figure 8.3 Image of disc implants with 10% PLS of the experimental bone composite harvested 7 days, grey scaled and in binary format via image J (n=3).

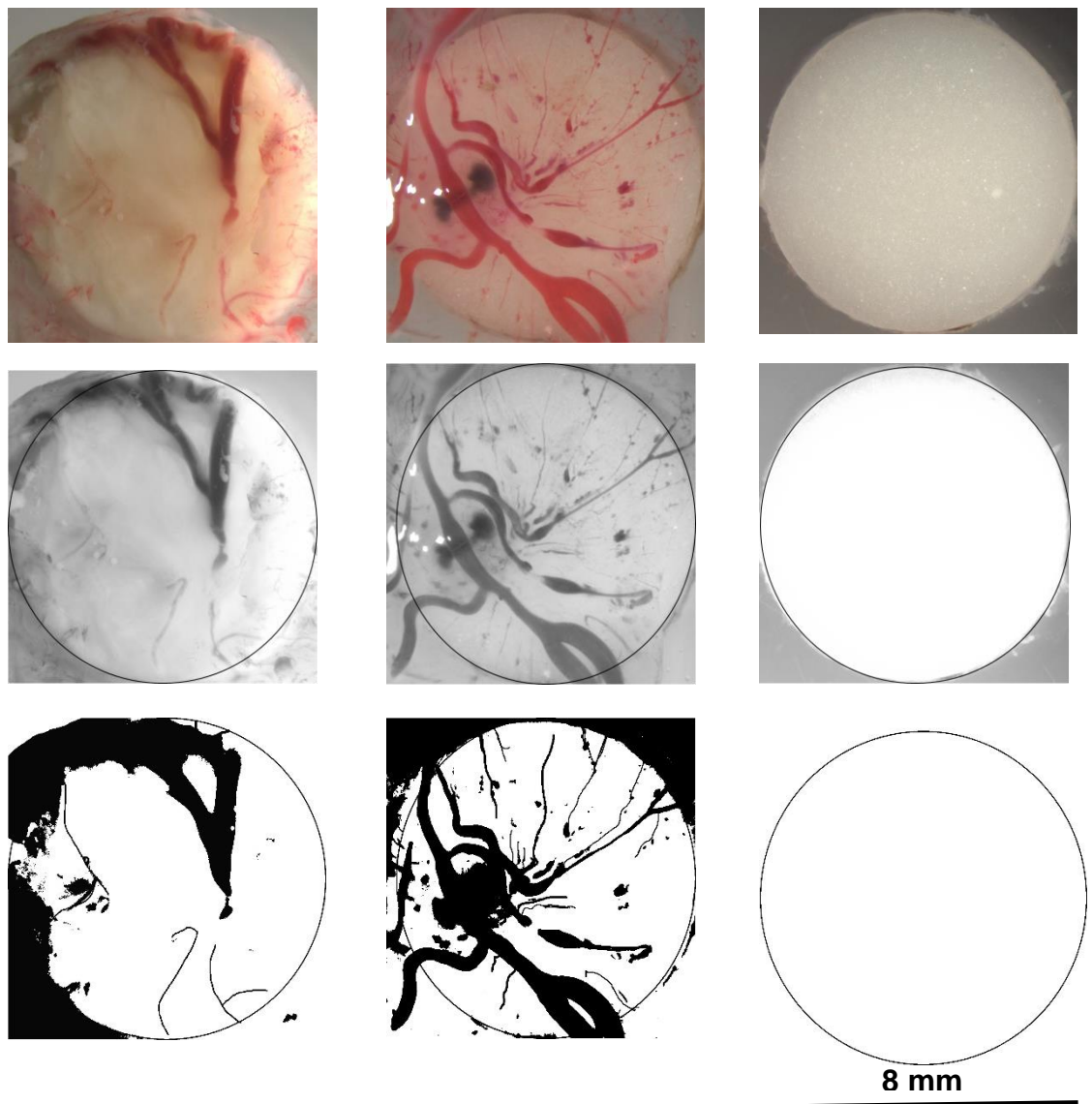


Figure 8.4 Image of disc implants with 4% MCPM of the experimental bone composite harvested 7 days, grey scaled and in binary format via image J (n=3).

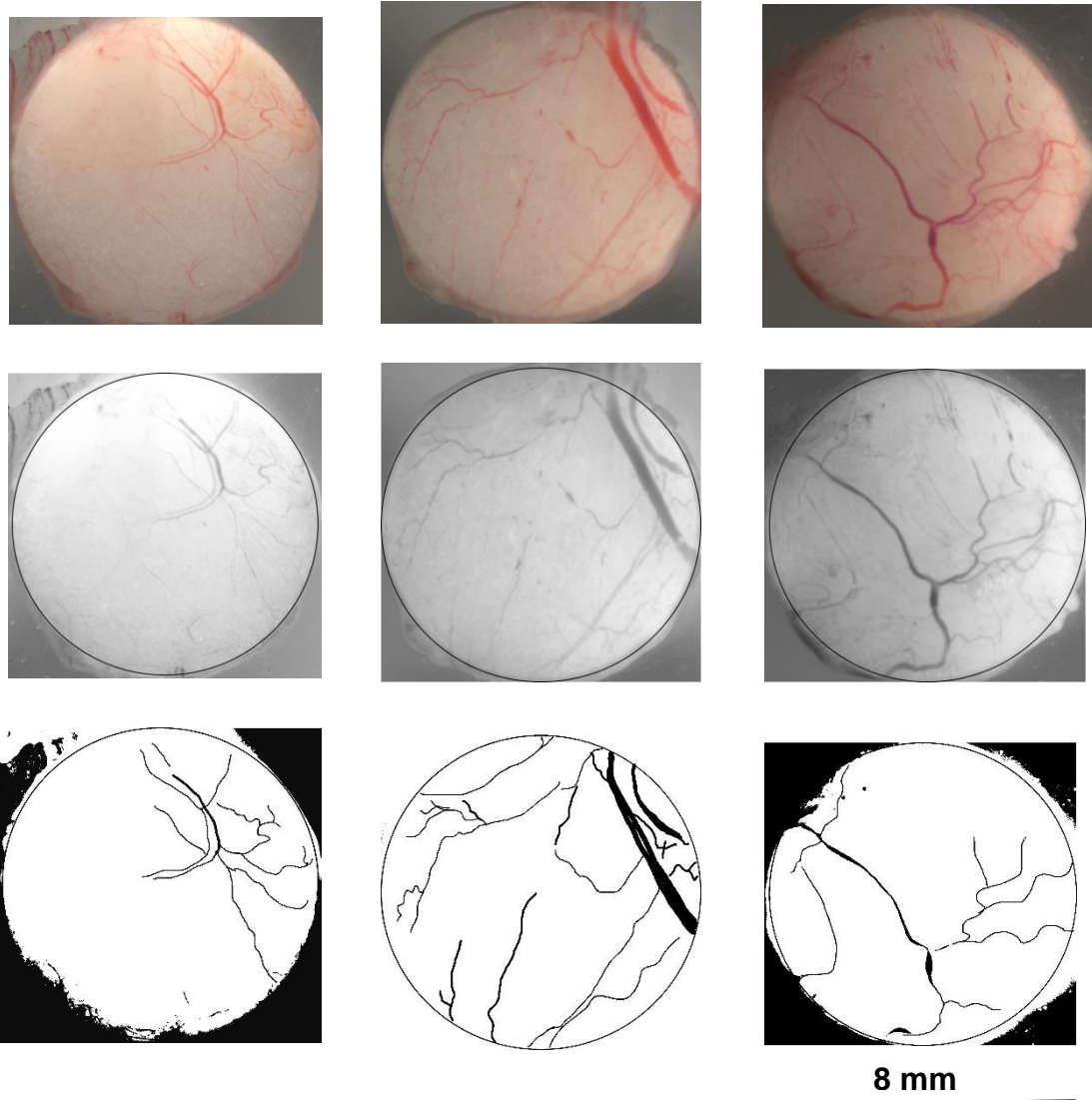


Figure 8.5 Image of disc implants with 16% MCPM of the experimental bone composite harvested 7 days, grey scaled and in binary format via image J (n=3).

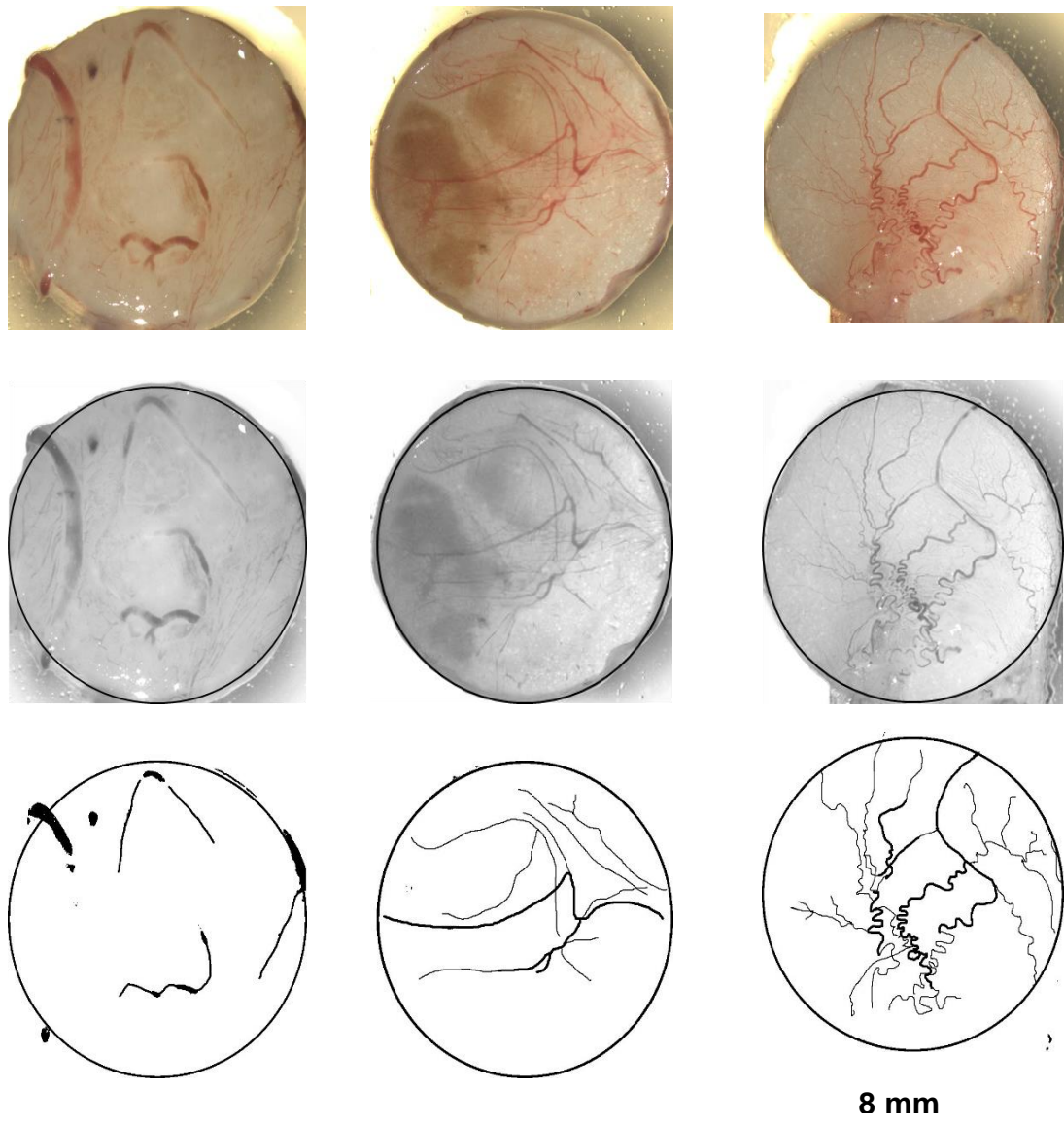


Figure 8.6 Image of disc implants with 5% PLS of the experimental bone composite harvested 7 days, grey scaled and in binary format via image J (n=3).

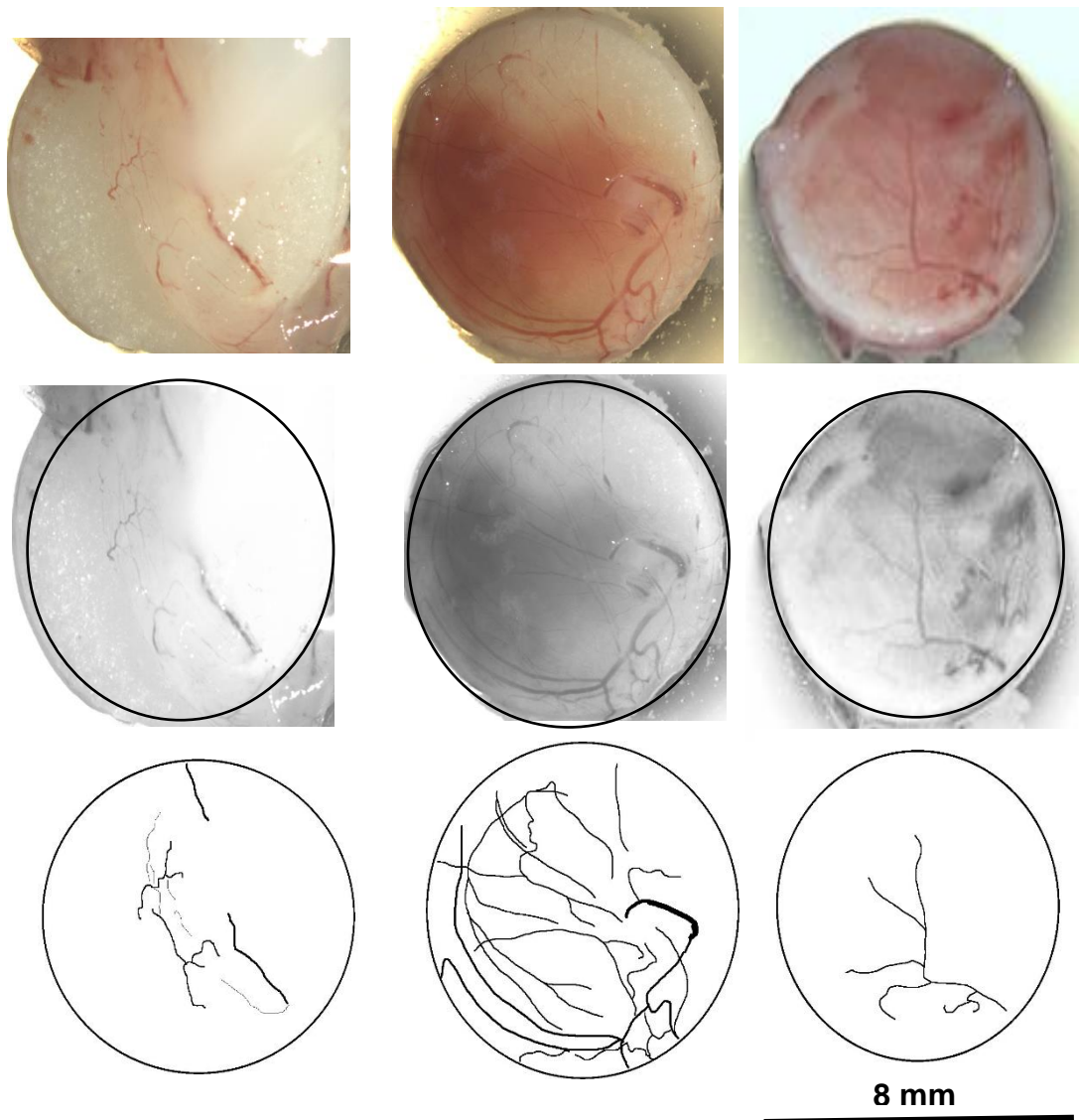


Figure 8.7 Image of disc implants with 8% MCPM of the experimental bone composite harvested 7 days, grey scaled and in binary format via image J (n=3).

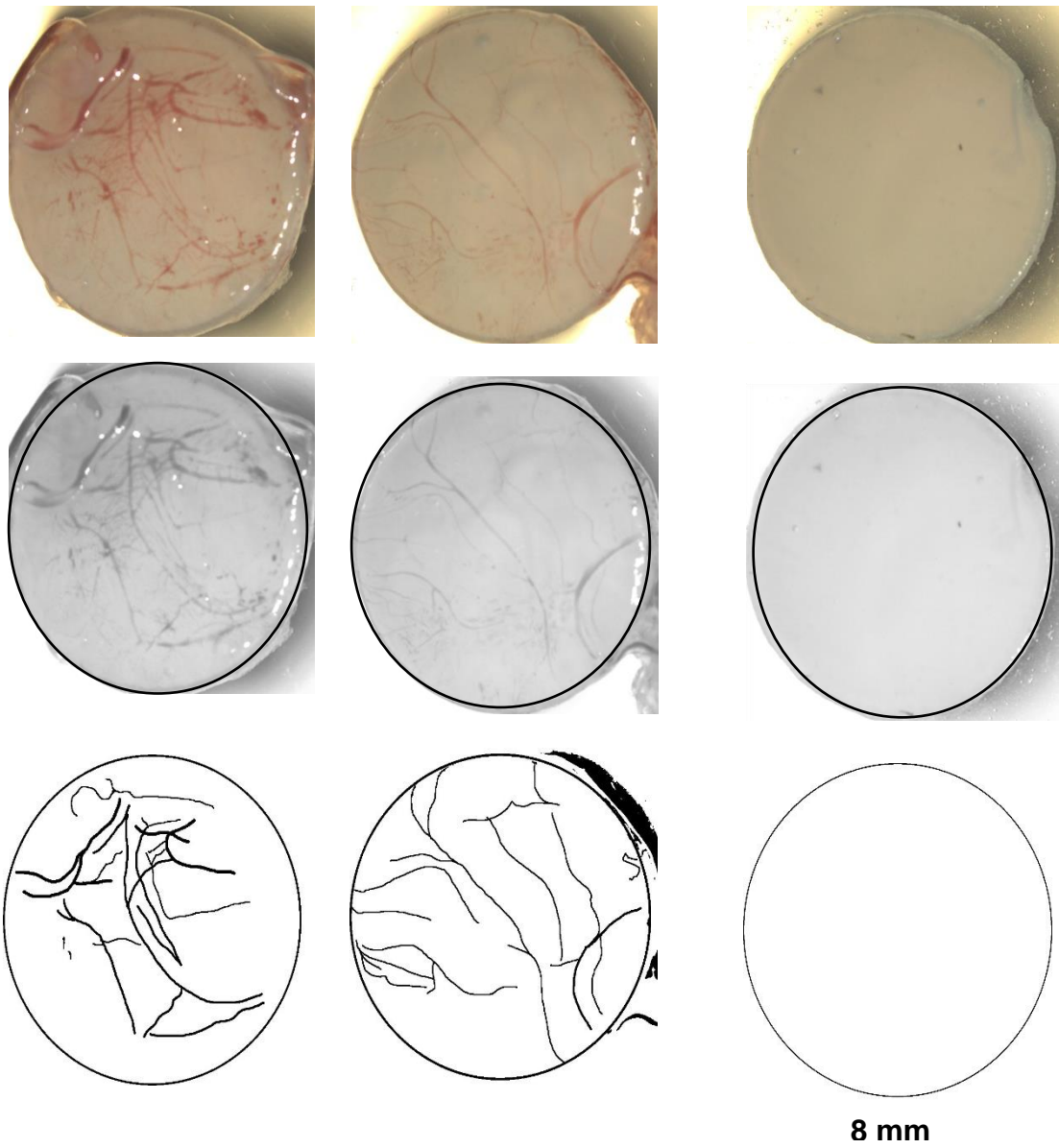


Figure 8.8 Image of disc implants with 0 % PLS of the experimental bone composite harvested 7 days, grey scaled and in binary format via image J (n=3).

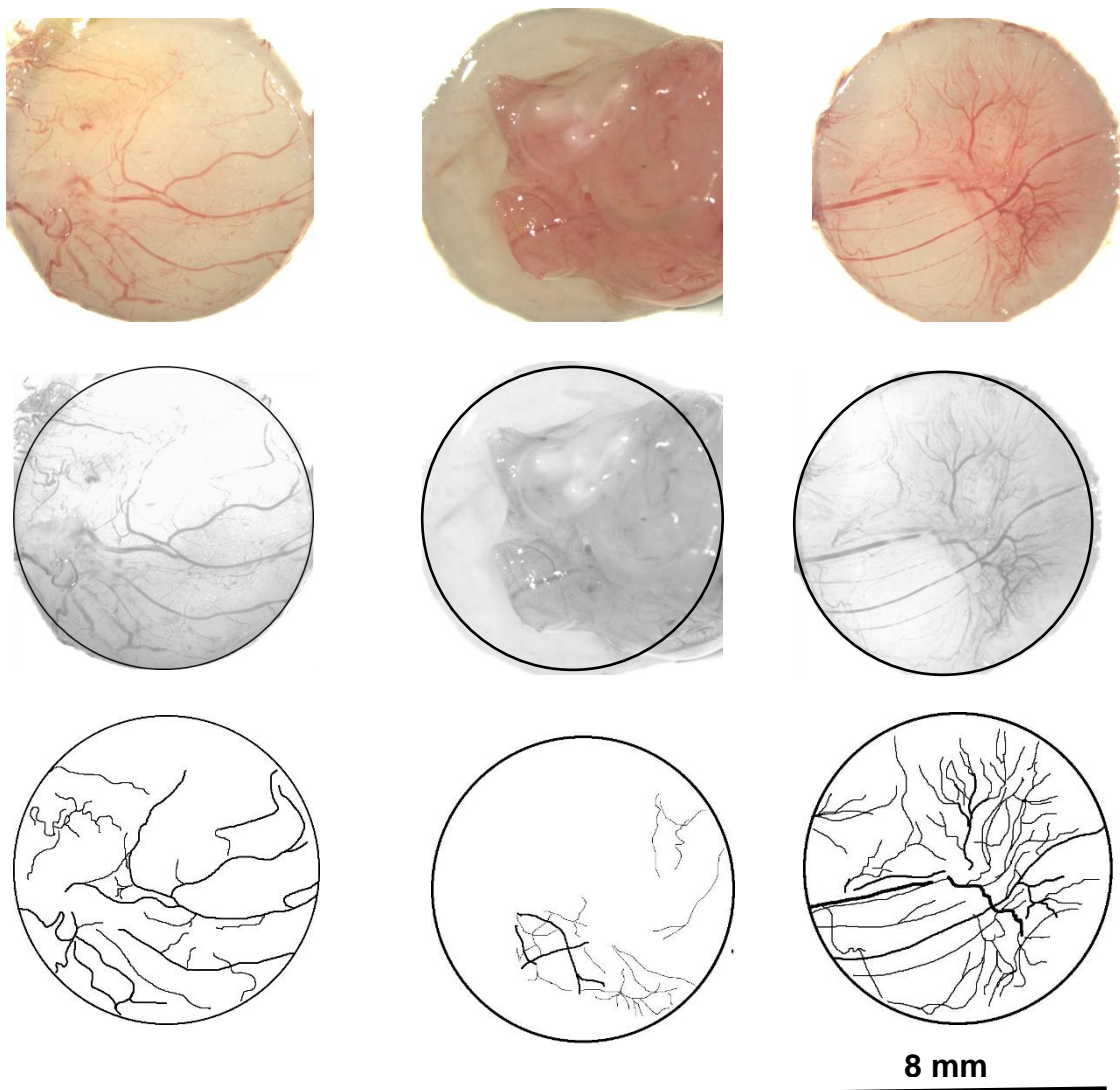


Figure 8.9 Image of disc implants with 4 % MCPM and 2 % PLS of the experimental bone composite harvested 7 days, grey scaled and in binary format via image J (n=3).

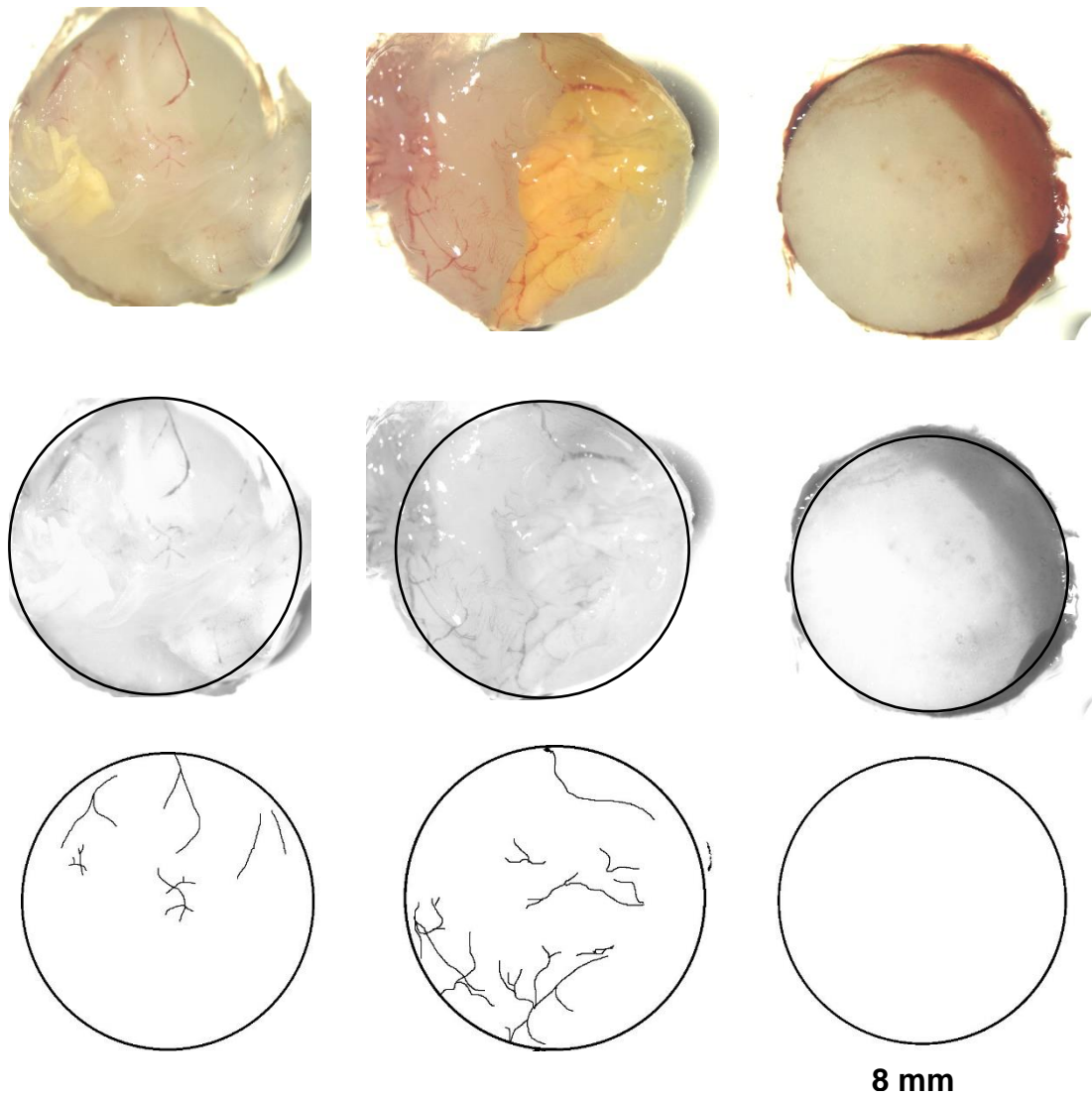


Figure 8.10 Image of disc implants with 4 % MCPM and 5 % PLS of the experimental bone composite harvested 7 days, grey scaled and in binary format via image J (n=3).

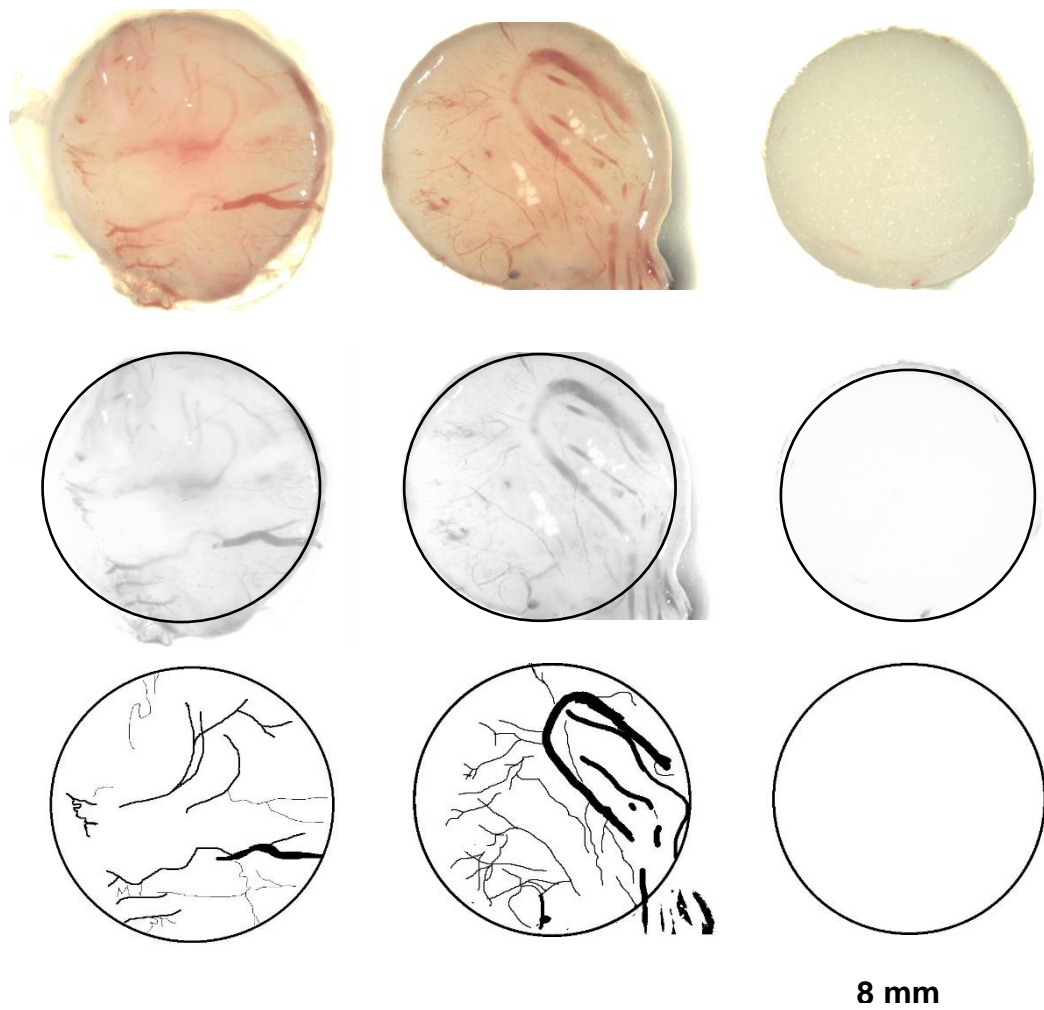


Figure 8.11 Image of disc implants with 8% MCPM and 2 % PLS of the experimental bone composite harvested 7 days, grey scaled and in binary format via image J (n=3).

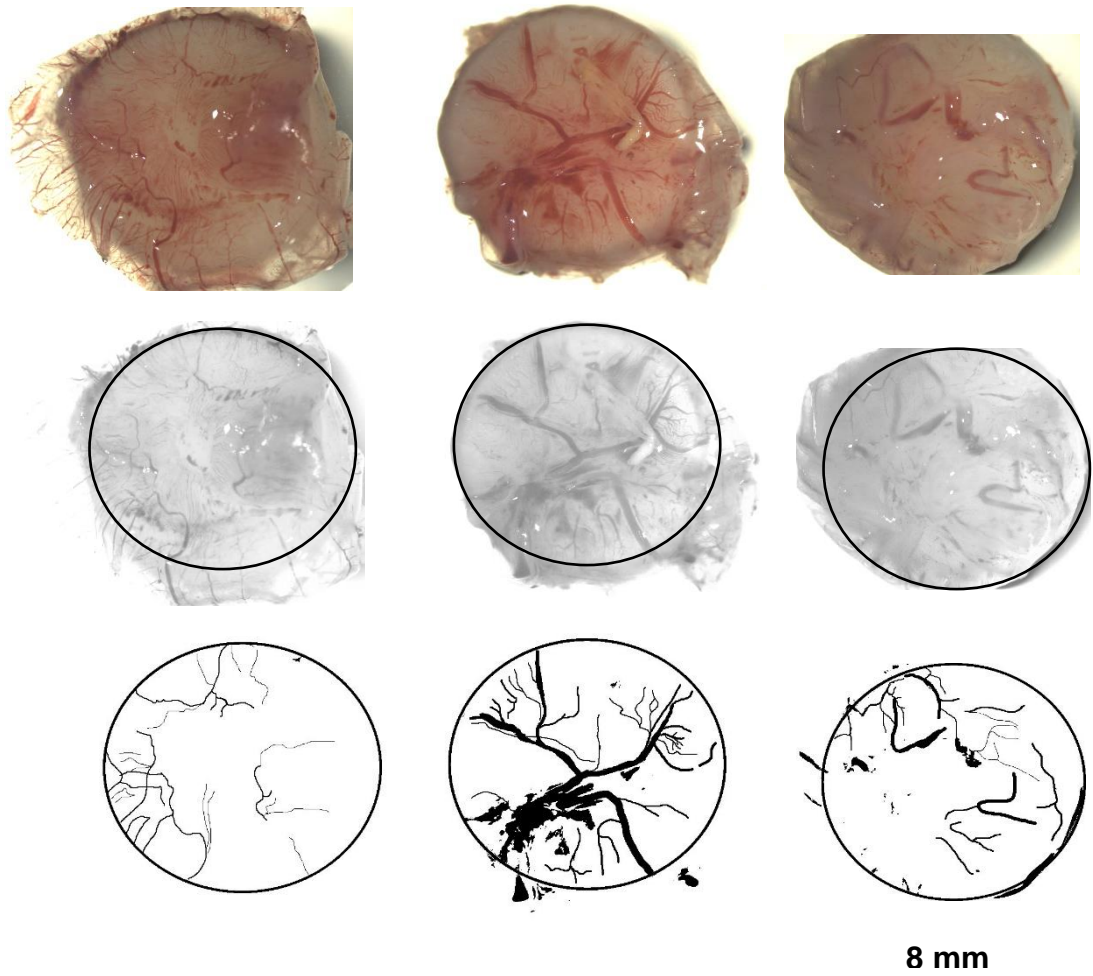


Figure 8.12 Image of disc implants with 8% MCPM and 5 % PLS of the experimental bone composite harvested 7 days, grey scaled and in binary format via image J (n=3).

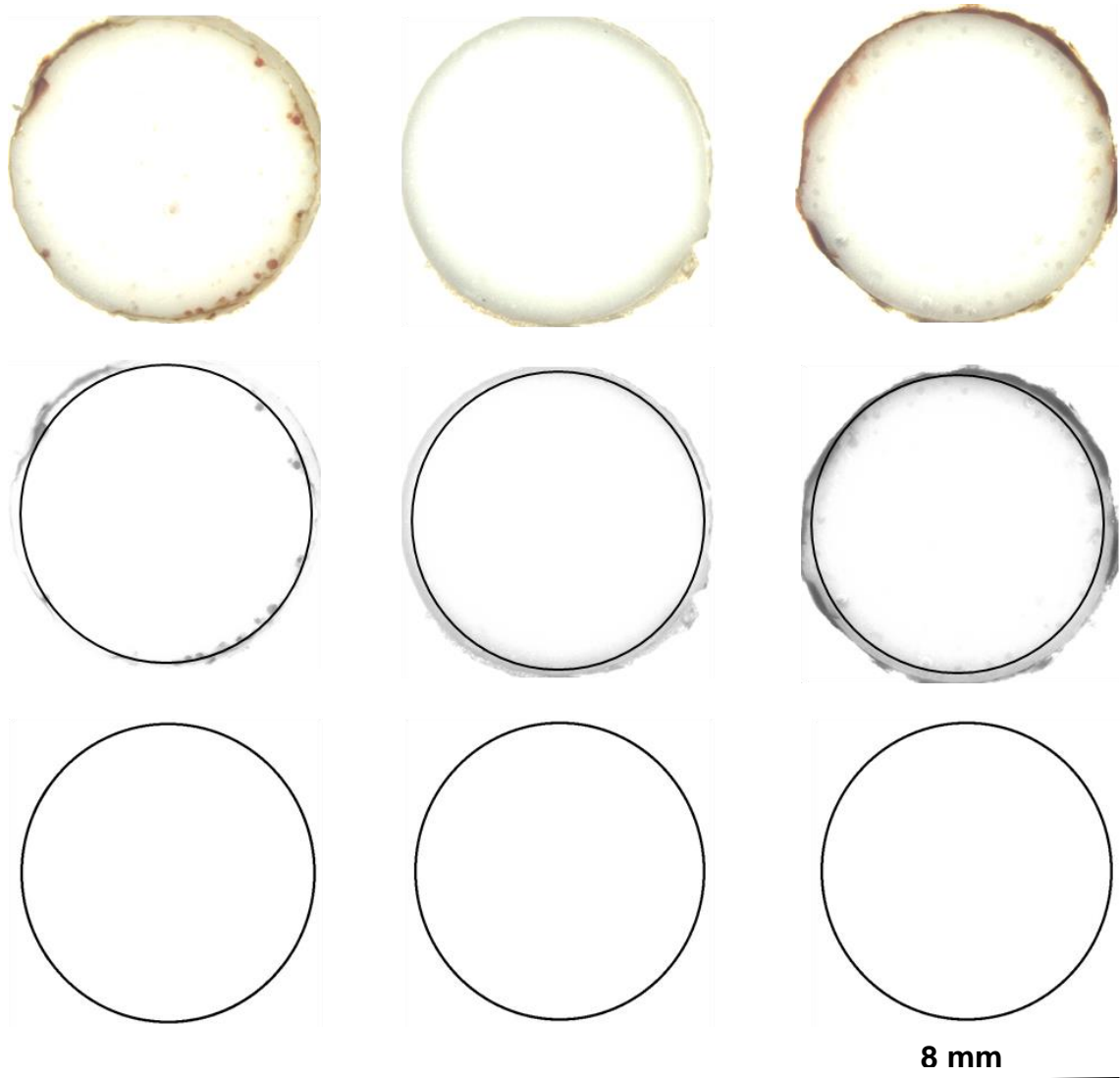


Figure 8.13 Image of disc implants of PMMA harvested 7 days, grey scaled and in binary format via image J (n=3).

Appendix B

ELSEVIER LICENSE TERMS AND CONDITIONS Mar 17, 2021

This Agreement between UCL -- Mayda Arshad ("You") and Elsevier ("Elsevier") consists of your license details and the terms and conditions provided by Elsevier and Copyright Clearance Center.

License Number	4998930549609
License date	Jan 30, 2021
Licensed Content Publisher	Elsevier
Licensed Content Publication	Surgery (Oxford)
Licensed Content Title	Anatomy of the vertebral column
Licensed Content Author	Vishy Mahadevan
Licensed Content Date	Jul 1, 2018
Licensed Content Volume	36
Licensed Content Issue	7
Licensed Content Pages	6
Start Page	327
End Page	332
Type of Use	reuse in a thesis/dissertation
Portion	figures/tables/illustrations
Number of figures/tables/illustrations	3
Format	both print and electronic
Are you the author of this Elsevier article?	No
Will you be translating?	No
Title	Modified Dental Composites for Bone Repair

Institution name	University College London
Expected presentation date	Mar 2021
Order reference number	Figures for spine and vertebra for Literature Review
Portions	Figure 1 on page 328. Figure 2, on page 329. Figure 3, on page 329
	UCL 51 Felbrigge Road
Requestor Location	Ilford, Essex IG3 8DW United Kingdom Attn: UCL
Publisher Tax ID	GB 494 6272 12
Total	0.00 GBP

SPRINGER NATURE LICENSE
TERMS AND CONDITIONS
Mar 17, 2021

This Agreement between UCL -- Mayda Arshad ("You") and Springer Nature ("Springer Nature") consists of your license details and the terms and conditions provided by Springer Nature and Copyright Clearance Center.

License Number	5026580098061
License date	Mar 12, 2021
Licensed Content Publisher	Springer Nature
Licensed Content Publication	Nature Materials
Licensed Content Title	Bioinspired structural materials
Licensed Content Author	Ulrike G. K. Wegst et al
Licensed Content Date	Oct 26, 2014
Type of Use	Thesis/Dissertation
Requestor type	academic/university or research institute
Format	print and electronic
Portion	figures/tables/illustrations
Number of figures/tables/illustrations	1
High-res required	no
Will you be translating?	no
Circulation/distribution	1 - 29
Author of this Springer Nature content	no
Title	Modified Dental Composites for Bone Repair
Institution name	University College London
Expected presentation date	Mar 2021
Order reference number	123
Portions	Figure 2
	UCL
	51 Felbrigge Road
Requestor Location	
	Ilford, Essex IG3 8DW
	United Kingdom
	Attn: UCL
Total	0.00 GBP